RLO/2438-77/1
UC-60

SITES FOR WIND POWER INSTALLATIONS:
Wind Tunnel Simulation of the Influence of Two-Dimensional Ridges on Wind Speed and Turbulence

Draft Final Report: Second Year

R. N. Meroney
V. A. Sandborn
R. J. B. Bouwmeester
M. A. Rider

Fluid Mechanics and Wind Engineering Program
Civil Engineering Department
Colorado State University
Fort Collins, Colorado 80523

July 1977

Prepared for the United States
Energy Research and Development Administration
Division of Solar Energy
Federal Wind Energy Program

ERDA Contract No. EY-76-S-06-2438, A001

CER77-78RNM-VAS-RB-MAR6

TABLE OF CONTENTS

TABLE OF CONTENTS (continued)

ABSTRACT

Wind tunnel studies of optimum sites for wind power turbines were made. A systematic evaluation of the flow over two-dimensional ridges is reported. Two-dimensional ridges with definite crests, such as ideal triangular or sinusoidal shapes, produce the greatest amplifications in local wind speed. Bluff, very steep and flat topped ridges do not produce as large an increase in velocity as the crest ridges. The ridges tested were of small characteristic size compared to the boundary layer thickness. The models correspond to ridges of the order of 100 meters or less in the atmosphere. For these ridges it is found that local viscous effects are of second order and the speedup of velocity can be predicted by inviscid flow considerations. Only near the surface (corresponding to approximately one to two ridge heights) are large changes in velocity observed. Wind velocity increases of the order of two times or greater than that of the approach velocity are measured at the crest of the triangular ridge. A slope of 1 to 4 (14 degrees) for the triangular ridge gives the optimum speedup at the crest.

The flow in the outer region of the boundary layers over the ridge was found to remain similar to the flow upstream of the ridge. The longitudinal turbulent velocity component was found to decrease slightly near the ridge surface as the flow progressed over the windward face of the ridge. The vertical turbulent velocity component increased slightly along the windward face of the ridge. The variation in turbulent velocities over the windward face of the ridge correspond to effect of a contraction on isotropic turbulence.

SITES FOR WIND-POWER INSTALLATIONS

Wind Tunnel Simulation of the Influence of Two-Dimensional Ridges on Wind Speed and Turbulence

INTRODUCTION

Selection of sites for wind power generation require a detailed knowledge of air flow over atmospheric terrain. Since the power from the wind is proportional to the cube of the speed, it is of critical importance that the wind conversion unit be located where maximum wind velocities occur. The atmospheric wind is greatly influenced by the local terrain features. It is well known that the wind over hills and ridges and local funneling effects can also produce high winds. Likewise surface roughness, obstructions, such as trees, buildings and local rock outcrops, will produce local reductions in the wind speed. All of these factors must be included in the selection of wind power sites.

For large span wind turbine units it is advantageous to have a uniform wind velocity that does not vary with vertical height. Use of optimum two-dimensional ridges will both amplify the wind velocity near the surface and make the velocity nearly constant with height. These results can be achieved even in the case of small ridges. The initial phase of the present wind tunnel study was focused on documenting details of the most optimum sites. Effects of ridge shape, approach velocity distribution, and stratification have been considered. Also factors such as the effect of the ridges on the turbulent velocities have been experimentally evaluated.

Details of the wind tunnel modeling of atmospheric flows are discussed in the present report, along with the experimental studies on flow over ridges.

LIST OF SYMBOLS

Symbol	Definition	Dimensions
A	constant King's Law	
B	constant King's Law	
C_f	friction coefficient	
C_p	pressure coefficient	
E_1, E_2	mean voltage of a hot wire, 1 normal, 2 yawed	V
e, e_1, e_2	voltage fluctuation	V
$\overline{e^2}$	mean square of voltage fluctuation	V^2
$\sqrt{\overline{e^2}}$	root mean square of voltage fluctuation	V
$\overline{e_1 e_2}$	mean of product of e_1 and e_2	V^2
H	form factor	
h	height of hill	L
m	exponent	F/L^2
p	pressure	VT
S_u	sensitivity dE/dU of a hot wire	$\frac{VT}{L}$
S_1	sensitivity dE/dU of a normal hot wire	$\frac{VT}{L}$
S_2	sensitivity dE/dU of a yawed hot wire	$\frac{VT}{L}$
S_v	sensitivity, $1/U\ dE/U\phi$, to angle	$\frac{VT}{L}$
U	local mean velocity	L/T
U_e	characteristic velocity	L/T
U_{TOT}	total velocity	L/T
$U_{F.S.}$, U_∞	free stream velocity	L/T
U_τ	friction velocity	L/T
u, v	velocity fluctuation in x-, y-direction	L/T
$\sqrt{\overline{u^2}}$, $\sqrt{\overline{v^2}}$	root mean square velocity fluctuations	L/T
$\overline{uv}$	time mean product of u and v	L^2/T^2

LIST OF SYMBOLS (continued)

Symbol	Definition	Dimensions
x	longitudinal direction	L
y	vertical direction	L
z	horizontal direction	L
ΔP	pressure difference	F/L^2
ΔS	mean velocity speedup	
δ	boundary layer thickness	L
δ^*	displacement thickness	L
η	nondimensional distance from wall, y/δ	
θ	momentum thickness	L
ν	kinematic viscosity	L^2/T
ρ	mass density	m/L^3
ρ_e	characteristic mass density	m/L^3
τ	shear stress	F/L^2
τ_e	characteristic shear stress	F/L^2
τ_{ref}	reference wall shear stress	F/L^2
τ_w	wall shear stress	F/L^2
$\tau_{w\ local}$	local wall shear stress	F/L^2
ϕ	angle of probe with x axis	

OBJECTIVES OF WIND TUNNEL STUDIES

The major objectives of the wind tunnel study of wind power sites are the modeling of "ideal" atmospheric flows over both basic and complex shapes. The shapes are related to typical hills and ridges that are encountered in field site terrain. The initial study was directed toward the evaluation of an ideal, optimum, two-dimensional ridge. The ideal case allows an evaluation of the major features of the flow and a check of digital techniques of modeling flow over atmospheric terrain. The initial results has shown that for the large Reynolds numbers encountered in atmospheric flows, viscous effects can be neglected in predicting the flow over moderately high ridges. The initial studies have been for ridges with heights small compared to the approach boundary layer thickness ($\frac{H}{\delta} \simeq 0.1$). For atmospheric boundary layers of the order of 1000 meters, the model scale correspond to ridge heights of the order of 100 meters. The ridge cord, which for the optimum triangular shape with slope of 1 to 4 is also of the order of the longitudinal turbulent scale. For atmospheric flows the longitudinal turbulent scales can range from 50 to several hundred meters depending on the approach topography. Detailed evaluation of both the mean and turbulent flow over the two-dimensional ridges has confirmed that viscous effects need not be included in the analysis of the mean flow. It was not foreseen in the initial phase of the wind tunnel study that the flow could be treated as inviscid. Indeed most computer models currently being developed for flow over terrain still employ elaborate viscous and turbulence models.

The modeling study also included effects of surface roughness and thermal stability. For the two-dimensional ridges roughness effects alter the approach boundary layer profile, but the flow over the ridge does not have time to more than produce a contraction of the oncoming flow. Thermal stratification will also alter the approach velocity distribution, but has only a secondary effect on the velocity speedup over the small scale, two-dimensional ridges studies. Obviously, stratification is expected to be important for large scale mountains.

The initial study documented the basic flow over optimum shapes. The flow over isolated, three-dimensional, ideal hills has also been evaluated. Again this study was made to provide a set of data from which computer modeling of complex terrain can be developed. The isolated three-dimensional hill does not produce the dramatic speedup of the ridge, since the flow both goes around and over the hill.

Evaluation of flow over less than ideal shapes was also made for the two-dimensional ridges. For very steep ridges, bluff cliffs and escarpments the flow fails to follow the local surface, and viscous separation regions result. The separation of flow leads to a reduction in the local speedup of the wind over these bluff ridges. An experimental evaluation of the separation effects is currently underway to better define the flows, so that they may be taken into account in selection of field sites.

Direct modeling of actual field sites will be done in the near future. As noted above the wind tunnel produces detailed modeling of the wind field over hills that are small compared to either the boundary layer thickness, or of the order of the turbulent scale. This "small" scale modeling produces the inviscid type flow pattern. The small scale modeling can accurately identify speedup effects and local separation regions. Further detail of the modeling between the wind tunnel and the atmosphere will be covered in the following section. In order to model terrain features, such as mountains or hills that are large compared to the boundary layer height, or turbulent scales a different approach is employed. Detailed models that include local terrain features, such as local roughness, trees and other obstructions are employed. Of equal importance is the need to specify a local pressure distribution, either associated with the freestream above the model, or at the model surface. The wind tunnel is constructed so that the ceiling can be raised or lowered to produce a desired pressure gradient. Note that for the small scale models the freestream flow was assumed to remain nearly constant. For the large scale field sites it will be necessary to make parametic studies of the pressure gradient over the models.

WIND TUNNEL MODELING OF ATMOSPHERIC FLOW

Atmospheric wind flows are associated mainly with large scale motions. A basic modeling parameter for fluid flow is the Reynolds number

$$Re = \frac{\rho U L}{\mu} \tag{1}$$

where ρ is the fluid density, U is the fluid velocity, μ is the coefficient of fluid viscosity and L is a characteristic length. Many characteristic lengths can be defined for specific modeling applications. Typically a length associated with the distance over which the boundary layer develops can be used to define a particular flow. Reynolds numbers of the order of 10^9 to 10^{10} may be obtained in the atmosphere. For the Colorado State University wind tunnel it is possible to obtain boundary layer Reynolds numbers along the test floor of the order of 10^8, Zoric and Sandborn, ref. 1. The analysis of Zoric and Sandborn, discussed below, demonstrates that for a sufficiently large Reynolds number the turbulent boundary layer develops to a similarity form. Thus, for Reynolds numbers greater than approximately 10^7 only second order differences are found for the outer region of turbulent boundary layers.

In the atmosphere the wind is driven by a large scale difference in pressure, however, the local flow behaves very much like a zero pressure gradient flow. A major difficulty with atmospheric winds are that they do not remain constant with time. However, for those times when a steady wind is present, the velocity distribution above the surface will be similar to the large Reynolds number boundary layers produced in the wind tunnel. Figure 1 shows typical zero pressure gradient velocity distributions that have been reported for a number of different Reynolds numbers. The velocity in the outer portion of the layer approaches closer the freestream value as the Reynolds number increases.

Mean Velocity Similarity - In order to simulate the atmospheric flow in the laboratory, a wind tunnel with a long test section was employed. The boundary layer at the start of the test section was artificially thickened with roughness. The thick boundary layer was then allowed to develop further over a smooth surface. The laboratory boundary layer cannot simulate the turning of wind direction with attitude encountered in the atmosphere. Figure 2 is a typical set of velocity distributions measured along the test section surface, ref. 1.

As can be seen on Figure 2, the boundary layer required approximately 20 feet of development to obtain a "similarity" shape. Evaluation of the surface shear stress along the test section was used to determine the equivalant x-distance Reynolds numbers. Measurement of the turbulent stress terms also indicate that they obtain a similarity, ref. 1. Formally a similarity of the mean velocity, U, and the shear stress, τ, can be postulated as

$$U = U_e \phi(\eta) \quad \text{and} \quad \tau = \tau_e (\eta) \quad \text{where} \quad \eta = \frac{z}{\delta_e} \tag{2}$$

where U_e is a characteristic velocity (which is taken as the freestream velocity), τ_e is a characteristic shear stress (local wall shear stress for zero pressure gradient flow and δ_e is a characteristic length (taken as the boundary layer thickness in Figure 2). The similarity conditions, eq. 2, can be substituted into the x-direction equation of motion together with the continuity equation to determine the conditions for which similarity can exist, ref. 1. In order for similarity to exist the equation of motion requires that

$$\frac{\rho U_e^2}{\tau_e} \frac{d\delta_e}{dx} = \text{constant} \tag{3}$$

Equation 3 points out that it was not necessary to specify three different characteristics for the boundary layer. Also if the characteristic length were taken as the "momentum" thickness of the boundary layer, equation 3 is just the "integral" or von Karman momentum equation (where the constant is 2, $\tau_e = \tau_w$ and $U_e = U_\infty$).

For both the wind tunnel boundary layer and for atmospheric boundary layers the actual Reynolds number cannot change greatly once the flow is established. Thus, the flow might be approximated as a constant Reynolds number flow. For constant Reynolds number the skin friction coefficient, $c_f(= \tau_w/\frac{1}{2}\rho U_\infty^2)$, would be constant, and equation 3 predicts that the characteristic length can at most be a linear function of x-distance. Zoric and Sandborn found that the lengths; momentum, displacement and boundary layer thickness approached linear functions of x-distance, even though the shear stress decreased slightly with distance down the wind tunnel. Sufficient data is usually not available to evaluate the thicknesses of the atmospheric boundary layer.

Turbulence Similarity - As noted, Zoric and Sandborn, ref. 1, also found that the turbulent velocity components and the turbulent shear stress obtained a similarity form. The distance downstream from the initial roughness to the point where similarity was obtained for the turbulent velocity components was roughly twice as far as that required for the mean velocity. The similarity has proven of great value in large Reynolds number flows, such as encountered at supersonic speeds, Sandborn, ref. 2. Use of the similarity relations, eq. 2, in the equation of motion leads to a relation between the turbulent shear stress (Reynolds stress) and the mean velocity, Sandborn and Horstman, ref. 3. The similarity relation for the turbulent and/or total shear stress was shown by Sandborn and Horstman to be an accurate means of relating the turbulence and mean flow for a very wide range of zero pressure gradient boundary layers. It is expected that the similarity concept will be valid for the atmospheric boundary layer. In both the case of mean and turbulent velocities the similarity should apply everywhere except in the viscous sublayer.

Figure 3 shows typical longitudinal and vertical turbulent velocity components measured in the large Reynolds number similarity region of the wind tunnel. The lower Reynolds number measurements of Klebanoff, ref. 4, which correspond to aerodynamic type flows, are also shown on Figure 3. With the exception of the region close to the surface, the longitudinal turbulent velocity components are similar, when ratioed to the local surface shear stress (characteristic shear stress), for both the low and high Reynolds numbers. It is expected that the equivalent smooth surface, large Reynolds number, atmospheric results would also agree closely with the measurements of Figure 3. For the vertical turbulent velocity component the lower Reynolds number data of Klebanoff does not agree with the larger Reynolds number results. The discrepancy between the measurements of Klebanoff and the larger Reynolds number results has not been resolved. It would appear that the discrepancy is not solely due to a Reynolds number effect, but may reflect such problems as local upstream pressure gradient effects. Sandborn, ref. 2, found that the high Reynolds number supersonic, zero pressure gradient flow data agree closely with the subsonic large Reynolds number measurements. The low Reynolds number data of Klebanoff appear to be more characteristic of the turbulence observed in increasing pressure gradient flows.

Turbulence Scale - The demonstration of the approach of large Reynolds number boundary layers to a similar form can be used as a strong point in favor of modeling the atmospheric boundary layer in wind tunnels. The gross features of relative magnitudes of the velocities are correctly modeled. However, it is not obvious that the magnitude of size of the turbulence in the atmosphere related to that in the laboratory is adequately modeled. An evaluation of the spectral energy content of the longitudinal turbulent velocity was made by Sandborn and Marshall, ref. 5. Figure 4 shows a comparison of the wind tunnel spectrum with similar spectra reported by Pond, Stewart and Burling, ref. 6, for wind over water, and by Grant, Stewart and Moilliet, ref. 7, for ocean flow in a tidal channel. As expected the wind tunnel spectra indicates a smaller scale at the smaller frequencies or wave numbers, but the higher frequency content of energy is identical to that of the atmospheric boundary layer. By comparison, Figure 5 shows the difference in spectra measured in the large Reynolds number wind tunnel boundary layer to data reported for typical aerodynamic boundary layers. These spectra demonstrate that the turbulent structure approach a similarity form at large Reynolds number, and that the present wind tunnel flow facility is capable of producing turbulence very much like those of the atmosphere.

Again the present discussion applies to the boundary layer outside the viscous sublayer. For heights of interest to wind power the turbulent spectra over relatively smooth terrain is nearly independent of height. Figure 6 is a set of spectra taken with hot wire anemometers mounted on a meteorological tower, Stankov, ref. 8. These atmospheric spectra were evaluated by an analog analizer, which allowed time averaging over one hour of time for each point.

No apparent change in the spectrum with height could be observed. Length scales (calculated from autocorrelation measurements) of the order of from 10 to 70 meters were determined from the hot wire data, ref. 8. A study of the spectra development in the wind tunnel was reported by Tieleman, ref. 9. Figure 7 shows Tieleman's measured spectra for a number of distances from the surface. The boundary layer was 88.9cm (35 inches) thick at the point where the data was measured. For the data furthest from the surface ($z = 1.27$cm, 0.500 in.) which corresponds to $z/\delta = 0.0143$, the spectra are similar, and no further change in shape occurs at greater distances. Thus, the viscous sublayer effects on turbulent structure are limited to values of z/δ less than 1% of the boundary layer thickness.

Thermal Effects - The Colorado State University wind tunnel was constructed so that both the air stream and the surface can be either heated or cooled independently. Thus, thermally stratified flows for a wide range of conditions are possible. A discussion of the modeling of stratified flows in the wind tunnel was given by Plate and Sandborn, ref. 10. For the atmosphere Monin and Obukhov, ref. 11, employed a "log-linear" velocity distribution to represent thermally stratified flow. Figure 8 show typical velocity distributions obtained in the wind tunnel for a number of cases. Both stable and unstable cases are shown. The length scale L used in Figure 8 is a stability length, ref. 10, and the coefficient α varies with the stability. For atmospheric flows McVehil, ref. 12, finds that α varies between 2 and 6 for unstable flows and is greater than 7 for stable stratified flows. Values of α greater than 10 have been reported. Figure 8 shows that the wind tunnel can model at least the moderate range of stable and unstable flows expected in the atmosphere.

Certain aspects of atmospheric flow are known to exist, which are generally not modeled in the wind tunnel. For example, cloud formation, thermal convection, and buoyancy can generate turbulence external from the surface boundary layer turbulence. Figure 9 shows typical turbulent intensity distributions reported for the atmosphere. Although there is considerable scatter in some of the data (determined from cup anemometers) it is apparent that the "outer region" level of turbulence is changing with time of day. As demonstrated in Figure 10, it is possible to introduce turbulence into the freestream of the wind tunnel to model special conditions, ref. 10, although buoyancy generated turbulence does not appear feasible. No detailed study of these high turbulence level flows has been undertaken.

WIND TUNNEL MODELING OF ATMOSPHERIC TERRAIN

For direct wind tunnel testing of aerodynamic shapes the model Reynolds number is made the same as the prototype. For simulation of terrain in the wind tunnel the model is normally scaled in relation to the boundary layer size. This scaling produces models which are of the correct size related to the wind tunnel turbulence scales. Obviously, the Reynolds number based on model size is much smaller than that of the atmospheric terrain. For the initial two-dimensional and three-dimensional hill studies a model height, H, to boundary layer thickness, δ, of approximately, $H/\delta \simeq 0.1$ was selected. The height of the atmospheric boundary layer can vary from as low as 300 meters (see Figure 9c for example) up to greater than 1000 meters. The height depends strongly on local flow conditions. Thus, for this initial set of measurements the models correspond to atmospheric hill heights from 30 to slightly over 100 meters. Note that this hill height is roughly of the same dimensions as the turbulent scales. Thus, the hill will act as a small perturbation in the flow and it is possible to assume that the freestream velocity is not affected. Secondly, it was assumed that atmospheric hills of this height would be the most likely candidates for small and moderate wind power sites. The results of the study suggest that hills with characteristic sizes of the order of the turbulence scale will produce a near inviscid speedup of the local wind. Thus, the small hills will be the most efficient amplifiers of the local wind, since larger hills and mountains may have correspondingly large viscous losses in wind energy.

The boundary layer similarity aspects, which are employed to justify the modeling of atmospheric boundary layer in the wind tunnel, exclude the "viscous sublayer". For the present wind tunnel studies the thickness of the sublayer can be estimated from the value of the surface shear stress. From the data given by Rider and Sandborn, ref. 13, the skin friction coefficient of the approach layer is approximately, $c_f \approx 0.0025$. This value of skin friction corresponds to a "shear stress" velocity, U_τ, of 0.38 meters per second. The viscous sublayer is taken as an arbitrary value of the non-dimensional length

$$\frac{y\,U_\tau}{\nu} \approx 5 \tag{4}$$

For the present flow this relation corresponds to a vertical distance of 0.024cm. Even a more conservative value of the length limits the complete "logarithm" velocity distribution to a vertical distance of no more than 0.5cm. At the crest of the hills the skin friction coefficient is of the order of $c_f \approx .0035$, which increases the shear stress velocity by roughly 18% and reduces the viscous region by the same amount. The complete sublayer region is limited to values of z/δ less than 0.01 and as such, have received little attention in the present modeling. For the atmosphere the equivalent sublayer is also limited to very small distances from the surface and would be of little interest in wind power site studies.

The modeling of viscous effects, such as flow separation, is not well documented. Although physical understanding of turbulent boundary layer separation has been advanced considerably in the past decade, Sandborn, ref. 14, it is still not possible to predict the effect of such parameters as Reynolds number on flow separation. In the past it was tactful to assume that boundary layer separation was a unique point with a unique velocity distribution. However, experimental measurements, ref. 14, produce a wide spectrum of possible separation profiles depending on flow history and local conditions. The wind tunnel modeling can be expected to identify regions where separation is likely to occur, and also produce some information on the extent of the separation region. Further experimental studies are still required to insure that this separation data obtained in the wind tunnel can be related directly to the field case. Certainly, studies of the effect of flow separation around model buildings have proven extremely valuable in predicting the local pressure loads on the structures.

RESULTS AND DISCUSSION

Mean Flow Over Ridges - Based on the preliminary studies made in the first year of the research program, it was evident that the maximum wind amplification would be achieved over two-dimensional ridges. The preliminary measurements demonstrated that sharp crested, triangular shaped ridges produced the optimum speedup of the approach flow. Detailed evaluation of these studies of ridge shape were completed and formally documented during the current year. The results reported by Rider and Sandborn, ref. 13, on the ridge shape evaluation is included as Appendix A of the present report.

During the present year detailed experimental evaluation of the optimum two-dimensional ridges with heights of the order of one tenth the boundary layer thickness were completed. The preliminary observation reported in the previous annual report, ref. 15, was that viscous effects appeared to be unimportant for the particular cases measured. It was possible to predict the magnitude of the speedup ratio over the two-dimensional ridges using an inviscid flow model. During the present year it was possible to document the fact that the inviscid approach was able to predict flows over the windward side of two-dimensional ridges, Derickson and Meroney, ref. 16. Thus, the velocity distribution at the crest of a two-dimensional, small, ridge can be predicted from an inviscid flow analysis, once the upstream approach velocity distribution is specified.

Detailed information on the mean flow over the two-dimensional ridges together with a formal analysis of the justification and limits on the application of the inviscid flow model are currently being prepared as a doctoral dissertation by Mr. R. J. B. Bouwmeester. A summary paper by Bouwmeester, et al., ref. 17, presented at Washington, D.C., in September covers some of the results to be presented in the thesis.

Turbulence Over Ridges - A detailed evaluation of the development of turbulence over two-dimensional ridges was made during the present year of study. Questions had arisen as to whether or not the speedup of flow over a ridge would give rise to large increases in the local turbulence. The presence of large fluctuations in the wind velocity would be a major objection to a particular wind site. The results of this aspect of the study was presented in a report by Rider and Sandborn, ref. 13, attached as Appendix B of this report. The basic result of this study was that the small ridge has only a small, predictable effect on the boundary layer turbulence. The similarity analysis of the mean and turbulent flow discussed in the section on "Wind Tunnel Modeling of Atmospheric Flow" demonstrates that the turbulence can be non-dimensionalized by a characteristic surface shear stress. It is found that the turbulence for a very wide range of flow conditions can be correlated by a similarity plot of the form shown in Figure 3. The data points shown on Figure 3 are taken from the results of the present study. If the flow conditions change rapidly it is found that the turbulence cannot respond quickly to the new conditions. Thus, the inertia of the turbulence tends to keep the distribution similar even for large changes in the surface conditions. Sandborn, and Horstman, ref. 3, demonstrated that the turbulent shear stress changes only near the surface to meet the new pressure gradient requirement. The outer part of the turbulent shear stress distribution required a very long time or distance before it can alter. For the present case of small ridges in a large boundary layer where direct viscous effects can be neglected it would also be expected that the turbulence cannot change appreciably. The results presented in the appendix show that only near the surface does any change in the turbulence occur. The actual change in the turbulence appears to be that which could have been predicted for turbulence undergoing a contraction of strain. The turbulent component in the direction of the mean flow is reduced in magnitude near the surface, while the vertical component of turbulence is slightly increased. Since it is expected that the horizontal component of the turbulence would be the most critical in wind turbine design, the results of Appendix B are considered to indicate that the turbulence over the upstream face of the small, two-dimensional ridges will not be a problem. Once the results are obtained it may appear obvious that the passive role of turbulence would be expected. However, most of the basic concepts of turbulent boundary layers and shear flows are so poorly understood that, such aspects as possible similarity of turbulence in large Reynolds number boundary layers, are still being questioned. The present results are an important check on the evolving turbulence "model", as well as a necessary conclusion that the turbulence on the windward face of a ridge does not cause wind turbine problems.

Effects of Roughness - A number of factors can and will effect the mean velocity distribution of the boundary layer in the atmosphere. A major factor will be surface roughness. Roughness which can range from smooth grass surfaces to large obstructions, such as trees and hills will act to reduce the wind velocity near the surface. Figure 11 shows the effect of roughness on the mean velocity profile in the special case studied; see Appendix B for identification of Case I (smooth) and Case II (rough surface). The mean velocities at the crest of the 1 to 6 slope hill is also shown in Figure 11b). The speedup ratio is approximately the same for the two cases shown in Figure 11. Thus, the major effect of the upstream roughness is to remove energy near the surface, which would decrease the power available to a wind turbine. The speedup ratio remains roughly the same for a given small ridge independent of the shape of the approach velocity distribution. Figure 8 of Appendix A shows the effect of Reynolds number of the speedup over a 1 to 4 slope ridge. As noted in Appendix A there is roughly an order of magnitude difference in the Reynolds number for the two profiles shown on Figure 8 (Appendix A). There is also roughly a factor of two difference in the boundary layer thickness for the two flows. For the two-dimensional, small ridges of similar shape the speedup factor is not sensitive to changes in Reynolds number or perhaps more general to the approach flow velocity distribution. Obviously, this conclusion can only be applied to the cases where the ridge dimensions are small compared to the boundary layer thickness.

Thermal Effects - A set of measurements of the mean and turbulent fluctuations over 1 to 4 and 1 to 6 slope triangular ridges for stably stratified flow was also made during the current study. Figure 12 shows a typical set of upstream and crest profiles for flow over the 1 to 4 ridge with a surface temperature of 0°C and a freestream temperature of 42°C. The freestream velocity was approximately 9 meters per second for both cases shown. The effect of thermal stratification on the speedup ratio appears to be extremely small in the area of interest to wind power sites. The inviscid flow model analysis indicated that mildly stable conditions will tend to decrease the speedup factor, while the unstable conditions tend to increase the speedup factor.

CONCLUSIONS

The present experimental program demonstrated that the two-dimensional, sharp crested ridge produced the optimum speedup of winds near the surface for a modeled atmospheric boundary layer. The results apply to ridge sizes that are small compared to the boundary layer height. The measurements indicate a slope of 1 unit rise to 4 units of length produce the maximum speedup. Steeper slopes produce a separation bubble or vortex at the foot of the ridge and less speedup at the crest. Smaller slopes fail to produce sufficient acceleration of the flow near the surface. The speedup ratio for the small ridges was only slightly altered by changes in Reynolds number, approach surface roughness or stable stratification.

For the small ridge, which corresponds to heights of the order of 100 meters or less in the atmosphere, the experimental measurements were found to be predicted by an inviscid flow analysis. This result is of major interest in the development of numerical models. The limitations will be that viscous separation does not occur in the flow field analyzed. It can be implied that, since viscous losses are not important for the small ridge, the particular type of flow will be the most efficient for wind power sites. Not only does the ridge increase the wind speed near the surface, but it also acts to produce a more nearly uniform velocity distribution above the surface. The uniform velocity distribution can be of great value particularly for the propeller type wind turbines. Note that the present results are for the ideal case where the prevailing wind is normal to the ridge, such as might occur along an ocean coast line for example.

Evaluation of the turbulent velocity field over the two-dimensional ridge was also made. The turbulent velocities respond as if the ridge acts as a contraction, or the flow near the surface has undergone a small strain. The turbulent velocity component in the direction of the mean flow is reduced in magnitude near the surface. The vertical turbulent velocity component increases in magnitude near the surface. Since the longitudinal turbulent velocity component is most likely to be important in the design of wind turbines, the effect of the ridge will not adversely affect turbine design.

RECOMMENDATIONS

The present study has demonstrated the feasibility of small two-dimensional ridges for wind power sites. It remains to document such details as what constitutes a two-dimensional ridge as opposed to a three-dimensional hill. Present results for the ideal (cone), three-dimensional hill show a reduction of nearly 50% in the speedup ratio over that of the ridge. Thus, if a wind power site choice is possible the two-dimensional ridge will produce far more wind power. A systematic evaluation of the effect of ridge length is required in order to determine the effect of ridge aspect ratio. The study has evaluated the optimum symmetrical ridge, however it may be possible to improve on the shape by varying the rearward face of the ridge. Since the rearward face of the ridge is usually a separation region, the inviscid modeling of the flow will not be valid over the downwind part of the ridge.

The obvious next step in the study is the modeling of actual atmospheric field sites. Both small hill and ridge sites as well as tall mountain sites need be modeled. For the small hills, the fact that viscous effects are unimportant makes it relatively easy to model the flow in the wind tunnel. For the larger mountain terrain where the atmospheric boundary layer and turbulence scales are small compared to the terrain more information is necessary in order to model the flow. Of critical importance are factors such as surface roughness and local pressure gradients. While these factors are simulated in the wind tunnel it is not always possible to specify what pressure gradient to model. The wind tunnel studies would be made with a range of possible freestream pressure gradients, for example, that might be encountered in the field case.

REFERENCES

1. Zoric, D., and Sandborn, V. A.: Similarity of Large Reynolds Number Boundary Layers, Boundary Layer Meteorology, Vol. 2, No. 3, pp. 326-333, 1972.
2. Sandborn, V. A.; Review of Turbulence Measurements in Compressible Flow, NASA Tech. Memo. X62,337, 1974.
3. Sandborn, V. A., and Horstman, C. C.; Boundary Layer Shear Stress in Subsonic and Supersonic Flow, Symposium on Turbulent Shear Flow, Penn. St. Univ., 1977.
4. Klebanoff, P. S.; Characteristics of Turbulence in a Boundary Layer With Zero Pressure Gradient, NACA TR 3178, 1954.
5. Sandborn, V. A., and Marshall, R. D.; Local Isotropy in Wind Tunnel Turbulence, Colo. St. Univ. Research Memo. No. 1, 1965.
6. Pond, S., Stewart, R. W., and Burling, R. W.; Turbulence Spectra in Wind Over Waves, Journ. of the Atmospheric Sci., Vol. 22, 1963.
7. Grant, H. L., Stewart, R. W., and Moilliet, A.; Turbulence Spectra From a Tidal Channel, Jour. of Fluid Mech., Vol. 12, 1962.
8. Stankov, B.; Some Characteristics of Turbulence in the Lower 200 Feet of the Atmosphere, Colo. St. Univ. Research Report CER70-71BS14, 1970.
9. Tieleman, H. W.; Viscous Region of Turbulent Boundary Layer, Colo. St. Univ. Report CER67-68HWT21, 1967.
10. Plate, E. J., and Sandborn, V. A.; Modeling of a Thermally Stratified Boundary Layer, Colo. St. Univ. Research Memorandum No. 8, 1966.
11. Monin, A. S., and Obukhov, A. M.; USSR Acad. Sci. Geophys. Institute Report No. 24, 1954.
12. McVehil, G. I.; Quart. Journ. Royal Met. Soc., Vol. 90, p. 136, 1964.
13. Rider, M. A., and Sandborn, V. A.; Boundary Layer Turbulence Over Two-Dimensional Hills, Colo. St. Univ. Tech. Report CER77-78MAR-VAS4, 1977.
14. Sandborn, V. A.; Boundary Layer Separation and Reattachment, NASA SP-304, p. 279, 1974.
15. Meroney, R. N., Sandborn, V. A., Bouwmeester, R. J. B., and Rider, M. A.; Sites for Wind Power Installations, Annual Report, Colo. St. Univ. Report CER76-77RNM-VAS-RB-MAR5, 1976.
16. Derickson, R. G., and Meroney, R. N.; A Simplified Physics Airflow Model for Evaluating Wind Power Sites in Complex Terrain, Proc. Summer Computer Simulation Conference, Chicago, Ill., 1977.
17. Bouwmeester, R. J. B., Meroney, R. N., Sandborn, V. A., and Rider, M. A.; The Influence of Hill Shape on Wind Characteristics Over Two-Dimensional Hills, Third Biennial Conference and Workshop on Wind Energy Conversion Systems, U. S. Energy Research and Development Administration, Division of Solar Energy, Washington, D. C., 1977.

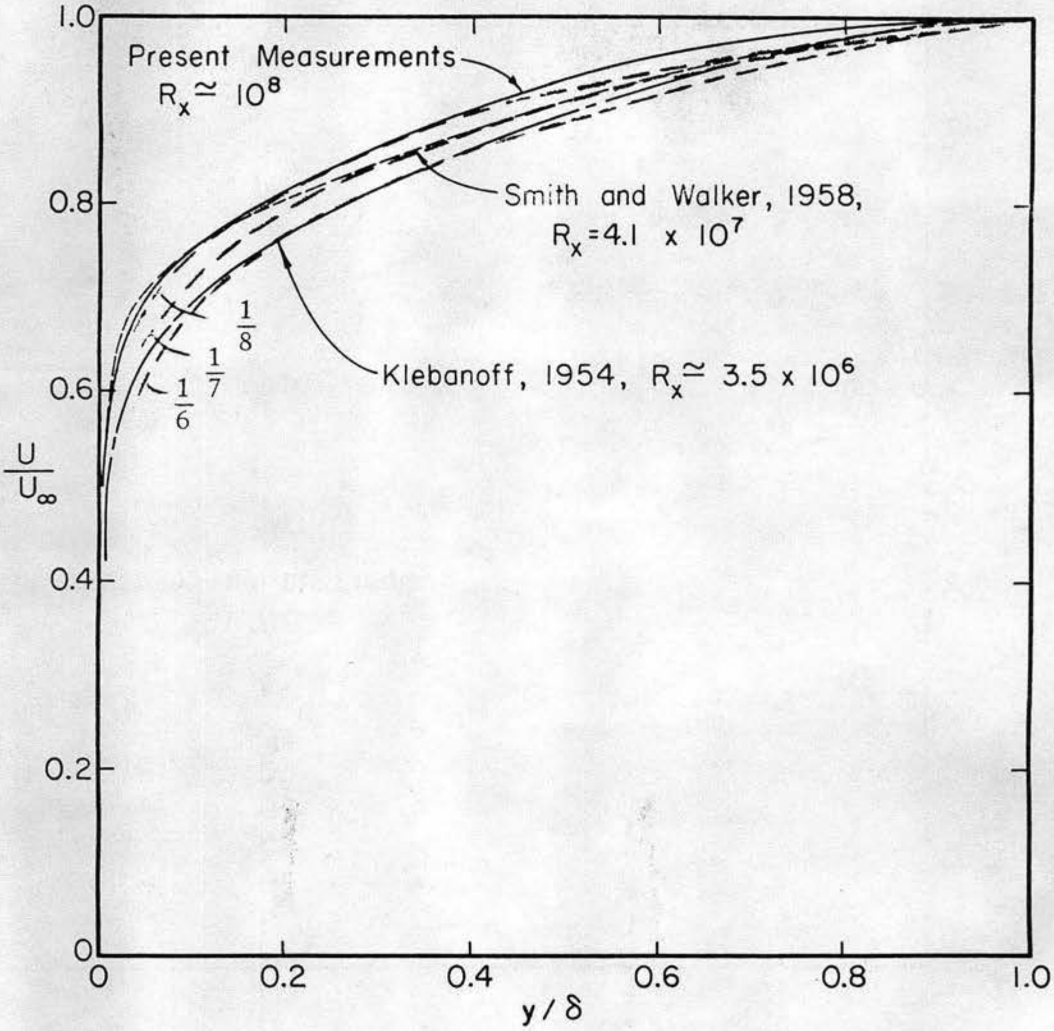

Figure 1. Zero Pressure Gradient, Boundary Layer Velocity Distributions

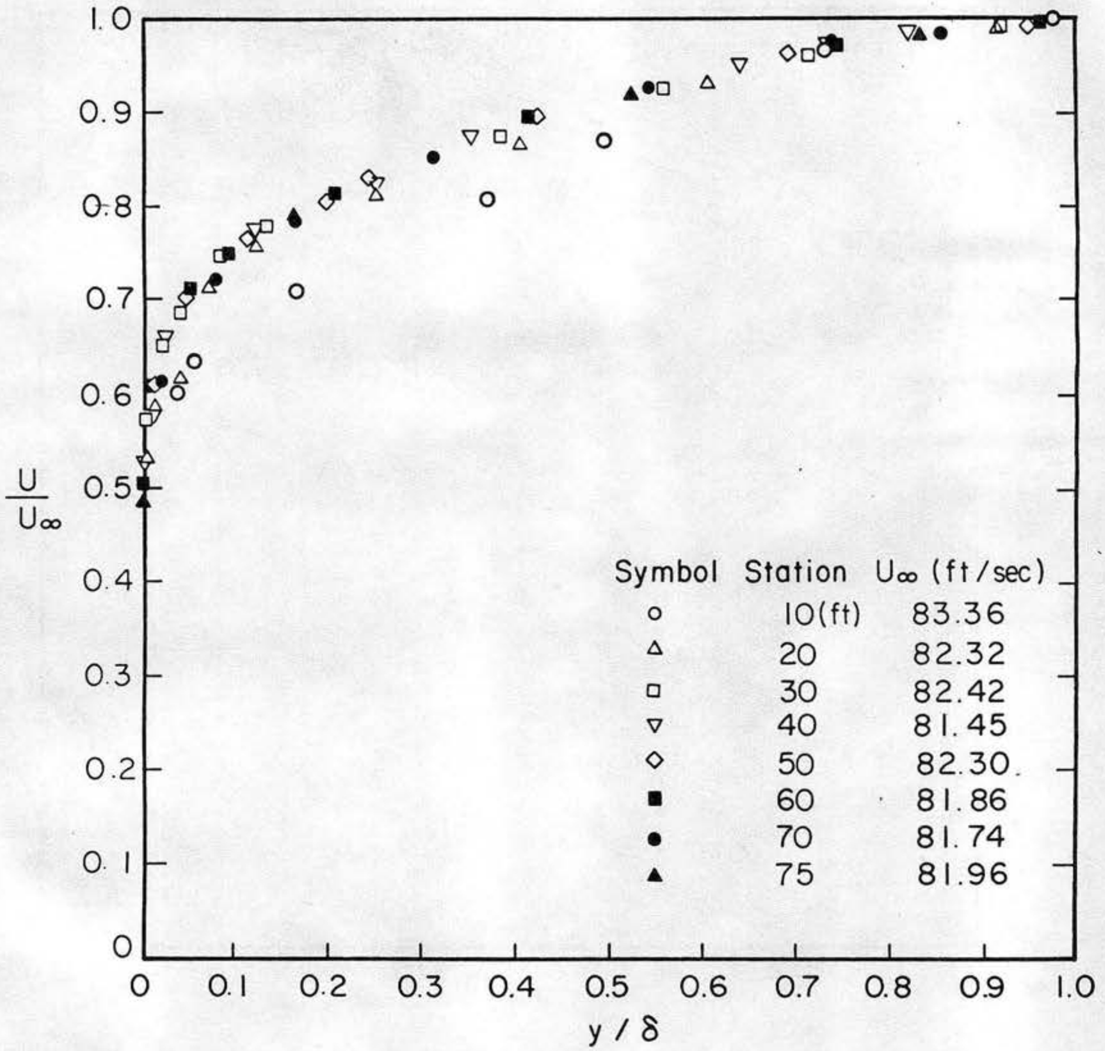

Figure 2. Development of a Large Reynolds Number, Zero Pressure Gradient, Boundary Layer

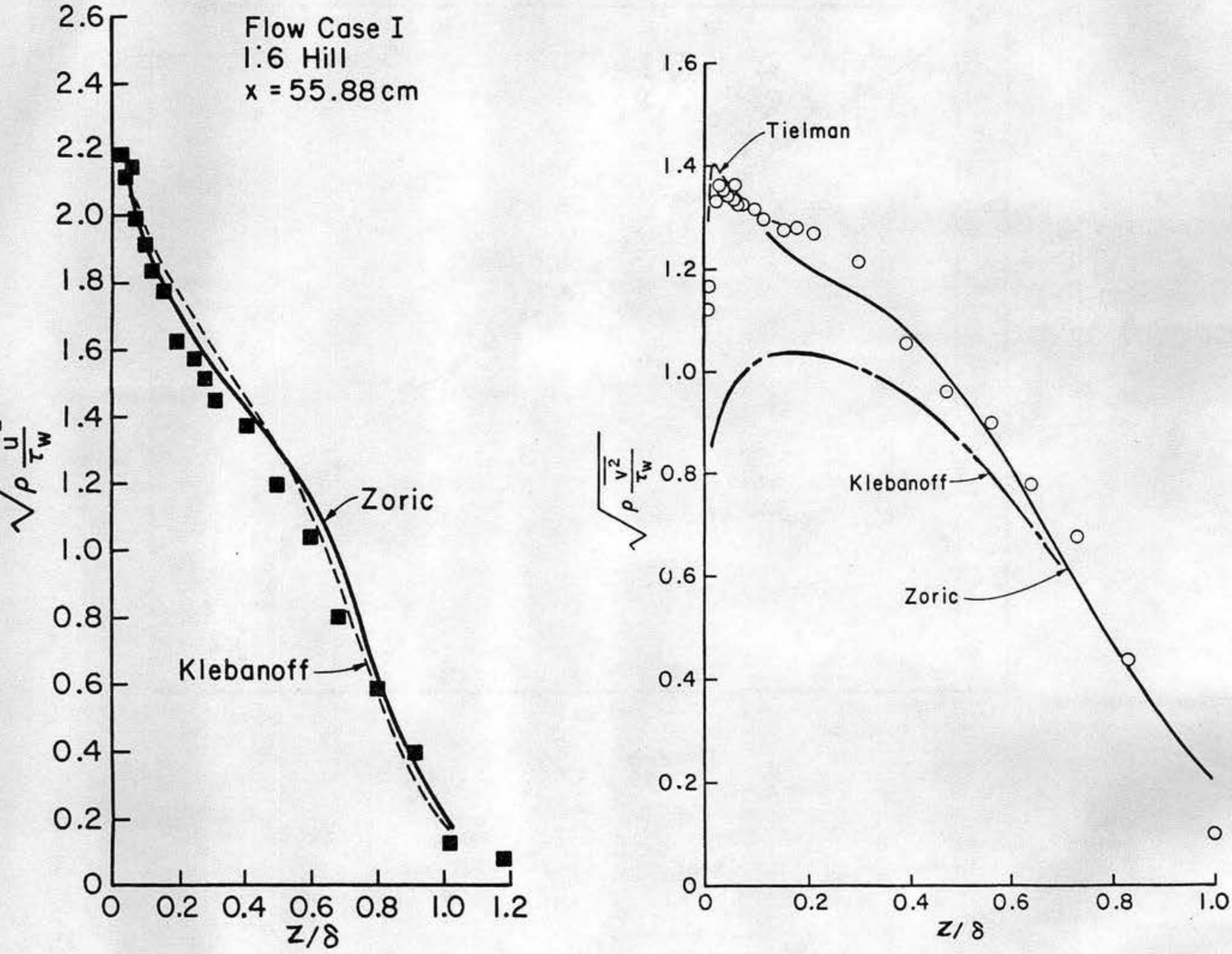

a) Longitudinal

b) Vertical

Figure 3. Turbulent Velocity Component Distributions in the Large Reynolds Number Boundary Layer

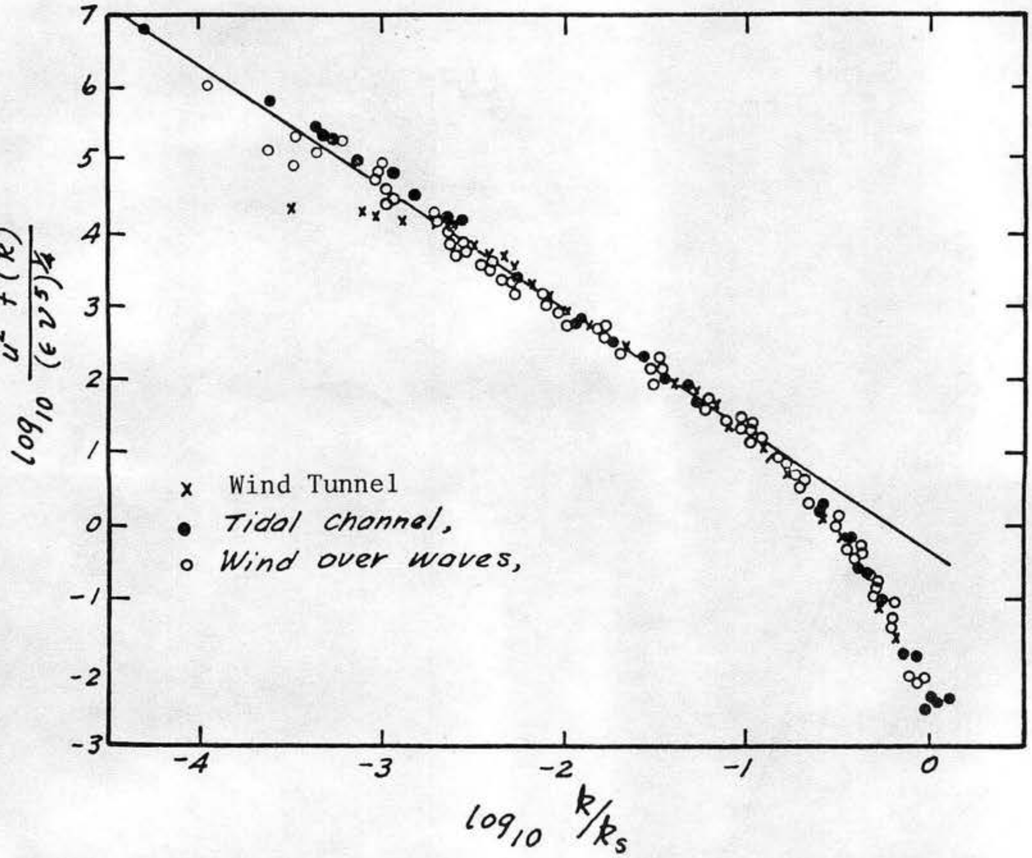

Figure 4. Spectra of the Longitudinal Turbulent Velocity in Large Reynolds Number Boundary Layers

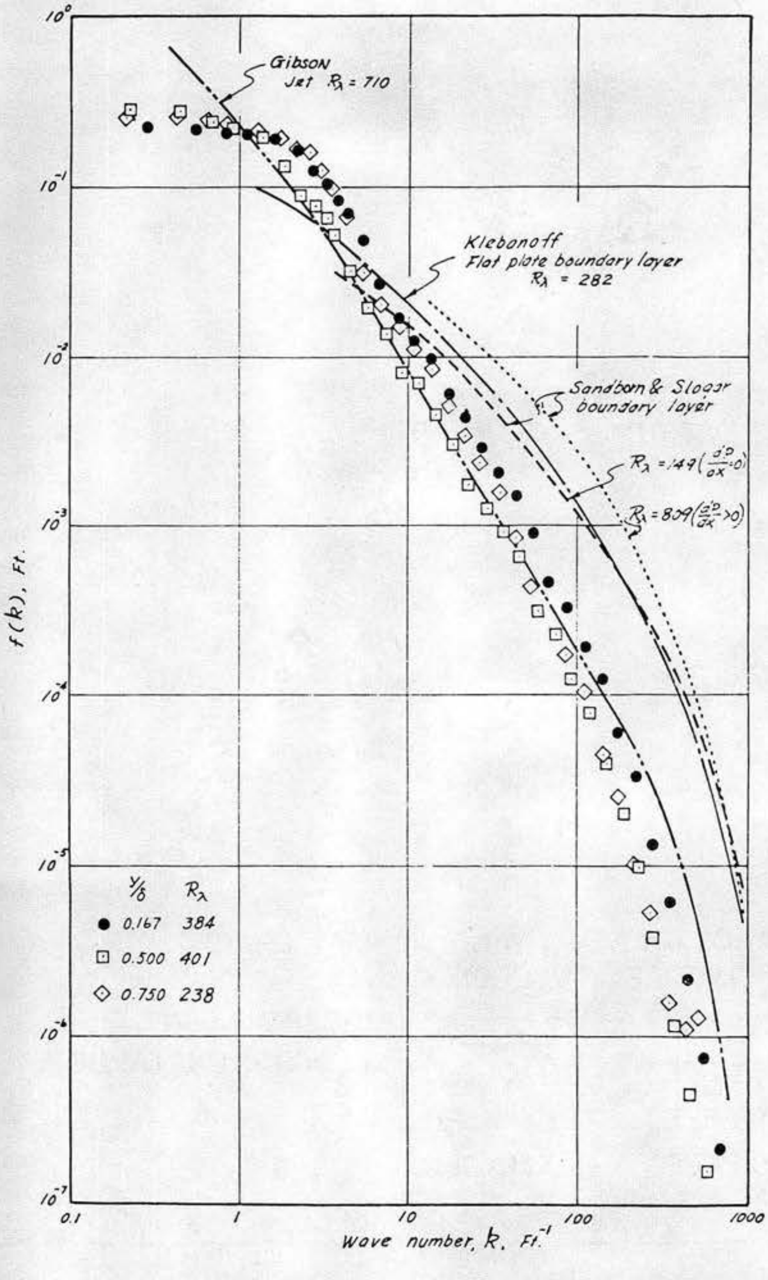

Figure 5. Comparison of Turbulence Spectra for a Wide Range of Reynolds Numbers

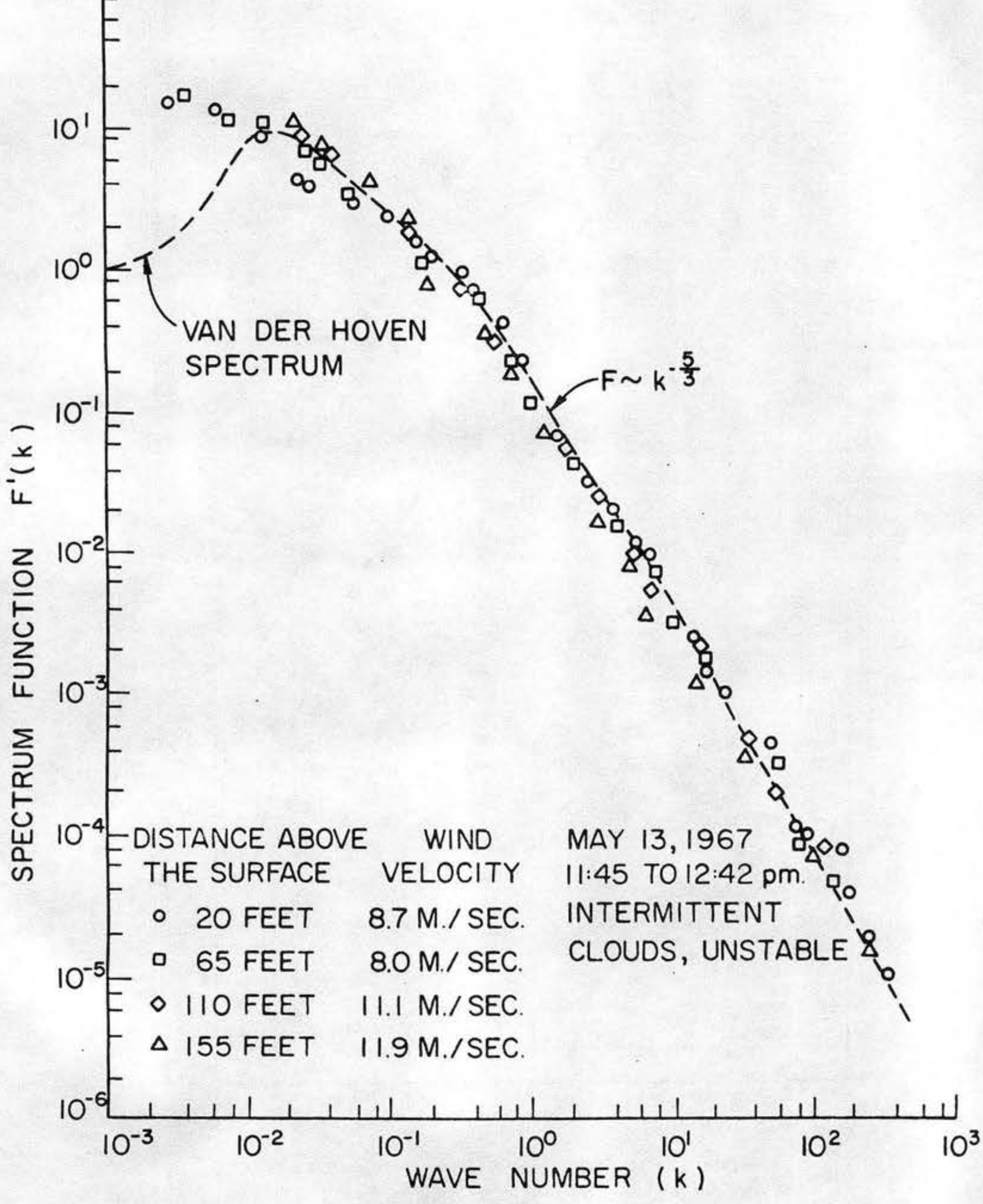

Figure 6. Spectrum of Turbulence in the Atmosphere

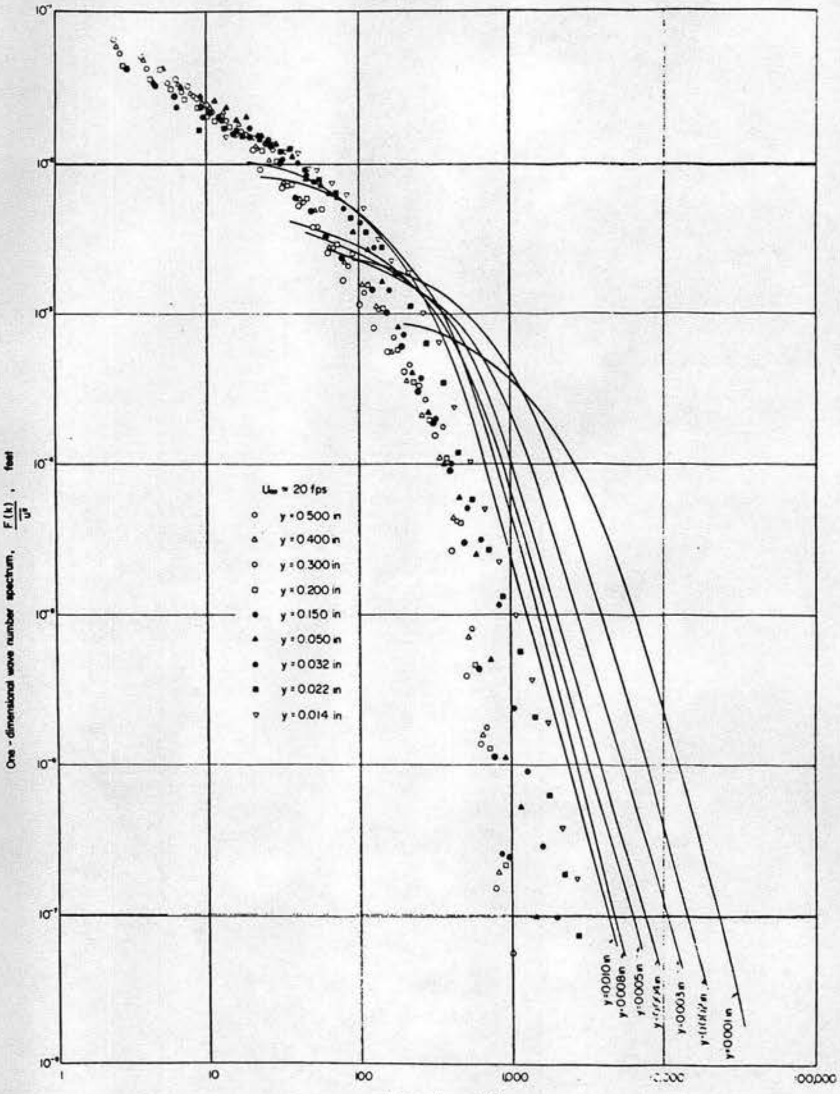

Figure 7. Variation of the Turbulent Spectra Near the Surface in the Wind Tunnel

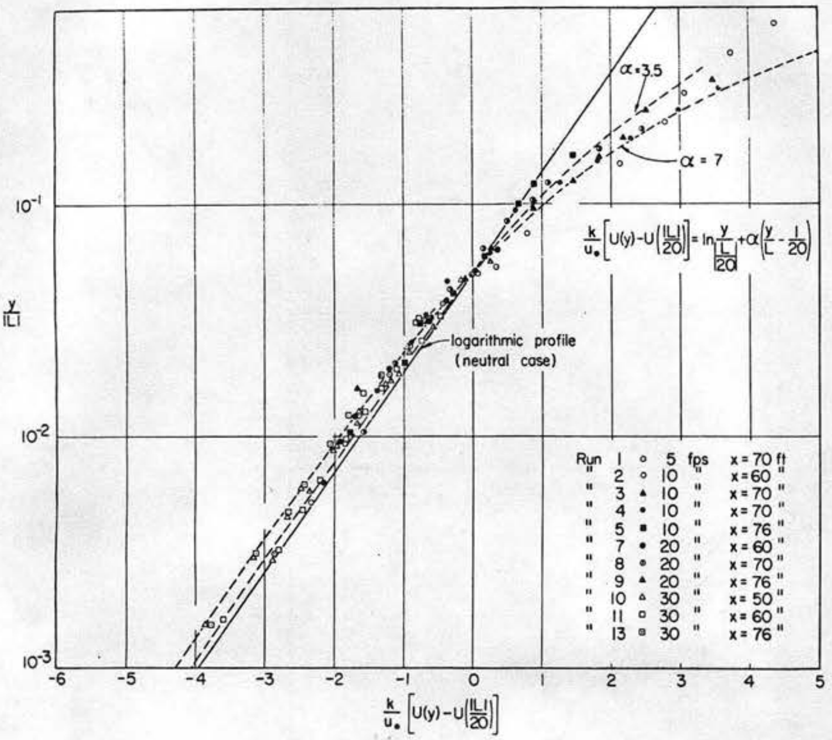

a) Stable

b) Unstable

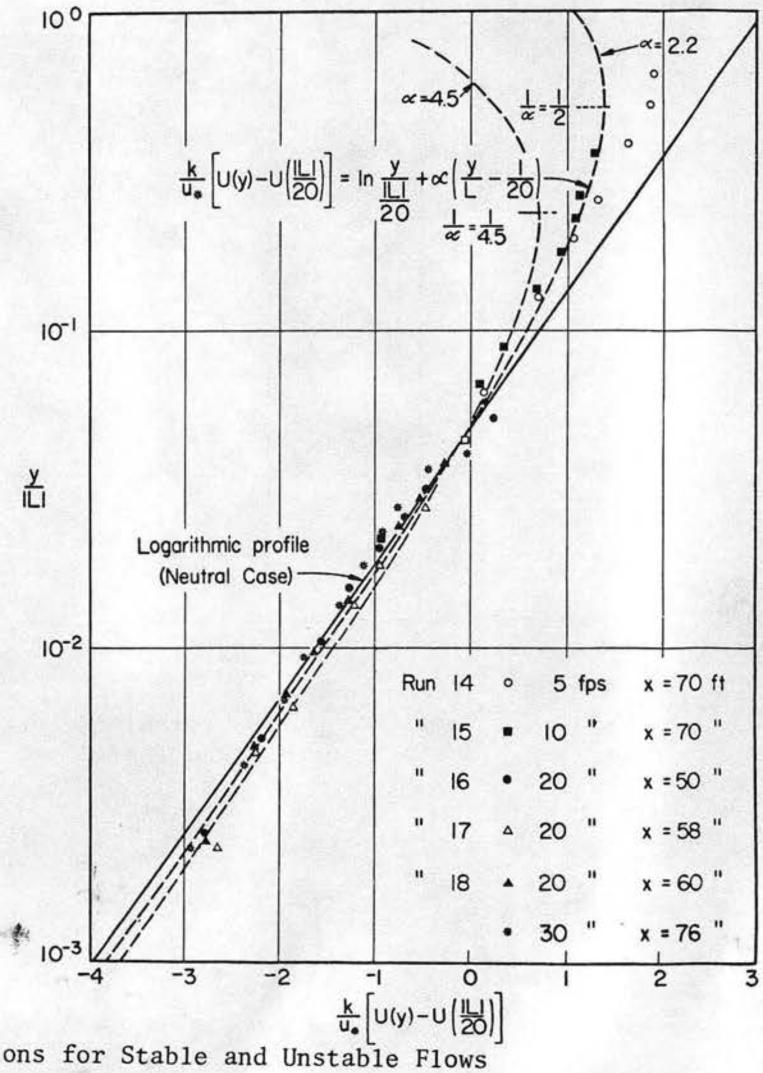

Figure 8. Velocity Distributions for Stable and Unstable Flows

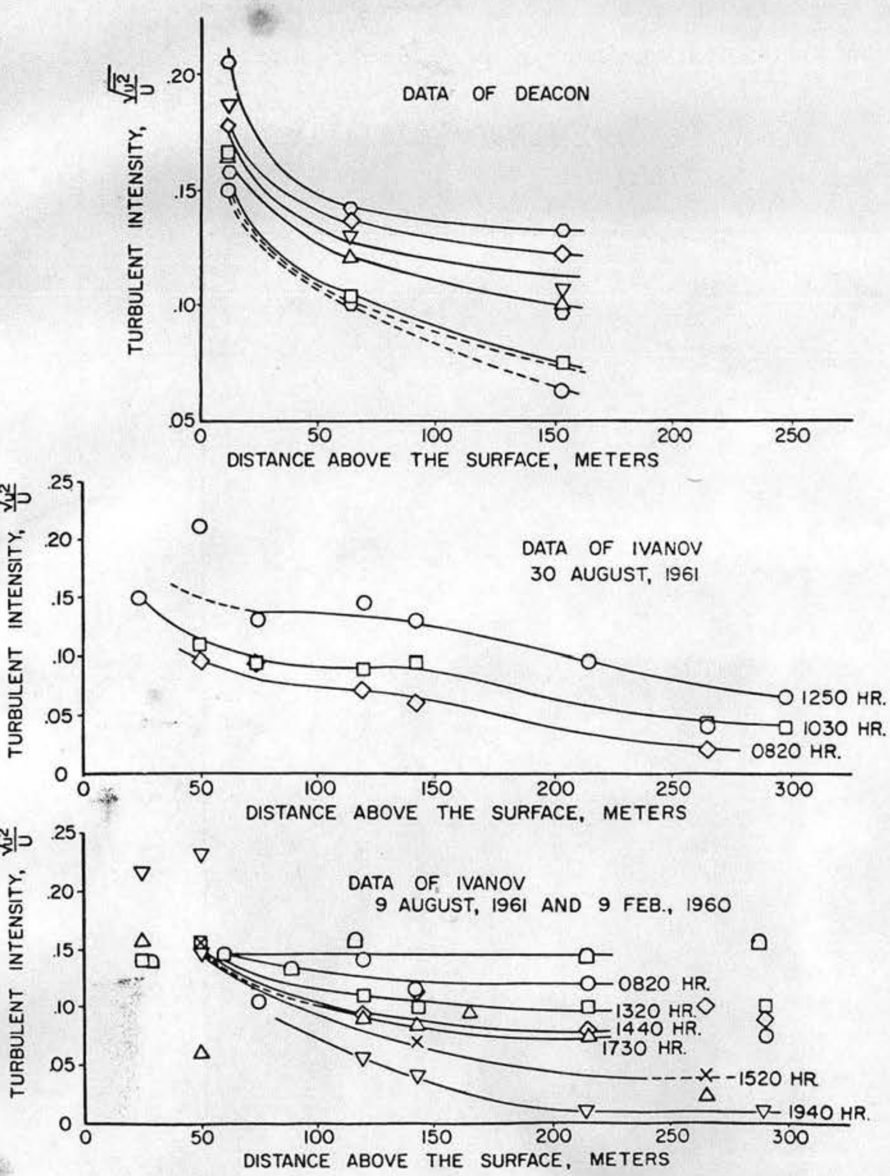

Figure 9. Atmospheric Turbulence Measurements

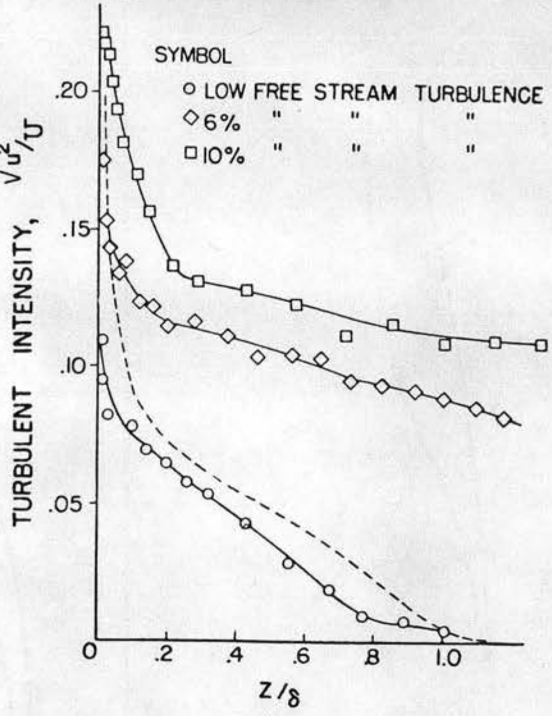

Figure 10. Turbulent Distribution in the Wind Tunnel Boundary Layer as a Function of the Freestream Turbulence

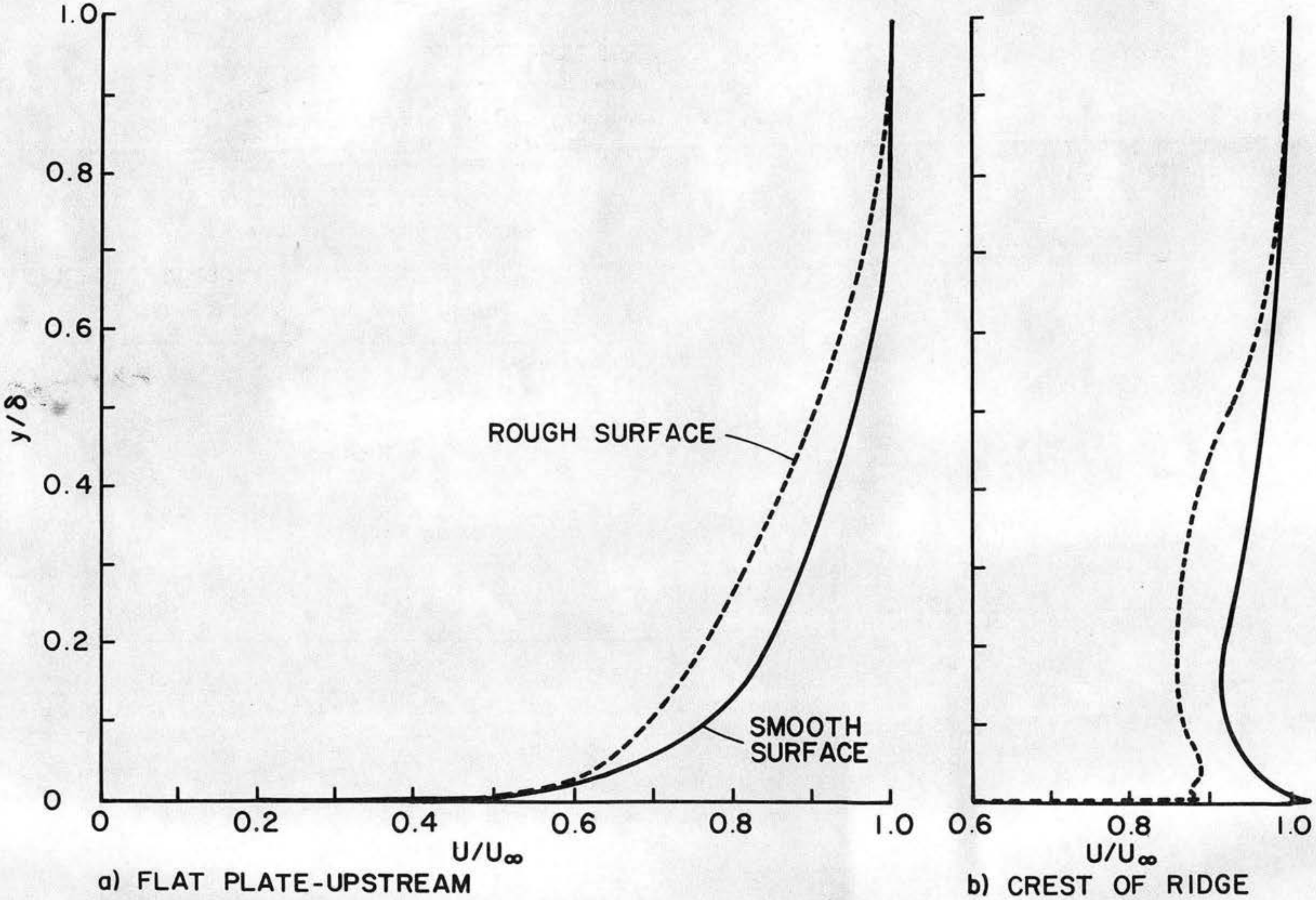

Figure 11. Effect of Surface Roughness on the Mean Velocity Distribution

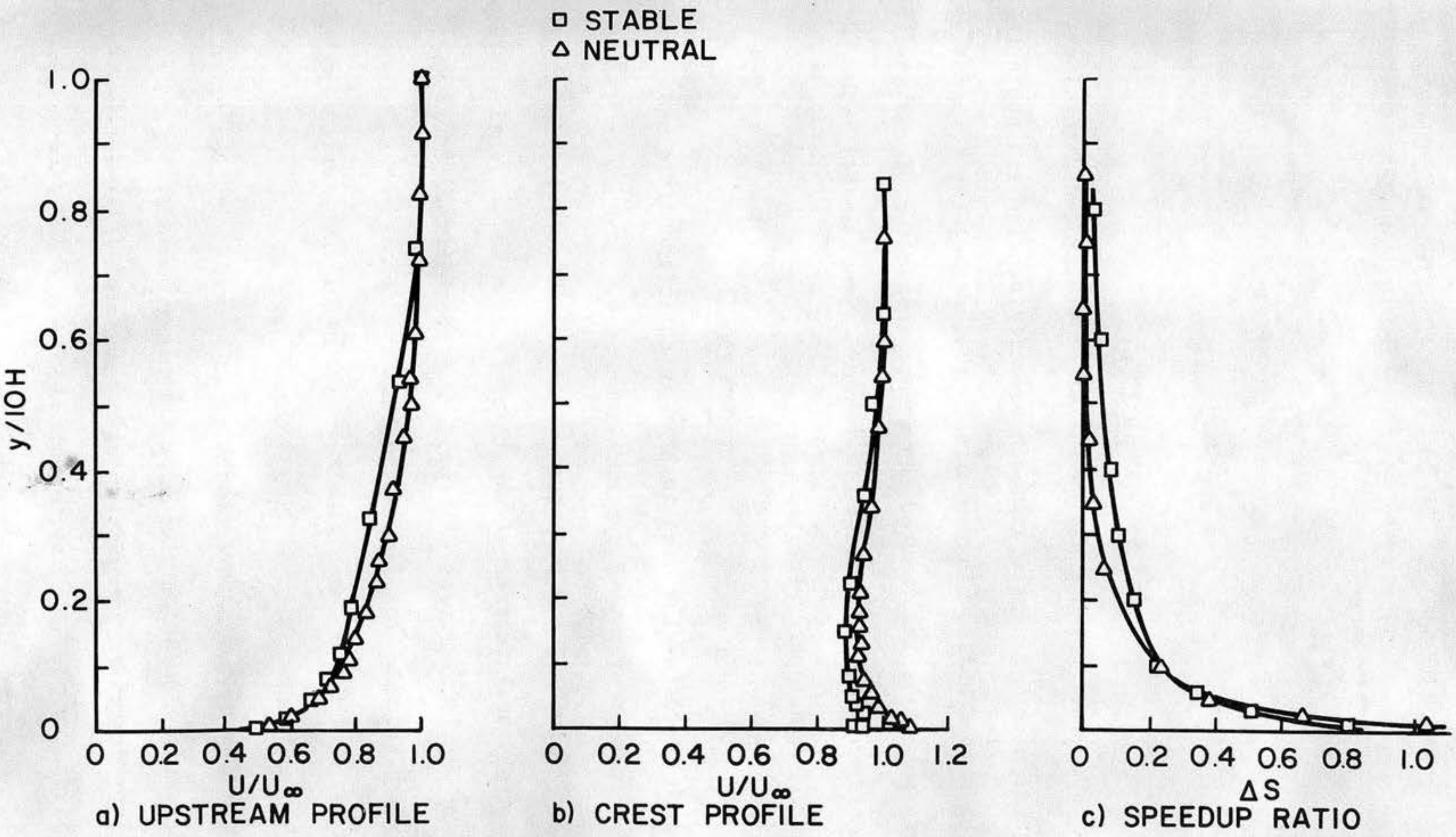

Figure 12. Evaluation of Stable Stratification on the Flow Over a Two-Dimensional Ridge

APPENDIX A

MEASUREMENTS OF THE MEAN AND LONGITUDINAL TURBULENT VELOCITIES OVER VARYING HILL SHAPES

by

Michael A. Rider

and

V. A. Sandborn

ABSTRACT

A systematic wind tunnel study of flow over two-dimensional hills was made. A single approach velocity profile was subjected to varying shaped hills. The results indicated that the triangular and sinusoidal hills produced the greatest speed up of the airstream in the region near the surface. The more abrupt models produced less of an increase in local velocity.

INTRODUCTION

Site selection for wind turbine installations is a major criteria for the success of a wind system. Topography is known to have very strong effects on the atmospheric winds. Particularly, in the lower atmosphere, the influence of the local terrain is extremely evident. Different hills or ridges will produce different degrees of speed up of the airstream as the flow approaches the summit. Thus, it is important to find the most likely location for the greatest possible power production.

A series of tests were conducted in a small wind tunnel to estimate the change in flow properties of a turbulent boundary layer as it moved over six different ridge models. Models of the same relief but different slope were investigated. The hills varied geometrically from triangular to sinusoidal and finally a box shape.

TEST SETUP

The measurements were made in a small .37 x .37 meter (transpiration) wind tunnel located at the Fluid Dynamics Laboratory at Colorado State University, Figure 1 . All tests were conducted with a zero pressure gradient.

As the flow entered the test section a series of five fences, 2.54 cm in height and spaced 10 cm apart were used to initiate the growth of the turbulent boundary layer, Figure 2. The last fence was followed by a 1.22 m reach of roughness. The roughness made from .5 cm diameter spheres ended 2.54 cm from the base of the models. The center of the models were positioned 1.35 m from the last boundary layer trip. A false floor covered the total test section, Figure 2. A horizontal hot-wire probe sampled the mean and the longitudinal velocities. Profiles were taken at locations 10.16 cm in front of the crest at the foot of the hills and at the crest of the hills.

The hill models were constructed from .32 cm masonite, Figure 3. All of the models were 43 cm in length. A traverse mounted on the underside of the tunnel was used to survey the flow. The traverse entered the tunnel behind the models and along the center line of the tunnel.

FLOW VISUALIZATION

To aid in the investigation several photographs were taken of smoke passing over the hills. The smoke, titanium tetrachloride, was released a few centimeters upstream of the foot of the hill models. All of the photographs were taken with a tunnel velocity of about 3 m/s. The shutter speed was varied to give different perspectives of the flow. The more revealing photographs are shown in Figure 4.

RESULTS

Of the shapes tested the triangular hill produced the greatest speedup at the crest. Table I lists the measured mean and turbulent velocity profiles for each hill. The approach profile was measured only once and was assumed to remain the same for all the tests. Figures 5a to 5f are plots of the measured non-dimensional mean velocity distributions. For all the figures the initial upstream profile is the same. With the exception of the rectangular hill (bluff body) there is always a decrease in velocity at the foot of the hill and a speedup at the crest. The boundary layer upstream of the foot of the hills experience an increasing pressure gradient, which can be seen in the smoke pictures to produce a local separation bubble for the bluff body. (Note that the smoke pictures of Figure 4 can be somewhat misleading due to shadow effects both along the upstream and downstream junctions between the model and the floor.)

Figure 6 is a plot of the fractional speedup

$$\Delta S \equiv \frac{\overline{U}(\frac{y}{10H})_{\text{crest}} - \overline{U}(\frac{y}{10H})_{\text{approach}}}{\overline{U}(\frac{y}{10H})_{\text{approach}}} \qquad (1)$$

The triangular and sinusoidal hills produce the greatest speedup effect. It is somewhat surprising that hill No. 4 shows considerably less speedup than the same slope triangular hill. The smoke pictures indicate that the separation effect in the lee of the triangular hills acts to in effect make the triangular hill appear to the flow to be higher.

Figure 7 is a plot of the longitudinal turbulent intensity distributions for the six hills. With the exception of the rectangular hill the turbulent intensities are greatly reduced at the crest of the hills.

It was noted by Rider, ref. 1, that a reduction in the longitudinal turbulent velocity component could be predicted from the theory for turbulence undergoing a contraction. The reduction in the longitudinal turbulence will be accompanied by a proportional increase in the vertical turbulent component, ref. 1.

The present study made in a small wind tunnel was limited to the use of boundary layer trips and roughness to increase the equivalent Reynolds number approach velocity profile. The equivalent Reynolds number estimated from the value of skin friction coefficient for the approach profile in $\sim 10^7$. A comparison of the present results for the triangular hill with similar results reported by Rider, ref 1, for a much longer boundary layer development length (Re $\sim 10^8$) are shown in Figure 8. The fractional speedup for both cases is quite similar. The larger flow facility velocity profile is somewhat fuller than the one employed in the small wind tunnel.

CONCLUDING REMARKS

Evaluation of the velocity speedup over different shaped hills show that triangular and sinusoidal geometry is preferred for wind power sites. The flat top hill does not give as large a speedup at the crest, due apparently to the absence of the separation that occurs for the "sharp" crested models. The present feasibility study suggests that reasonably small scale flow systems may be employed to determine the gross features of hill shapes on the speedup.

REFERENCES

1. Rider, Michael A. (1977) Boundary Layer Turbulence Over Two-Dimensional Hills, M. S. Thesis, Colorado State University, Department of Civil Engineering.

Table I. Measured Mean and Turbulent Velocity Distributions

a) Initial Approach Profiles

POSITION 10.16CM FROM CREST

FREE STREAM VELOCITY 17.87M/S

BAROMETRIC PRESSURE 24.70IN HG

TUNNEL TEMP. 73.0F

DATE 4/26/76 TIME 2.30

DENSITY .9896E+00 KG/CM

A= 11.533 B= 3.333 C= .50 Y= 25.40

Y CM	E VOLTS	RMS MV	DE/DU M/S	U M/S	RMSU	YN	UN
.40	4.488	171.20	.0719	6.67	2.381	.016	.373
1.47	4.713	141.00	.0552	10.26	2.555	.058	.574
3.42	4.821	115.00	.0492	12.34	2.337	.135	.691
6.17	4.896	100.20	.0456	13.92	2.197	.243	.779
8.71	4.946	92.00	.0434	15.05	2.118	.343	.842
11.47	4.999	79.50	.0413	16.30	1.925	.451	.912
14.26	5.034	57.70	.0400	17.16	1.444	.561	.960
16.64	5.054	35.10	.0392	17.67	.895	.655	.989
19.99	5.062	17.90	.0389	17.87	.460	.787	1.000

Table I. (Continued)

b)

FOR HILL 1

FREE STREAM VELOCITY 17.67M/S

TUNNEL TEMP. 72.0F

DENSITY .9896E+00 KG/CM

POSITION 10.16CM FROM CREST

BAROMETRIC PRESSURE 24.74IN HG

DATE 4/26/76 TIME 11.30

A= 11.533 B= 3.333 C= .50 Y= 25.40

Y CM	E VOLTS	RMS MV	DE/DU M/S	U M/S	RMSU	YN	UN
.53	4.351	187.80	.0863	4.93	2.176	.021	.279
1.63	4.625	155.80	.0609	8.75	2.557	.064	.495
4.42	4.803	113.10	.0501	11.98	2.256	.174	.678
6.82	4.871	95.00	.0468	13.38	2.031	.268	.757
9.08	4.948	89.20	.0434	15.09	2.058	.357	.854
11.03	4.963	80.40	.0427	15.44	1.882	.434	.874
12.39	4.991	73.10	.0416	16.11	1.757	.488	.911
14.42	5.019	57.40	.0405	16.79	1.416	.568	.950
16.53	5.041	38.10	.0397	17.34	.960	.651	.981
18.54	5.048	23.10	.0394	17.51	.586	.730	.991
20.00	5.054	19.80	.0392	17.67	.505	.788	1.000

FOR HILL 1

FREE STREAM VELOCITY 18.15M/S

TUNNEL TEMP. 73.0F

DENSITY .9844E+00 KG/CM

POSITION 0.00CM FROM CREST

BAROMETRIC PRESSURE 24.66IN HG

DATE 4/27/76 TIME 11. 0

A= 11.334 B= 3.333 C= .50 Y= 25.40

Y CM	E VOLTS	RMS MV	DE/DU M/S	U M/S	RMSU	YN	UN
.17	4.927	83.00	.0436	15.08	1.906	.007	.831
.36	4.927	85.00	.0436	15.08	1.952	.014	.831
1.51	4.927	94.00	.0436	15.08	2.158	.059	.831
3.21	4.943	88.00	.0429	15.45	2.052	.126	.851
5.98	4.968	84.00	.0419	16.04	2.006	.236	.884
8.41	5.005	79.00	.0405	16.94	1.953	.331	.933
11.08	5.024	64.00	.0398	17.41	1.610	.436	.959
13.64	5.044	42.00	.0390	17.92	1.076	.537	.987
16.19	5.051	23.00	.0388	18.10	.593	.637	.997
18.95	5.052	16.00	.0387	18.12	.413	.730	.998
20.43	5.053	13.00	.0387	18.15	.336	.804	1.000

Table I. (Continued)

c)

FOR HILL 2

FREE STREAM VELOCITY 17.75M/S

TUNNEL TEMP. 72.0F

DENSITY .9896E+00 KG/CM

POSITION 10.16CM FROM CREST

BAROMETRIC PRESSURE 24.74IN HG

DATE 4/26/76 TIME 12. 0

A= 11.533 B= 3.333 C= .50 Y= 25.40

Y CM	E VOLTS	RMS MV	DE/DU M/S	U M/S	RMSU	YN	UN
.30	4.243	162.50	.1012	3.77	1.606	.012	.212
.25	4.501	162.80	.0707	6.85	2.302	.010	.386
2.50	4.694	130.50	.0564	9.92	2.316	.099	.559
3.83	4.781	114.60	.0513	11.54	2.234	.151	.650
5.61	4.852	98.10	.0477	12.98	2.058	.221	.731
7.01	4.881	93.00	.0463	13.60	2.009	.276	.766
9.58	4.942	86.30	.0436	14.95	1.979	.377	.843
11.75	4.986	76.70	.0418	15.99	1.835	.462	.901
14.06	5.010	59.40	.0409	16.57	1.454	.554	.933
16.01	5.039	41.90	.0398	17.29	1.053	.630	.974
18.45	5.050	23.00	.0394	17.56	.584	.726	.989
19.97	5.057	19.30	.0391	17.74	.493	.786	1.000

FOR HILL 2

FREE STREAM VELOCITY 18.56M/S

TUNNEL TEMP. 73.0F

DENSITY .9844E+00 KG/cm

POSITION 0.00CM FROM CREST

BAROMETRIC PRESSURE 24.66IN HG

DATE 4/27/76 TIME 10.30

A= 11.334 B= 3.333 C= .50 Y= 25.40

Y CM	E VOLTS	RMS MV	DE/DU M/S	U M/S	RMSU	YN	UN
.17	4.920	86.00	.0439	14.92	1.961	.007	.804
.46	4.926	88.00	.0436	15.05	2.018	.018	.811
.88	4.941	91.00	.0430	15.40	2.118	.035	.830
2.25	4.952	95.00	.0425	15.66	2.234	.089	.844
4.38	4.964	87.00	.0420	15.94	2.069	.172	.859
6.35	4.994	83.00	.0409	16.66	2.031	.250	.898
9.10	5.016	75.00	.0400	17.21	1.873	.358	.927
11.63	5.048	60.00	.0389	18.02	1.543	.458	.971
13.79	5.061	43.00	.0384	18.36	1.119	.543	.989
16.47	5.066	24.00	.0383	18.49	.627	.648	.996
20.43	5.069	17.00	.0382	18.56	.446	.804	1.000

Table I. (Continued)
d)

FOR HILL 3
FREE STREAM VELOCITY 17.75M/S
TUNNEL TEMP. 73.0F
DENSITY .9896E+00 KG/CM

POSITION 10.16CM FROM CREST
BAROMETRIC PRESSURE 24.72IN HG
DATE 4/26/76 TIME 12.45

A= 11.533 B= 3.333 C= .50 Y= 25.40

Y CM	E VOLTS	RMS MV	DE/DU M/S	U M/S	RMSU	YN	UN
.35	4.236	167.40	.1023	3.70	1.637	.014	.208
1.26	4.564	158.30	.0655	7.78	2.418	.050	.438
2.71	4.714	123.40	.0551	10.28	2.238	.107	.579
4.19	4.801	106.90	.0502	11.94	2.128	.165	.673
6.91	4.888	94.60	.0460	13.75	2.057	.272	.775
9.73	4.941	88.20	.0436	14.93	2.021	.383	.841
12.09	4.995	71.30	.0414	16.20	1.720	.476	.913
13.88	5.024	60.40	.0403	16.91	1.497	.546	.953
15.95	5.038	43.70	.0398	17.26	1.098	.628	.972
18.15	5.047	26.20	.0395	17.49	.664	.714	.985
19.98	5.057	17.40	.0391	17.74	.445	.787	1.000

FOR HILL 3
FREE STREAM VELOCITY 18.46M/S
TUNNEL TEMP. 73.0F
DENSITY .9844E+00 KG/CM

POSITION 0.00CM FROM CREST
BAROMETRIC PRESSURE 24.66IN HG
DATE 4/27/76 TIME 9.10

A= 11.334 B= 3.333 C= .50 Y= 25.40

Y CM	E VOLTS	RMS MV	DE/DU M/S	U M/S	RMSU	YN	UN
.14	5.011	81.00	.0402	17.08	2.013	.006	.925
.37	4.990	82.00	.0410	16.57	1.999	.015	.897
.62	4.966	85.00	.0420	15.99	2.026	.024	.866
.76	4.957	90.00	.0423	15.77	2.127	.030	.855
1.83	4.934	94.00	.0433	15.24	2.173	.072	.825
2.76	4.943	90.00	.0429	15.45	2.098	.109	.837
4.72	4.961	85.70	.0422	15.87	2.033	.186	.860
6.63	4.972	81.90	.0417	16.13	1.963	.261	.874
8.74	5.007	75.30	.0404	16.98	1.865	.344	.920
11.07	5.031	62.50	.0395	17.59	1.582	.436	.953
13.71	5.054	43.10	.0387	18.17	1.114	.540	.985
15.43	5.057	28.10	.0386	18.25	.729	.607	.989
18.07	5.063	20.90	.0384	18.41	.545	.712	.997
20.41	5.065	12.30	.0383	18.46	.321	.804	1.000

Table I. (Continued)

e)

FOR HILL 4 POSITION 10.16CM FROM CREST

FREE STREAM VELOCITY 17.52M/S BAROMETRIC PRESSURE 24.72IN HG

TUNNEL TEMP. 73.0F DATE 4/26/76 TIME 1.15

DENSITY .9896E+00 KG/CM

A= 11.533 B= 3.333 C= .50 Y= 25.40

Y CM	E VOLTS	RMS MV	DE/DU M/S	U M/S	RMSU	YN	UN
.77	4.185	193.30	.1110	3.22	1.742	.030	.184
1.60	4.453	178.80	.0752	6.19	2.378	.063	.354
3.60	4.715	124.40	.0551	10.30	2.259	.142	.588
5.16	4.813	103.70	.0496	12.18	2.090	.203	.695
7.50	4.886	93.00	.0461	13.71	2.019	.295	.782
9.55	4.936	85.60	.0439	14.82	1.952	.376	.846
11.47	4.968	78.20	.0425	15.56	1.839	.452	.888
14.11	5.012	61.40	.0408	16.62	1.505	.555	.948
16.52	5.036	39.60	.0399	17.21	.993	.650	.982
18.45	5.044	23.50	.0396	17.41	.594	.726	.994
19.99	5.048	19.20	.0394	17.51	.487	.787	1.000

FOR HILL 4 POSITION 0.00CM FROM CREST

FREE STREAM VELOCITY 18.23M/S BAROMETRIC PRESSURE 24.66IN HG

TUNNEL TEMP. 73.0F DATE 4/27/76 TIME 10.10

DENSITY .9844E+00 KG/CM

A= 11.334 B= 3.333 C= .50 Y= 25.40

Y CM	E VOLTS	RMS MV	DE/DU M/S	U M/S	RMSU	YN	UN
.14	4.680	120.20	.0562	10.05	2.141	.005	.552
.53	4.794	118.00	.0497	12.21	2.373	.021	.670
1.72	4.858	107.00	.0466	13.54	2.296	.068	.743
3.44	4.912	95.00	.0442	14.73	2.150	.136	.808
5.72	4.954	86.00	.0424	15.70	2.026	.225	.861
7.60	4.985	80.00	.0412	16.45	1.941	.299	.902
9.96	5.008	71.00	.0403	17.01	1.760	.392	.933
12.29	5.041	56.00	.0391	17.84	1.431	.484	.979
14.21	5.048	39.00	.0389	18.02	1.003	.560	.988
16.26	5.051	26.00	.0388	18.10	.670	.640	.993
18.67	5.053	18.00	.0387	18.15	.465	.735	.996
20.43	5.056	14.00	.0386	18.23	.363	.804	1.000

Table I. (Continued)
f)

FOR HILL 5
FREE STREAM VELOCITY 17.85M/S
TUNNEL TEMP. 73.0F
DENSITY .9896E+00 KG/CM

POSITION 10.16CM FROM CREST
BAROMETRIC PRESSURE 24.70IN HG
DATE 4/26/76 TIME 2.50

A= 11.533 B= 3.333 C= .50 Y= 25.40

Y CM	E VOLTS	RMS MV	DE/DU M/S	U M/S	RMSU	YN	UN
.41	4.282	196.00	.0954	4.16	2.055	.016	.233
1.94	4.637	155.00	.0601	8.94	2.579	.076	.501
3.42	4.749	124.00	.0531	10.93	2.336	.135	.612
5.93	4.848	102.00	.0479	12.90	2.131	.234	.722
8.63	4.917	90.70	.0447	14.39	2.030	.340	.806
11.05	4.968	81.00	.0425	15.56	1.905	.435	.872
13.62	5.015	66.90	.0407	16.69	1.645	.536	.935
15.85	5.044	45.30	.0396	17.41	1.144	.624	.975
18.34	5.056	27.10	.0392	17.72	.692	.722	.993
19.99	5.061	20.00	.0390	17.84	.513	.787	1.000

FOR HILL 5
FREE STREAM VELOCITY 18.23M/S
TUNNEL TEMP. 73.0F
DENSITY .9844E+00 KG/CM

POSITION 0.00CM FROM CREST
BAROMETRIC PRESSURE 24.66IN HG
DATE 4/27/76 TIME 10. 0

A= 11.334 B= 3.333 C= .50 Y= 25.40

Y CM	E VOLTS	RMS MV	DE/DU M/S	U M/S	RMSU	YN	UN
.24	4.864	90.00	.0463	13.67	1.943	.009	.750
.53	4.854	90.00	.0468	13.46	1.923	.021	.738
1.58	4.862	100.00	.0464	13.63	2.154	.062	.748
3.25	4.905	94.00	.0445	14.58	2.113	.128	.800
5.36	4.933	88.00	.0433	15.21	2.032	.211	.835
7.83	4.974	80.00	.0416	16.18	1.921	.308	.888
10.90	5.009	68.00	.0403	17.03	1.687	.406	.934
12.91	5.042	50.00	.0391	17.87	1.279	.508	.980
15.84	5.052	28.00	.0387	18.12	.723	.624	.994
18.49	5.055	17.60	.0386	18.20	.456	.728	.998
20.43	5.056	13.50	.0386	18.23	.350	.804	1.000

Table I. (Completed)

g)

FOR HILL 6
FREE STREAM VELOCITY 17.75M/S
TUNNEL TEMP. 73.0F
DENSITY .9896E+00 KG/cm

POSITION 10.16CM FROM CREST
BAROMETRIC PRESSURE 24.70IN HG
DATE 4/26/76 TIME 2.10

A= 11.533 B= 3.333 C= .50 Y= 25.40

Y CM	E VOLTS	RMS MV	DE/DU M/S	U M/S	RMSU	YN	UN
2.99	4.806	88.00	.0500	12.04	1.761	.118	.678
3.30	4.821	94.00	.0492	12.34	1.910	.130	.695
5.39	4.878	97.10	.0464	13.53	2.091	.212	.762
8.14	4.930	89.80	.0441	14.68	2.036	.320	.827
10.62	4.974	81.30	.0423	15.70	1.923	.418	.885
12.68	5.005	71.80	.0411	16.44	1.749	.499	.926
14.52	5.032	59.70	.0400	17.11	1.491	.572	.964
16.64	5.050	40.20	.0394	17.56	1.021	.655	.989
18.47	5.055	27.10	.0392	17.69	.691	.727	.997
19.99	5.057	19.10	.0391	17.74	.488	.787	1.000

FOR HILL 6
FREE STREAM VELOCITY 18.51M/S
TUNNEL TEMP. 73.0F
DENSITY .9844E+00 KG/CM

POSITION 0.00CM FROM CREST
BAROMETRIC PRESSURE 24.66IN HG
DATE 4/27/76 TIME 9.30

A= 11.334 B= 3.333 C= .50 Y= 25.40

Y CM	E VOLTS	RMS MV	DE/DU M/S	U M/S	RMSU	YN	UN
.29	4.580	196.00	.0629	8.37	3.117	.012	.452
.68	4.640	200.00	.0587	9.36	3.407	.027	.506
1.53	4.770	183.00	.0510	11.74	3.589	.060	.634
3.11	4.881	126.00	.0456	14.04	2.766	.123	.759
4.81	4.940	100.00	.0430	15.38	2.325	.189	.831
6.95	4.977	87.00	.0415	16.25	2.095	.274	.878
9.01	5.006	76.00	.0404	16.96	1.880	.355	.916
11.60	5.041	64.00	.0391	17.84	1.635	.457	.964
13.76	5.054	46.00	.0387	18.17	1.189	.542	.982
16.21	5.065	30.00	.0383	18.46	.784	.638	.997
18.52	5.066	19.00	.0383	18.49	.497	.729	.999
20.42	5.067	15.00	.0382	18.51	.392	.804	1.000

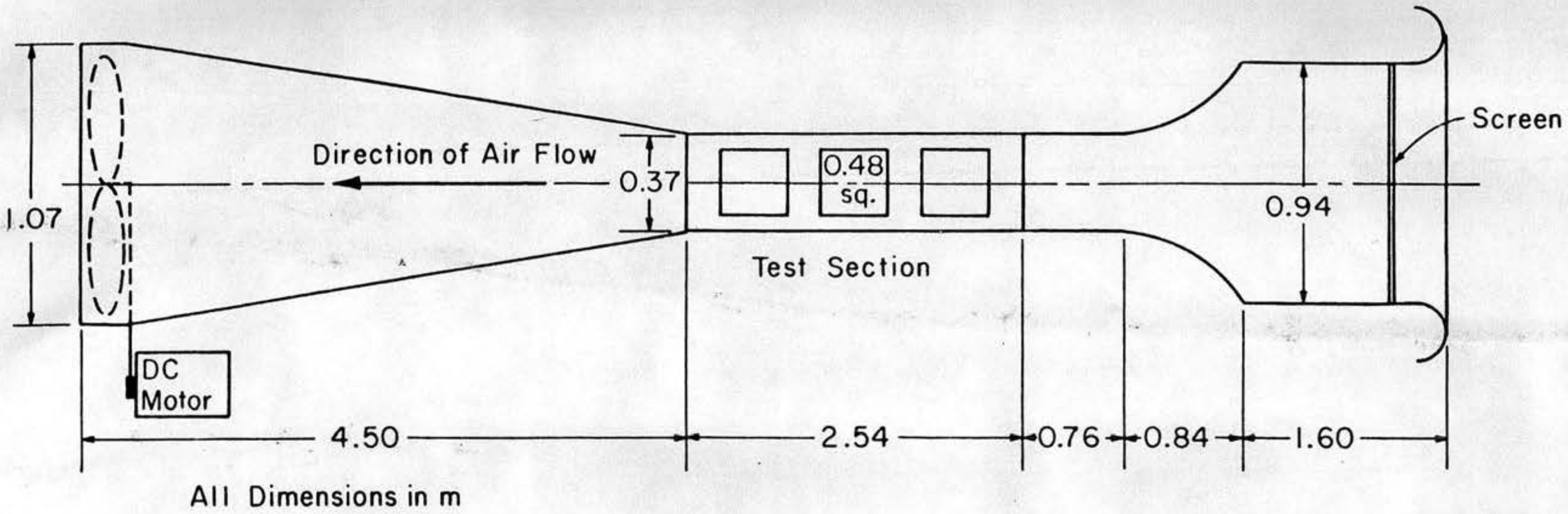

Figure 1 TRANSPIRATION WIND TUNNEL
FLUID DYNAMICS & DIFFUSION LABORATORY
COLORADO STATE UNIVERSITY

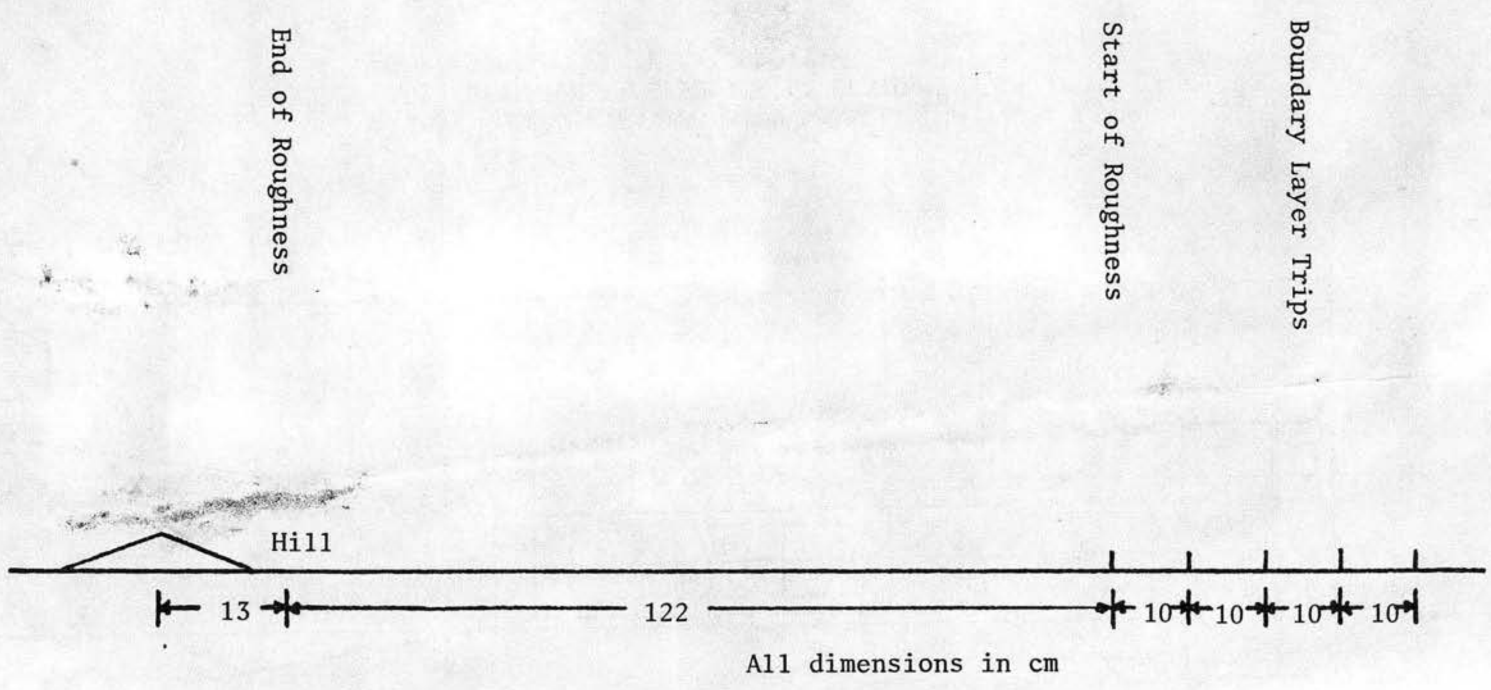

Figure 2. Wind Tunnel Setup

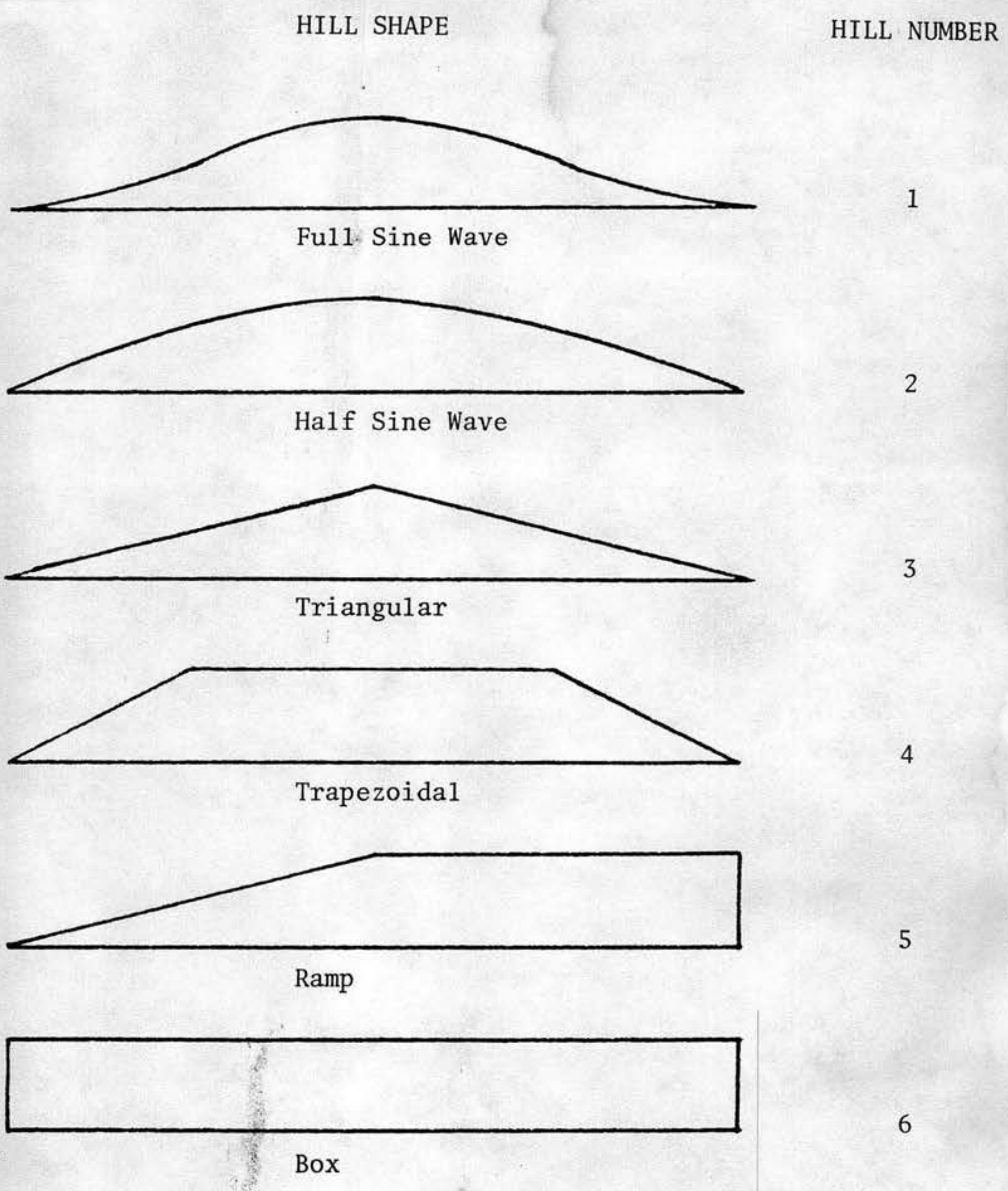

Figure 3. Hill Shapes

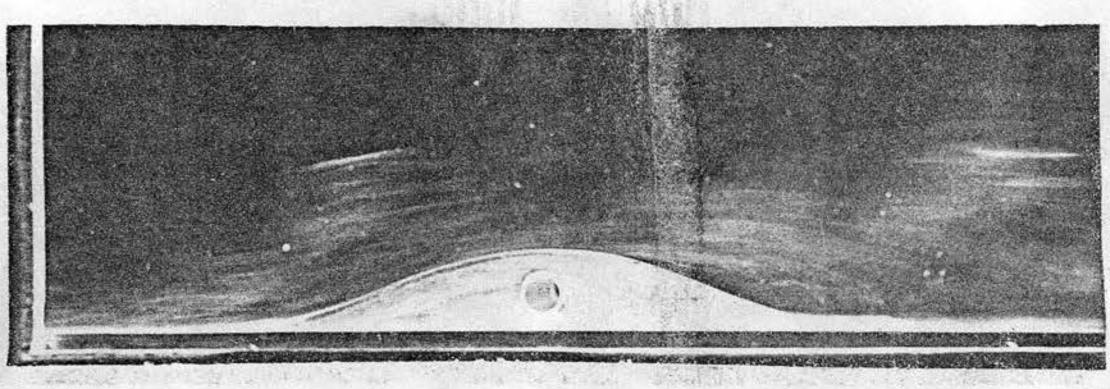

a) Full Sine Wave

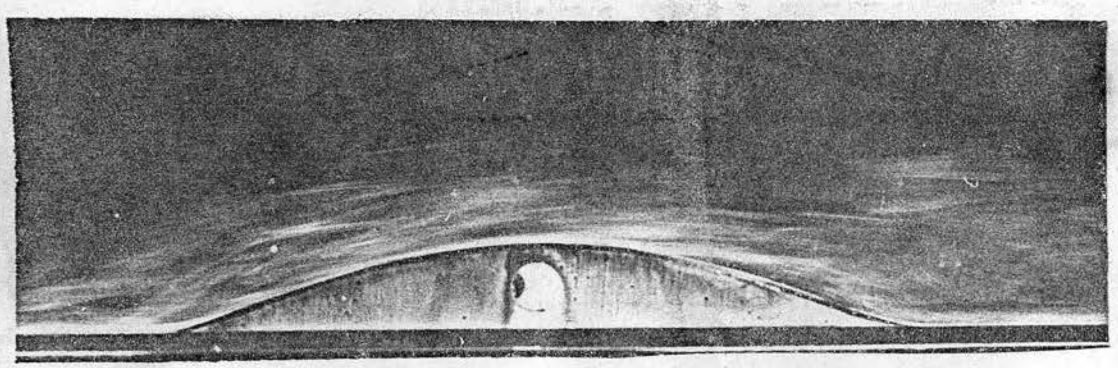

b) Half Sine Wave

c) Triangular

Figures 4a, b, c. Flow Visualization

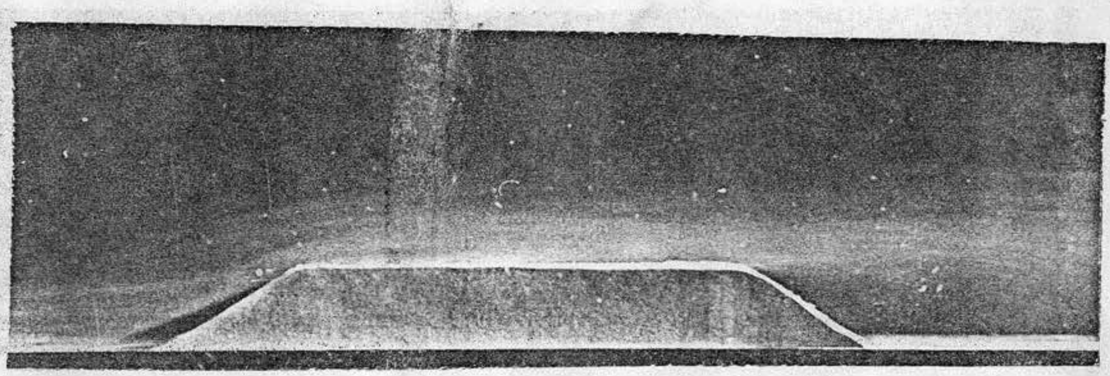

d) Trapezoidal

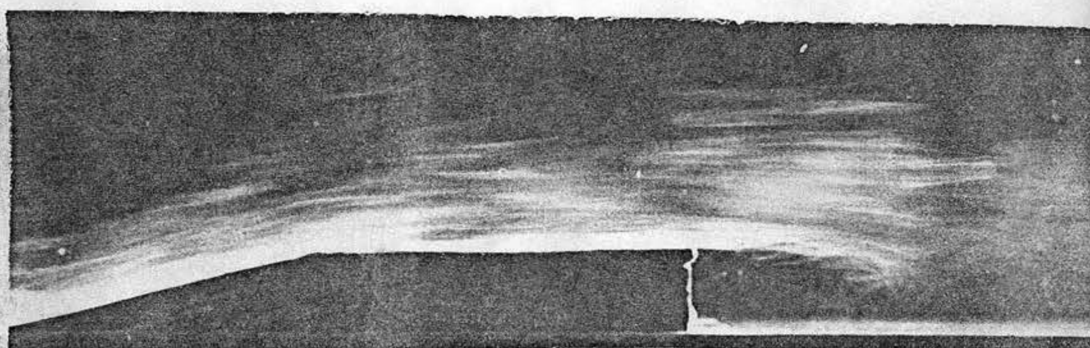

e) Ramp

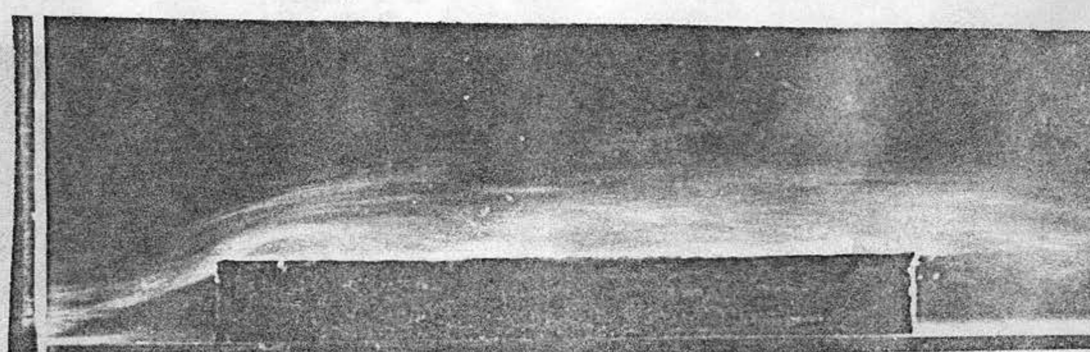

f) Box

Figures 4d, e, f. Flow Visualization (Completed)

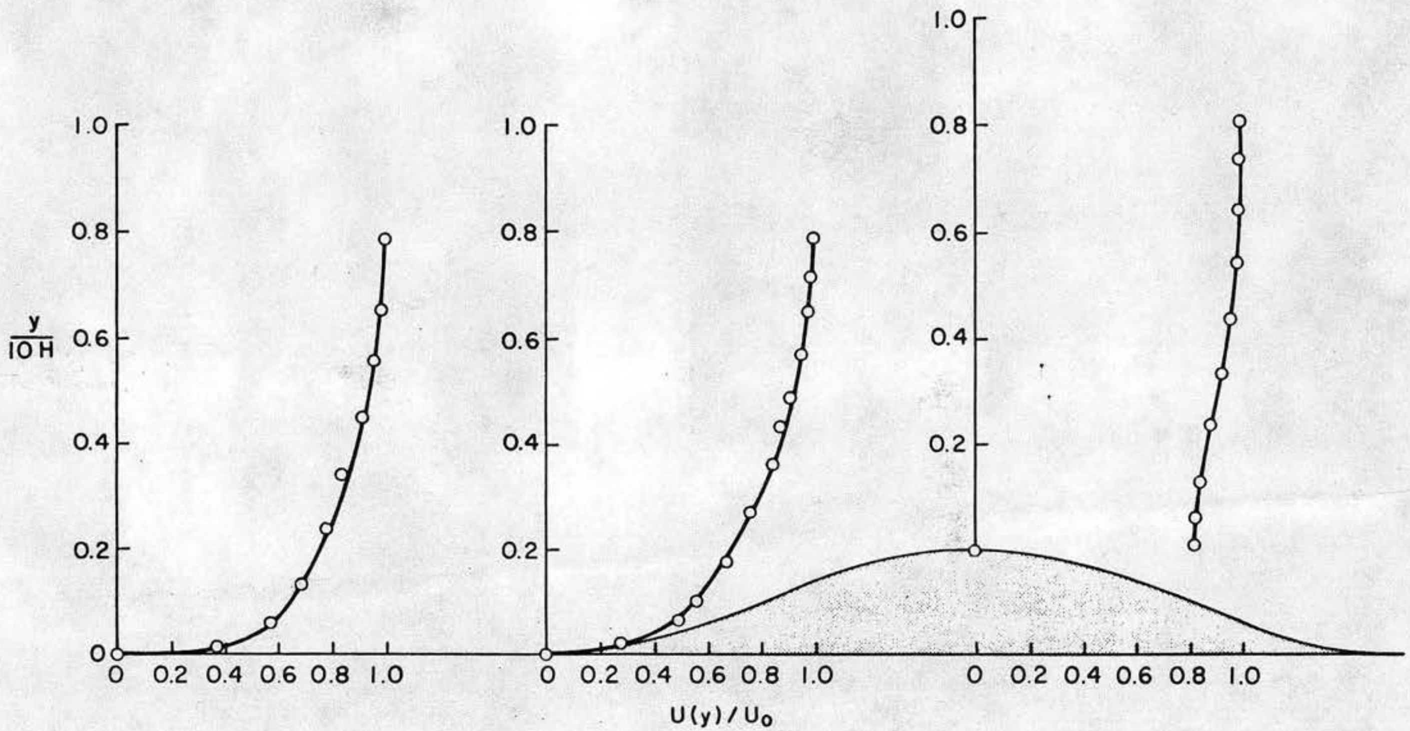

Figure 5a. Velocity Profile for Hill Models

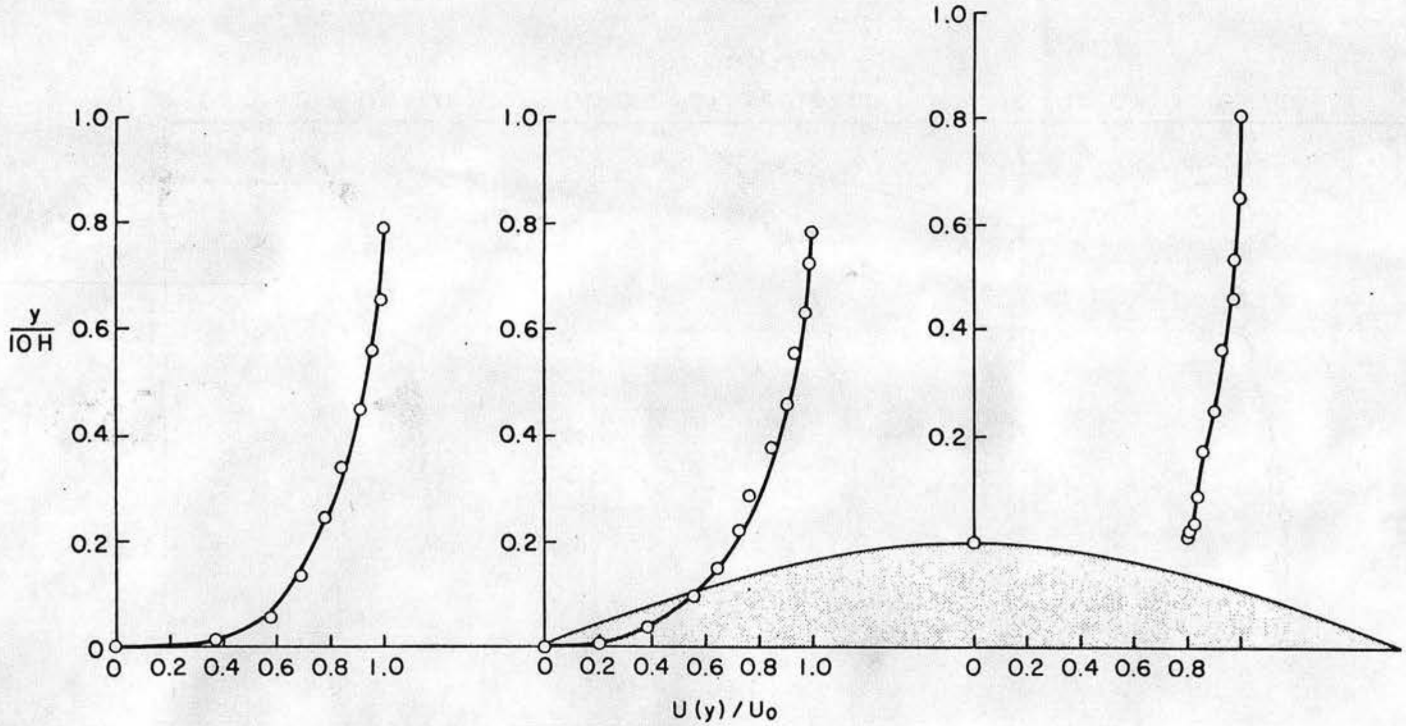

Figure 5b. Velocity Profile for Hill Models

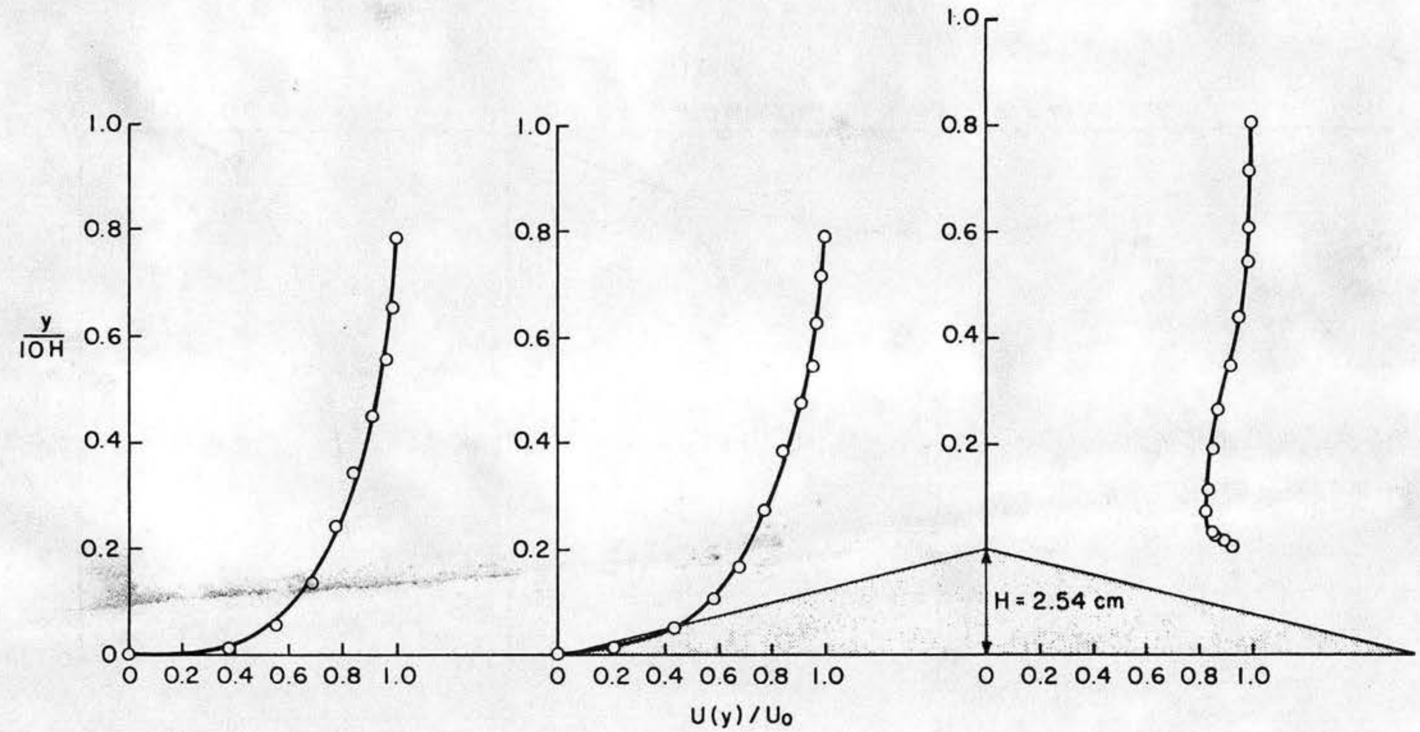

Figure 5c. Velocity Profile for Hill Models

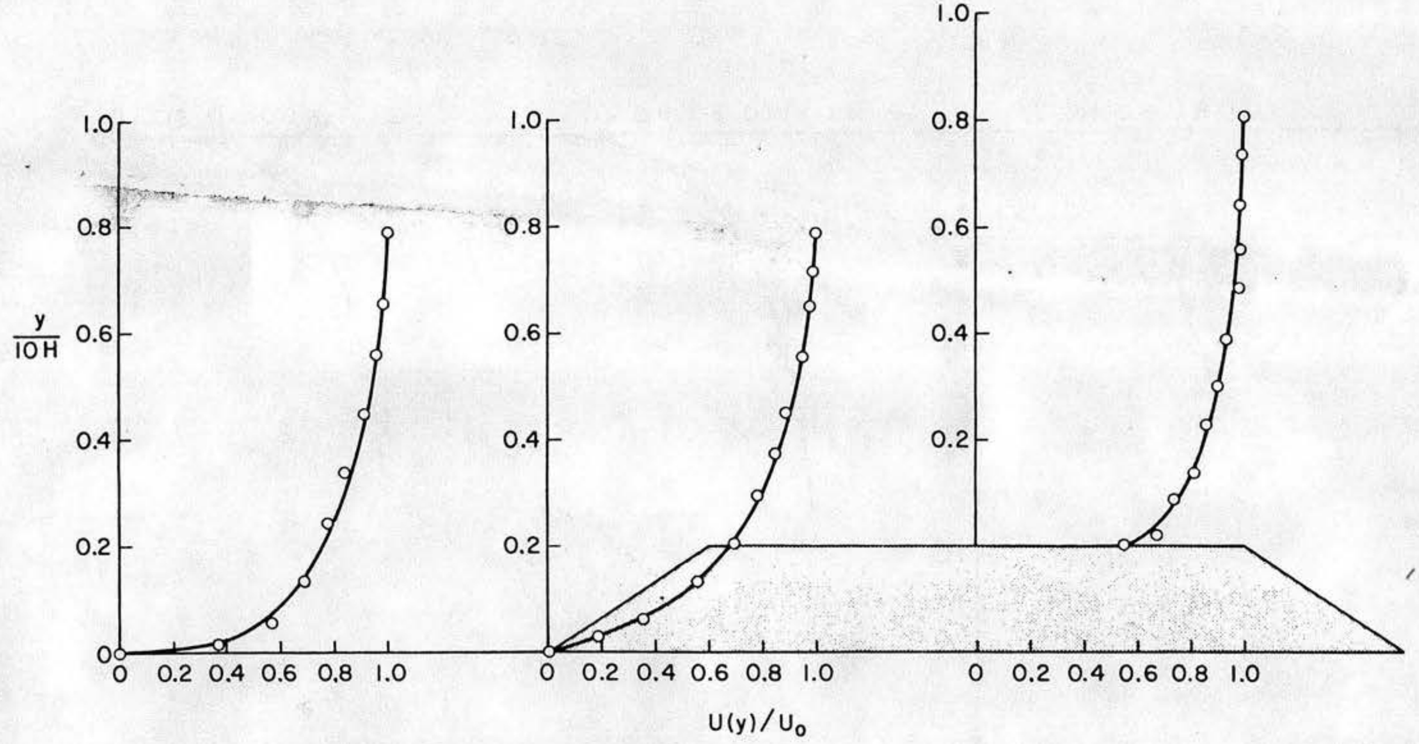

Figure 5d. Velocity Profile for Hill Models

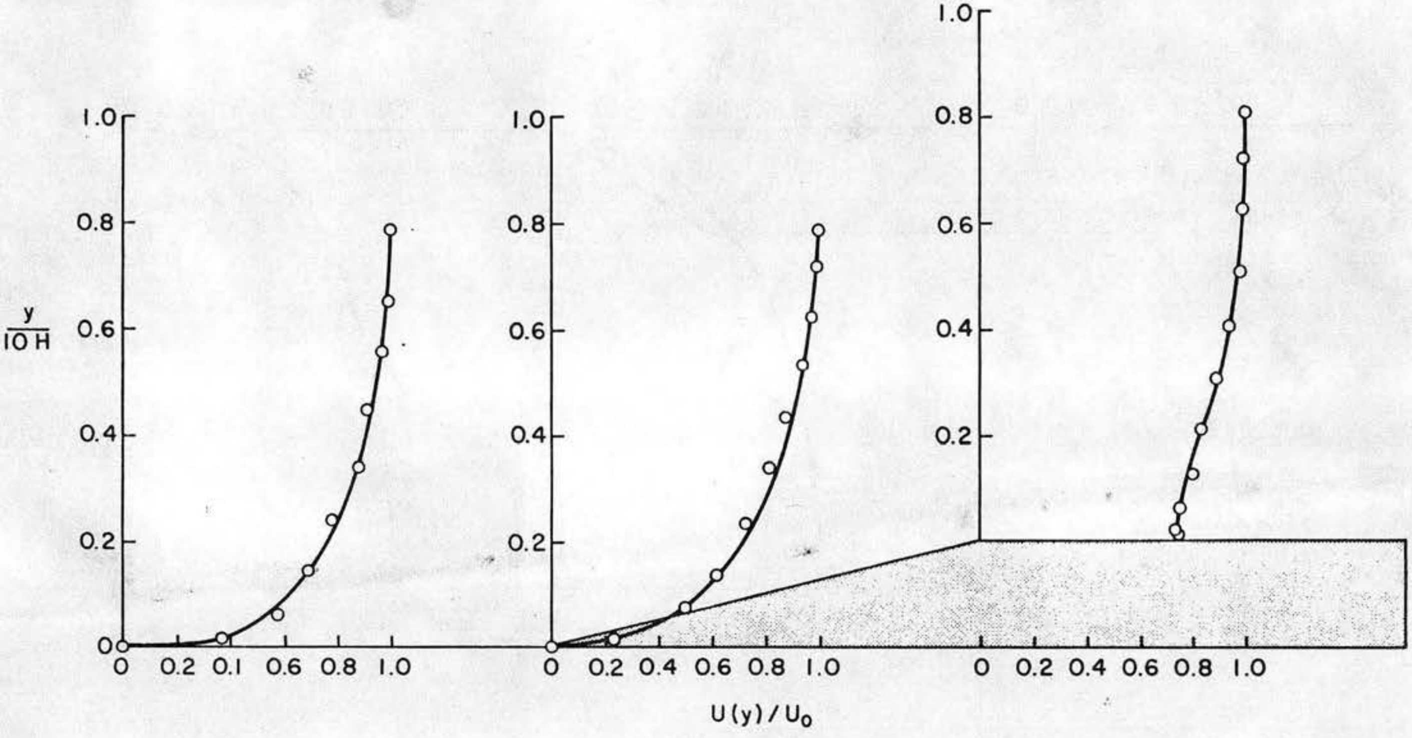

Figure 5e. Velocity Profile for Hill Models

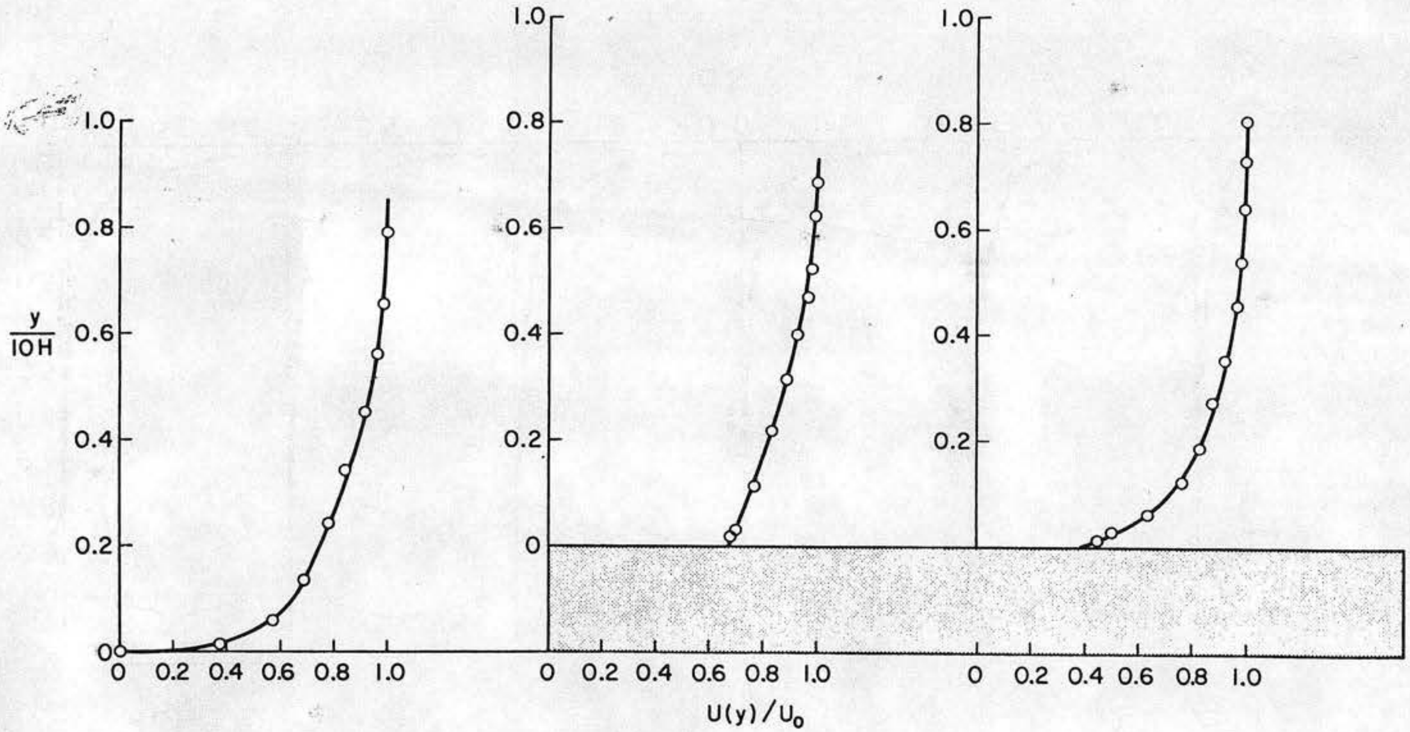

Figure 5f. Velocity Profile for Hill Models

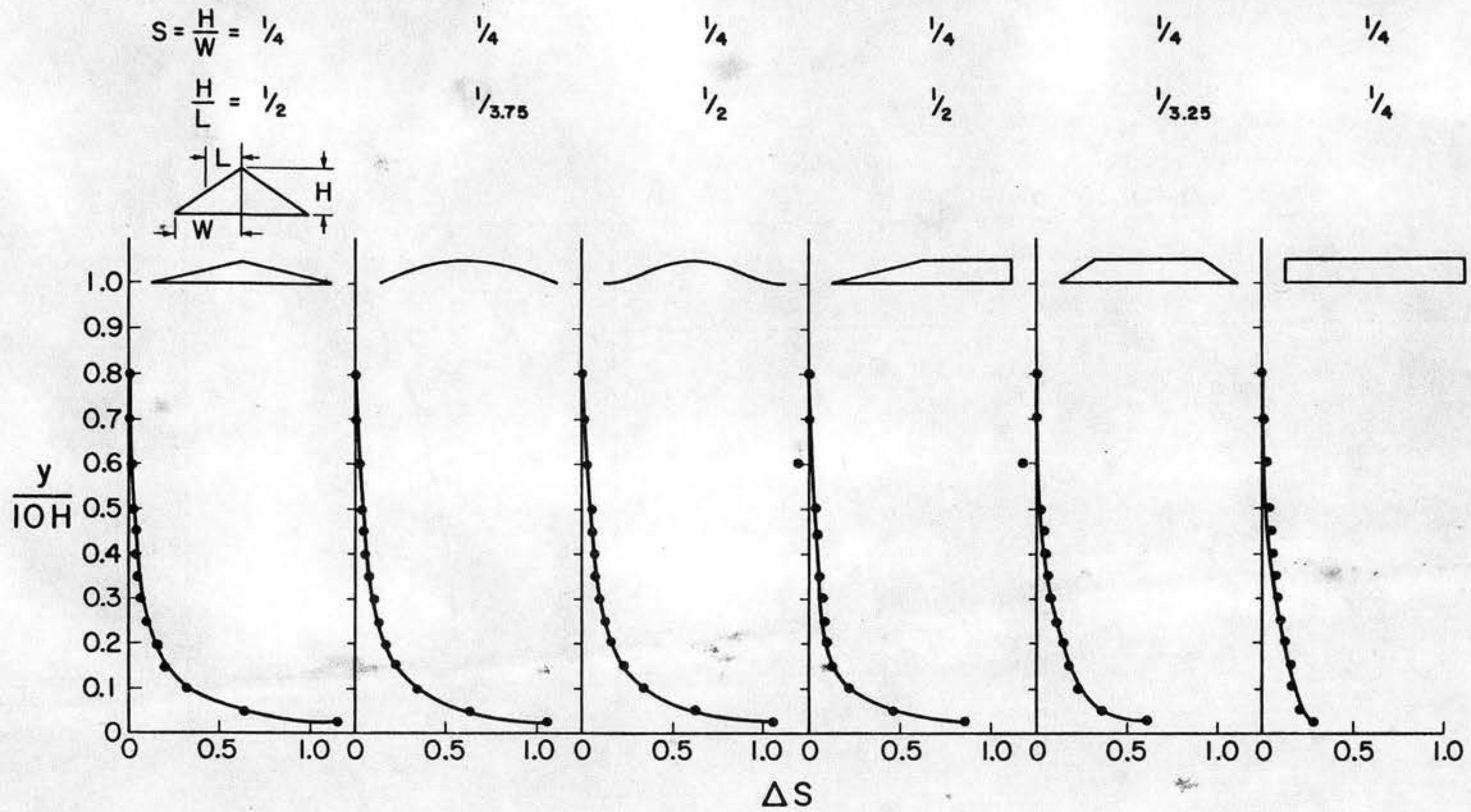

Figure 6. Velocity Speedup Between Approach Flow and Crest

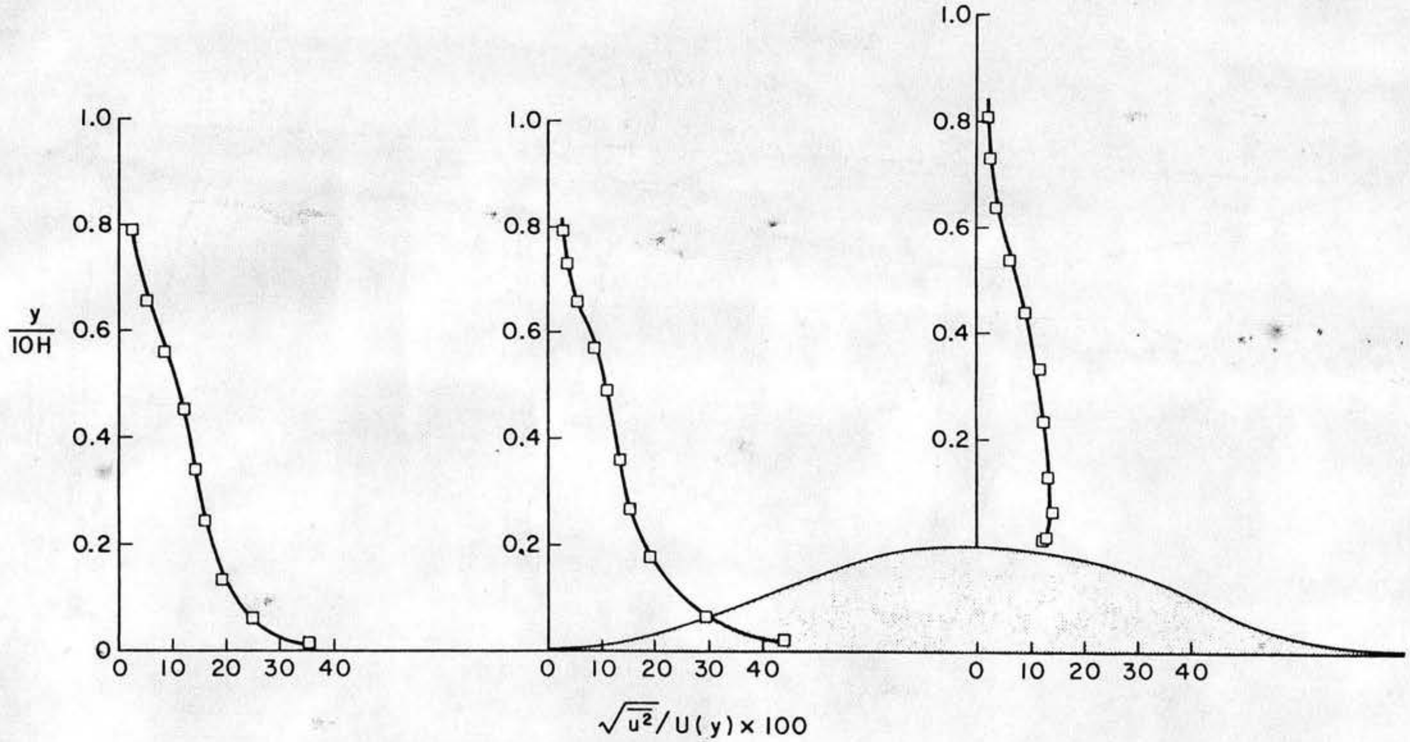

a) Full Sine Wave

Figure 7a. Longitudinal Turbulent Component Hill Model

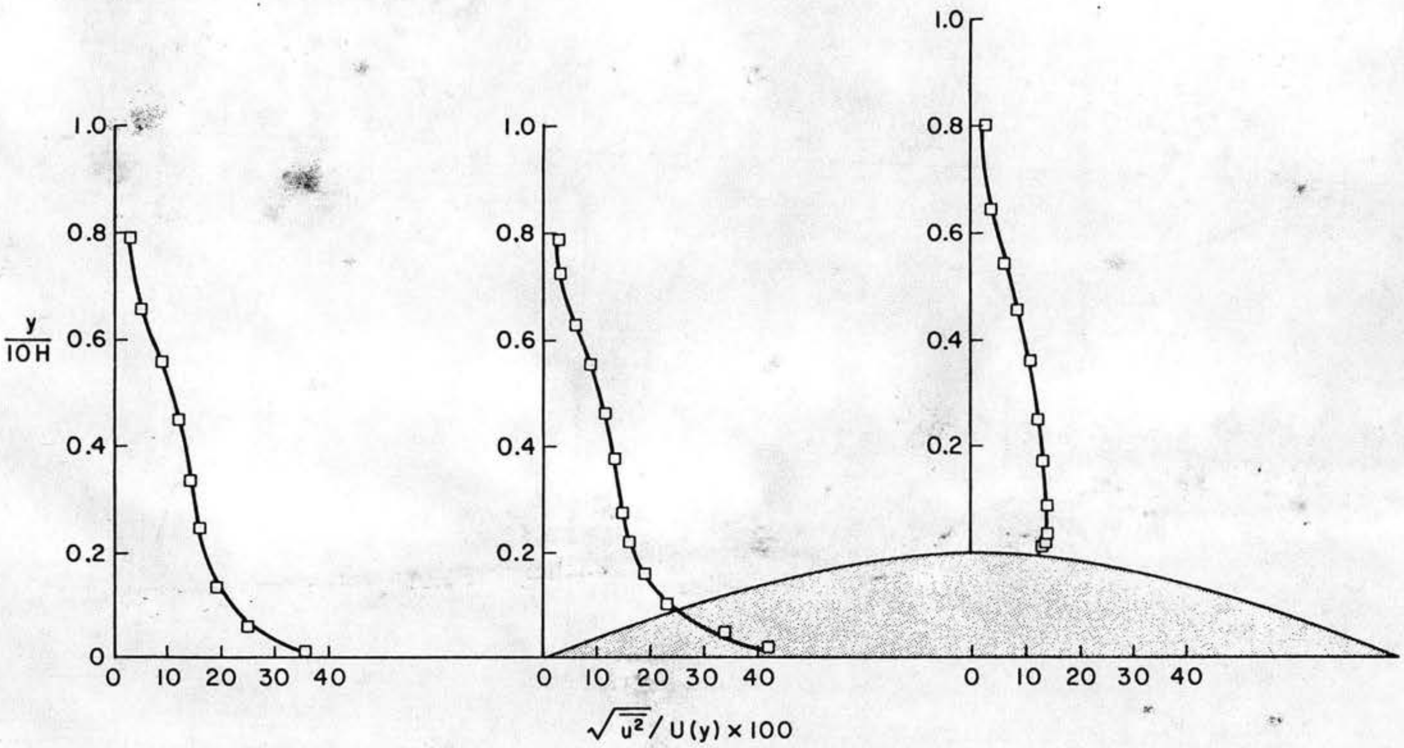

b) Half Sine Wave

Figure 7b. Longitudinal Turbulent Component Hill Model (Continued)

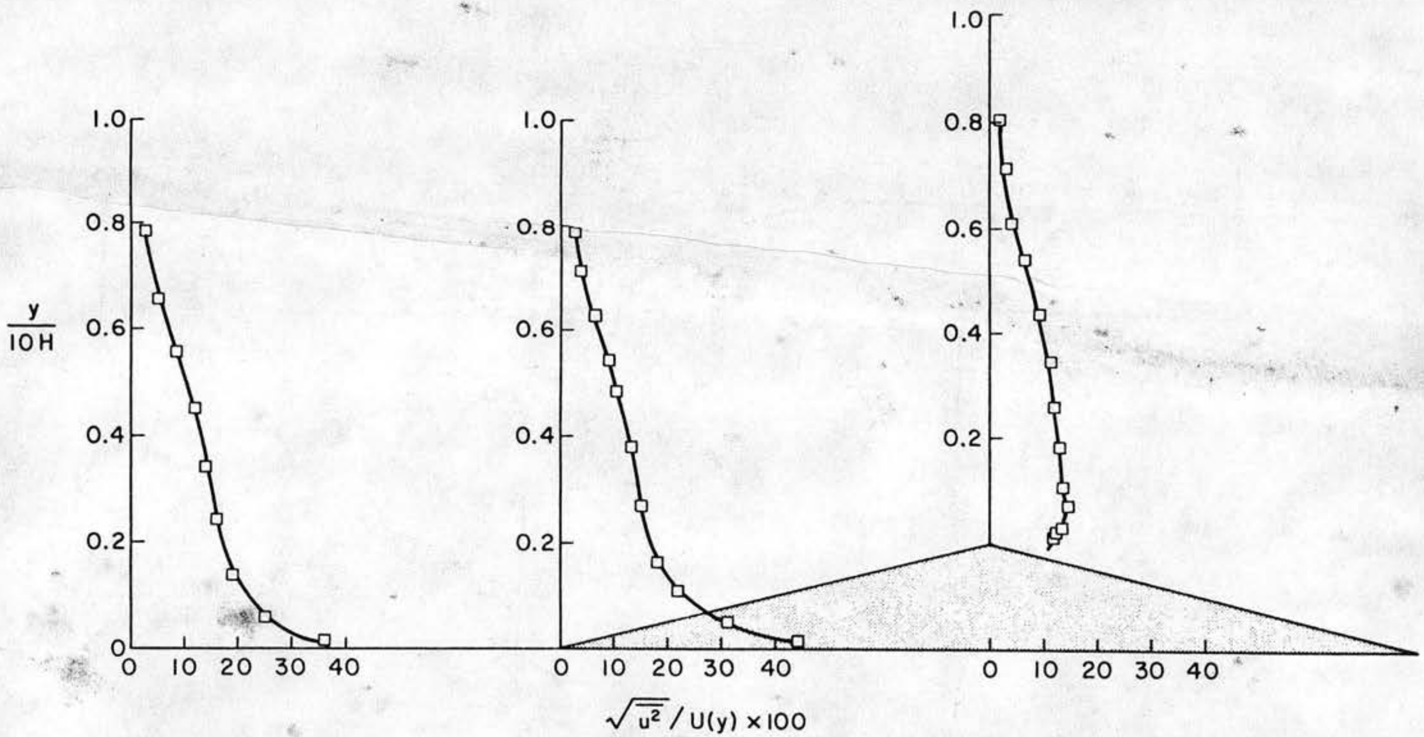

c) Triangular

Figure. 7c. Longitudinal Turbulent Component Hill Model (Continued)

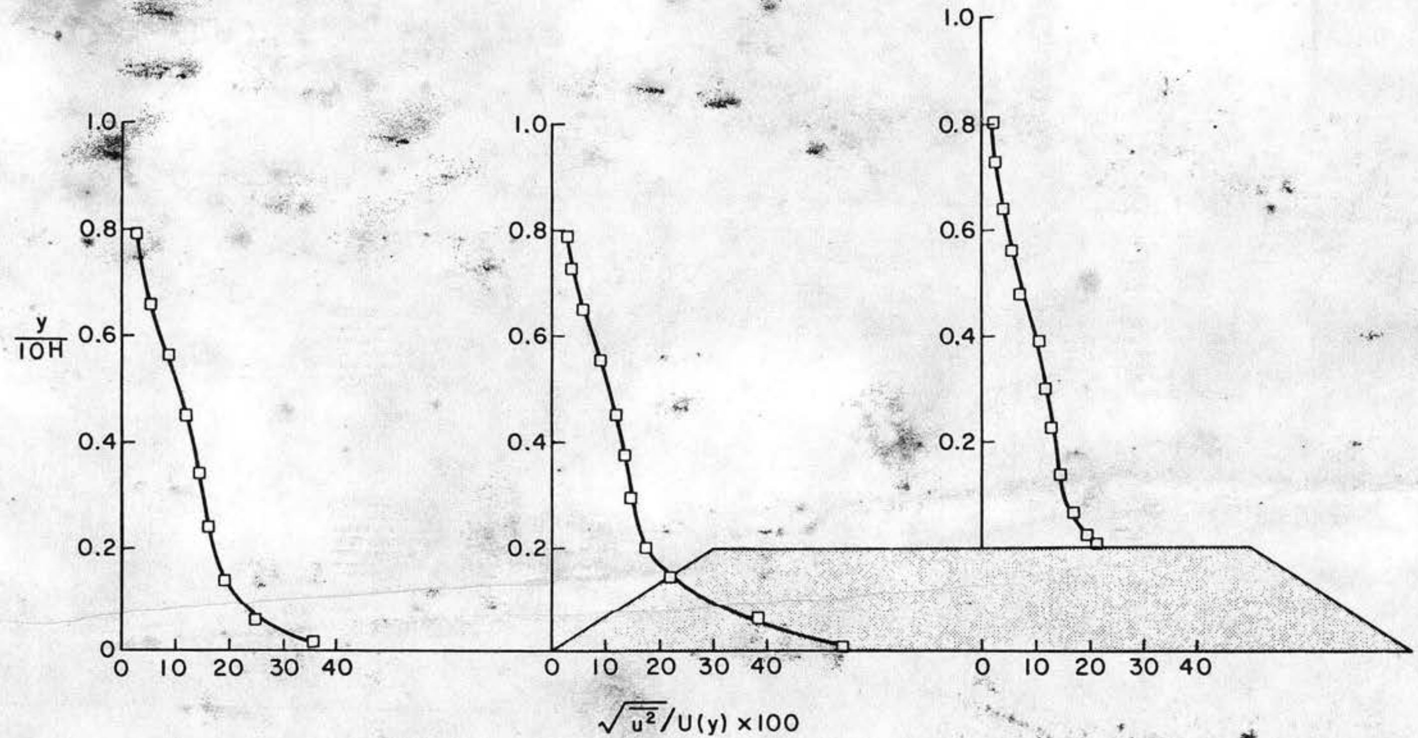

d) Trapezoidal

Figure 7d. Longitudinal Turbulent Component Hill Model (Continued)

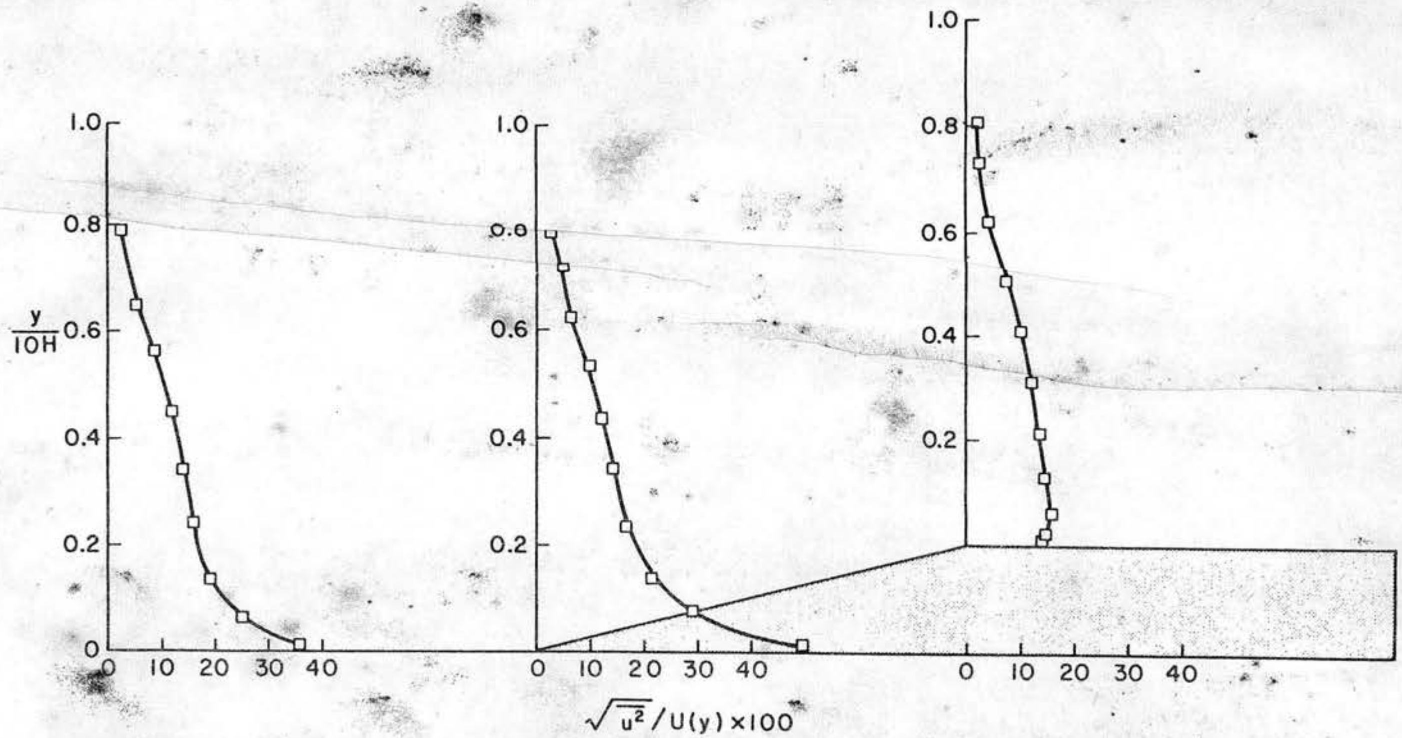

e) Ramp

Figure 7e. Longitudinal Turbulent Component Hill Model (Continued)

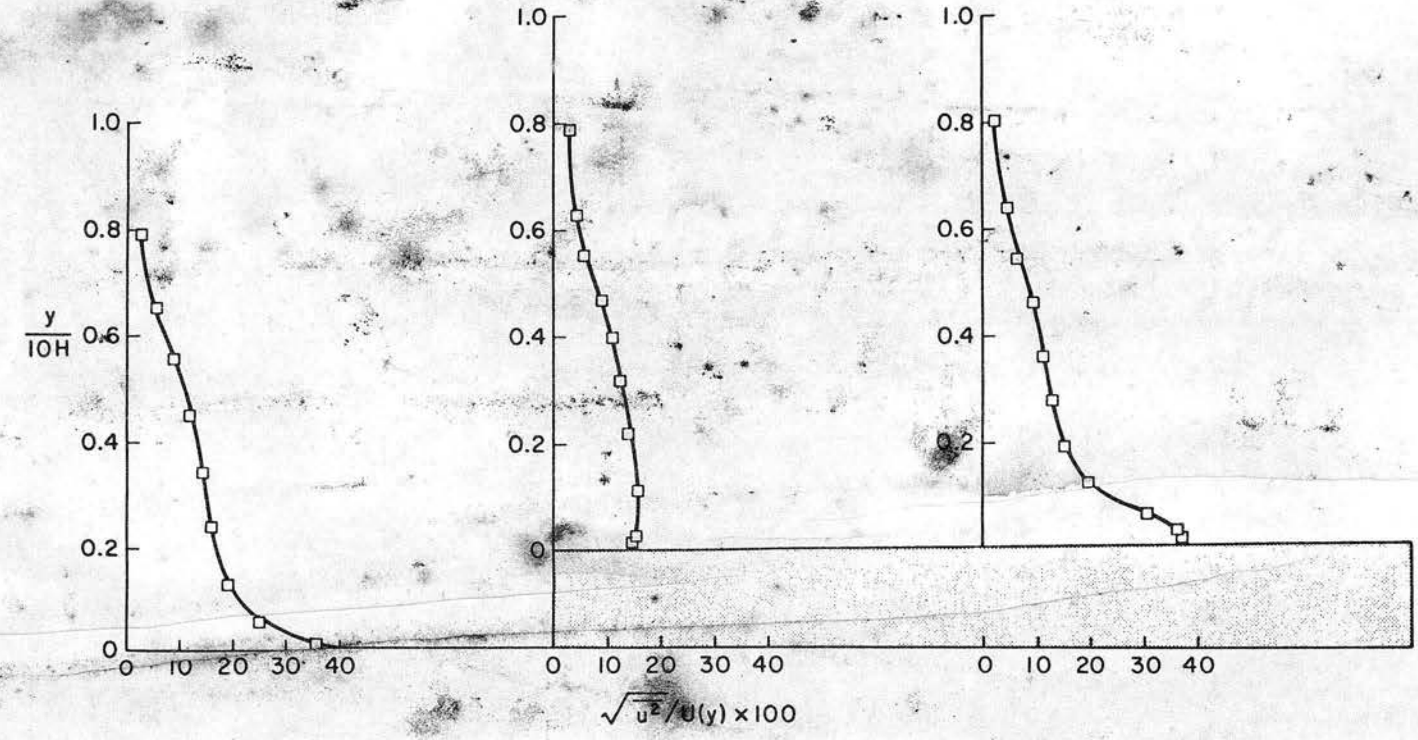

f) Box

Figure 7f. Longitudinal Turbulent Component Hill Model (Completed)

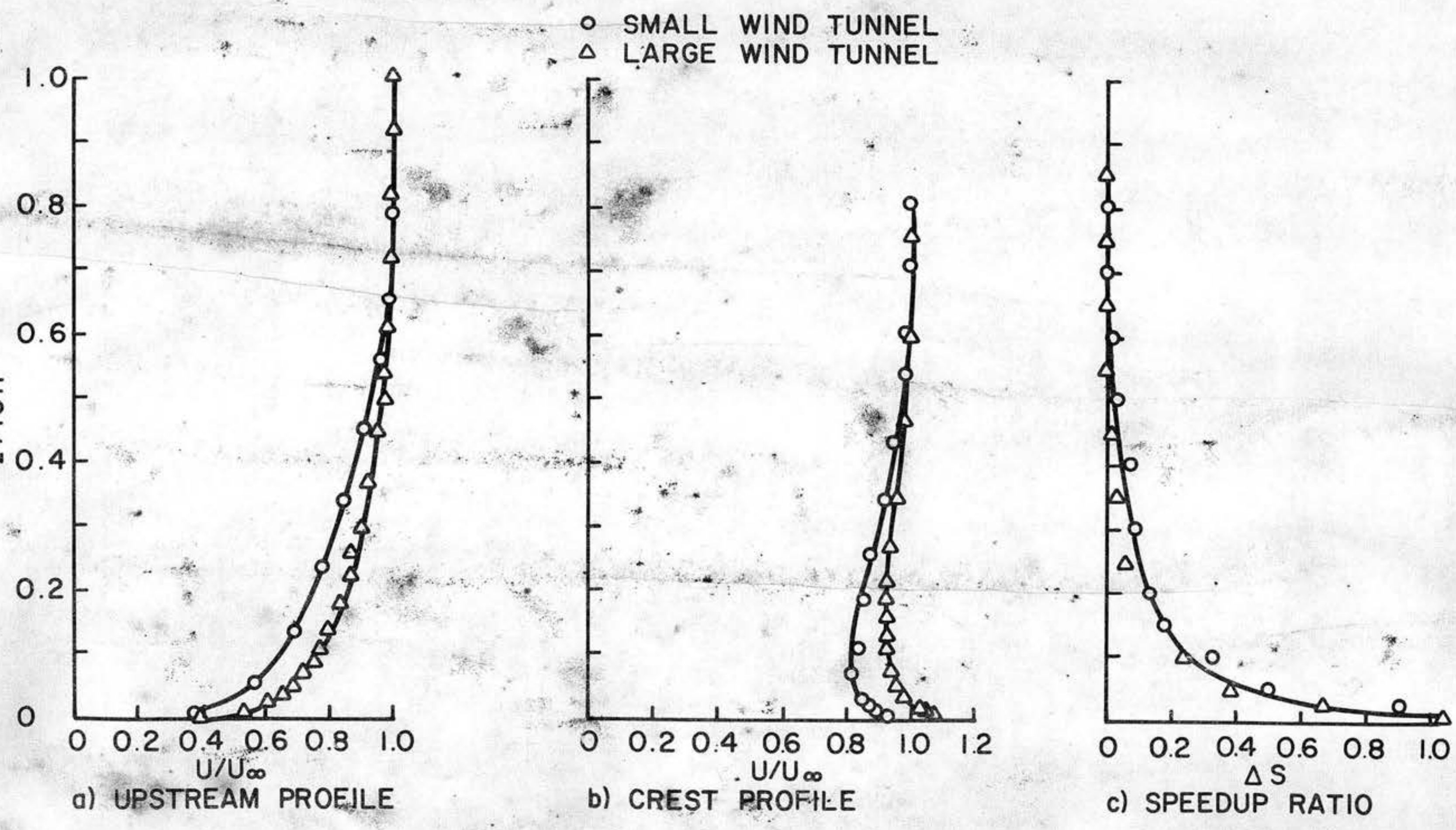

Figure 8. Comparison of Data From Two Similar Triangular Hills

APPENDIX B

BOUNDARY LAYER TURBULENCE OVER TWO-DIMENSIONAL HILLS

by

Michael A. Rider

and

V. A. Sandborn

SUMMARY

Measurements of the mean and turbulent velocities for turbulent boundary layers over two-dimensional hills have been made. Triangular hills, with aspect ratios (height to vertical distance to crest) of 1:2, 1:4, and 1:6, were subjected to two different approach turbulent boundary layer flows. Mean velocities, longitudinal and vertical turbulent velocities, Reynolds stress and the wall static pressure distributions are reported for a number of positions upstream, along, and at the crest of the hills.

As the flow advances up the hills, systematic changes in the mean and turbulent velocities occurred in the region near the hill surface. The flow in the outer region of the boundary layers above the hills were found to remain similar to the flow upstream of the hill. As the flow passed from the base of the hill to the crest there was an increase in mean velocity, shear stress, and vertical turbulent velocity near the surface. The longitudinal turbulent velocity was found to decrease in magnitude as the flow progressed from the base to the crest of the hill.

ACKNOWLEDGMENTS

This study was made possible by the Energy Research and Development Administration Contract EY-76-S-06-2438. Their support is gratefully acknowledged. The authors wish to thank Dr. R. N. Meroney and Mr. R. J. B. Bouwmeester for their valuable assistance in the research measurements and discussions on various aspects of the study. The authors would also like to thank Dr. J. A. Peterka and Dr. P. Wilbur for critically reviewing the report.

Chapter I

INTRODUCTION

Annual mean and peak wind velocities are available for general areas throughout the United States and the world. This information is critical for the development of wind power. However, rarely will the data be recorded at a proposed wind power site. It would be very beneficial to the wind power engineer to be able to predict from general wind data the flow characteristics at a specific location.

Needed, for a wind power site, are reliable estimates of the local flow properties. If the available wind data for the general area is at a station some distance from the site a means to correlate the desired information would be required.

In general, the approach terrain will affect the mean and turbulent flow properties. Moreover, to utilize the speedup affect of a hill, the predicted change in the airstream properties would be required. There are literally endless combinations of approach flow conditions and hill configurations. This study was limited to investigating two approach flow conditions and three two-dimensional triangular shaped model hills.

The investigation started with a turbulent boundary layer developed over a flat plate with a zero pressure gradient. The turbulent boundary layer was then subjected to one of three triangular shaped hills. Aspect ratios of the hills were (rise over run) 1:2, 1:4, and 1:6. Surveys were made of the mean velocity, the longitudinal and vertical turbulent velocities and the shear stress distributions. The measurement gave a reference to how these different flow properties change in magnitude over a two-dimensional ridge. Next by adding upstream roughness a different turbulent boundary layer was formed. The measurements during this flow case consisted of the mean velocity and the longitudinal turbulence.

The flat plate case represented a calibration point from which to build. In an effort to model atmospheric boundary layers in the wind tunnel, Zoric and Sandborn (1,2) have shown that similarity of turbulent boundary layers does exist for large Reynolds numbers. With their measurements in the Meteorological Wind Tunnel at Colorado State University, Sandborn and Zoric have documented that for a flat plate turbulent boundary layer with a zero pressure gradient similarity of the mean and turbulent velocities were present. When the turbulent quantities $\sqrt{\overline{u^2}}$, $\sqrt{\overline{v^2}}$ and $\overline{uv}$ are normalized by dividing by the local wall shear and multiplying by the density each of the turbulent flow properties follow a similarity curve.

Chapter II

THEORETICAL BACKGROUND

To utilize wind power to the fullest in a particular area the local terrain effects must be known. Different hills or ridges will produce different degrees of speedup of the airstream as it approaches the summit. Thus, to take advantage of the speedup it is important to find the most advantageous location and to choose a proper wind system for the local conditions. The mean velocity distribution is of primary interest, but turbulent quantities must be known to insure structural stamina. The present study was directed toward evaluating the effect of a hill on a flow. The fundamental concerns were the mean velocity and the longitudinal turbulent velocity component distributions. Also sought were the vertical turbulent velocity component and shear stress distributions.

Of specific interest was how far up into the boundary layer would the impression of the hill be evident. Due to inertia of the flow, the outer reaches of the boundary layer were expected to remain similar to that upstream. The only portion of the flow expected to change was the region closest to the wall.

It was known prior to the test that there would be a speedup of the mean velocity in the region nearest the wall. Furthermore, the increase in velocity gradient would produce an increase in surface shear stress. Not as obvious was the change in the turbulent components. A report by Ribner and Tucker (3), which discussed turbulence in a contracting stream gave some insight. Although the report dealt with isotropic turbulent flows which were undergoing simple contraction, it was felt the results could give an insight to the present problem.

Ribner and Tucker showed that when a flow was subjected to a contraction the longitudinal turbulent velocity component decreased and the lateral component increased. Regarding the hill as a local contraction, it was anticipated that similar results would be found.

Surface Shear Stress Evaluation

Two methods were used to determine the skin friction. The empirical Ludwieg-Tillmann equation and the "law of the wall."

The Ludwieg-Tillmann skin friction relation reads

$$C_f \equiv \frac{\tau_w}{1/2\ U_\infty^2} = .246 \times 10^{-.678H} \left(\frac{U_\infty \theta}{\nu}\right)^{-.268} \tag{1}$$

where: the momentum thickness is

$$\theta \equiv \int_0^\delta \frac{U}{U_\infty} \left(1 - \frac{U}{U_\infty}\right) dy$$

the form factor is

$$H \equiv \frac{\delta^*}{\theta}$$

the displacement thickness is

$$\delta \equiv \int_0^\delta \left(1 - \frac{U}{U_\infty}\right) dy$$

and δ is the boundary layer thickness.

Justification for using this relation is based on earlier work reported by Tieleman (4). During his experiments Tieleman required skin friction measurements at several points in the wind tunnel. To check the reliability of the Ludwieg-Tillmann equation, Tieleman compared direct measurements from a floating element shear plate and values determined from the Ludwieg-Tillmann equation (1), Figure 1.

The agreement shown on Figure 1 demonstrated that the Ludwieg-Tillmann equation was adequate for the flat plate--zero pressure gradient boundary layers.

The "law of the wall", credited to Prandtl (5), applies to the region nearest the wall where viscous effects are important. Nondimensionally the "law of the wall" reads

$$\frac{U}{U_\tau} = f\left(\frac{U_\tau y}{\nu}\right) \tag{2}$$

where $U_\tau^2 \equiv \frac{\tau_w}{\rho}$

Patel (6) gives the following definitions of f for the given flow conditions

(a) a linear sublayer

$$U/U_\tau = U_\tau y/\nu \tag{3a}$$

(b) a fully turbulent region

$$U/U_\tau = A \log_{10}\left(\frac{U_\tau y}{\nu}\right) + B \tag{3b}$$

(c) a transition zone

$$U/U_\tau = A \log_{10}\left[\left(\frac{U_\tau y}{\nu}\right) + C\right] + B \tag{3c}$$

Where the constants A, B and C are believed universal. From his work and other investigators, Patel assigns the following values for the fully turbulent region.

$$A = 5.5 \quad \text{and} \quad B = 5.45 \quad .$$

The "law of the wall" is limited to zero and moderate pressure gradients. Patel suggests the "law of the wall" may be used to determine the surface shear stress for pressure gradients in the range

$$0 > \frac{\nu}{(\rho U_\tau^3)} \frac{dP}{dX} > -.007 \tag{4}$$

within approximately 6%. For the zero and moderate pressure gradients, both the Ludwieg-Tillmann and the "law of the wall" give approximately the same value for the shear stress. Figure 2 gives values of C_f evaluated for the flat plate flow of the present study.

Shear Stress Distribution Evaluation

The following similarity method reported by Sandborn and Horstman (7) to evaluate turbulent boundary layer shear stress distributions of the approach flow was used for the present study. This theoretical model accurately predicted the shear stress distributions over a flat plate--zero pressure gradient flow. Figure 3 is a comparison of the shear stress measured by Zoric and Sandborn and another by Klebanoff with the similarity predictions. The solid line is the shear stress distribution evaluated directly from the mean velocity profile.

For a turbulent boundary layer the equation of motion in the x-direction is

$$\rho U \frac{\partial U}{\partial x} + \rho\ V \frac{\partial U}{\partial y} = \frac{\partial p}{\partial x} + \frac{\partial \tau}{\partial y} \tag{5}$$

where the shear stress τ is made up of two parts. The two parts are the mean and the turbulent stress

$$\tau \equiv \mu \frac{\partial U}{\partial y} + \rho \overline{uv} \tag{6}$$

The boundary conditions require that at the wall

$$\tau = \tau_w \quad \text{and} \quad \frac{d\tau}{dy} = \frac{dp}{dx}$$

where p is the surface static pressure. Also at the outer limit of the turbulent boundary layer the shear stress approaches zero.

Sandborn assumed for a compressible flow (although for the present study an incompressible flow is assumed) the following similarity

$$\rho U = \rho_e U_e f_{\rho U}(\eta)$$

$$U = U_e f_U(\eta)$$

$$\tau = \tau_e \psi(\eta) \tag{7}$$

where $\rho_e U_e$ is a characteristic mass flow, U_e the characteristic velocity and τ_e as the characteristic shear stress. η is a non-dimensional variable resulting from dividing the vertical distance y by the characteristic length δ_e. Evaluating the differentials in terms of the similarity variables gives

$$\frac{\partial U}{\partial x} = f_U \frac{\partial U_e}{\partial x} + U_e \frac{\partial f_U}{\partial x} = f_U \frac{\partial U_e}{\partial x} - \frac{U_e}{\delta} \frac{d\delta}{dx} \eta f_U' U \tag{8}$$

$$\frac{\partial U}{\partial y} = \frac{U_e}{\delta} f_U' \tag{9}$$

and from continuity

$$\rho V = - \int_o^\eta \delta \frac{\partial \rho_e U_e}{\partial x} f_{\rho U} d\eta + \rho_e U_e \frac{d\delta}{dx} \int_o^\eta f_{\rho U}' \eta d\eta \tag{10}$$

Substituting in the similarity values into the equation of motion yields

$$\rho_e U_e f_{\rho U}[f_U \frac{\partial U_e}{\partial x} - \frac{U_e}{\delta} \frac{d\delta}{dx} \eta f_U'] + \frac{U_e}{\delta} f_U'[- \delta \frac{\partial \rho_e U_e}{\partial x} \int_o^\eta f_{\rho U} d\eta$$

$$+ \rho_e U_e \frac{d\delta}{dx} \int_o^\eta f_{\rho U}' \eta d\eta] = - \frac{\partial p}{\partial x} + \frac{\tau_w}{\delta} \psi' \quad . \tag{11}$$

Solving for ψ' and integrating gives

$$\psi \equiv \frac{\tau}{\tau_e} = \frac{\rho_e \delta_e U_e}{\tau_e} \frac{dU_e}{dx} \left(\int_o^{\eta} f_{\rho U} f_U d\eta - \eta \right) \left(\frac{\delta_e U_e}{\tau_e} \frac{d\rho_e U_e}{dx} \right.$$

$$\left. + \frac{\rho_e U_e^2}{\tau_e} \frac{d\delta_e}{dx} \right) \int_o^{\eta} \{ f_U' \int_o^{\eta'} f_{\rho U} d\eta' \} \, d\eta + C \qquad (12)$$

For similarity it is required that the equation (11) be independent of x. Requiring that for compressible flow

$$\frac{\delta_e \rho_e U_e}{\tau_e} \frac{dU_e}{dx} = A \text{ (a constant independent of } x) \qquad (13)$$

and

$$\frac{\delta_e U_e}{\tau_e} \frac{d\rho_e U_e}{dx} + \frac{\rho_e U_e^2}{\tau_e} \frac{d\delta_e}{dx} = B \text{ (a constant independent of } x) \qquad (14)$$

For incompressible flow, $\frac{\delta \rho_e}{\delta x} = 0$, thus the similarity requirements are

$$\rho \frac{\delta U_e}{\tau_e} \frac{dU_e}{dx} = A \qquad (13a)$$

$$\rho \frac{U_e^2}{\tau_e} \frac{d\delta}{dx} = B \qquad (14a)$$

To evaluate equation (12) the following similarity characteristics were used: $U_e = U_\infty$, $\rho_e = \rho_\infty$, $\tau_e = \tau_w$, and δ_e, the characteristic length, was equal to δ where $\delta = y$ at $\tau = 0$. The final form of equation (12) for an incompressible flat plate flow, with a zero pressure gradient is

$$\psi \equiv \frac{\tau}{\tau_w} = 1 - \frac{U_\infty^2}{U_\tau^2} \frac{d\delta}{dx} \int_o^{\eta} \{ \frac{d(U/U_\infty)}{d\eta} \int_o^{\eta_1} (\frac{U}{U_\infty}) \, d\eta_1 \} \, d\eta \qquad (15)$$

where $U_\tau^2 \equiv \frac{\tau_w}{\rho}$ and the boundary condition at $\eta = 0 (\frac{\tau}{\tau_w} = 1)$ was used to evaluate the constant of integration.

TURBULENT VELOCITY COMPONENT SIMILARITY

Work by different experimenters show that similarity does exist in the total shear stress and the turbulent velocity terms. Measurements by Zoric (2) at high Reynolds numbers and Klebanoff (8) at low Reynolds numbers demonstrate this within experimental limits, (10). Figures 3 and 4 show the agreement of the total shear stress distribution when referenced to the wall shear stress and the boundary layer thickness. When referenced similarly, the longitudinal component, $\sqrt{\frac{\rho\overline{u^2}}{\tau_w}}$, compares well for $y/\delta \geq .05$, Figure 5. The vertical turbulent component, $\sqrt{\frac{\rho\overline{v^2}}{\tau_w}}$, distributions do not agree as well as the total shear stress or the longitudinal turbulent component, Figure 6. The measurements of Zoric do not show the drop in the $\sqrt{\overline{v^2}}$ as did that of Klebanoff. An additional set of data recorded by Tieleman (4) very close to the wall reveal a very distinct maximum followed by a sharp decline in the vertical turbulent component.

It is important to point out that the turbulent quantities $\sqrt{\overline{u^2}}$, $\sqrt{\overline{v^2}}$ and $\overline{uv}$ will be presented, unless indicated, nondimensionalized by multiplying by the density and the furthest upstream estimations of the wall shear stress. The study of Sandborn and Horstman (7) suggest the characteristic wall shear stress may be the upstream value when rapid pressure changes occur. Also, as the flow continues over the hills direct quantitative changes in the turbulence terms can easily be compared. In the derivation of the similarity relation between the shear stress and the mean flow the characteristic values are not defined.

Thus, the characteristic shear stress and characteristic length need not be the local wall shear stress and the local boundary layer thickness. For rapid distortion the turbulent properties apparently cannot change quickly, so they will be convected along by the mean flow without undergoing major changes. As noted, the work of Sandborn and Horstman suggested that an upstream value of the surface shear stress may be a possible choice for the present flow cases. For the present evaluation a value of wall shear stress at a specific upstream location (x = 55.8 cm from the crest for smooth surface case, and x = 50.8 cm from the crest for the rough surface case) was used for the characteristic shear stress. The particular locations are somewhat arbitrary, but were selected to be upstream of where the flow is disturbed by the presence of the hill.

The characteristic length must reflect the distortion of the boundary layer coordinate system as the layer develops. If it is assumed that the hill models influence only the part of the boundary layer near the surface and not that of the outer part of the layer; then a characteristic length equivalent to the layer development without the hill might be employed. This assumption of neglecting the perturbation of the hill on the boundary layer thickness length obviously would only be valid when the approach layer is thick compared to the hill height. For the present study it was found that the boundary layer thickness develops nearly linear with x-distance, Zoric and Sandborn (1). The present undisturbed boundary layers for both the smooth and rough surfaces appeared to grow at a rate of 1 cm for every 10 cm in the x-direction. Thus, the characteristic length, δ_e, was taken as the extrapolated boundary layer thickness (in the ratio of 1 to 10) from the measured approach profile thickness. Again this selection of a characteristic length is somewhat arbitrary. It is mainly justified in that it appears to produce a good correlation of the turbulence data over the hills in the outer part of the boundary layer. Other coordinate changes, such as following streamline paths, have been suggested, however for rapid distortions the boundary layer thickness appears to produce the most consistent correlation.

BOUNDARY CONDITIONS

In the atmosphere a wide spectrum of possible approach conditions might exist. In general the effect of a small hill in a deep boundary layer will depend on the energy distribution within the approach flow. The thicker the boundary layer the less the energy will be distributed in the region near the surface; thus the less will be the speedup effect of the hill. Local roughness of the approach surface will also act to remove more energy near the surface (which will also be seen in a thickening of the boundary layer). It is apparent that the higher the hill compared to the boundary layer thickness the larger will be the speedup. Likewise for boundary layers of the same thickness, but different surface roughness, the one over a smoother surface will produce the greater speedup. Two different approach turbulent boundary layers are considered in the present study. The first case is that of a smooth surface, while the second is produced by a long fetch of roughness.

Classical boundary layer theory generally employs a coordinate system which is perpendicular to the surface at all points along and near the surface (curvilinear coordinates). Over the hills this requirement of a curvilinear coordinate can also be expected to be valid.

However, for engineering applications of velocity distributions for wind power use, surveys and data in the vertical direction are desired. For the present study a simple rectangular coordinate system was employed, both for measurements and analysis. The x-distance coordinate originated at the crest of the hill and was measured positive in the upstream direction along the tunnel floor. The y-direction coordinate was measured positive from the local surface of the model at each x-location.

Evaluation of the local surface shear stress from equations (1) or (2) requires the curvilinear-boundary layer coordinate system be employed. As a demonstration of the deviation from boundary layer theory in the use of a vertical coordinate, an estimate of the surface shear from the law-of-the-wall concept was made for both a vertical and a curvilinear-coordinate evaluation, Figure 7. The deviation shown in Figure 7 is mainly important in the lower portion of the hill.

Chapter III

EXPERIMENTAL SETUP

The measurements were taken in the Meteorological Wind Tunnel located in the Fluid Dynamics and Diffusion Laboratory at Colorado State University. The purpose of the experiment was to make surveys of flow characteristics over models of hills emersed in deep turbulent layers. The following sections will discuss the experimental facility equipment and technique.

Wind Tunnel Facility

As mentioned above the measurements were performed in the recirculating Meteorological Wind Tunnel, Figure 8. The flow rate in the tunnel is controlled by a variable-pitch, variable-speed propeller and can be set between 0.3 and 37 m/s with no more than one-half percent deviation from the desired velocity. The test section is approximately 1.8 m square, 27 m in length, and is proceeded by a 9:1 contraction. A zero pressure gradient along the length of the test section was maintained with the adjustable ceiling. The ambient temperature was kept at a constant within $\pm 1/2°C$ by the tunnel air conditioning system.

The experimentation was scheduled in two parts. Each of the two parts had different upstream conditions, however, there were features which were similar to both. At the entrance to the test section during both tests a 1.22 m long section of 1.27 cm gravel fastened to the floor followed by a 3.80 cm high sawtooth fence spanning the width of the tunnel was used to prompt the formation and growth of a large turbulent boundary layer.

In the initial test, a false floor was installed to which the models were secured, Figure 9. The false floor was comprised of three sections--the approach ramp, horizontal test section, and the trailing down ramp. The floor originated 5.60 m from the sawtooth fence. The approach ramp, constructed from .32 cm masonite, was at an angle of 0.84° with the horizontal and had a length of 1.30 m. Following the upstream ramp was a 8.55 m long test section. This section was built from 1.91 cm plywood. The models tested were mounted directly on the plywood. Masonite, .32 cm thick, was then used in assembling the trailing ramp. This ramp was .90 m in length and formed on angle of -1.21° with the horizontal.

During the second test there was no false floor. However, a roughness beginning at 1.83 m from the sawtooth fence and ending at 11.43 m gave a different approach velocity profile, Figure 10. The roughness was made up of aluminum sheets with ribs .16 cm in height. The ribs were randomly spaced normal and parallel to the flow. In this phase of the experimentation the models were mounted directly on the aluminum floor of the wind tunnel.

As mentioned above, a sawtooth boundary-layer trip was used to prompt the growth of turbulent boundary layer. A similarity velocity profile was attained within 6.1 m of the test section entrance. During the initial test the models were set 14.0 m from the entrance and during the second 18.6 m. For both flows the ceiling of the wind tunnel was adjusted to produce a near zero pressure gradient in the free streams of the test section. A slight acceleration occurred along the approach ramp.

Model Description

A series of triangular-shaped hills were designed and used for the tests, Figure 11. The models were constructed using 9 cross-section ribs made of 1.27 cm Plexiglas. The hill surface was placed over the ribs, and was made of .32 cm thick Plexiglas. The crest height of each was 5.08 cm and with aspect ratios of 1/2, 1/4 and 1/6. All models were 183 cm in length. Each of the models were equipped with static pressure taps.

Instrumentation

Actuator and Carriage

The measurements for this experiment required vertical surveys (y-direction) of the flow at particular longitudinal points (x-direction) along the center of the tunnel. To accomplish this the existing carriage of the wind tunnel was employed. The carriage had been constructed on a rail and wheel system. The rails 101.6 cm from the floor run the full length of the test section. This allows the carriage to be positioned at any desired point in the x-direction. A control unit outside the tunnel monitors the vertical movement of the probes and probe support through the boundary layer. This actuator system, with a total traverse of 65 cm, provided a constant voltage change for a particular change in height.

In both tests a stop rod attached tightly to the probe support would make contact with the floor prior to the other instruments. The purpose of the stop rod was to protect the probes from being driven into the floor and possibly damaged. In addition, because the vertical distance between the bottom of the stop rod and the probes were known, y_o was known, Figure 11. An electric indicator was triggered when the stop rod contacted the floor. During the second set of tests a .00254 cm dial indicator was employed to determine more accurately the y-locations of the probes within .5 cm of the wall.

Static Pressure Measurements

Four different probes were used to measure the static pressure. The particular probe used depended on the location of the desired measurements. While making measurements of the mean velocity in the boundary layer above the surface of the hill, two probes were used as static pressure references. A commercial cylindrical pitot-static tube was used along with a commercial disk probe. In general, cylindrical probes are acceptable for free stream and boundary-layer measurements. However, as this type probe nears the wall of the tunnel and in particular the surface of the hill errors occur due to the rapidly varying flow direction. Specifically, the flow becomes something other than parallel to the axis of the cylindrical probe. To compensate for the error due to "pitch" angle between the airflow and pitot-static tube, measurements were made with the disk probe in the vicinity of the surface.

The disk probe samples the local static pressure through a small static tap drilled in the center of the .62 cm thin disk. The disk probe gave systematically lower static pressure readings, but was found to be insensitive to "pitch" angles of ±30°. The geometry of the disk probe restricted measurements near the surface. The cylindrical probe had a diameter of .18 cm with an elliptical nose. The static taps were located 2.22 cm from the support stem. This probe had a .040 cm hole for total pressure measurements.

Static pressure measurements were also taken on the surface of the models and the floor of the tunnel. Each of the models contained a set of static pressure taps distributed over the centerline of the hill, Figure 12. The static taps, sharp edged and .064 cm in diameter, were drilled perpendicular to the model surface. On the floor of the tunnel, static probes constructed from .079 cm i.d. and .139 cm o.d. brass tubing were used. The end of the tubes were soldered closed and a series of taps were drilled in a circle around the circumference of the tubing. The probes were secured to the wall of the tunnel.

When making static pressure measurements, the reference was the static pressure in the free stream. A commercial pitot-static tube .318 cm diameter was used. It was a cylindrical probe with an elliptical nose. The total pressure tap in the tip of the nose was .079 cm in diameter. The static taps were 5.08 cm from the support stem. The only static pressures reported are wall static pressures upstream and on the hills. The purposes of the other static pressure probes were to correct the measurements of the disk probe and their use as reference pressures.

Velocity Measurements

Three different probes were used to measure the total pressure. Two of the probes were commercial pitot-static tubes described earlier and the third was a commerical Kiehl probe.

The two pitot-static probes were used mainly for control and calibration. The pitot-static tube used to survey the static pressure above the hill was also incorporated as a standard used to calibrate the hot-wire probes. The second, which was maintained as a static-pressure reference, monitored the tunnel flow. This second probe was fixed in the free stream approximately 1 m ahead of the models.

The mean velocity measurements made during the surveys were sampled with the Kiehl probe. This probe has the capability of measuring total pressure even when the flow angles are ±40°. The disk probe pressure was used as a reference.

For the range of velocities measured in the present study all three probes agreed with the laboratory standard pitot probe. No correction to the readings were made because of the total pressure probes.

Turbulence and Shear Stress Measurements

Two types of hot-wire data were recorded. In the initial test a cross-wire system was used, while in the second a single horizontal wire fulfilled the requirement. The cross wire employed was not of the usual x wire type, but had one wire normal and one wire yawed to the flow. Both probes were constructed in the Fluid Dynamics and Diffusion Laboratory at Colorado State University. The wire in both cases was 80% platinum and 20% iridium and 1.02×10^{-3} cm in diameter. The length of the wires varied but all were approximately .16 cm. The wires were soldered at each end to a support which was protruding from a ceramic probe shielded by brass tubing. The sensor was then secured to the actuator system. A detailed discussion of the evaluation of the hot-wire output is given in Appendix A.

The hot wires were operated with commercial constant temperature anemometers. The output of the anemometers was amplified and read with mean d.c., and true r.m.s. voltmeters. The voltmeters were equipped with R-C time constants to allow long time averages of the signals. An analog multiplier was employed to obtain the product of the fluctuating output of the cross wires. The multiplier circuit was checked using a sine-wave generator.

Two capacitance pressure transducers were used for pressure measurements. The transducers were calibrated using a standard water micromanometer. These transducers are equipped with self-environmental control to maintain a constant operating temperature. Figure 13 is a schematic of the equipment setup.

Chapter IV

RESULTS AND DISCUSSION

The major effect of a hill is to increase the local velocity near the surface. This effect is of great importance in wind power application. The alteration of the mean wind profile will also be expected to alter the turbulence near the surface. Thus, the present study was directed at evaluating the effect of the hill on the mean and turbulent properties. Such data is needed in order to design wind power units.

Mean Velocity

Primary consideration for wind power is the change in the mean velocity distribution. It was found as the flow proceeded down the tunnel that similarity was maintained, Figure 14. At the windward foot of the model hills a slowdown of the airstream near the surface was evident. Once the flow passed over the base of the hill there was a continuous increase of the velocity near the surface. The greatest speedup for all models tested was recorded at the crest. The similarity was maintained in the outer region of the flow, Figure 15. It is important to note that the outer flow pressure was fixed approximately constant which would help the flow to remain similar in the outer region. The largest increase in velocity for the first flow case was recorded with the 1:4 hill followed by the 1:6 and finally the 1:2, Figure 16.

Flow case II with increased upstream roughness produced the same results for the two models tested, 1:2 and 1:6, Figure 17.

The 1:2 and 1:6 model hills caused a greater mean velocity speedup for flow case I than for flow case II. Flow case I, with a .17 power law profile, produced a maximum speedup, ΔS, of .62 for the 1:6 model hill and .33 for the 1:2 model hill where

$$\Delta S = \frac{U_{crest}(\eta) - U_{upstream}(\eta)}{U_{F.S.}} \tag{16}$$

and $\eta_{crest} = \eta_{upstream} \simeq 0.5$. The 1:4 model hill gave the maximum speedup of .68 for the same flow case. Flow case II, representing a .26 power law profile, was subjected to maximum speedups of .43 and .26 for the 1:6 and 1:2 model hills respectively.

Note that the turbulence terms are non-dimensionalized by dividing by τ_w or τ_{ref}. As described earlier τ_w are values calculated for upstream profiles. The values used were $\tau_w = .1074\ n/m^2$ for flow case I at $x = 5.88$ cm and $.0952\ n/m^2$ at $x = 50.80$ cm for flow case II.

Longitudinal Turbulent Velocities

The longitudinal turbulent velocities in both flow cases varied in the same manner. At the foot of the hill the greatest magnitudes were recorded. This was succeeded by a continuous decrease in $\sqrt{\overline{u^2}}$ near the surface with the decrease being greatest at the crest. A greater decrease in the longitudinal turbulent velocity component was noted for the second flow case with the larger values of approach turbulence. The alteration of the turbulence was restricted to that region near the wall, Figures 18, 19, 20, 21.

The longitudinal turbulent velocity component, $\sqrt{\overline{u^2}}$, compared closely with that found by Zoric (2) for the first test, Figure 22. As expected for the second flow case the $\sqrt{\overline{u^2}}$ component did not agree with Zoric but was higher. In both cases the measurements of the longitudinal turbulent velocity component were reproducible, Figure 23.

Vertical Turbulent Component

The vertical turbulent component, $\sqrt{\overline{v^2}}$, which was measured only in flow case I also varied as it passed over the hill. This turbulent component decreased up to the base of the hill, following them was a continuous increase in $\sqrt{\overline{v^2}}$ to the crest. The change only involved the flow near the surface, Figures 24 and 25. As discussed in Chapter II the increase in $\sqrt{\overline{v^2}}$ was expected from results for a contracting flow. When compared to Zoric's data in the outer region, the values obtained for $\sqrt{\overline{v^2}}$ were close. However, when compared to Tieleman's data (4) near the wall the measurements appear to be somewhat lower, Figure 26. (The data reported by Tieleman (4) were taken at a station almost 30 meters downstream in the tunnel compared to the present data taken at a distance of 14 meters.) The disagreement may in part be attributed to the strong velocity and turbulent gradients acting on the yawed wire in this region. Tieleman compensated for the gradients when he presented his results. A discussion of this is given by Sandborn (12). In addition, the first flow case may not be a true flat plate flow. There could have been some change in the flow because of the false floor.

Shear Stress Distribution and Surface Static Pressure

As the flow passed from the furthest upstream station toward the base of the hills there was a decrease in surface shear stress and an increase in the surface static pressure. After passing the foot of the hill, the trend reversed and an increase in wall shear was present. The surface static pressure decreased along the reach of the hill. Figure 27 shows the change in surface shear stress and surface static pressure as friction and pressure coefficients where

$$C_f = \frac{\tau_{wall\ local}}{1/2\ \rho U^2_{local}} \tag{17}$$

and

$$C_p = \frac{P_{static\ local} - P_{static\ F.S.}}{1/2\ \rho U^2_{local}} \tag{18}$$

The surface shear stress at each station was estimated using the Ludwieg-Tillmann equation and the "law of the wall." The values found using the "law of the wall" may be somewhat questionable for the pressure gradients obtained. Based on work done by Patel (5) which was described earlier, the "law of the wall" applies within approximately 6% in the range of

$$0 > \frac{\nu}{(\rho U_\tau^3)} \frac{dP}{dx} > -.007 \tag{4}$$

For the present study the range was exceeded. For the 1:6 hill an average of about $\Delta \simeq .032$ was computed. As a result, the values obtained for the wall shear stress on the surface of the hill would be expected to be consistently high. However, the numbers obtained do give approximate values. For the 1:6 and 1:2 hills the Ludwieg-Tillmann equation gives lower values than the "law of the wall."

The affect of the hill on the shear stress distribution was a local one. The shear stress distribution remained unaffected in the outer region. Near the wall the distribution changed accordingly with the wall shear stress, Figure 28. For Figures 28 ai, aii, bi, ci, cii, 29, and 30 all the points shown were calculated from the similarity equation (15). For the other cases shown on Figure 28 the data points were evaluated from the cross-wire data. The curves through the cross-wire data were faired using the upstream similarity distribution and an approximate extrapolation to the known surface shear stress value. The local slope of most of the shear stress curves at the wall ($\partial\tau/\partial y|_{y=0} = \partial P/\partial x$) are very steep, and as such were not shown on the fairings.

In Chapter II an explanation was given for the method used to evaluate the upstream shear stress distributions. Because the analysis depends on the mean velocity measurements and not the direct measure of the Reynolds stresses it was possible to evaluate for both flow cases the upstream shear stress distribution. When compared to Zoric's data, it was found that the shear stress distribution of the first test was repeatedly lower, Figure 29. Again this is attributed to the false floor. The second flow case yielded a similar result. However, these results were higher than that found in flow case I but still less than what Zoric found, Figure 30.

The Reynolds stresses, $\overline{uv}$, were employed to evaluate the vertical turbulent velocity component $\sqrt{\overline{v^2}}$. The cross correlation $\overline{uv}$ was the most uncertain term to evaluate. It was believed that a multiplying circuit used in the measurements did not function as well as desired. The result was a greater scatter in the data for the $\overline{uv}$ terms. Determination of the $\sqrt{\overline{v^2}}$ terms was also affected but since it is presented as a square root the scatter does not appear so pronounced.

Chapter V

CONCLUSIONS

The present investigation studied two different flow cases subjected to three different triangular hills. These two-dimensional model hills with aspect ratios of 1:2, 1:4 and 1:6 changed the mean and turbulent properties of the flow near the surface. From the experimental evidence the following conclusions can be drawn.

1. As the flow progressed from the upstream station to the crest there was no effect from the hill on the flow properties in the outer region. The flow properties included are mean velocity and the longitudinal and vertical turbulent velocities along with the shear stress.

2. For the region near the wall there was a velocity speedup as the flow passed over the hill with the maximum above the crest. The greatest speedup was for the 1:4 hill.

3. The longitudinal turbulent velocity, $\sqrt{\overline{u^2}}$, increased to the foot of the hill then decreased as the flow passed over the hill. The decrease is greater for a turbulent boundary layer with larger turbulent velocities. The decrease is on the order of 12%.

4. The vertical turbulent velocity $\sqrt{\overline{v^2}}$ decreased as the flow approached the base of the hill then increased to the summit. Both the increase in the vertical turbulent velocity and the decrease in the longitudinal turbulent velocity were consistent with theoretical results for a contracting flow.

5. The shear stress term $\overline{uv}$ and the wall shear stress decreased from the upstream station to the base of the hill. Over the hill an increase of the shear stress was found.

6. A decrease in surface pressure and increase in wall shear coincided with the increase in mean velocity. The opposite was true when the mean velocity decreased.

REFERENCES

1. Zoric, D. and Sandborn, V. A.: Similarity of Large Reynolds Number Boundary Layers. Boundary Layer Meteorology, Vol. 2, No. 3, pp. 326-333, 1972.

2. Zoric, D. L.: Approach of Turbulent Boundary Layer to Similarity. Ph.D. Dissertation, Colorado State University, Report CER68-69DLZ9, 1968.

3. Ribner, H. S. and Tucker, M.: Spectrum of Turbulence in a Contracting Stream. National Advisory Committee for Aeronautics Rep. 1113, 1953.

4. Tieleman, H. W.: Viscous Region of Turbulent Boundary Layer. Ph.D. Dissertation, Colorado State University, Report No. CER67-68HWT21, 1967.

5. Prandtl, L.: Recent Results of Turbulence Research. NACA Tech. Memo. 720, 1933.

6. Patel, V. C.: Calibration of the Preston Tube and Limitations on Its Use in Pressure Gradients. J. Fluid Mech., Vol. 23, Part 1, pp. 185-208, 1965.

7. Sandborn, V. A. and Horstman, C. C.: Boundary Layer Shear Stress in Subsonic and Supersonic Flow. Symposium on Turbulent Shear Flow, Pennsylvania State University, 1977.

8. Klebanoff, P. S.: Characteristics of Turbulence in a Boundary Layer with Zero Pressure Gradient. NACA TN 3178, 1954.

9. Sandborn, V. A.: Class Notes for Experimental Methods in Fluid Mechanics. Civil Engineering Department, Colorado State University, CER71-72VAS40, 1972.

10. Sandborn, V.A.: A Review of Turbulence Measurements in Compressible Flow. NACA Tech. Memo., X62, 337, March, 1974.

11. Schlichting, H.: Boundary Layer Theory. McGraw-Hill Book Company, Inc., New York, 1960.

12. Sandborn, V. A.: Effect of Velocity Gradients on Measurements of Turbulent Shear Stress. Colorado State University, AIAA J., Vol. 14, No. 3, pp. 400-402, March, 1976.

FIGURES

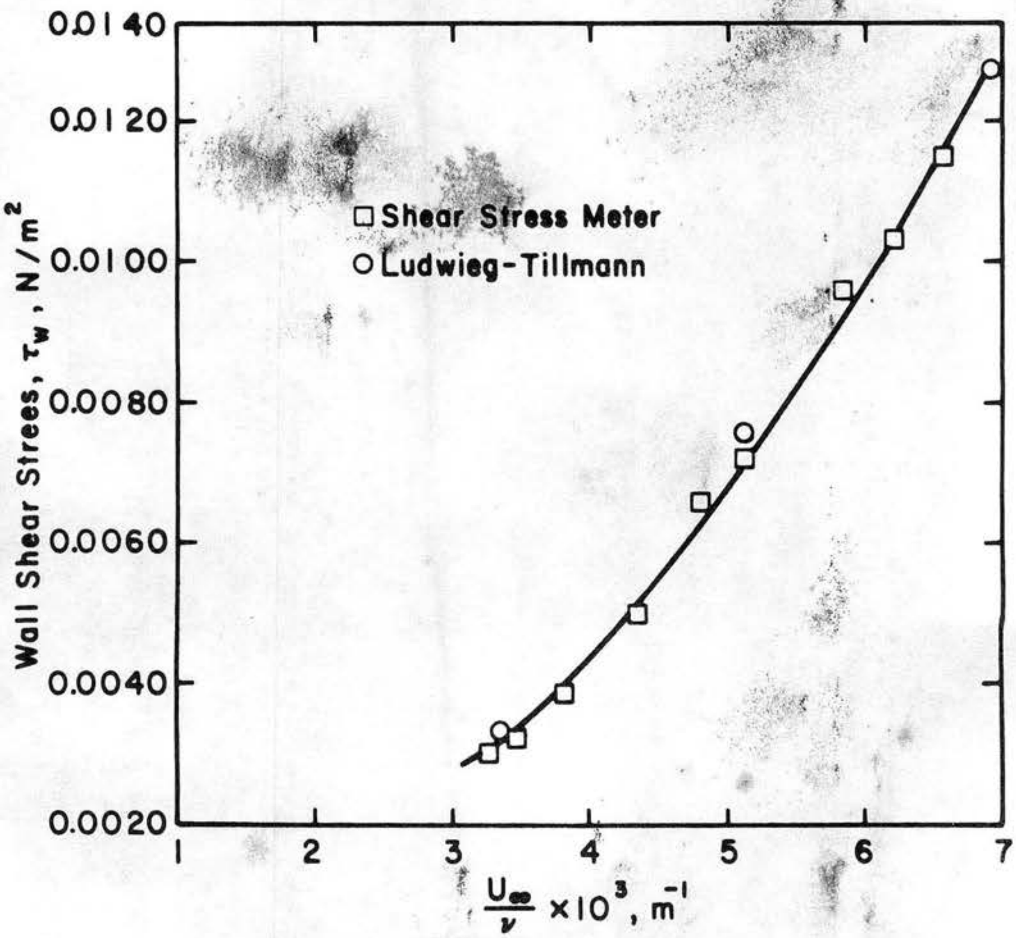

Figure 1. Comparison of Ludwieg-Tillmann equation and shear-stress meter (4).

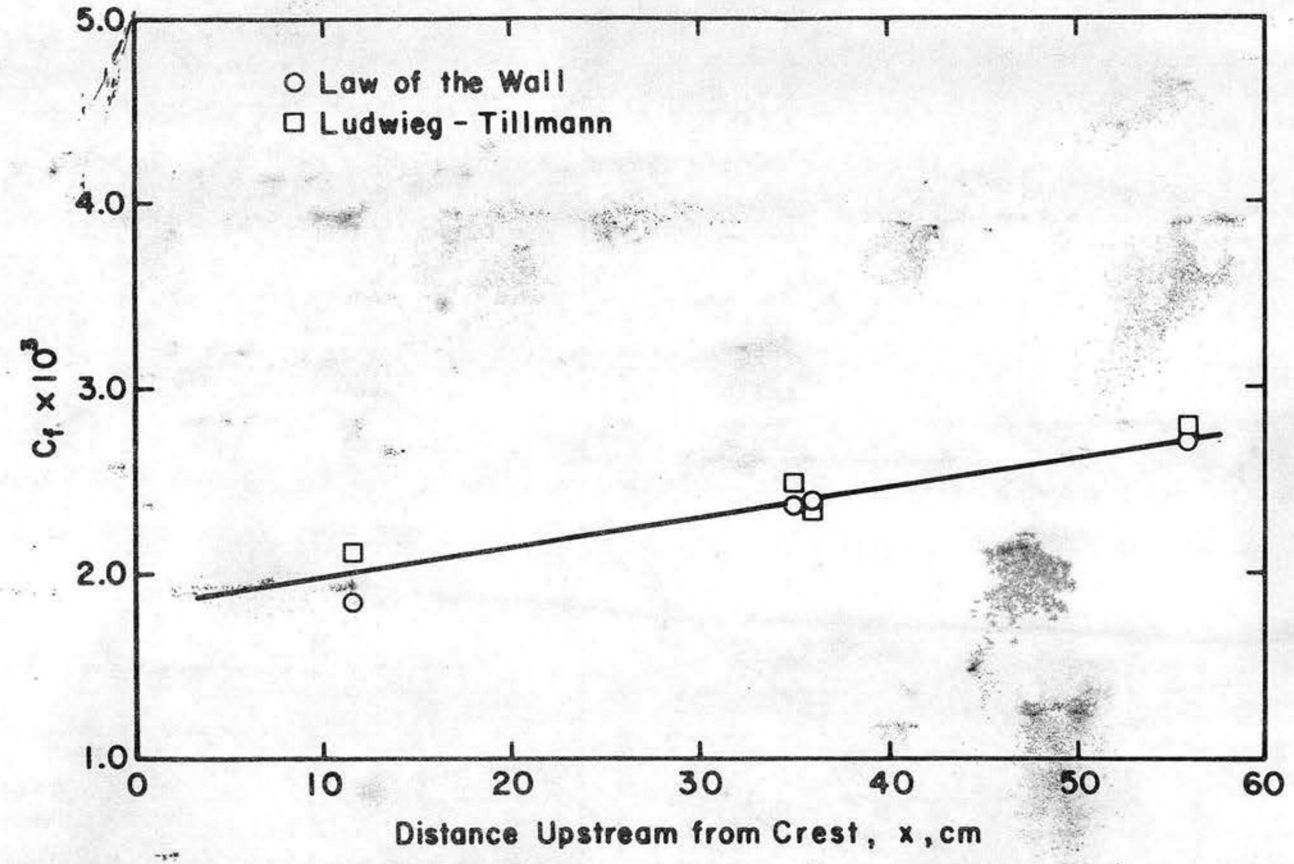

Figure 2. Comparison of shear stress evaluated by Ludwieg-Tillmann equation and "law of the wall" on flat plate.

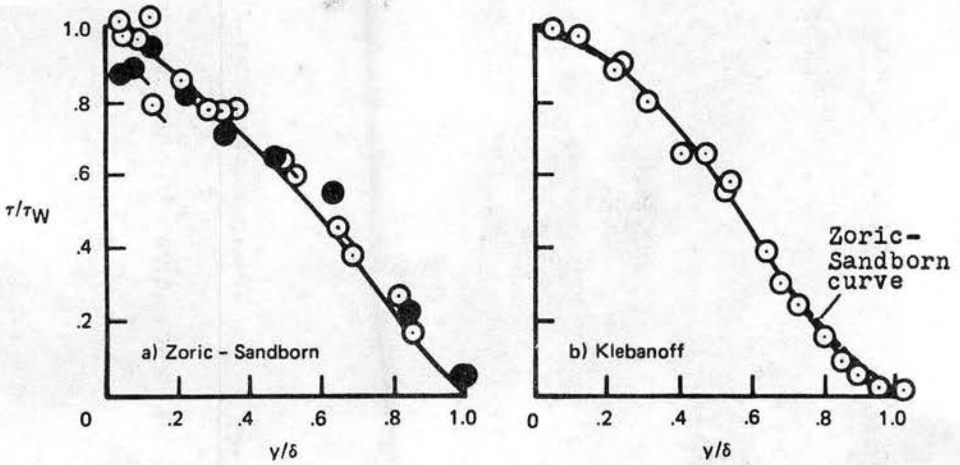

Figure 3. Comparison of shear stress distribution zero pressure gradient and values determined from equation 15,(7).

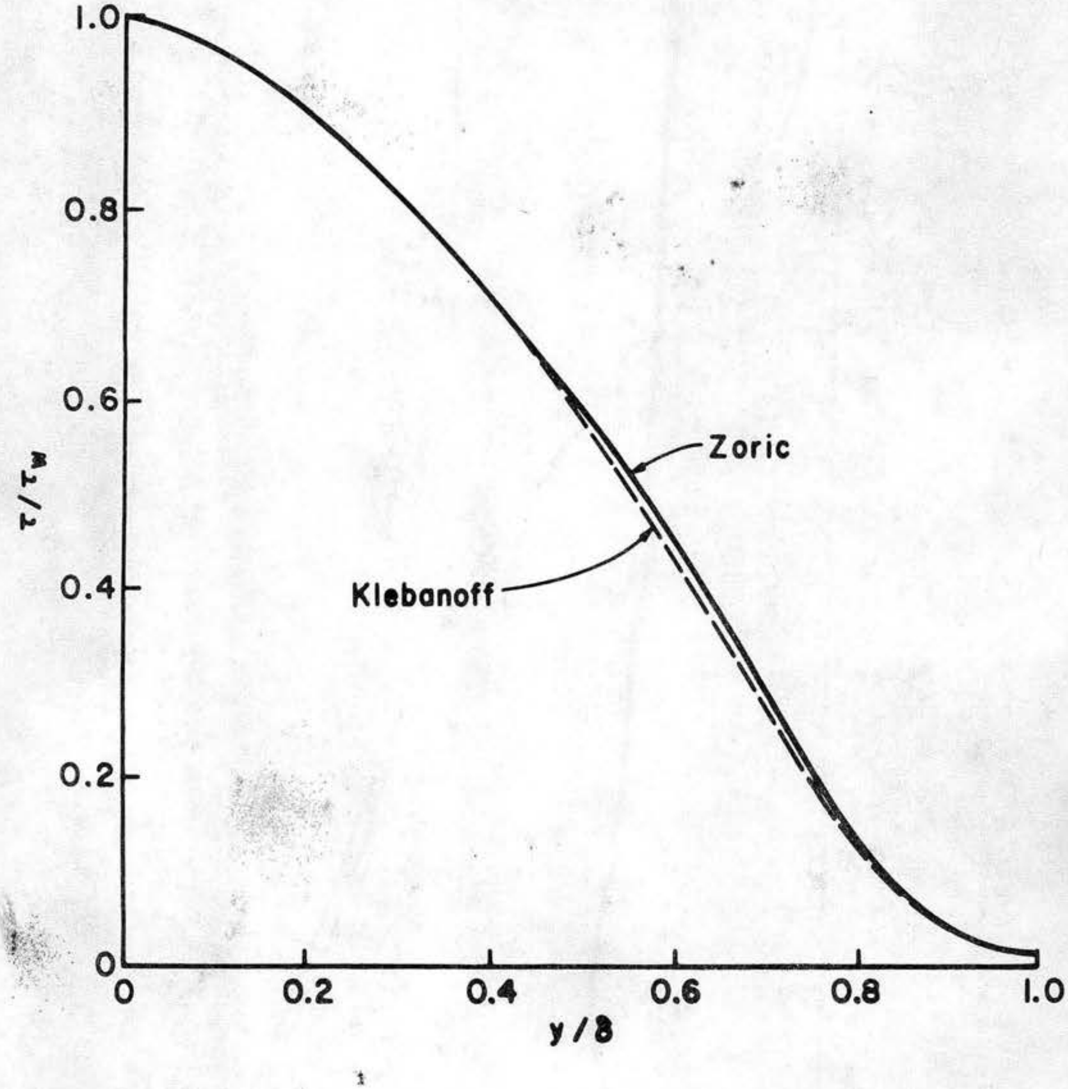

Figure 4. Comparison of shear stress measurements by Klebanoff and Zoric (10).

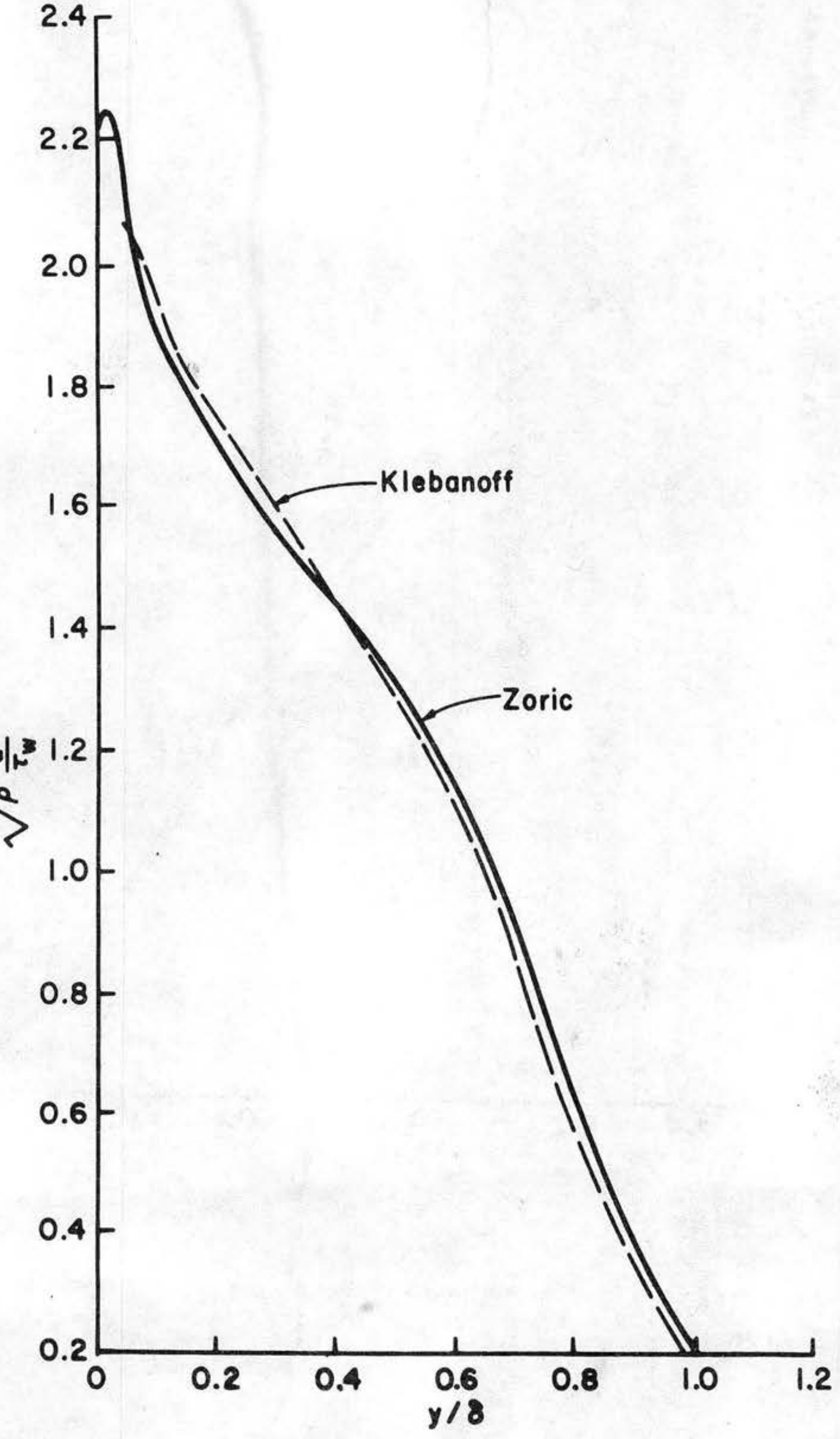

Figure 5. Comparison of flat plate longitudinal turbulent velocity distribution of Klebanoff and Zoric (10).

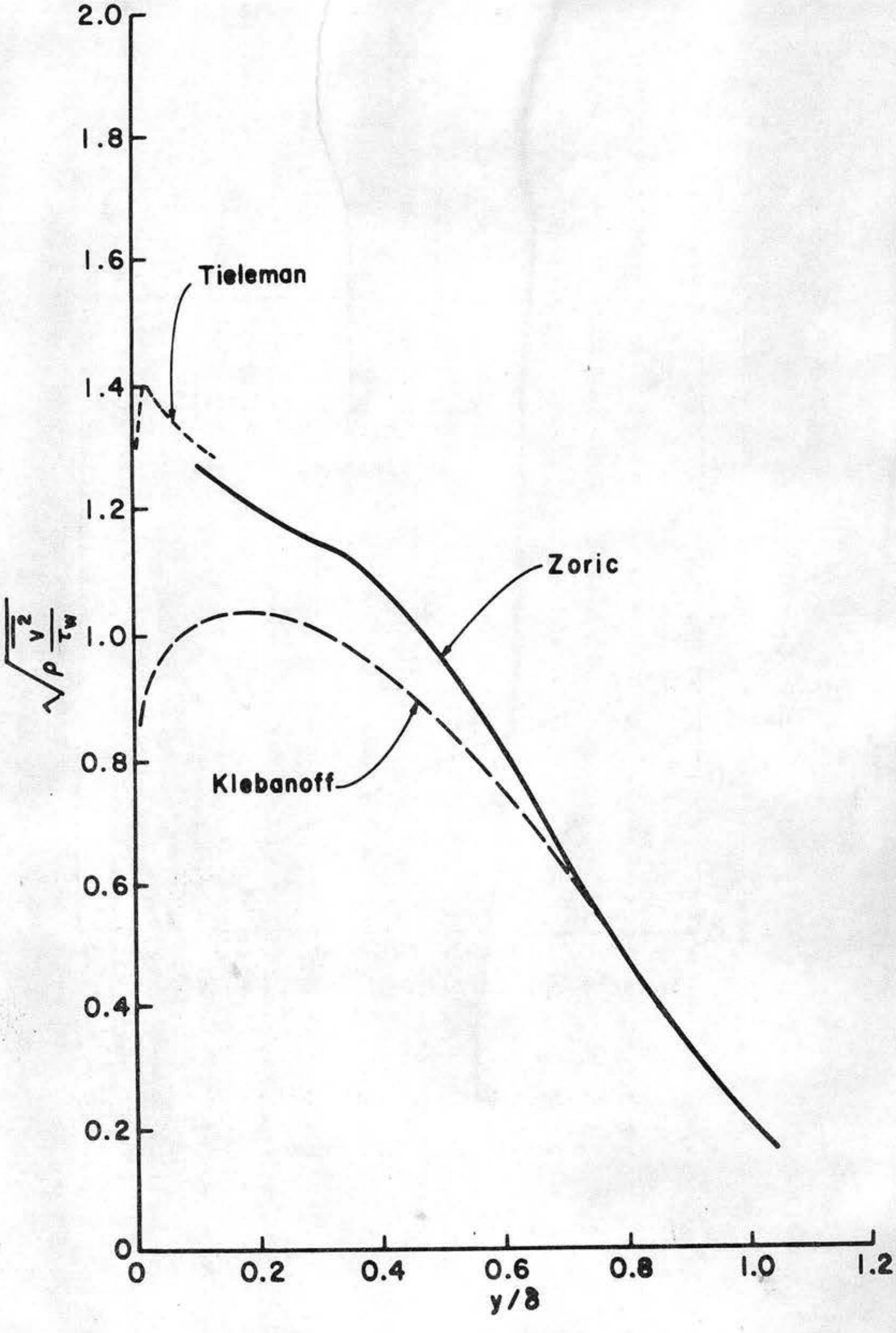

Figure 6. Comparison of flat plate vertical turbulent velocity distribution of Klebanoff, Zoric and Tieleman (10).

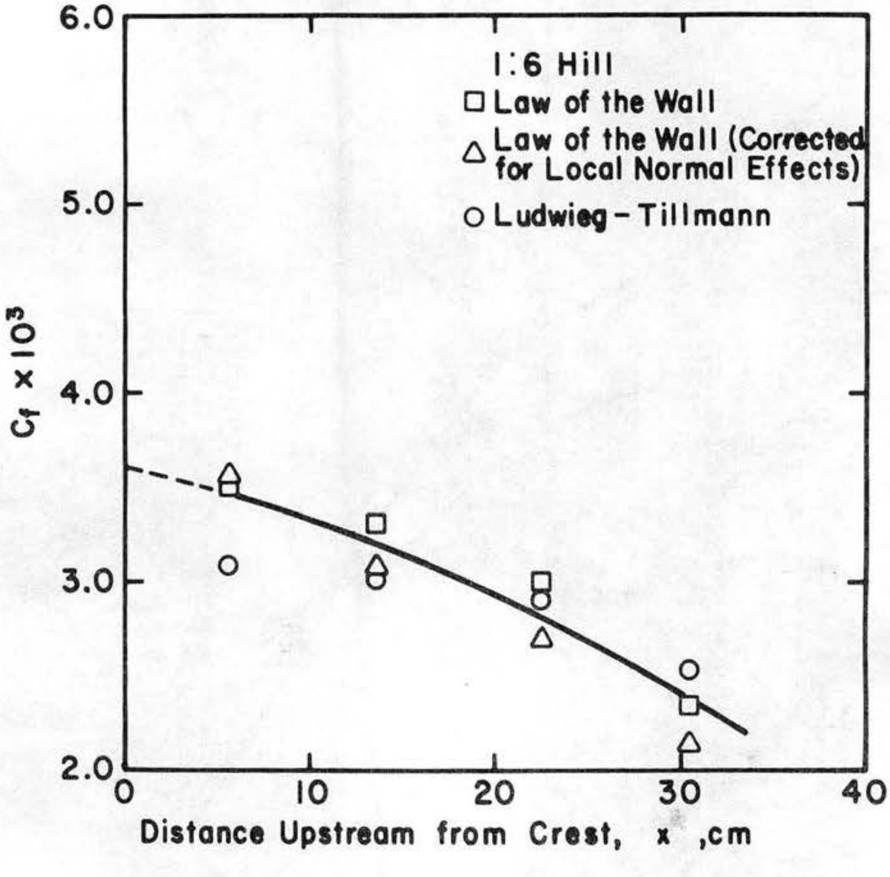

Figure 7. Shear stress evaluated by the "law of the wall" for standard coordinates and curvilinear coordinates.

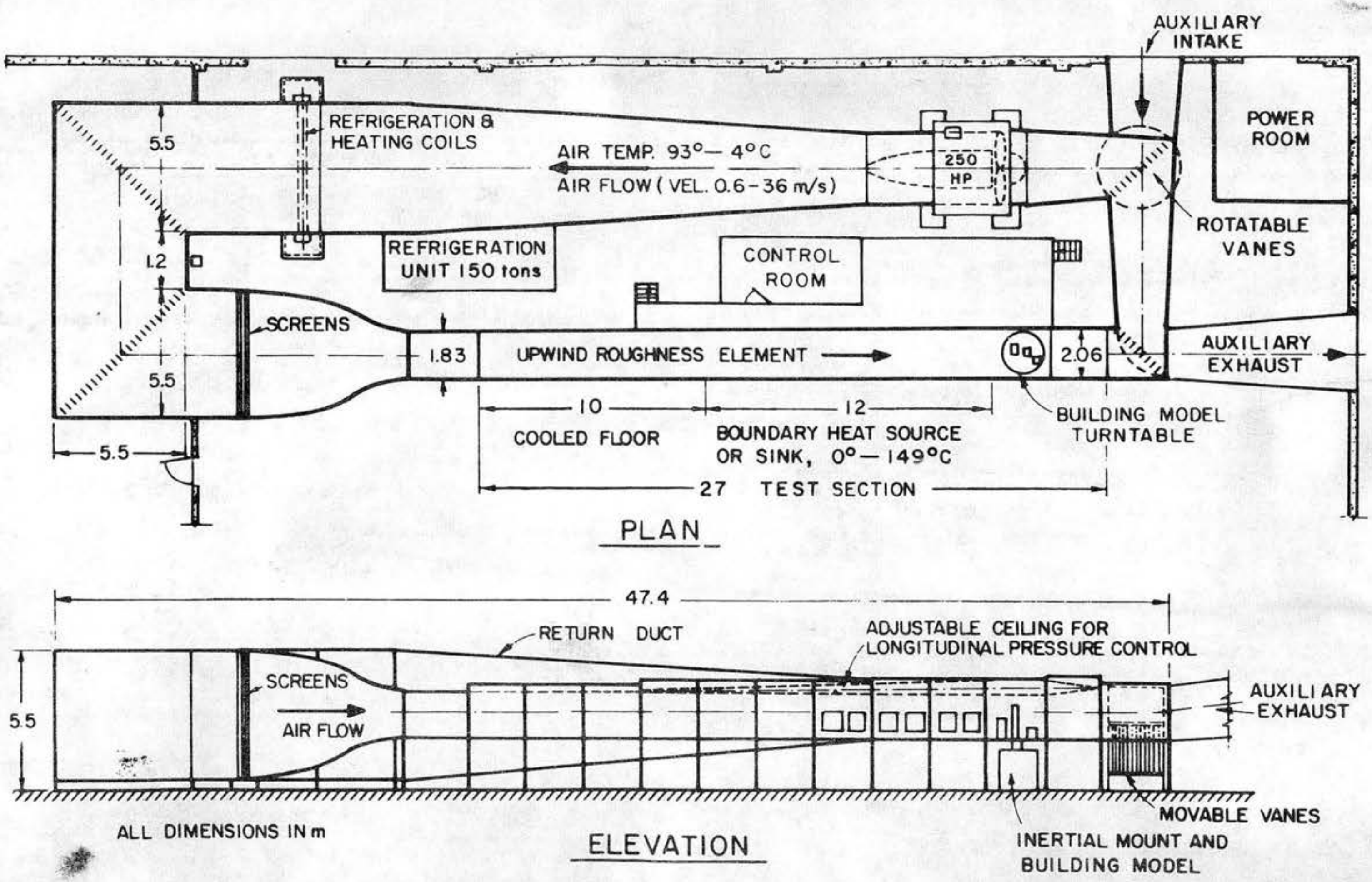

Figure 8. METEOROLOGICAL WIND TUNNEL (Completed in 1963)

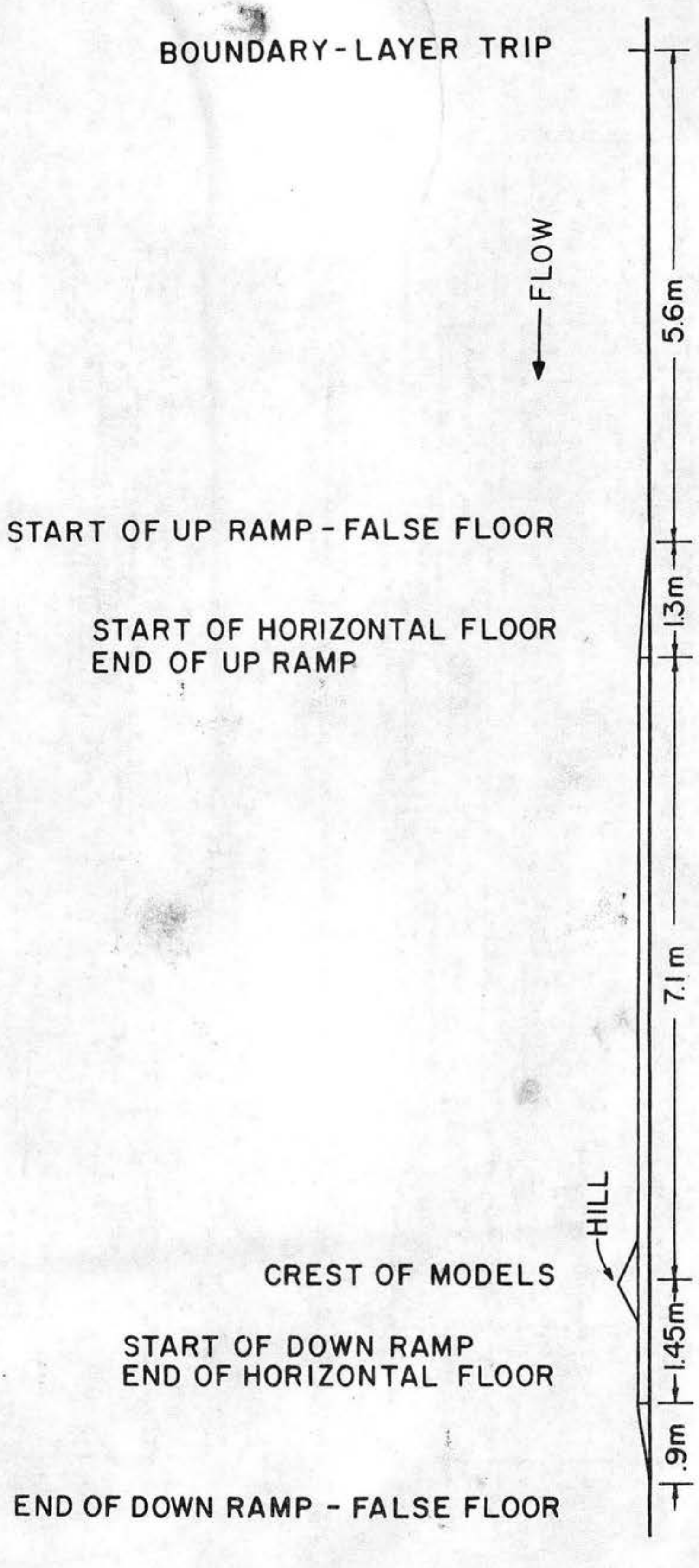

Figure 9. Tunnel setup for flow case I.

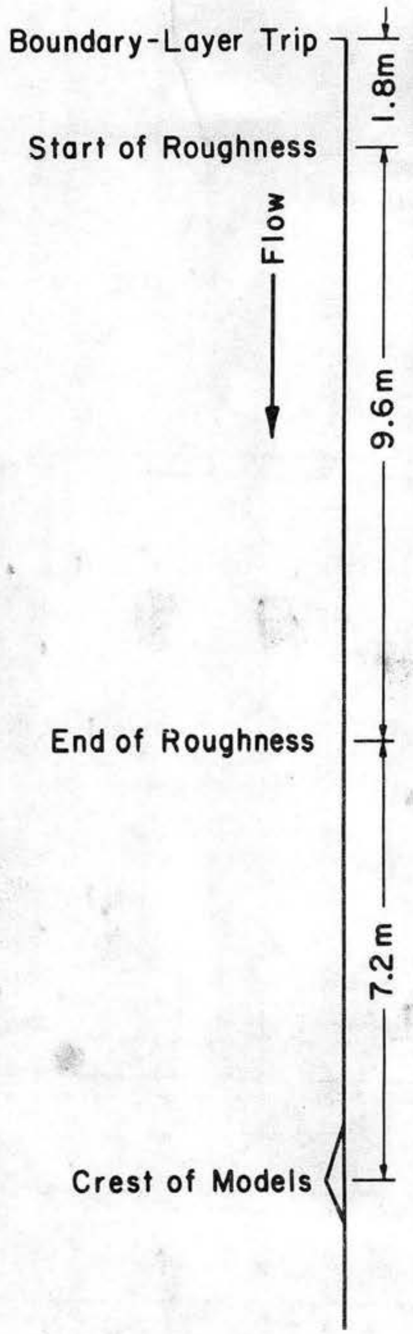

Figure 10. Tunnel setup for flow case II.

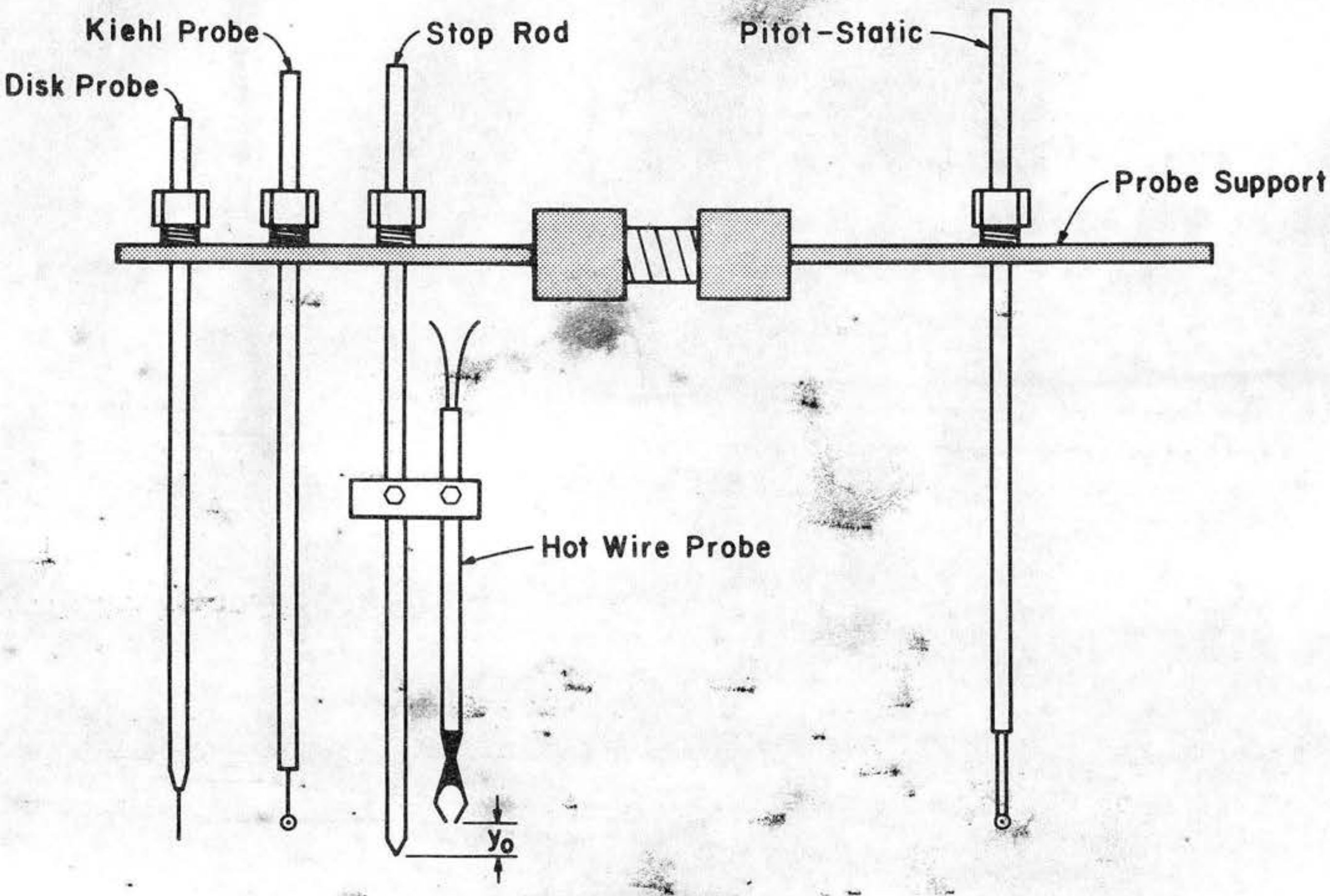

Figure 11. Schematic of probes.

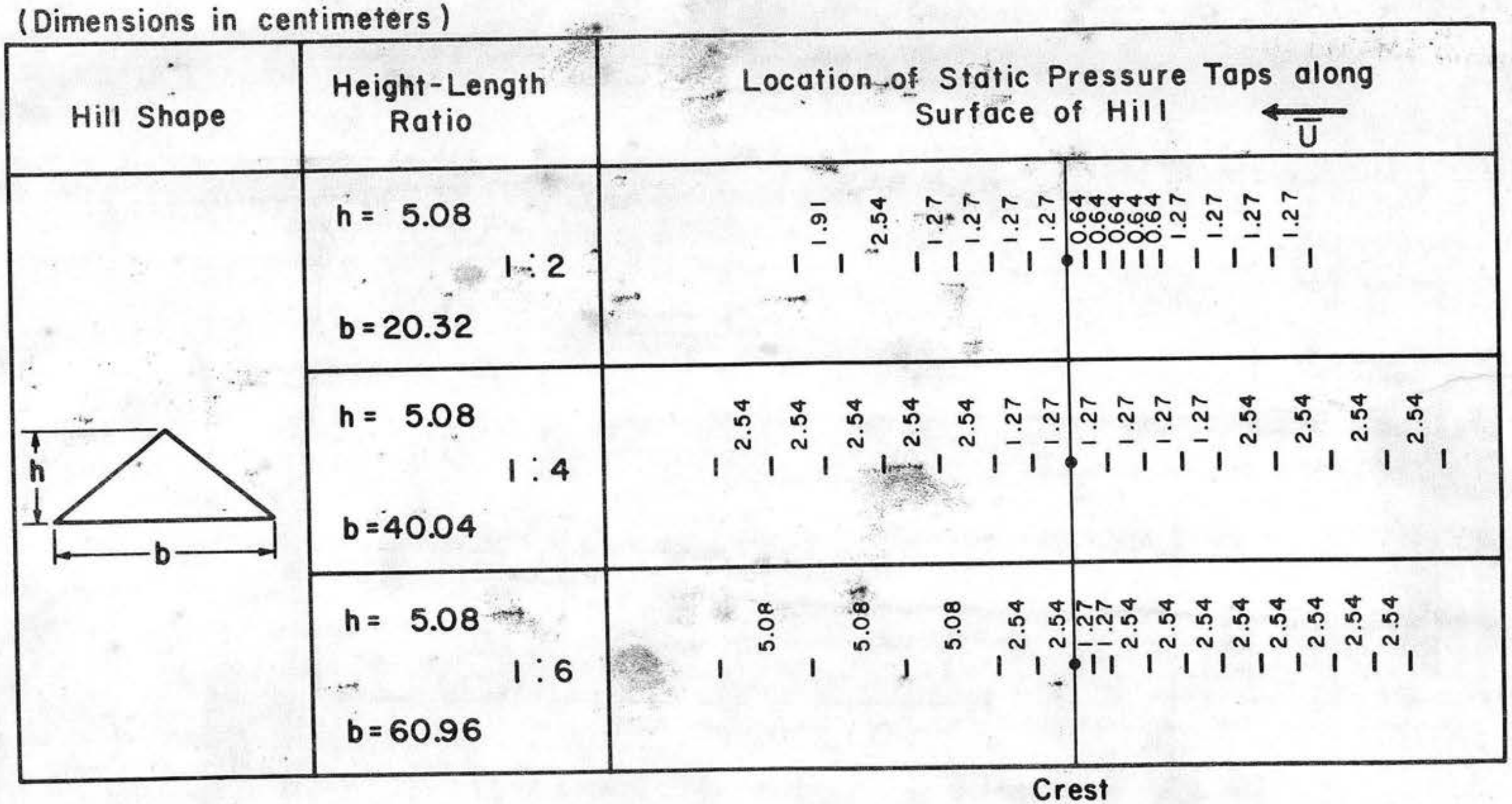

Figure 12. Model description and instrumentation location.

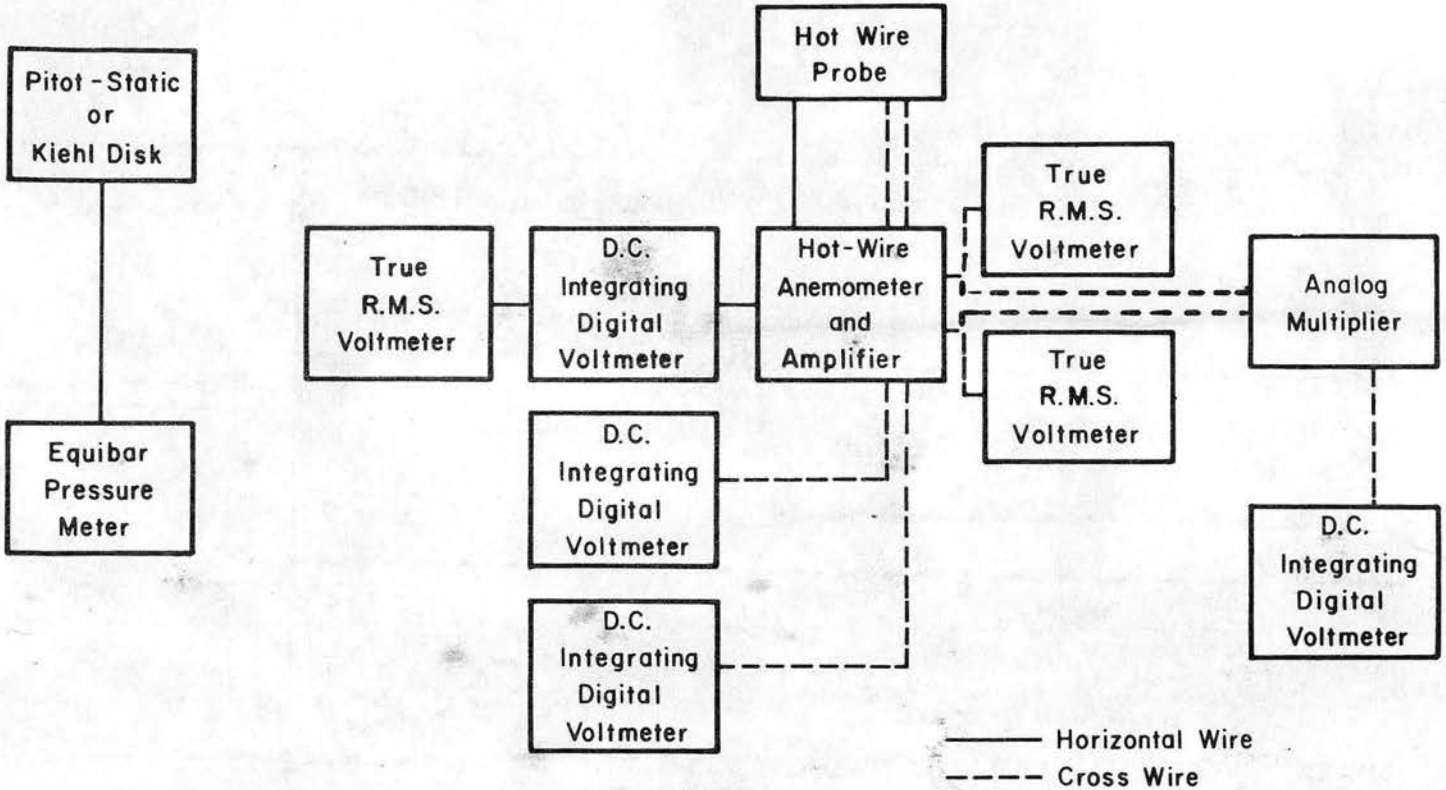

Figure 13. Schematic of equipment setup.

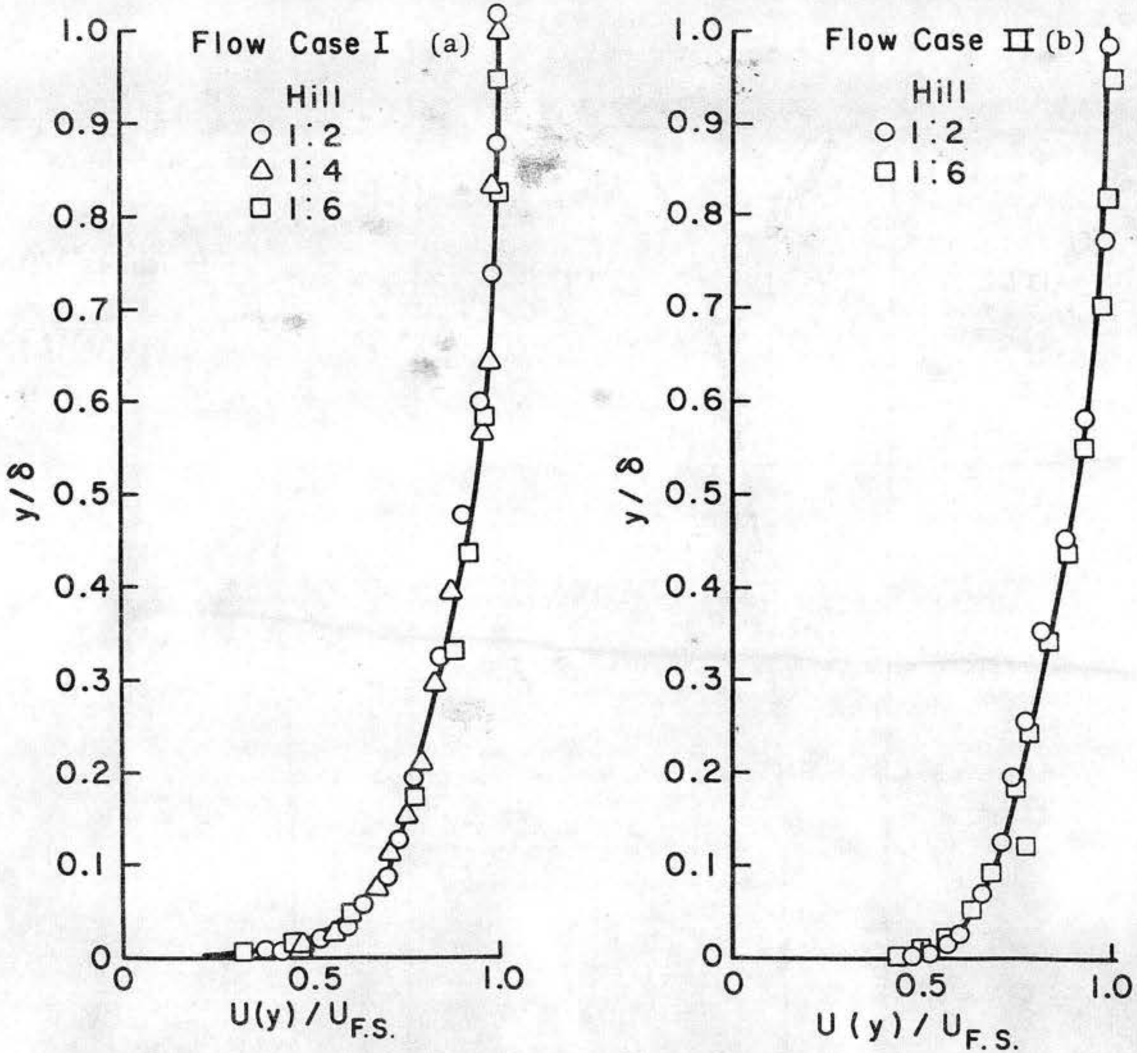

Figure 14. Velocity similarity profiles for both flow cases.

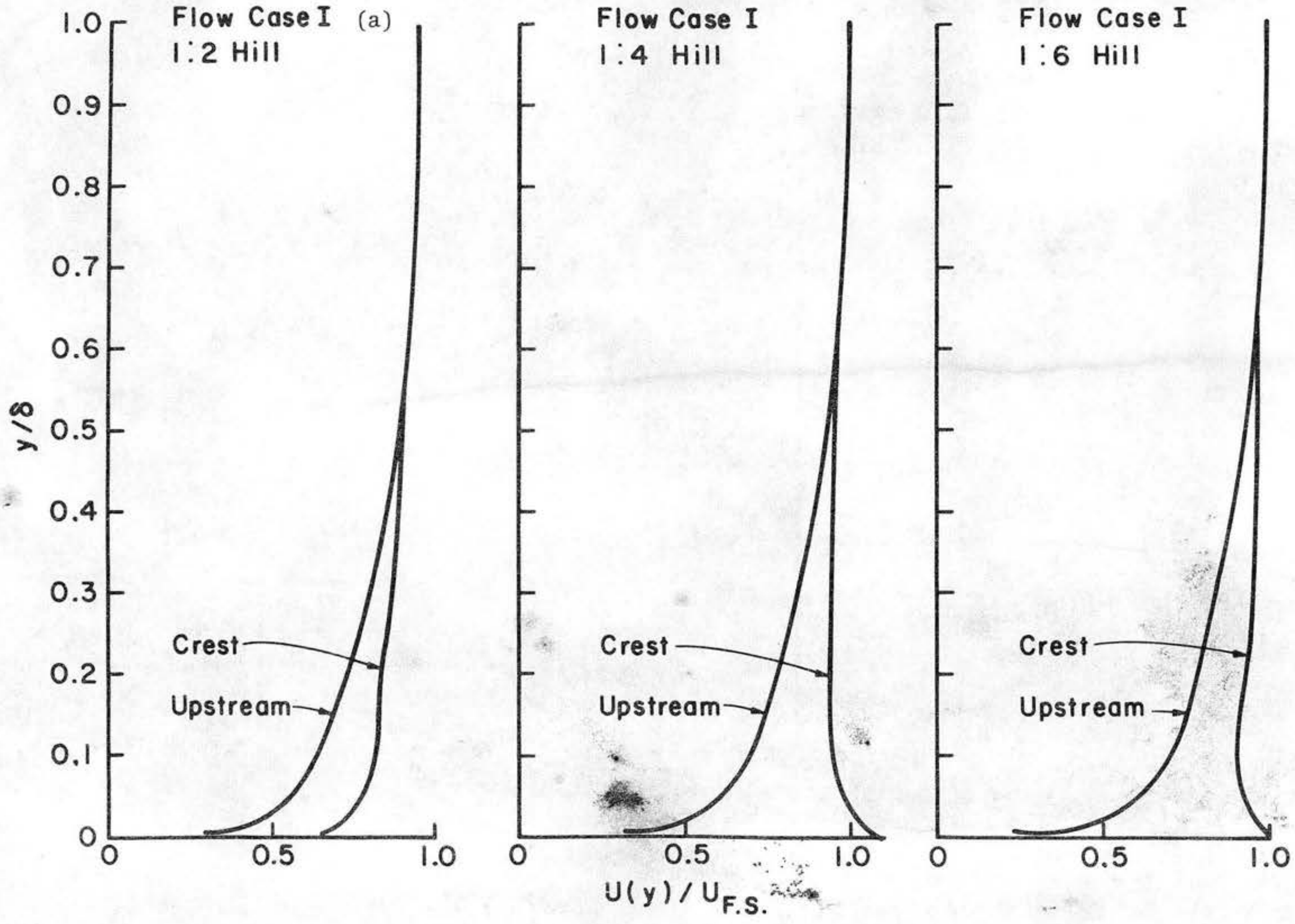

Figure 15a. Upstream similarity velocity profiles and velocity profiles at the crest.

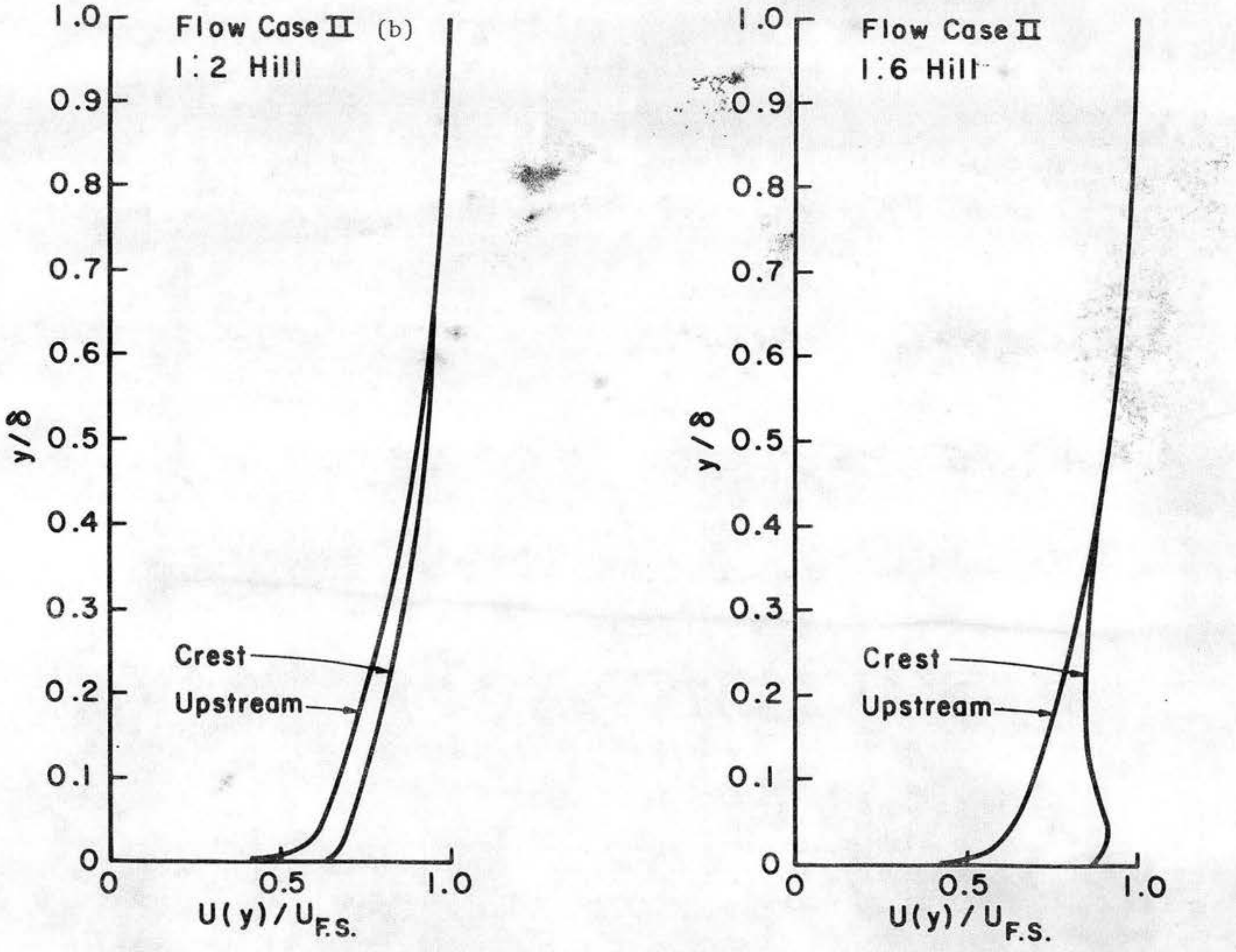

Figure 15b. Upstream similarity velocity profiles and velocity profiles at the crest.

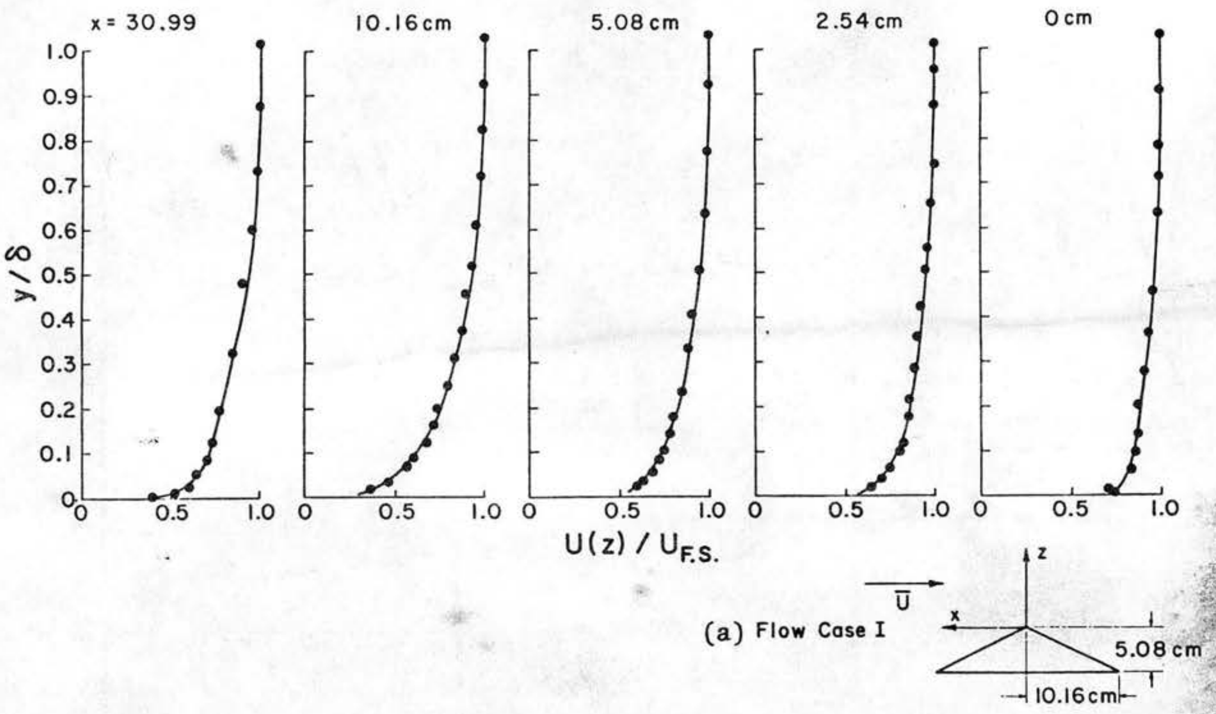

Figure 16a. Velocity profiles flow case I.

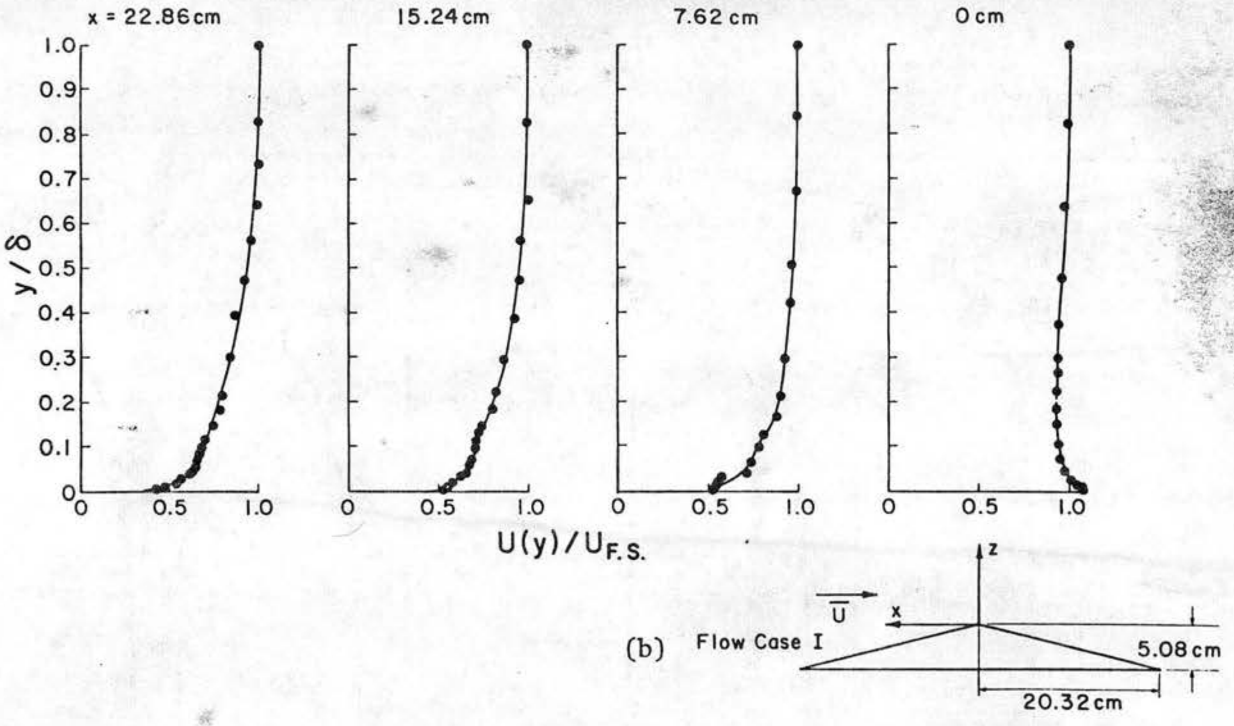

Figure 16b. Velocity profiles flow case I.

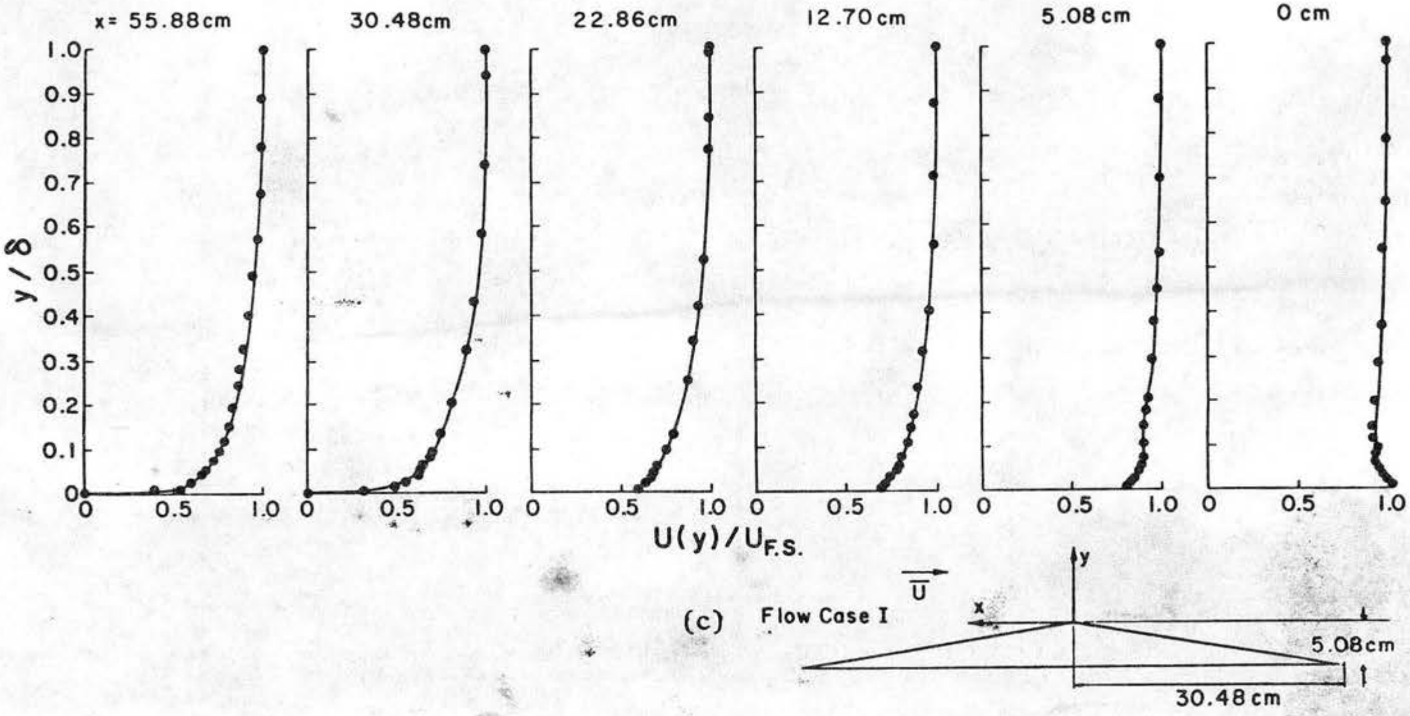

Figure 16c. Velocity profiles flow case I.

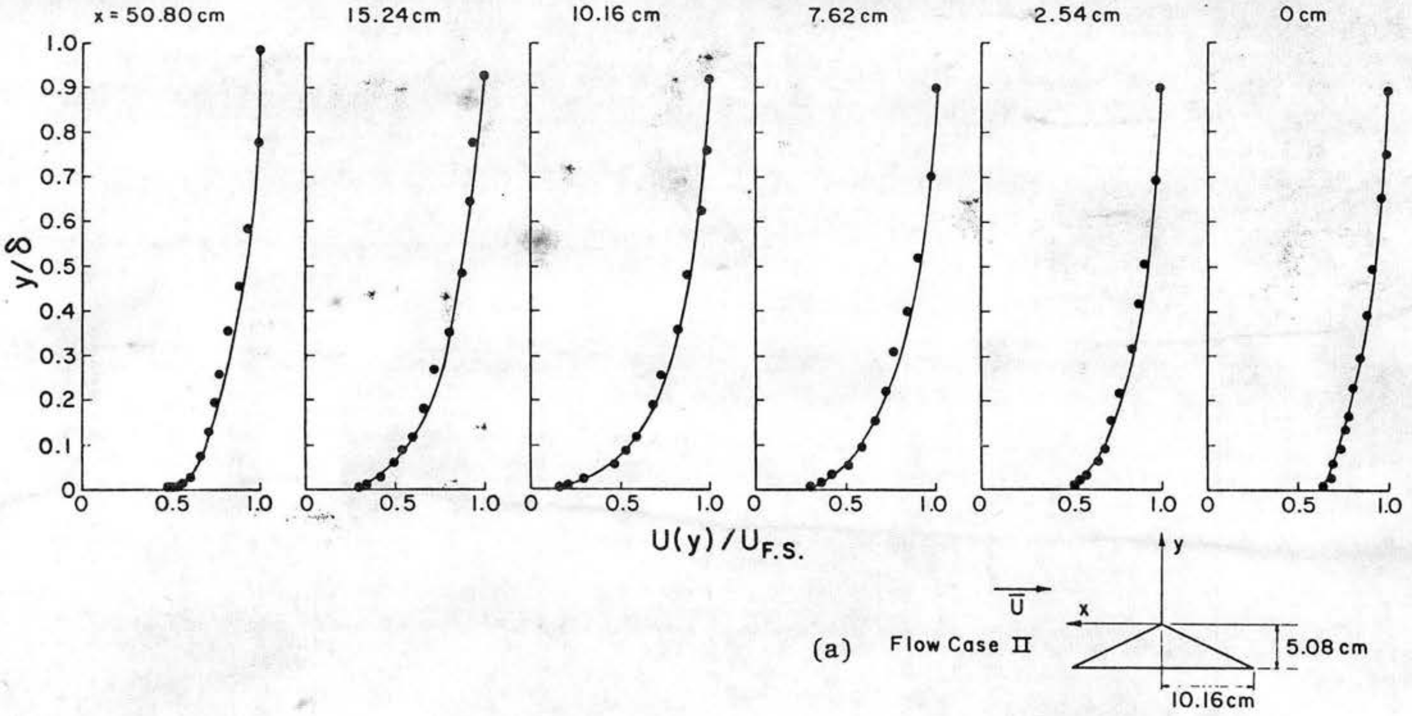

Figure 17a. Velocity profiles flow case II.

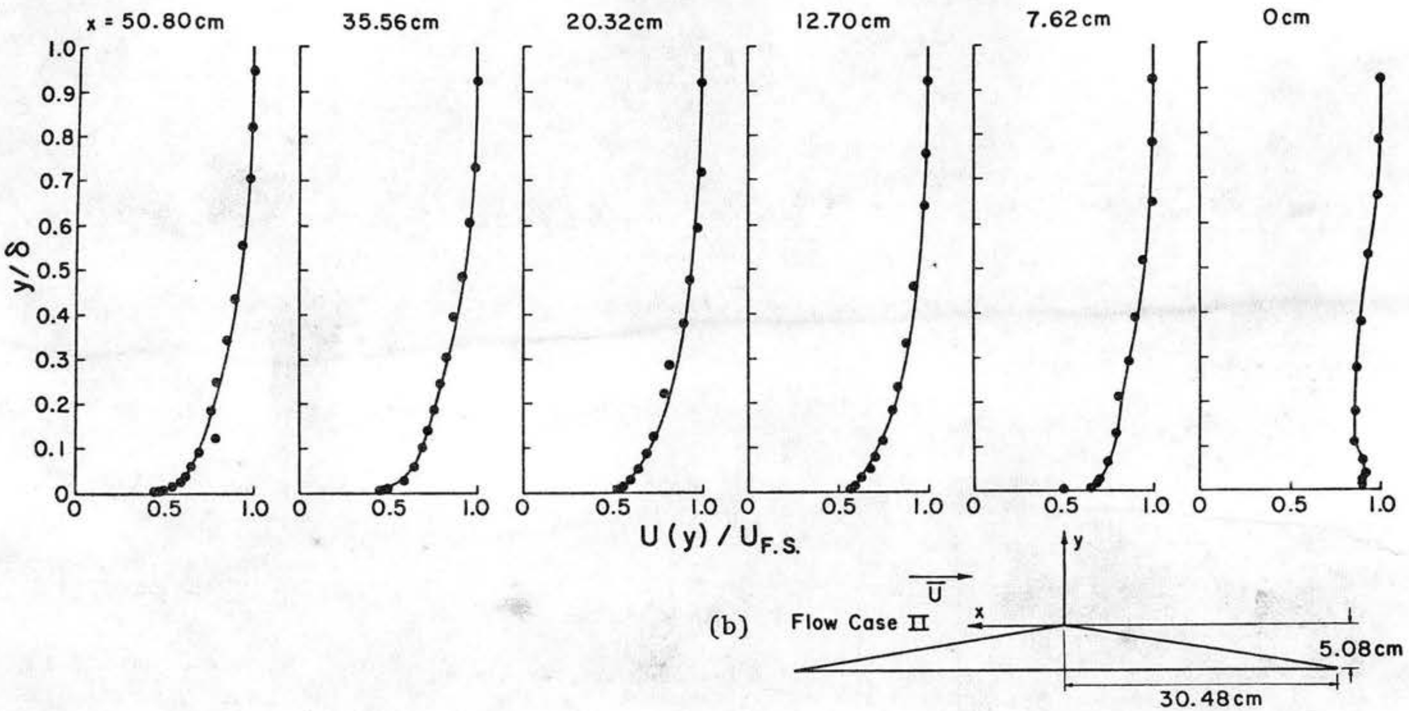

Figure 17b. Velocity profiles flow case II.

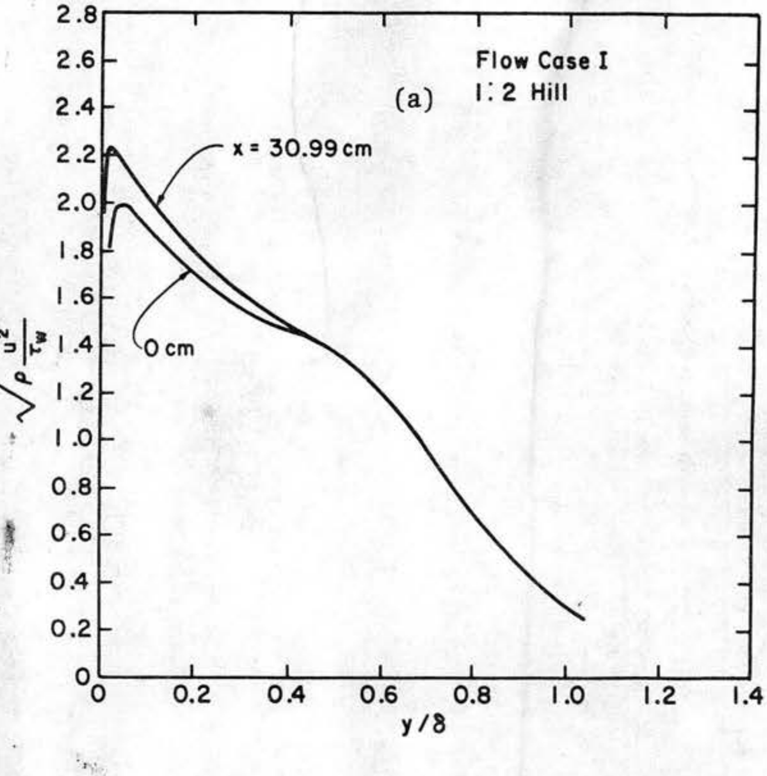

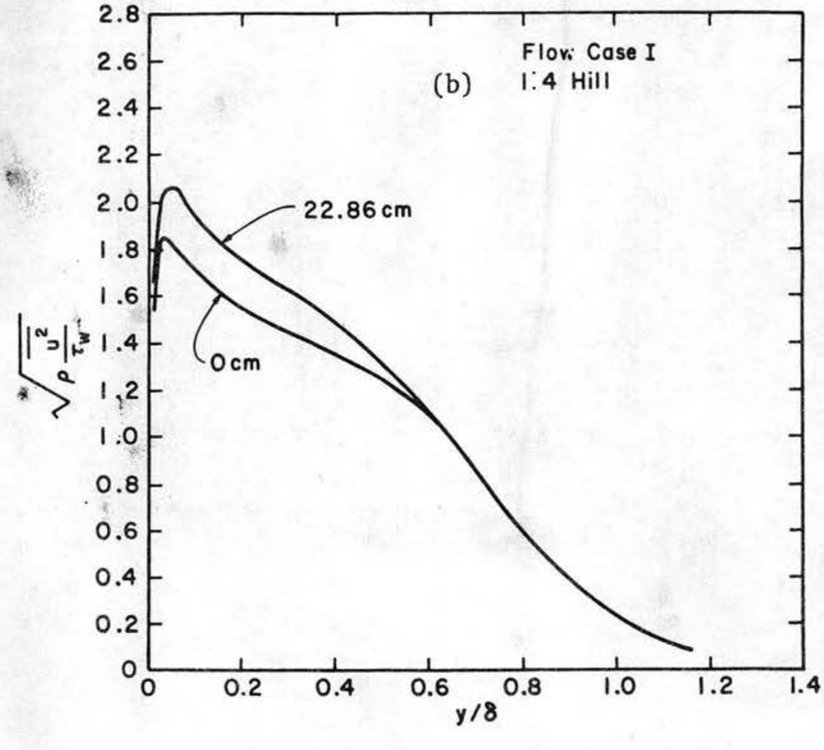

Figure 18. Upstream $\sqrt{\rho \frac{\overline{u^2}}{\tau_w}}$ measurements compared to $\sqrt{\rho \frac{\overline{u^2}}{\tau_w}}$ measurements at crest. Flow case I.

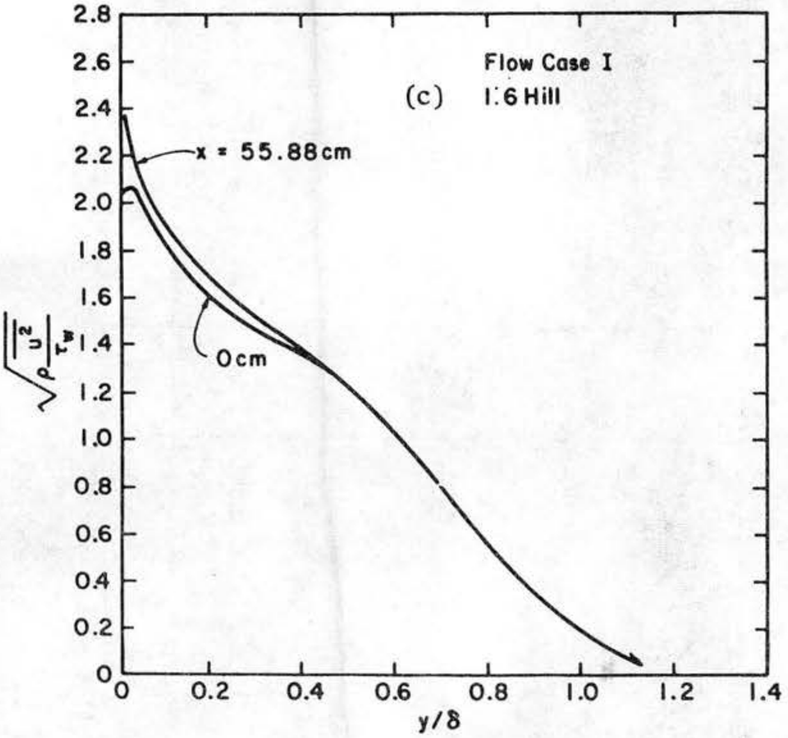

Figure 18 continued. Upstream $\sqrt{\rho \frac{\overline{u^2}}{\tau_w}}$ measurements compared to $\sqrt{\rho \frac{\overline{u^2}}{\tau_w}}$ measurements at crest. Flow case I.

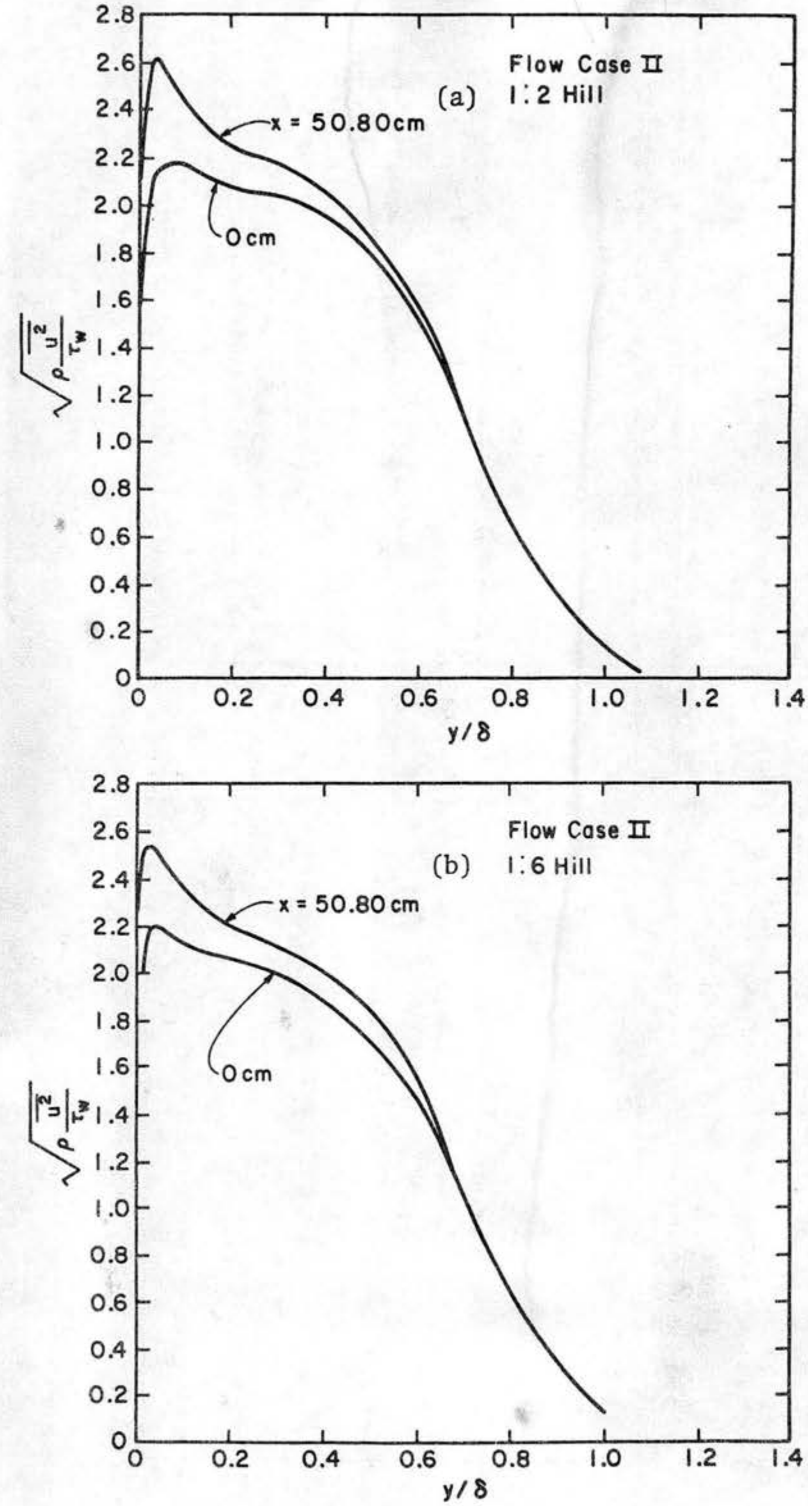

Figure 19. Upstream $\sqrt{\rho \frac{\overline{u^2}}{\tau_w}}$ measurements compared to $\sqrt{\rho \frac{\overline{u^2}}{\tau_w}}$ measurements at crest. Flow case II.

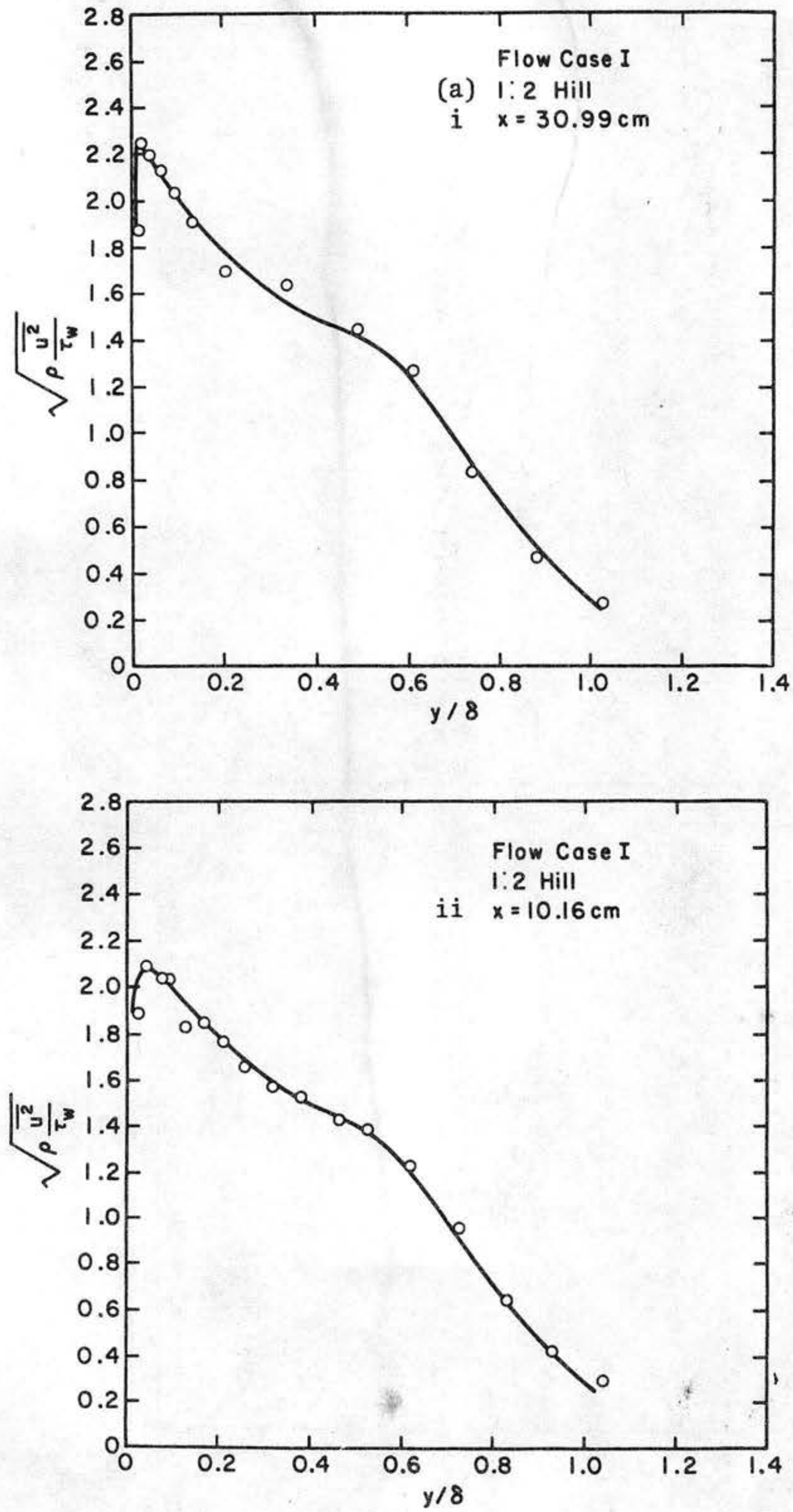

Figure 20. $\sqrt{\rho \frac{\overline{u^2}}{\tau_w}}$ profiles flow case I.

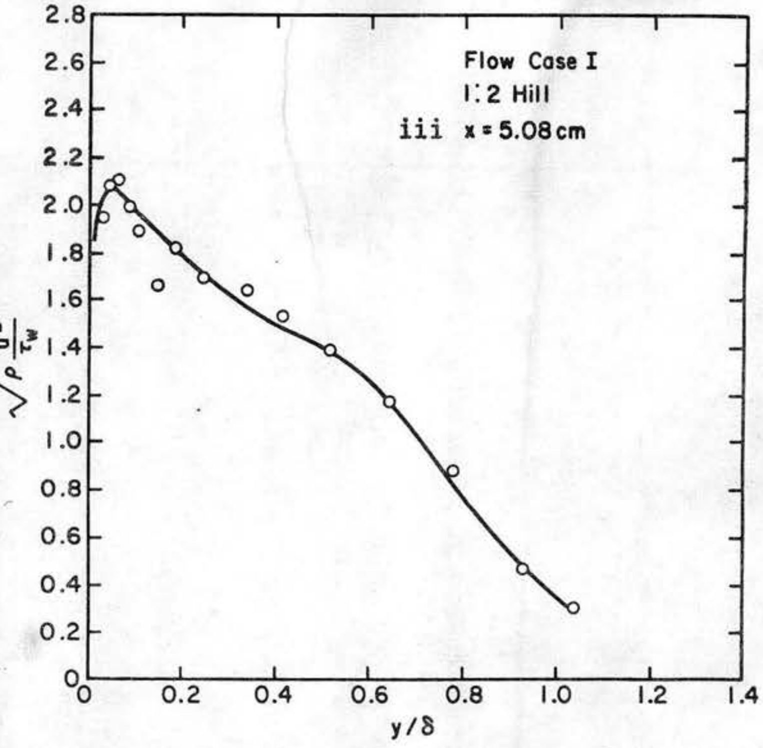

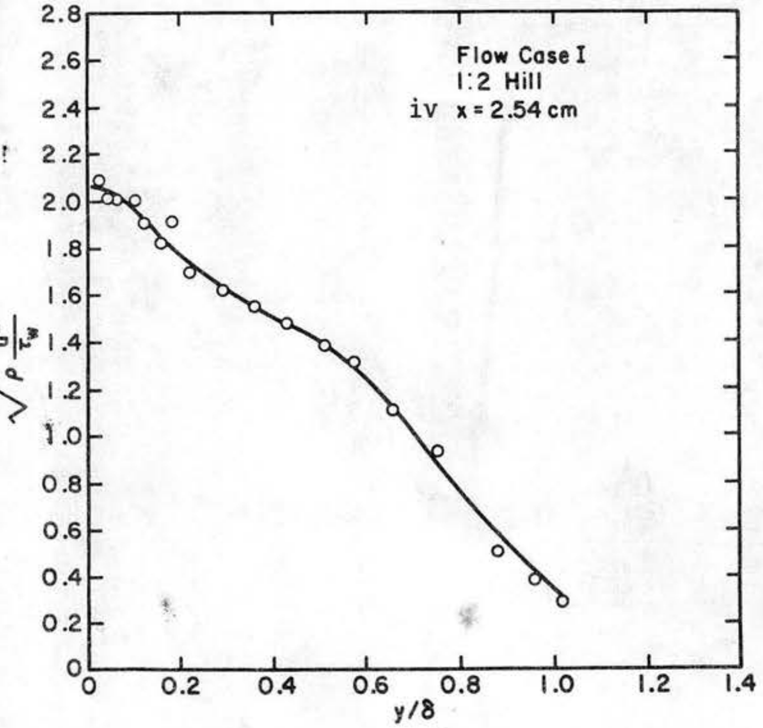

Figure 20. $\sqrt{\rho\,\frac{\overline{u^2}}{\tau_w}}$ profiles flow case I (continued).

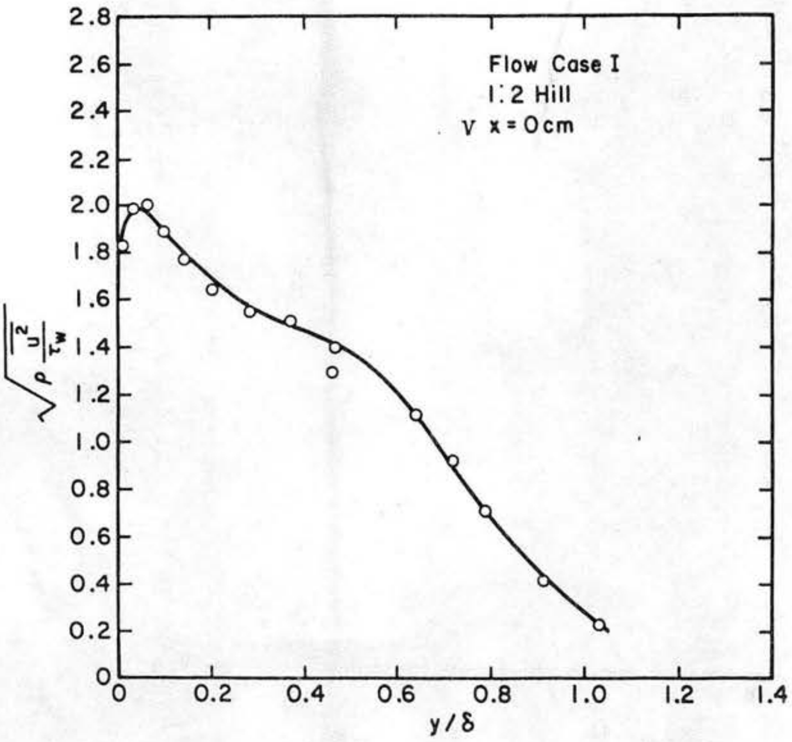

Figure 20. $\sqrt{\rho \frac{\overline{u^2}}{\tau_w}}$ profiles flow case I (continued).

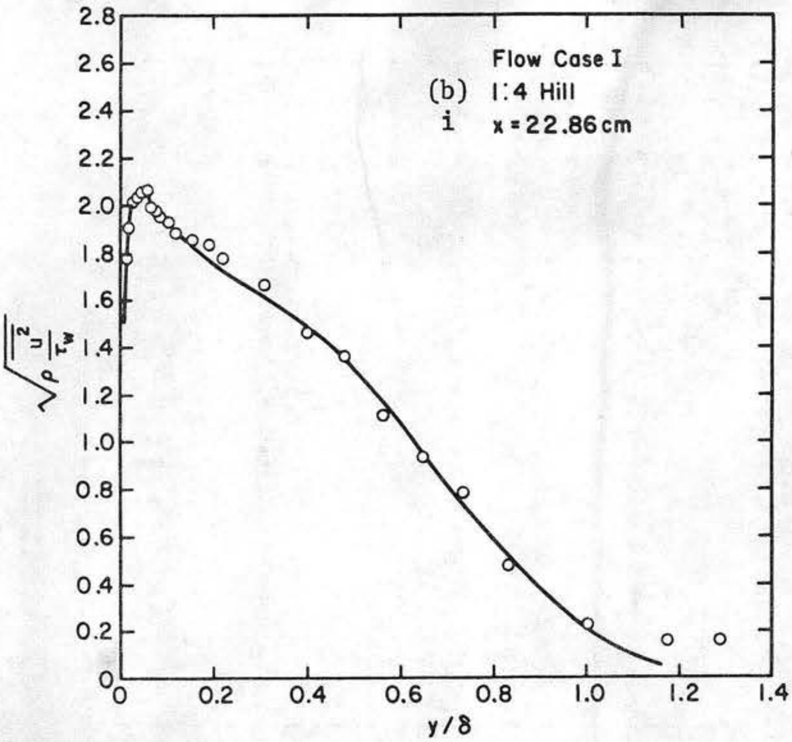

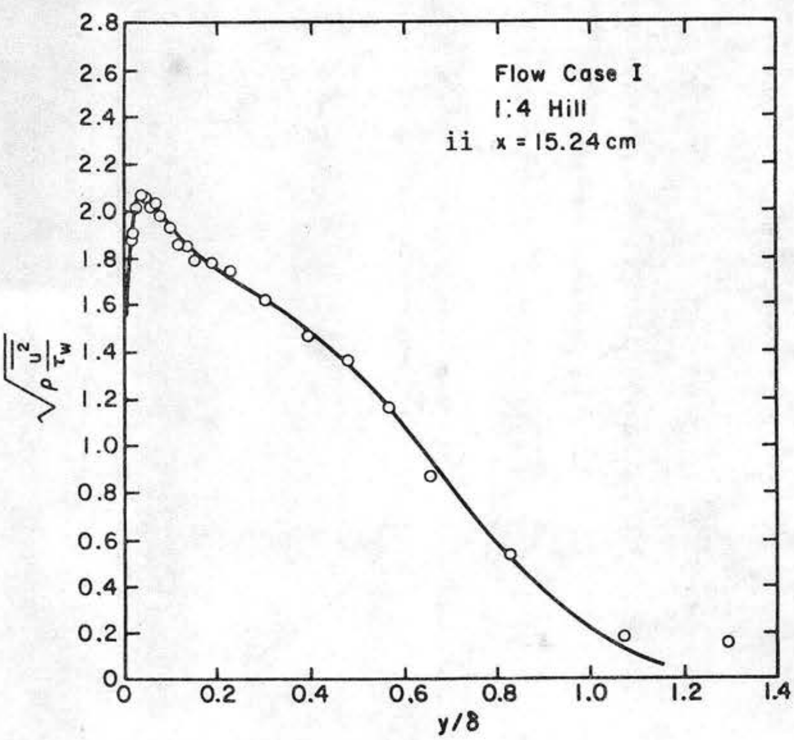

Figure 20. $\sqrt{\rho \frac{\overline{u^2}}{\tau_w}}$ profiles flow case I (continued).

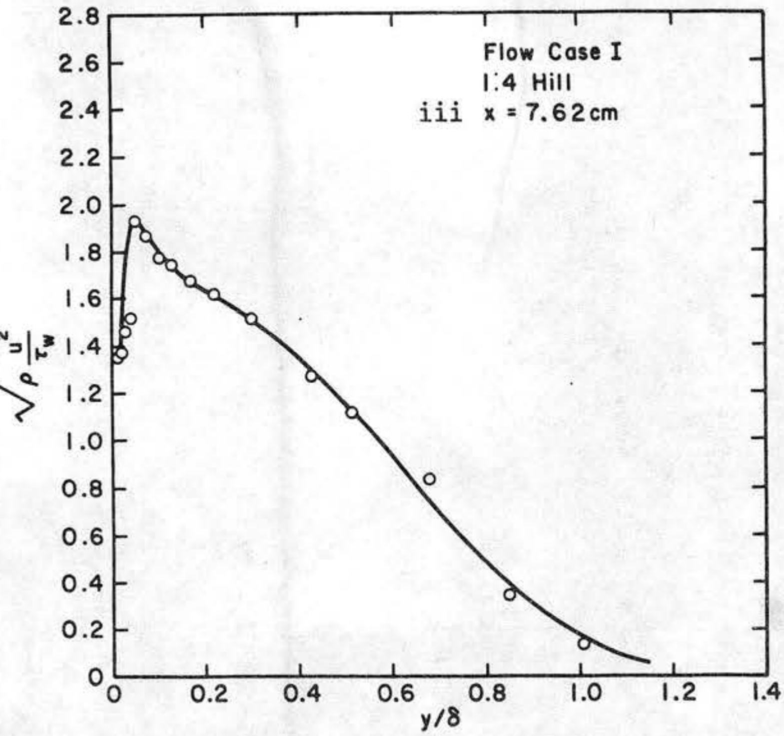

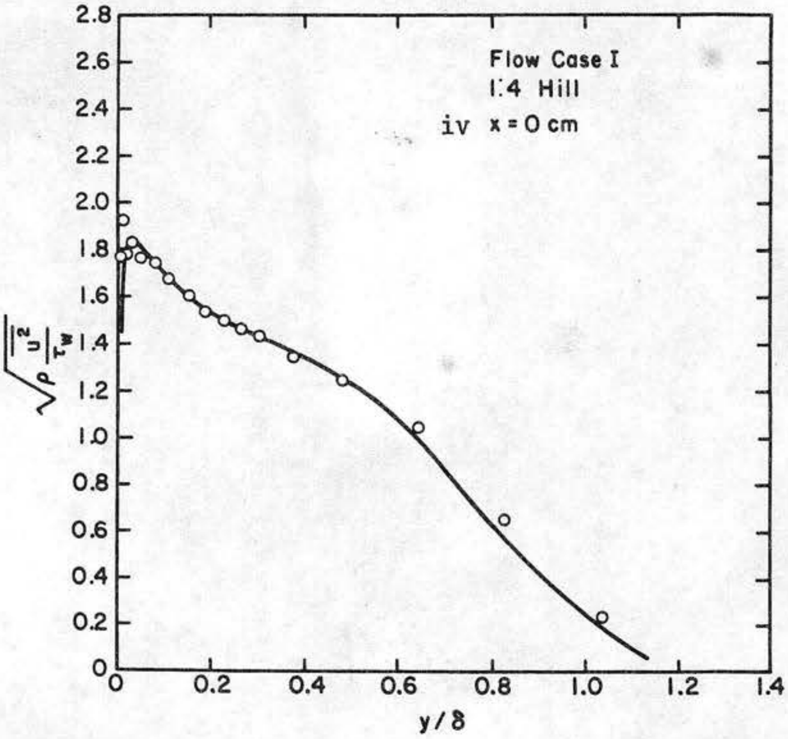

Figure 20. $\sqrt{\rho \frac{\overline{u^2}}{\tau_w}}$ profiles flow case I (continued).

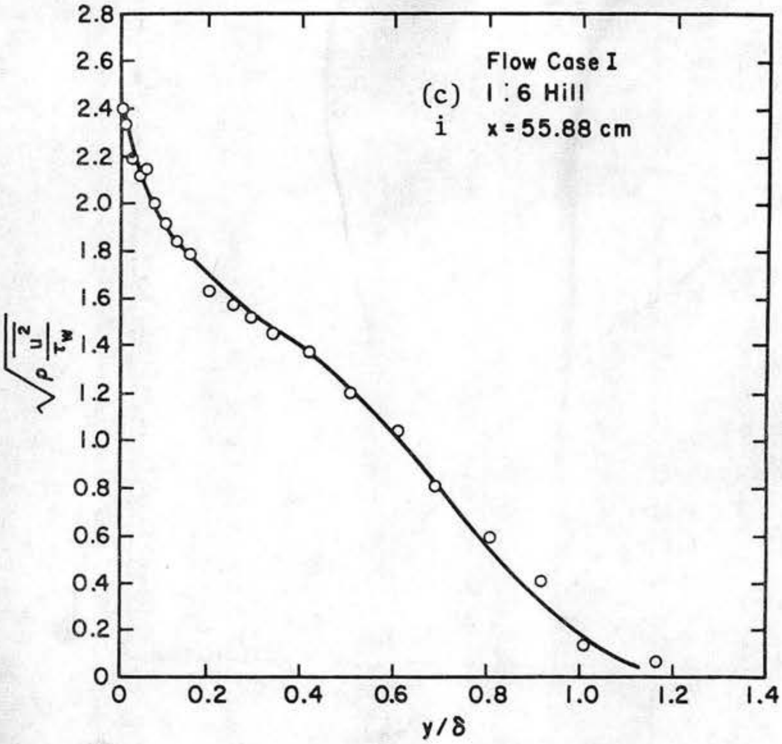

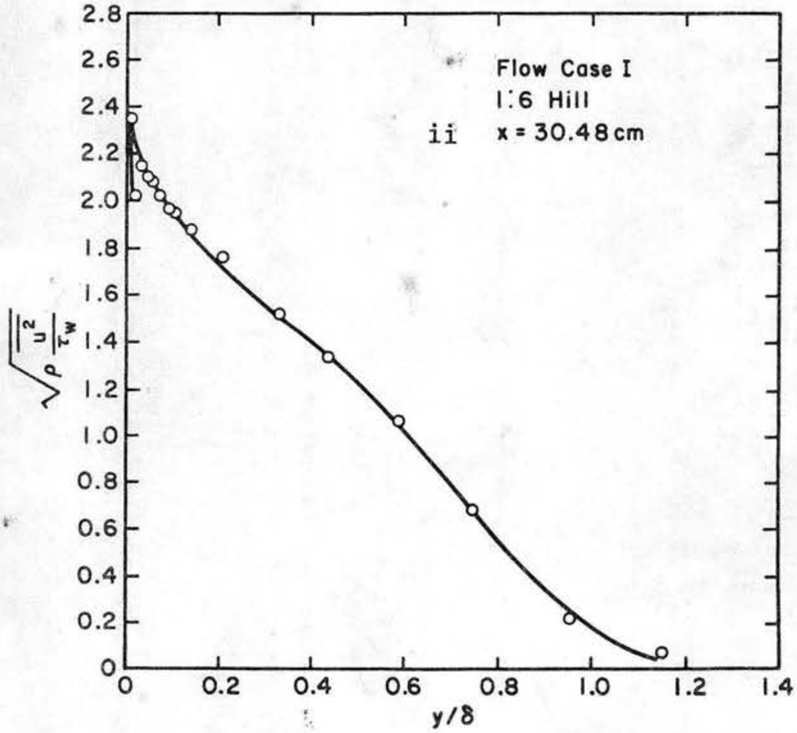

Figure 20. $\sqrt{\rho \frac{\overline{u^2}}{\tau_w}}$ profiles flow case I (continued).

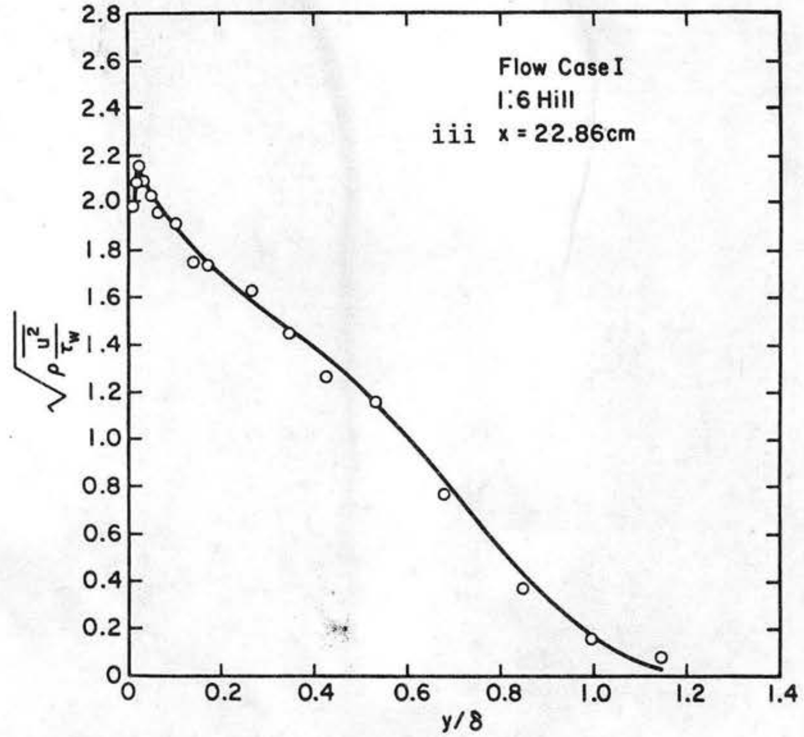

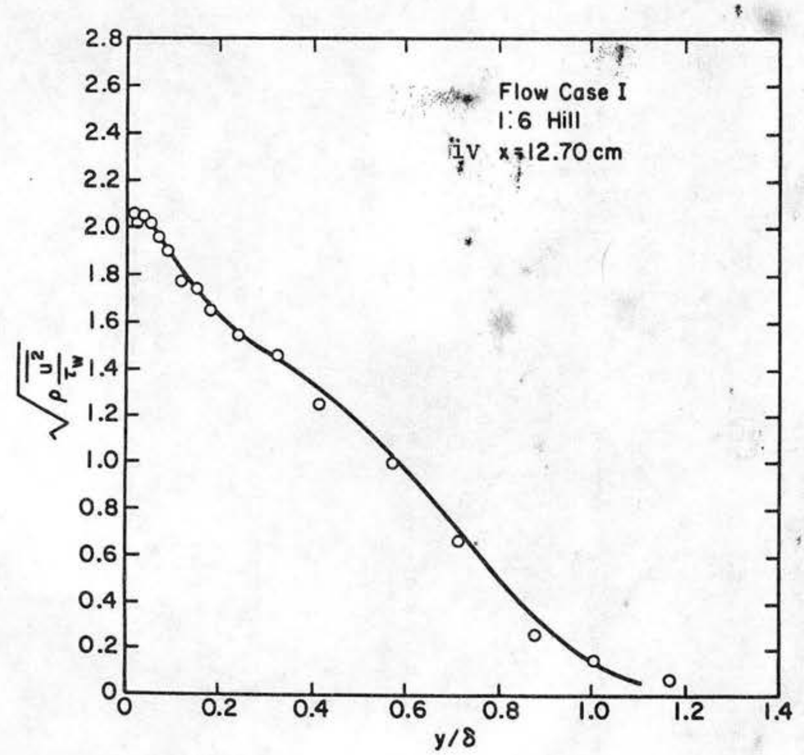

Figure 20. $\sqrt{\rho \frac{\overline{u^2}}{\tau_w}}$ profiles flow case I (continued).

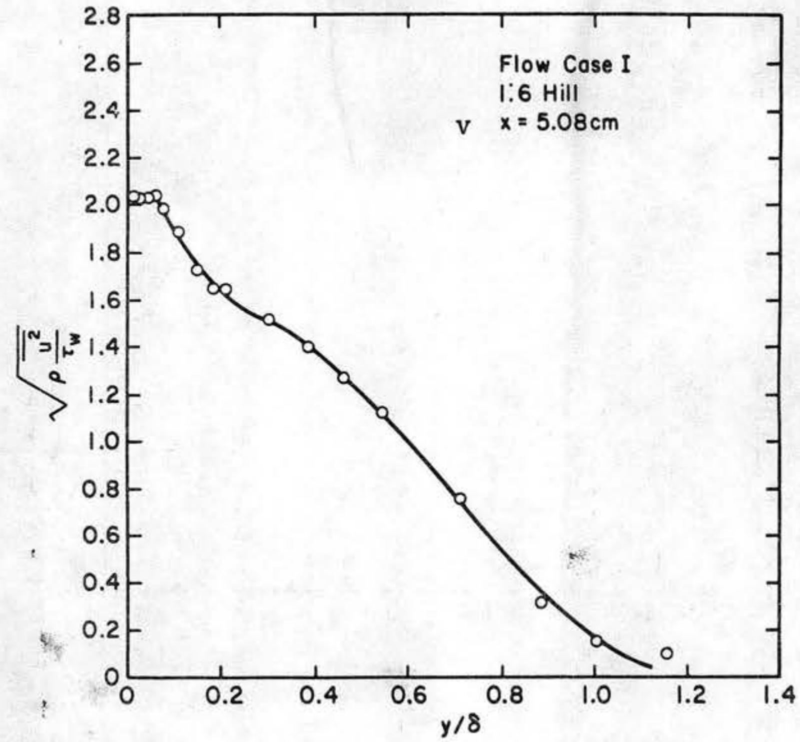

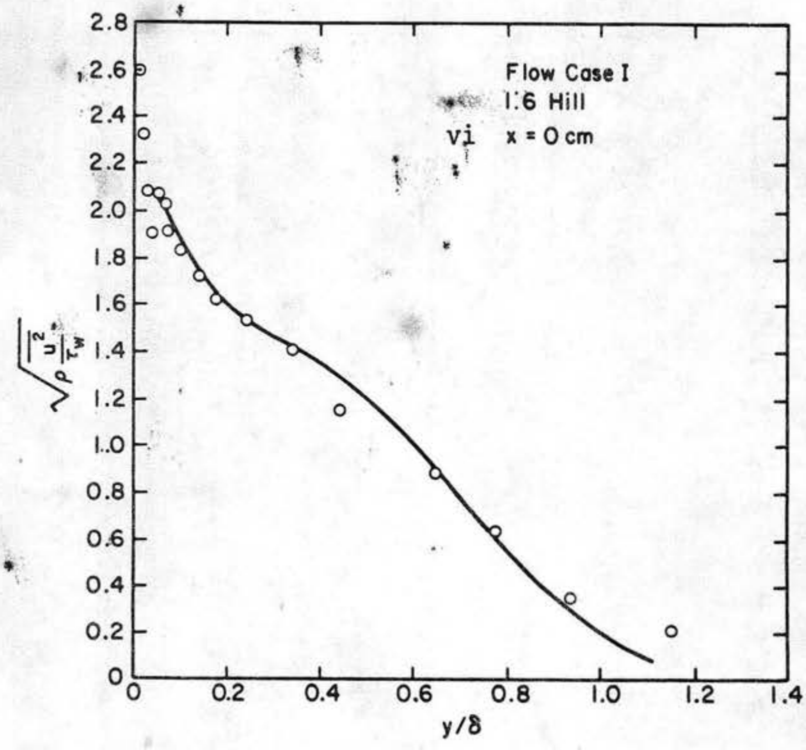

Figure 20. $\sqrt{\rho \frac{\overline{u^2}}{\tau_w}}$ profiles flow case I (completed).

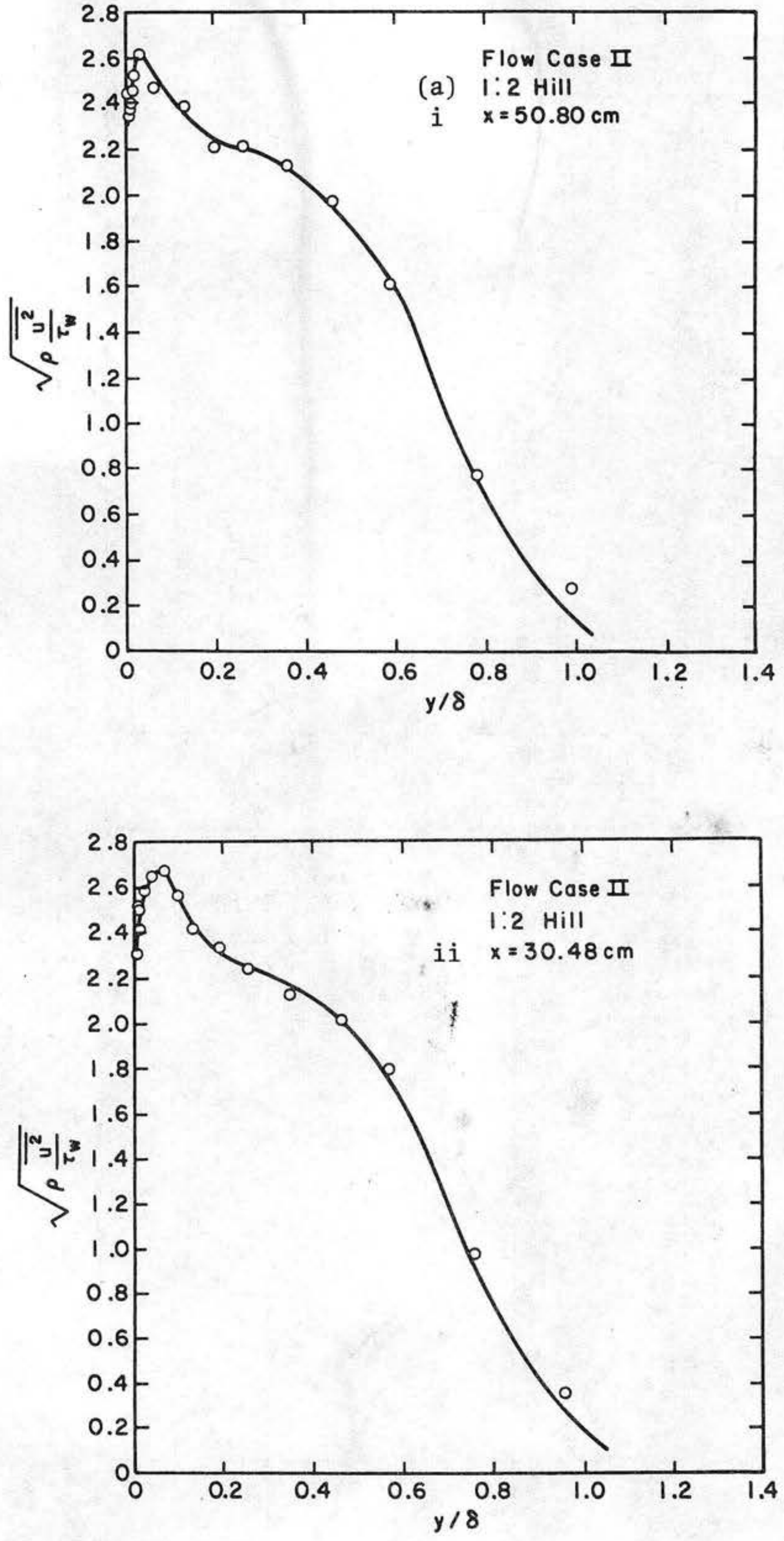

Figure 21. $\sqrt{\rho \frac{\overline{u^2}}{\tau_w}}$ profiles flow case II.

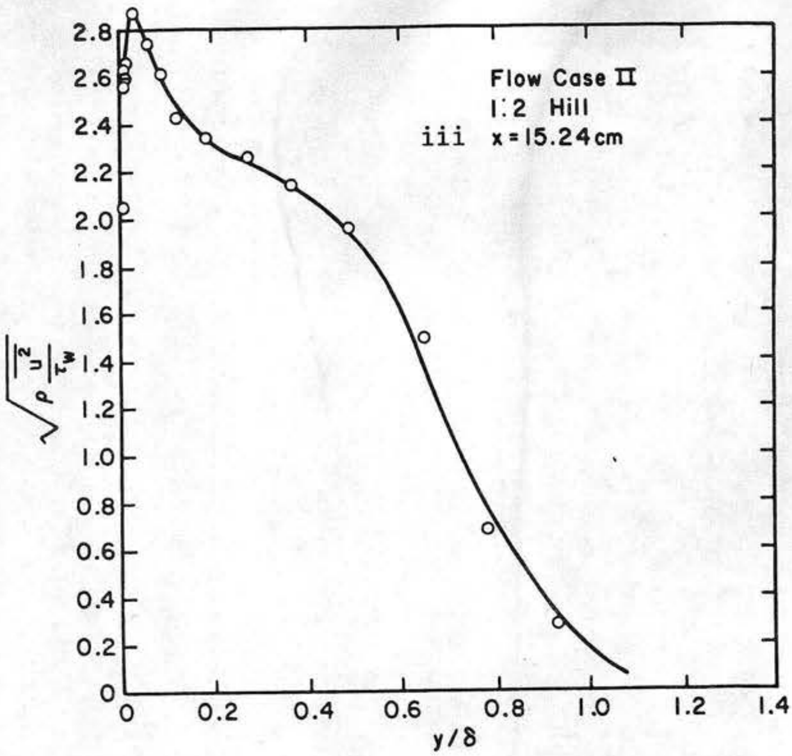

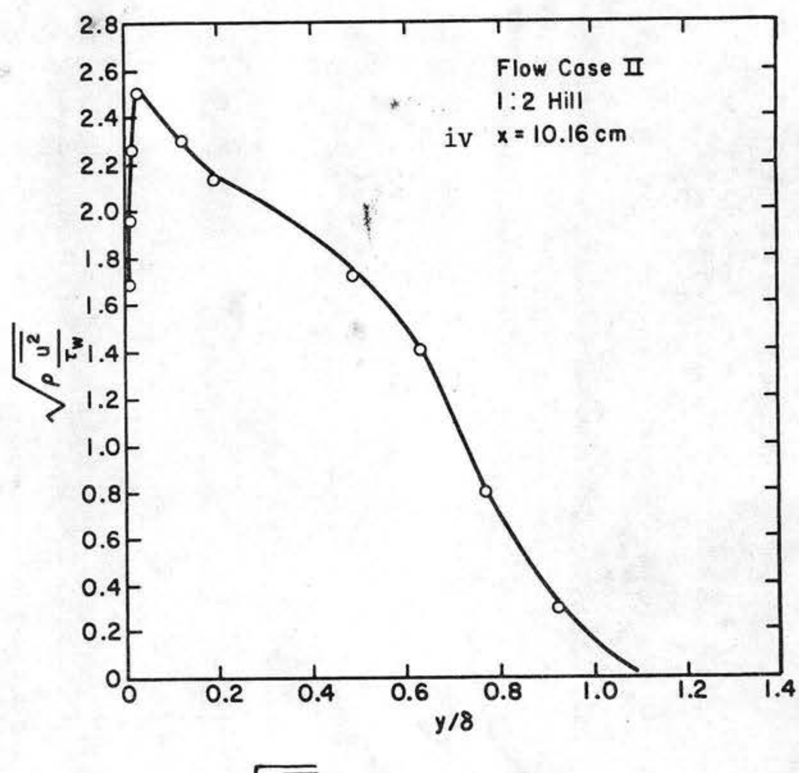

Figure 21. $\sqrt{\rho \frac{\overline{u^2}}{\tau_w}}$ profiles flow case II (continued).

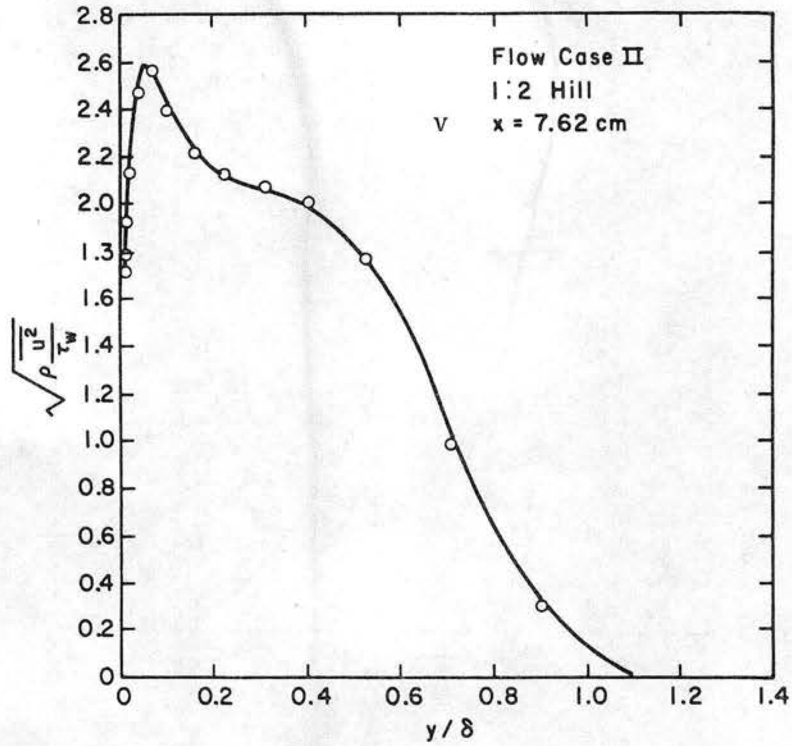

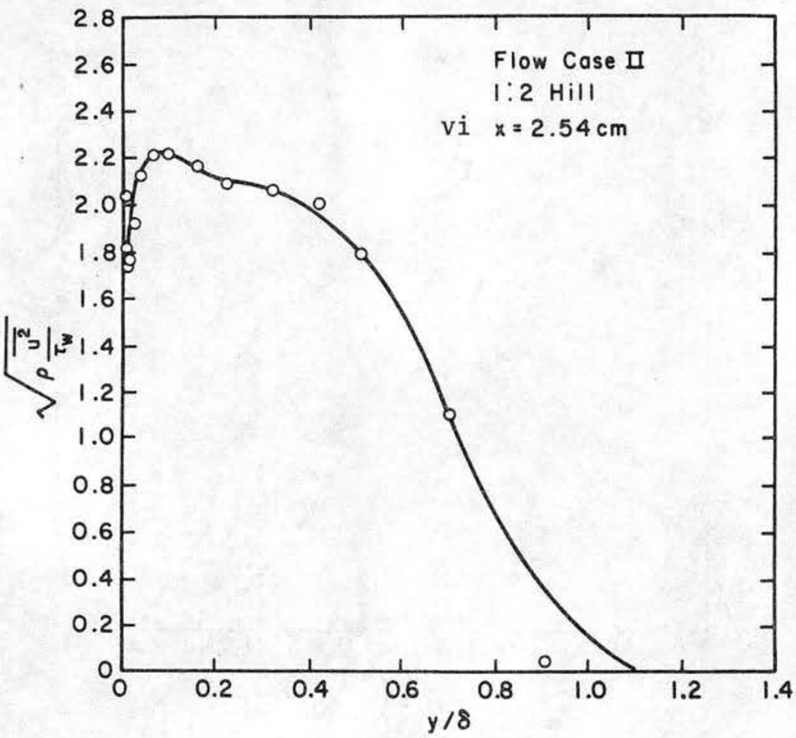

Figure 21. $\sqrt{\rho \frac{\overline{u^2}}{\tau_w}}$ profiles flow case II (continued).

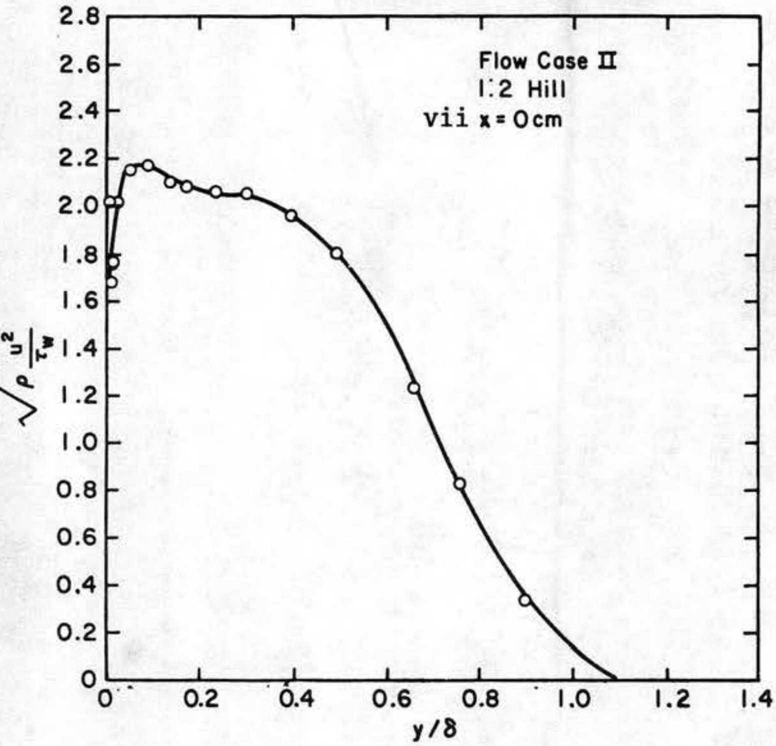

Figure 21. $\sqrt{\rho \frac{\overline{u^2}}{\tau_w}}$ profiles flow case II (continued).

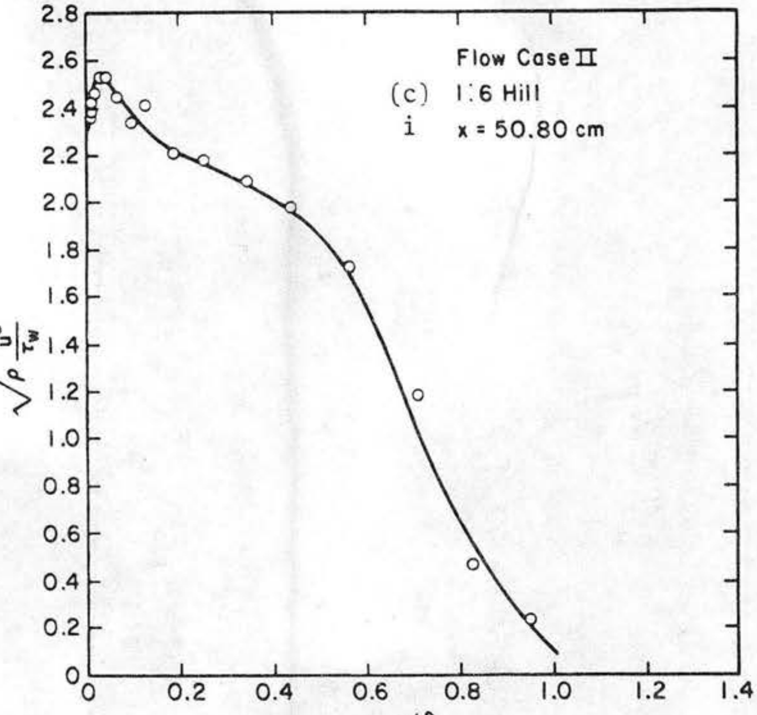

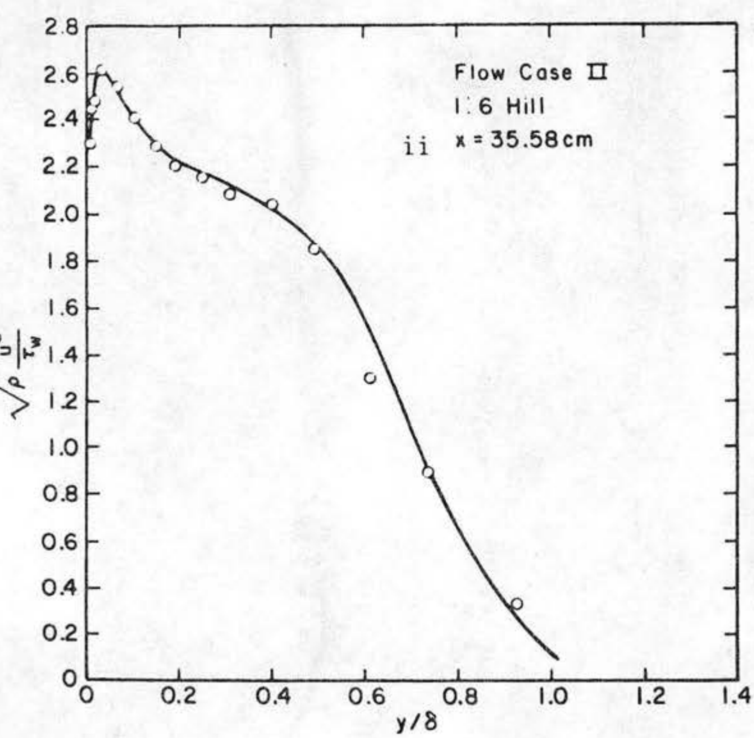

Figure 21. $\sqrt{\rho \frac{\overline{u^2}}{\tau_w}}$ profiles flow case II (continued).

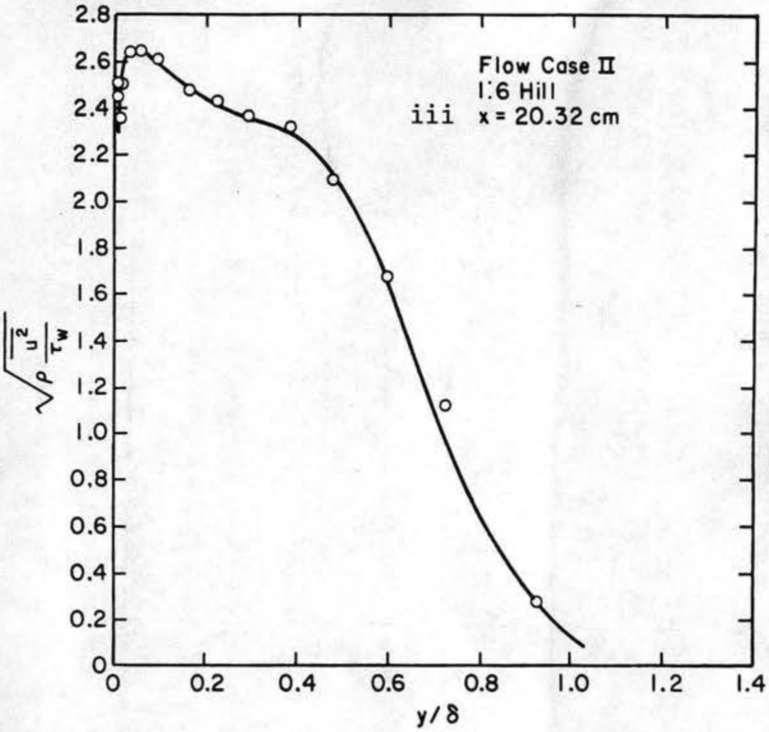

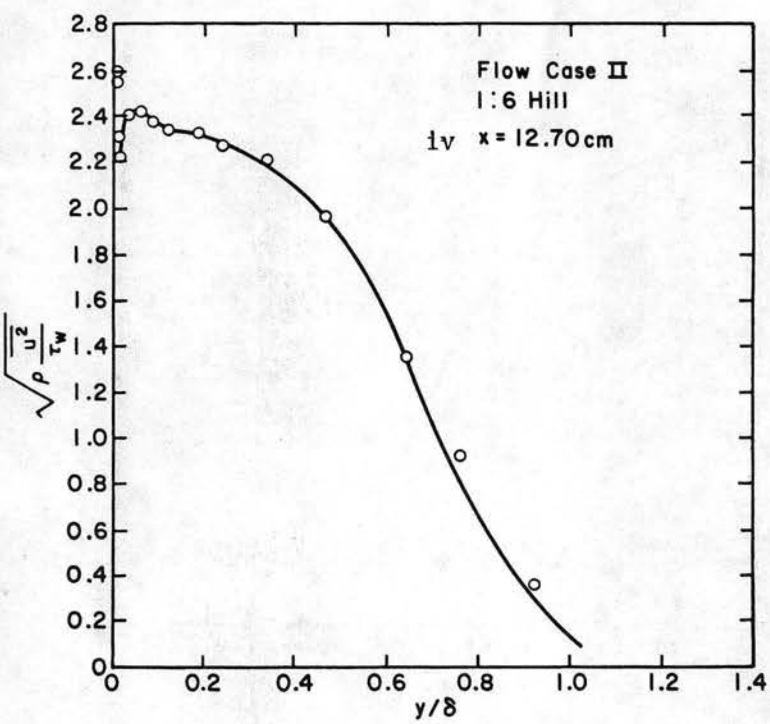

Figure 21. $\sqrt{\rho \frac{\overline{u^2}}{\tau_w}}$ profiles flow case II (continued).

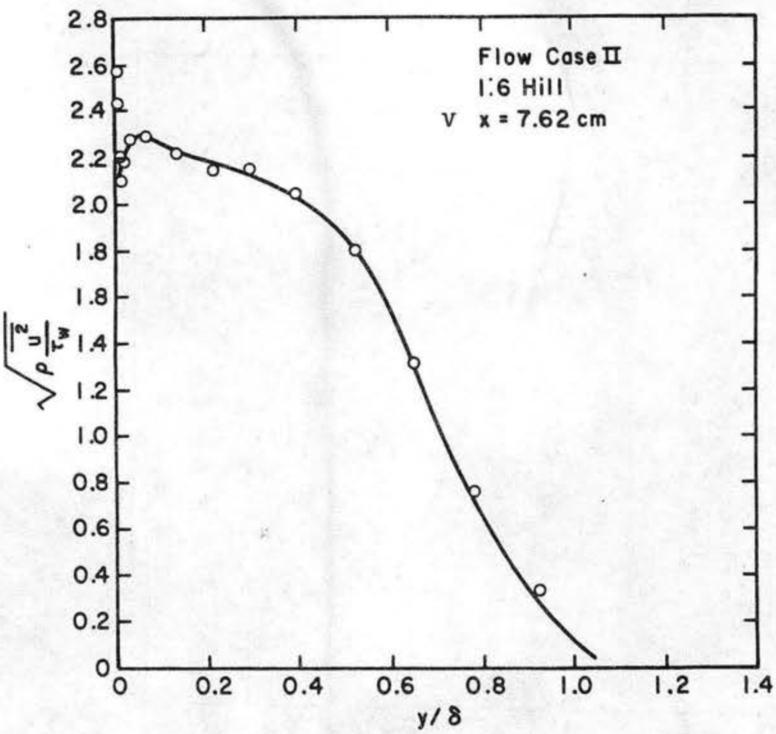

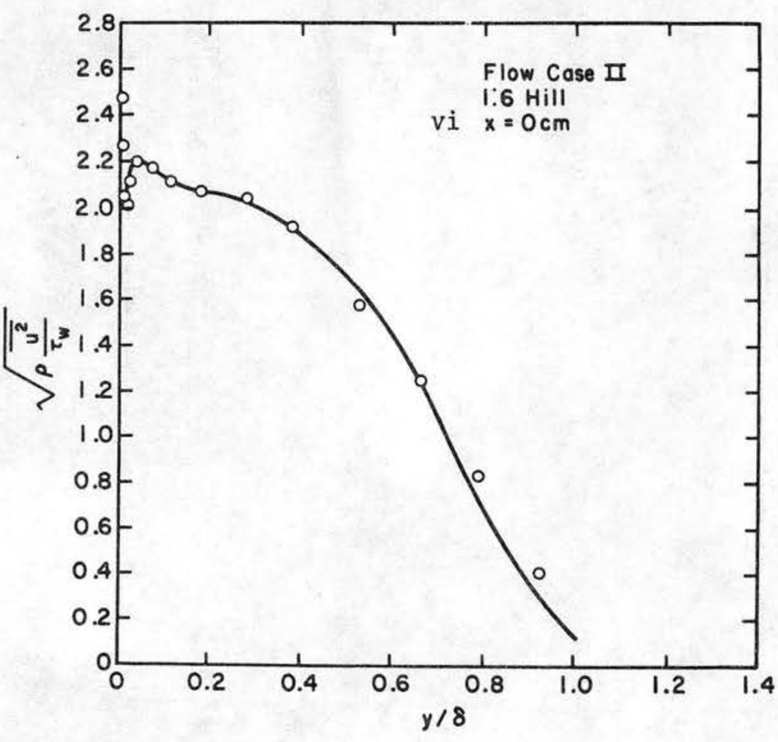

Figure 21. $\sqrt{\rho \frac{\overline{u^2}}{\tau_w}}$ profiles flow case II (completed).

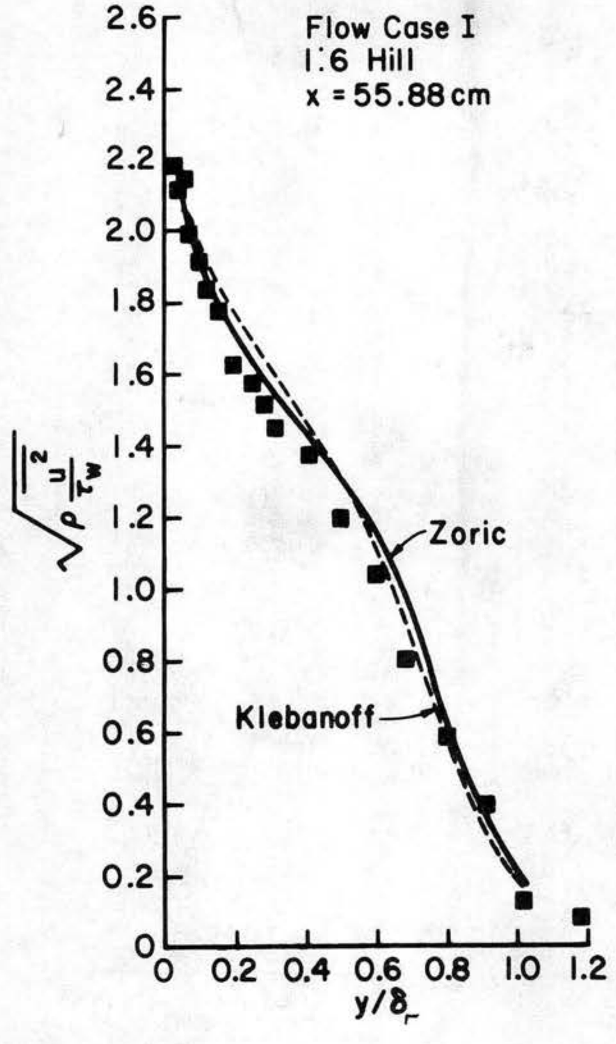

Figure 22. Comparison of upstream $\sqrt{\rho \frac{\overline{u^2}}{\tau_w}}$ measurements to those of Zoric and Klebanoff. Flow case I.

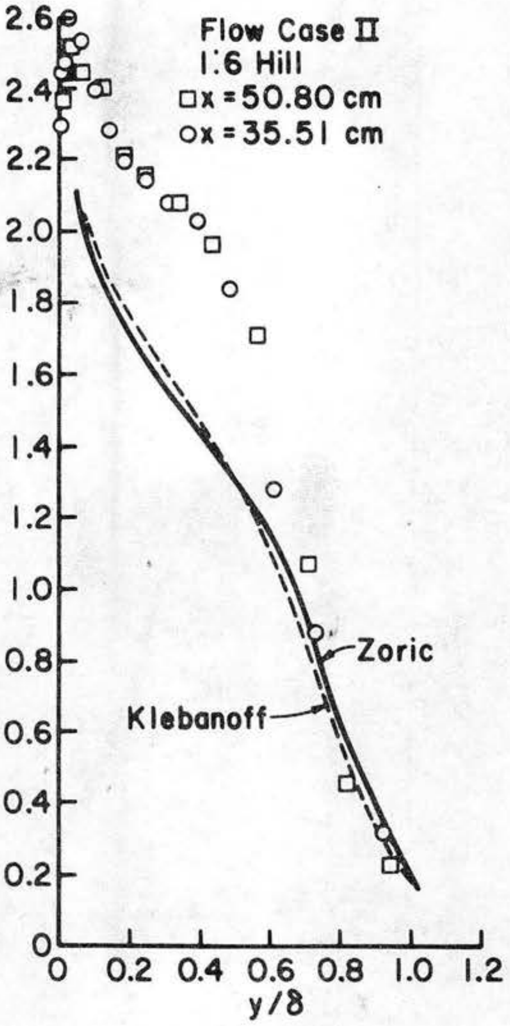

Figure 23. Comparison of upstream $\sqrt{\rho \frac{\overline{u^2}}{\tau_w}}$ measurements to those of Zoric and Klebanoff. Flow case II.

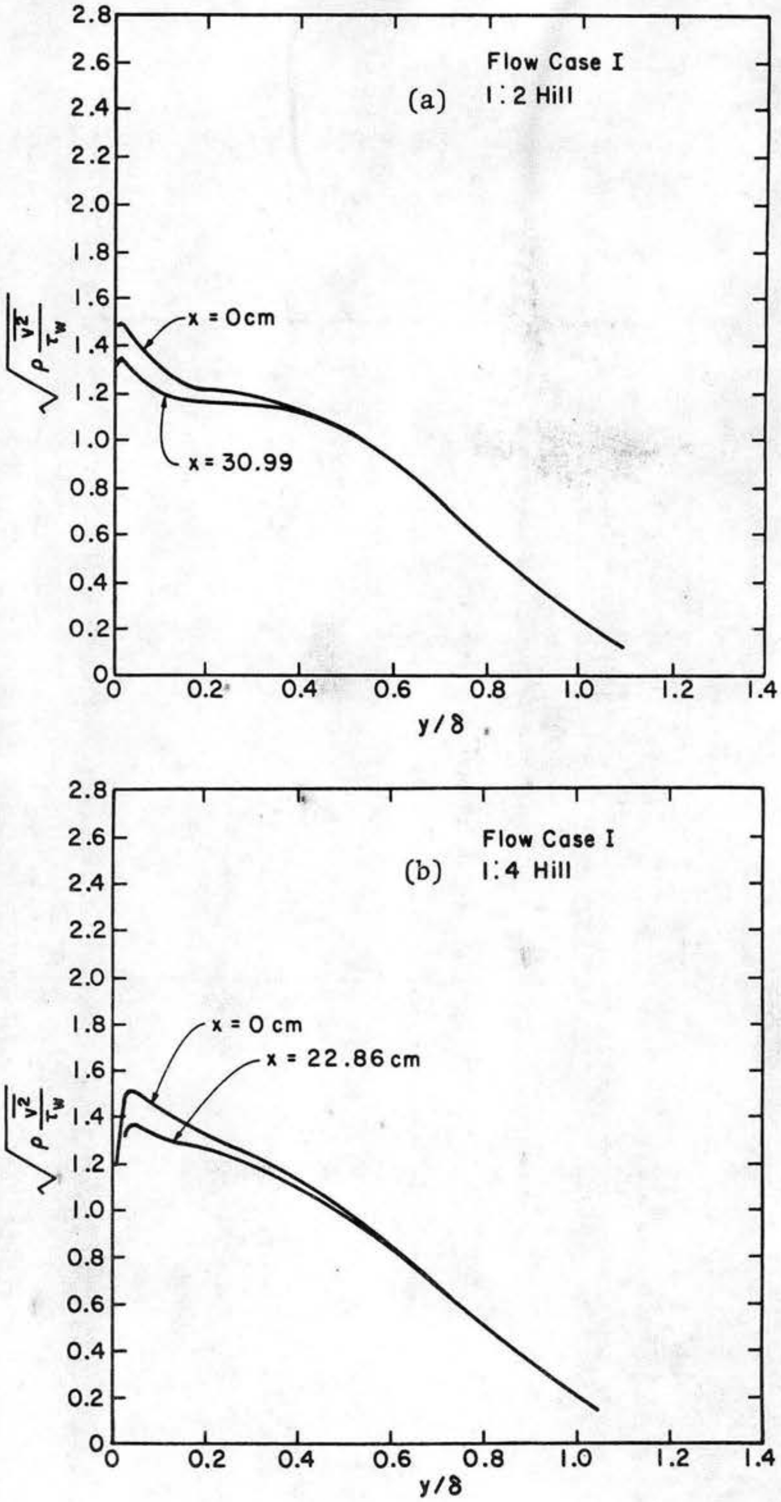

Figure 24. Upstream $\sqrt{\rho \frac{\overline{v^2}}{\tau_w}}$ measurements compared to $\sqrt{\rho \frac{\overline{v^2}}{\tau_w}}$ measurements at crest. Flow case I.

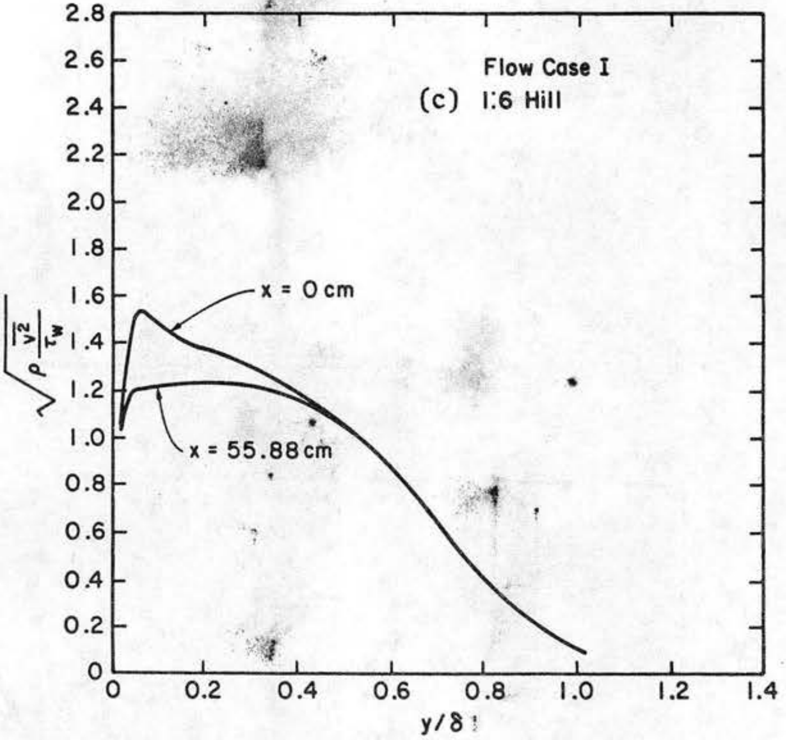

Figure 24. Upstream $\sqrt{\rho \frac{\overline{v^2}}{\tau_w}}$ measurements compared to $\sqrt{\rho \frac{\overline{v^2}}{\tau_w}}$ measurements at crest. Flow case (continued).

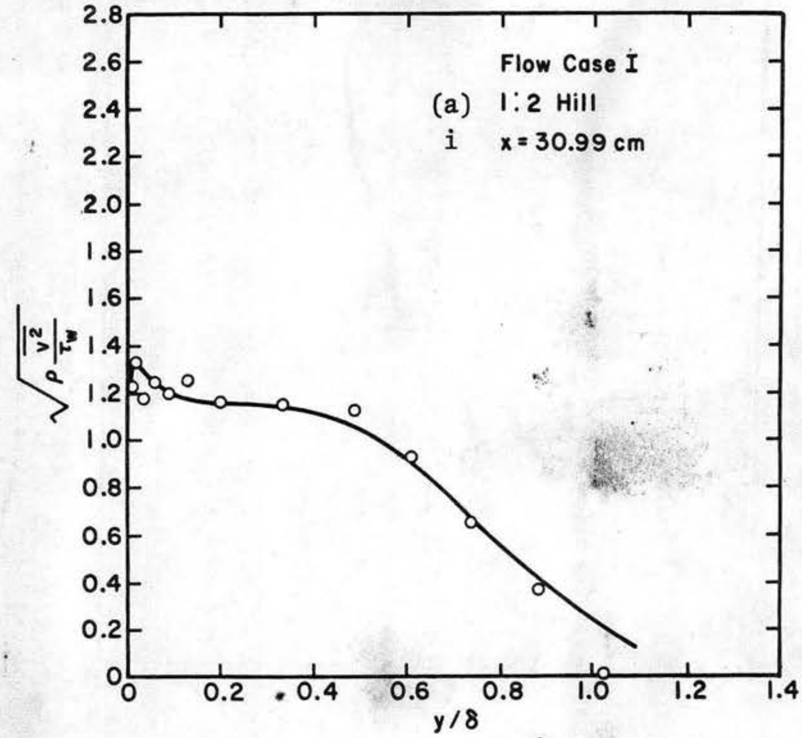

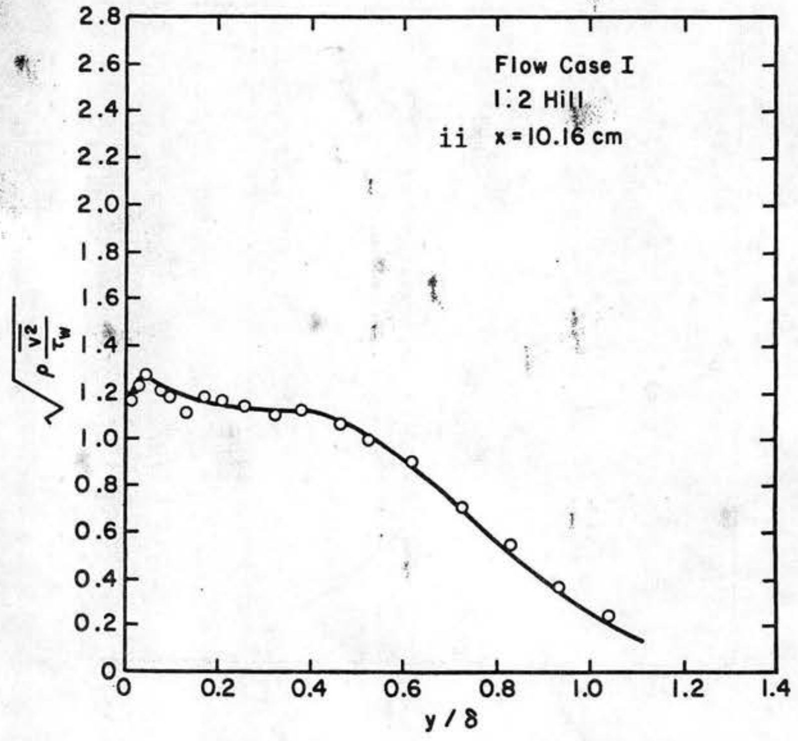

Figure 25. $\sqrt{\rho \frac{\overline{v^2}}{\tau_w}}$ profiles flow case I.

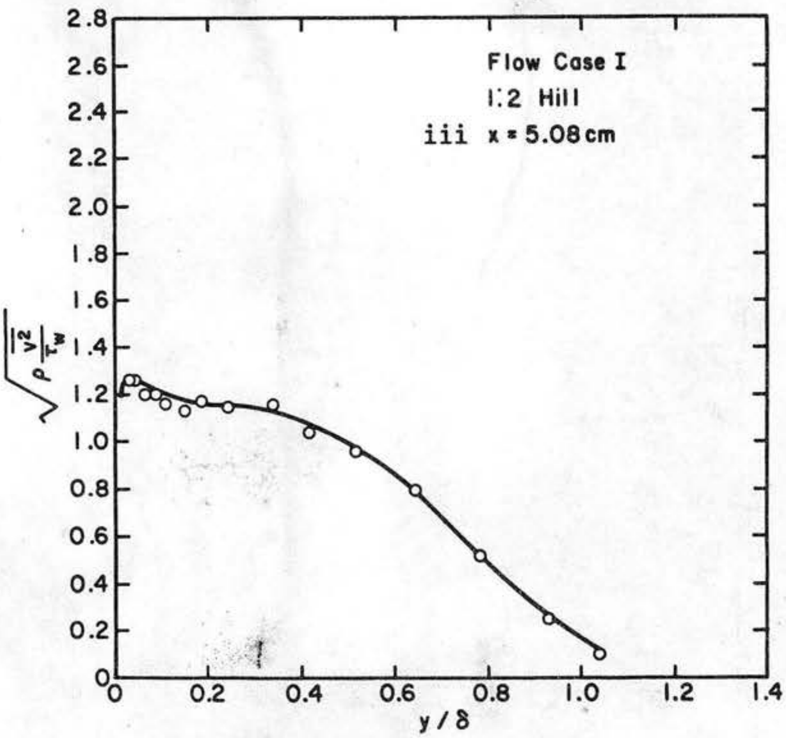

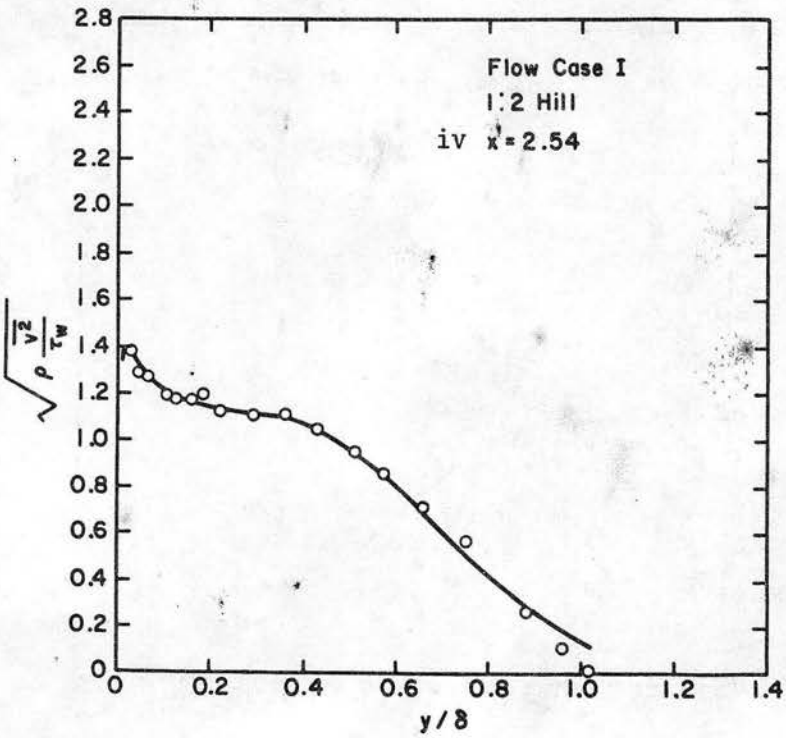

Figure 25. $\sqrt{\rho \frac{\overline{v^2}}{\tau_w}}$ profiles flow case I (continued).

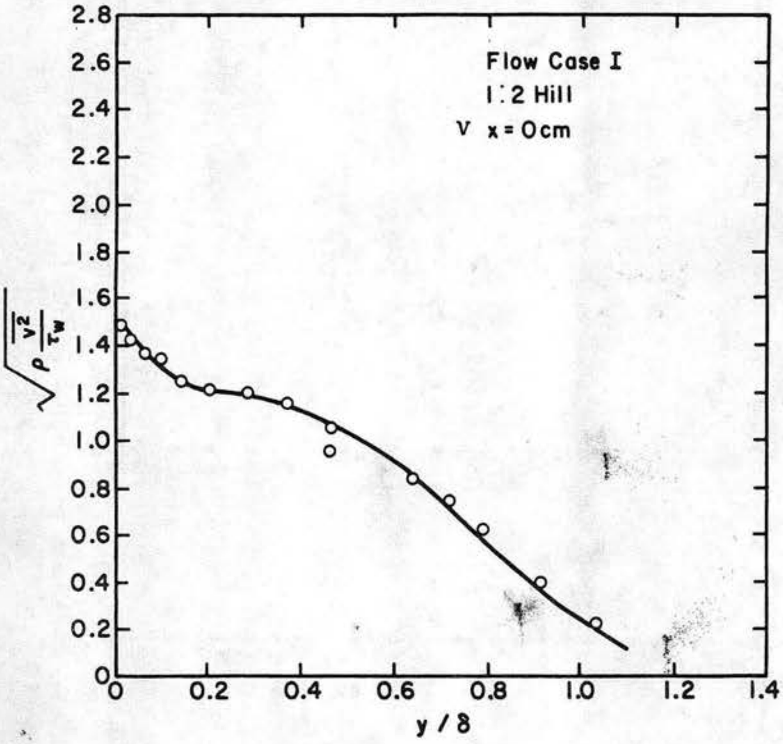

Figure 25. $\sqrt{\rho \frac{\overline{v^2}}{\tau_w}}$ profiles flow case I (continued).

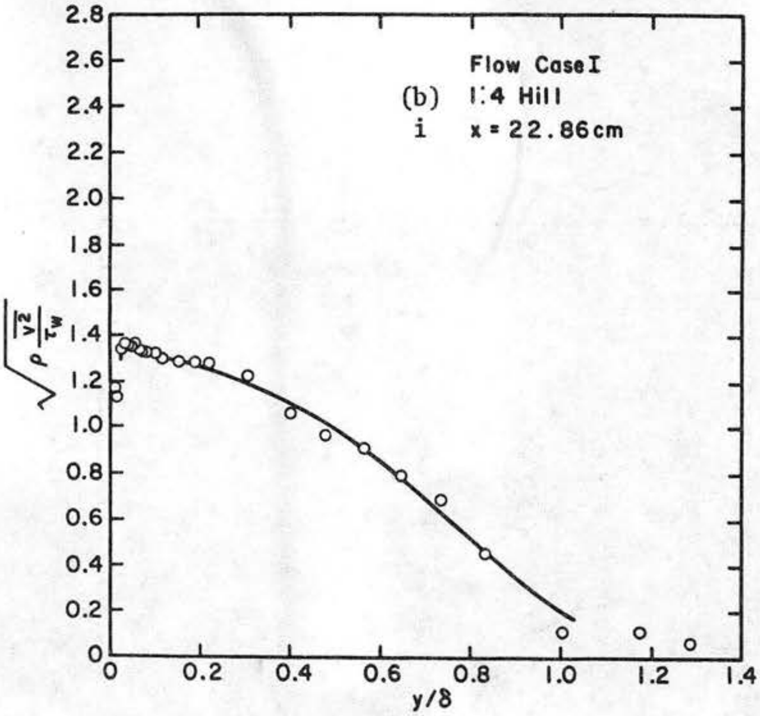

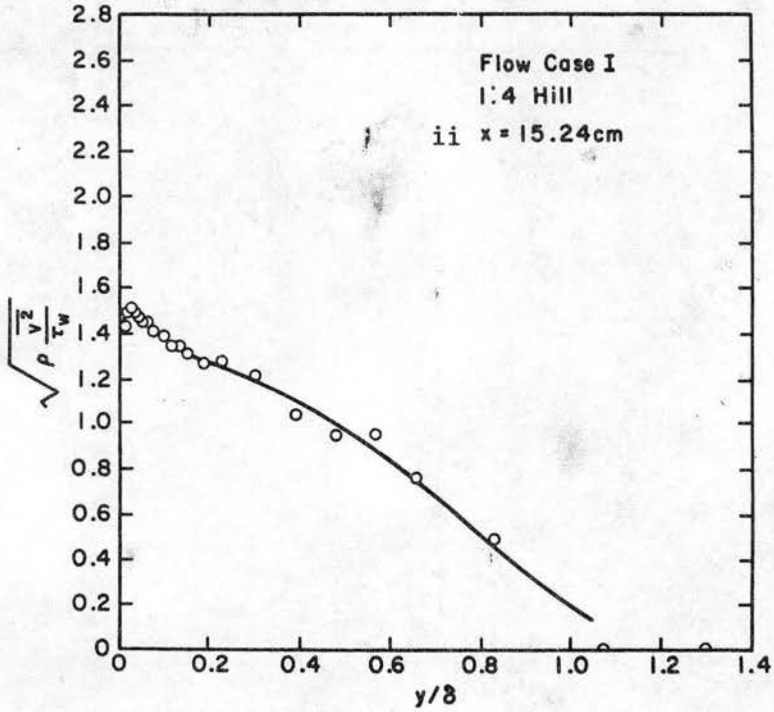

Figure 25. $\sqrt{\rho \frac{\overline{v^2}}{\tau_w}}$ profiles flow case I (continued).

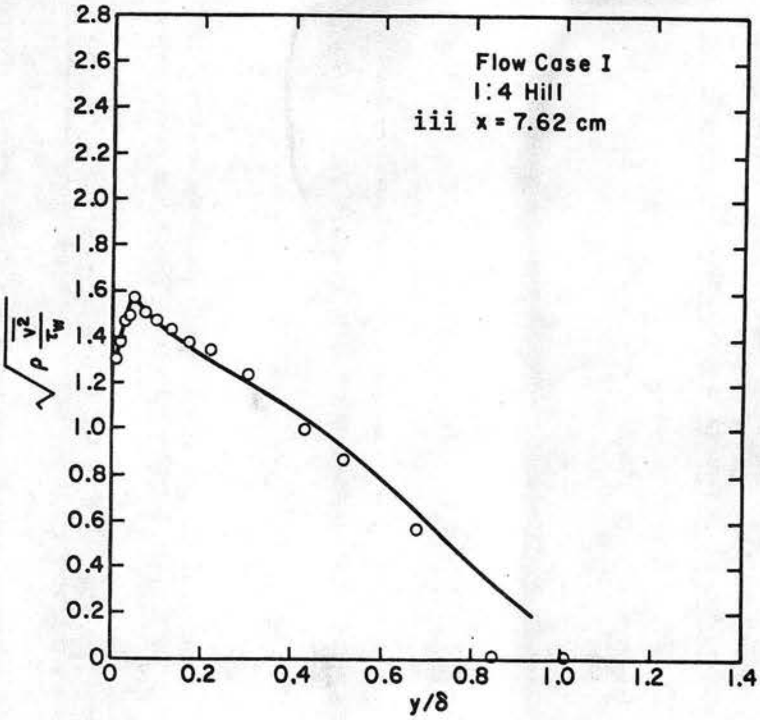

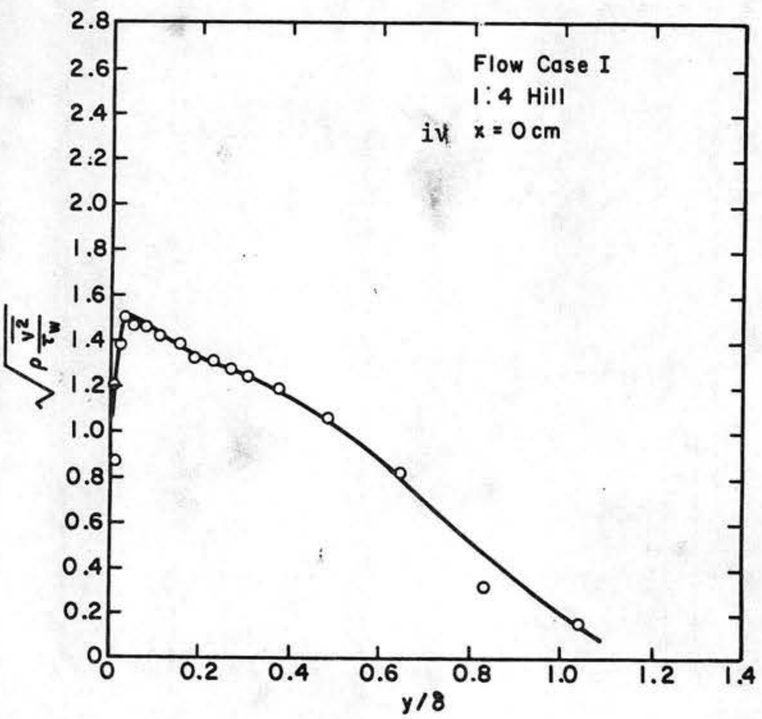

Figure 25. $\sqrt{\rho \frac{\overline{v^2}}{\tau_w}}$ profiles flow case I (continued).

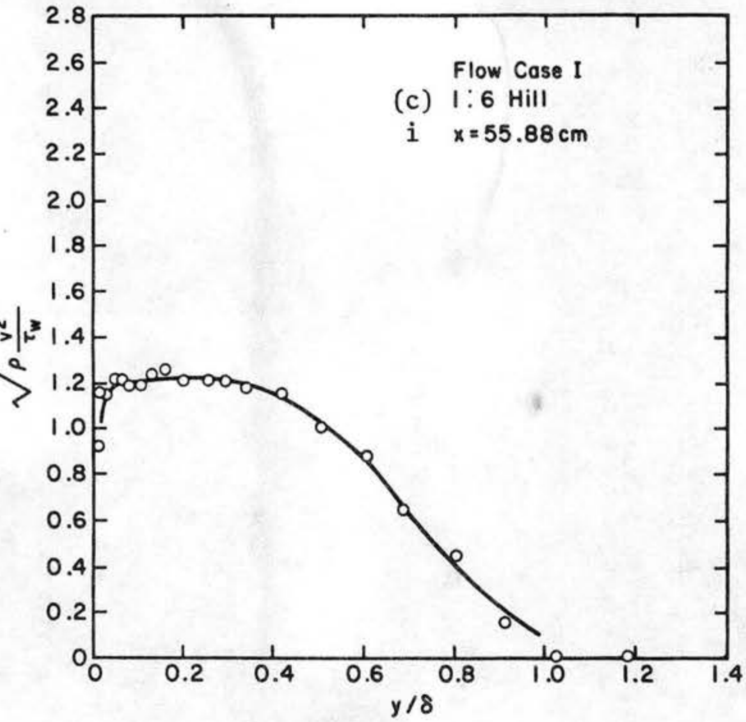

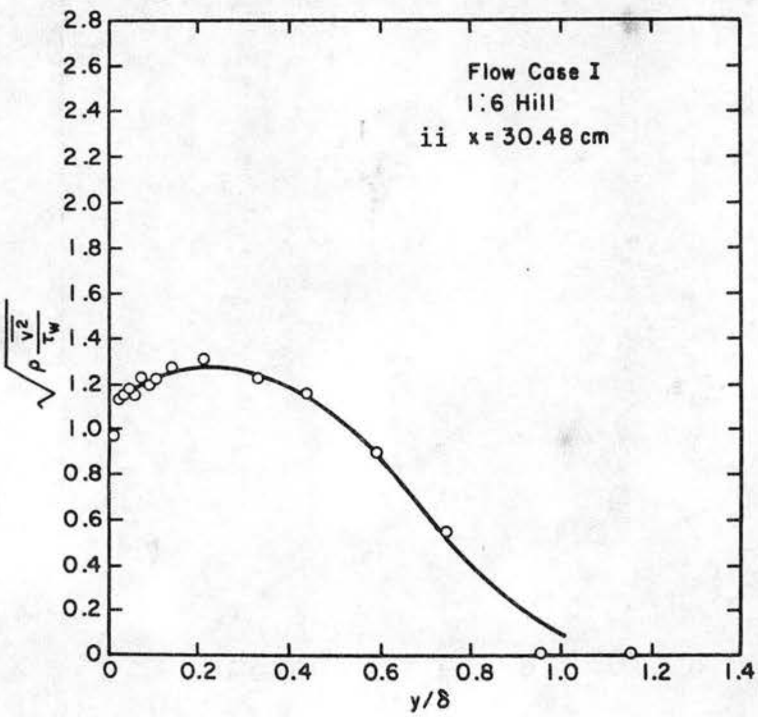

Figure 25. $\sqrt{\rho \frac{\overline{v^2}}{\tau_w}}$ profiles flow case I (continued).

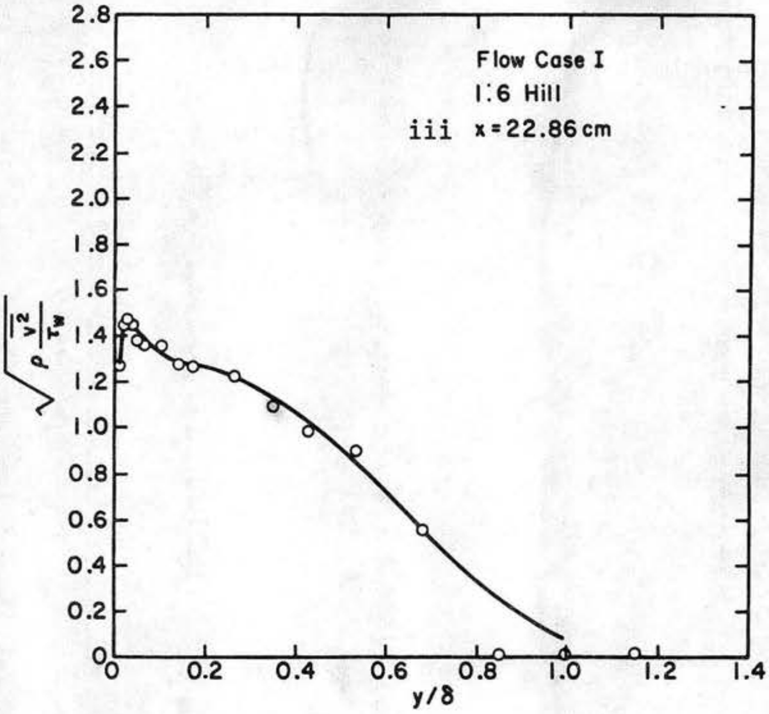

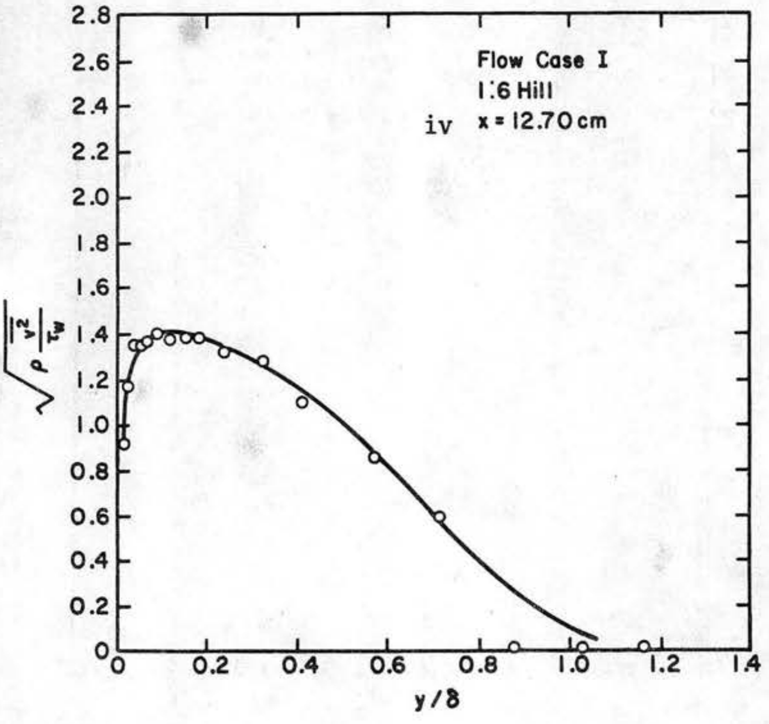

Figure 25. $\sqrt{\rho \frac{\overline{v^2}}{\tau_w}}$ profiles flow case I (continued).

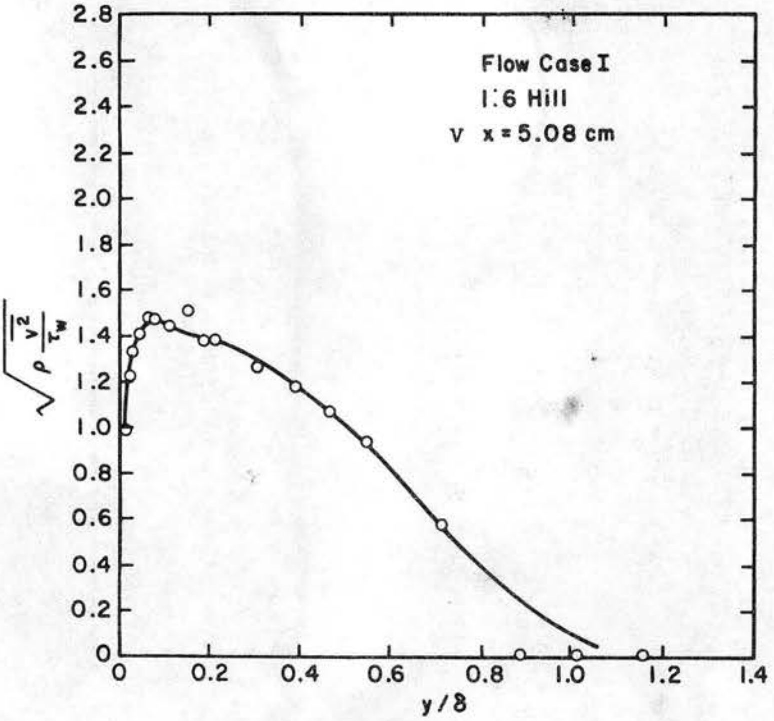

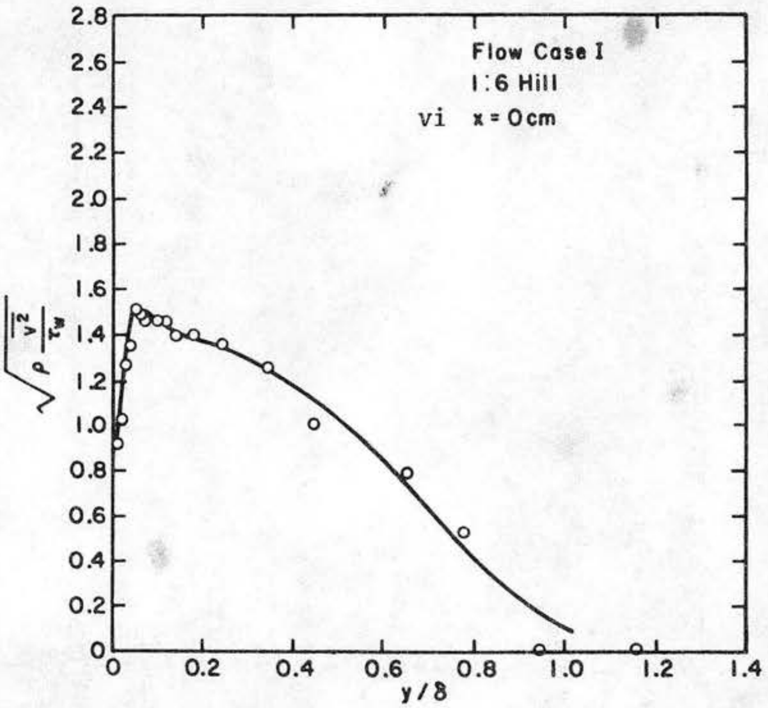

Figure 25. $\sqrt{\rho \frac{\overline{v^2}}{\tau_w}}$ profiles flow case I (completed).

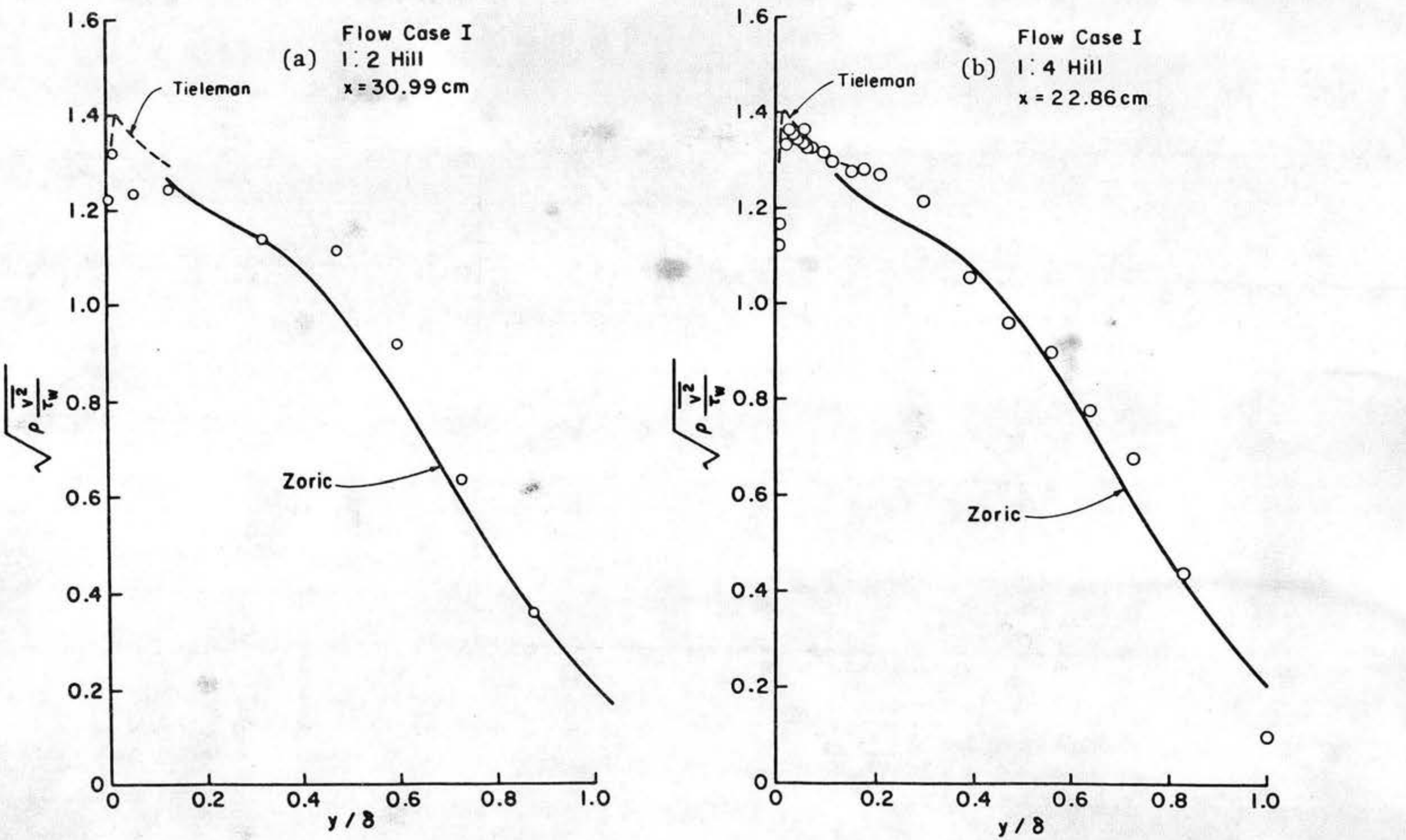

Figure 26. Comparison of $\sqrt{\rho \frac{\overline{v^2}}{\tau_w}}$ measurements to those of Zoric and Tieleman. Flow case I.

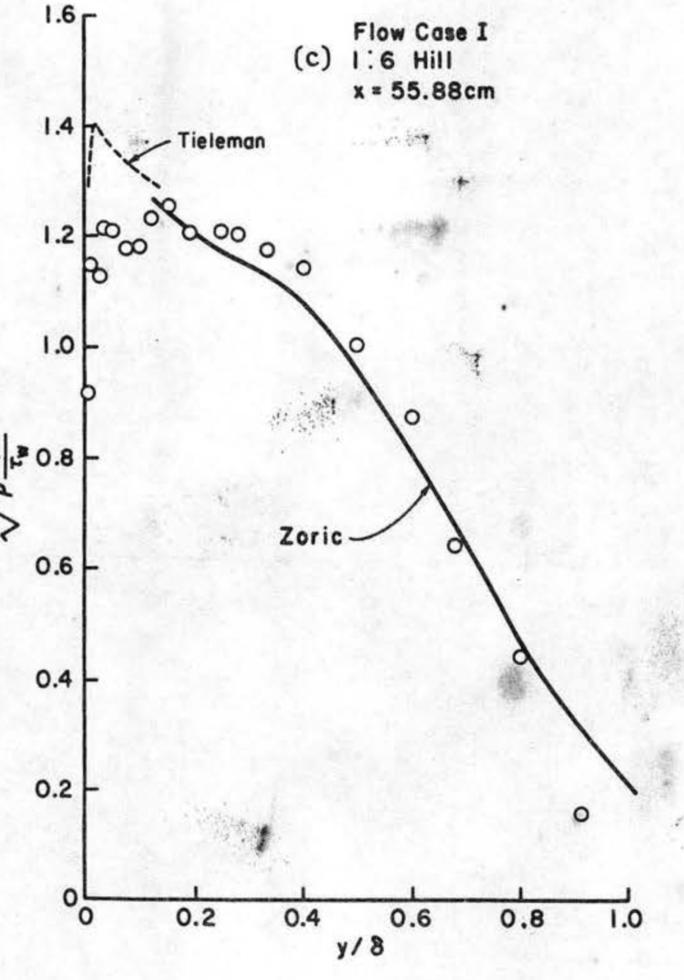

Figure 26. Comparison of $\sqrt{\rho \frac{\overline{v^2}}{\tau_w}}$ measurements to those of Zoric and Tieleman. Flow case I (continued).

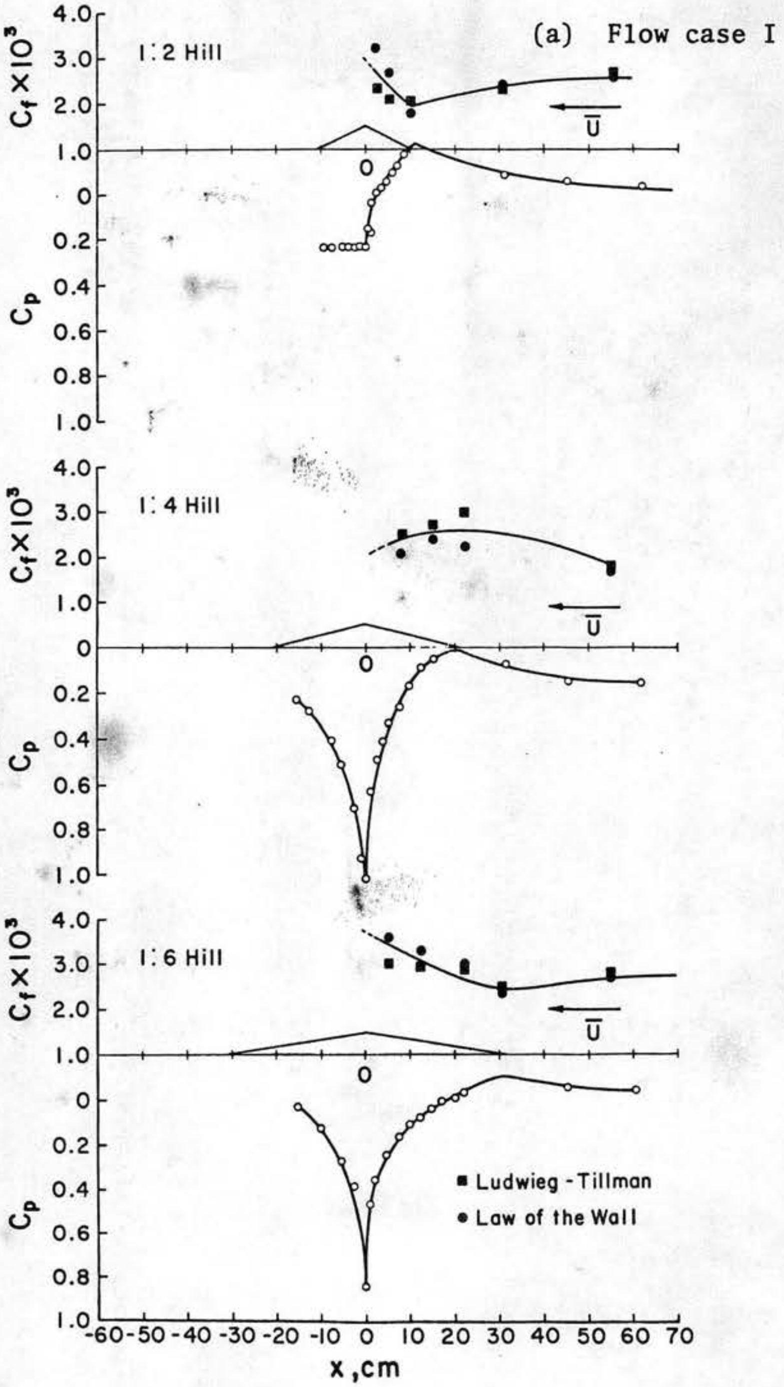

Figure 27. Wall, shear stress, and static pressure distribution. Flow case I.

(b) Flow case II

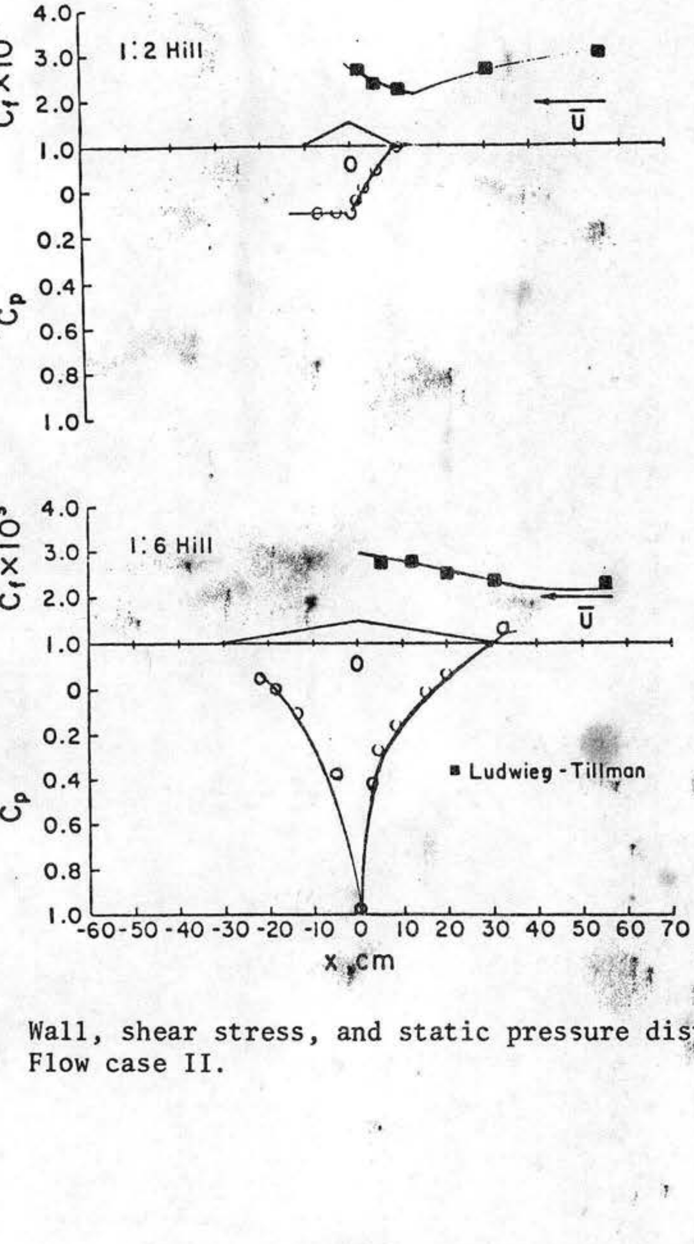

Figure 27. Wall, shear stress, and static pressure distribution. Flow case II.

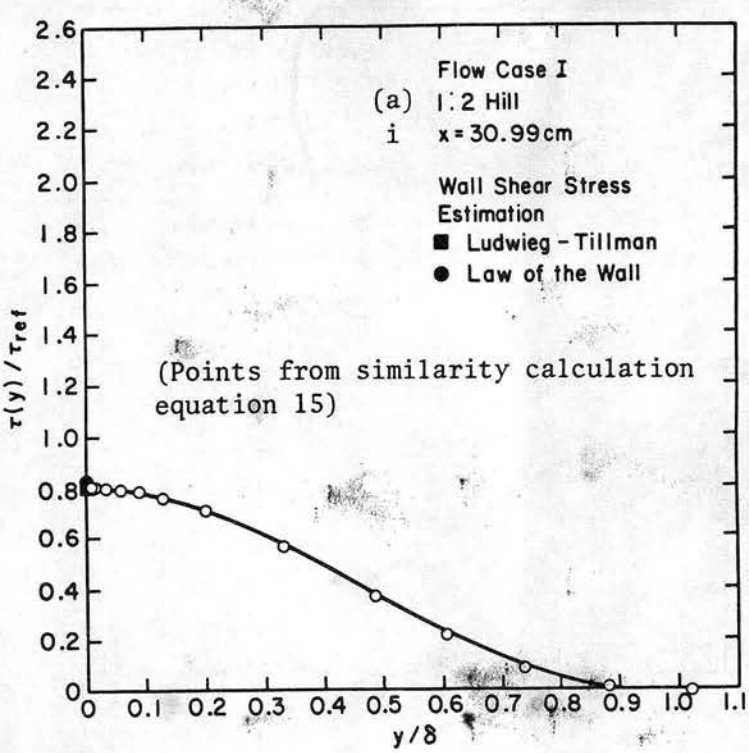

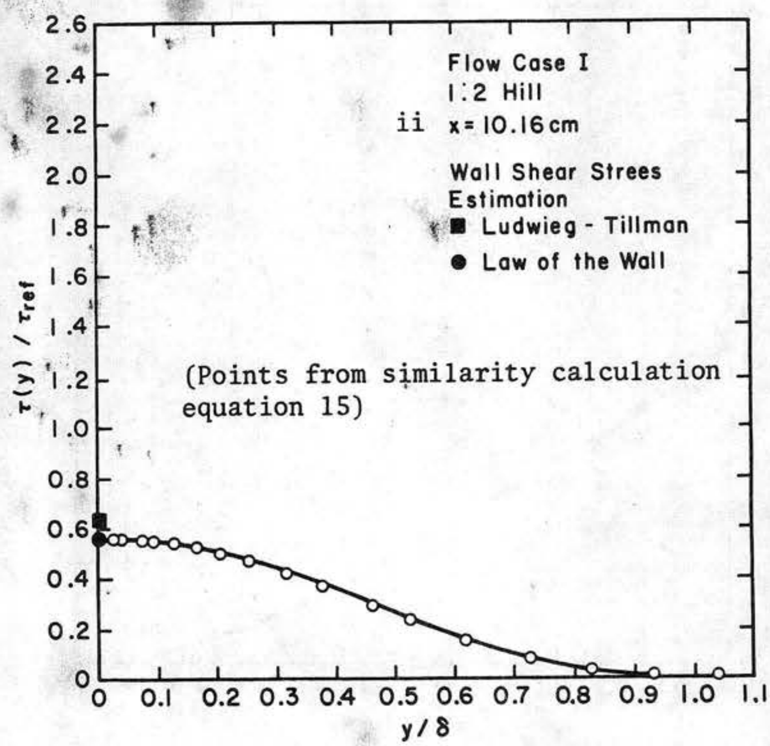

Figure 28. Shear stress distribution flow case I.

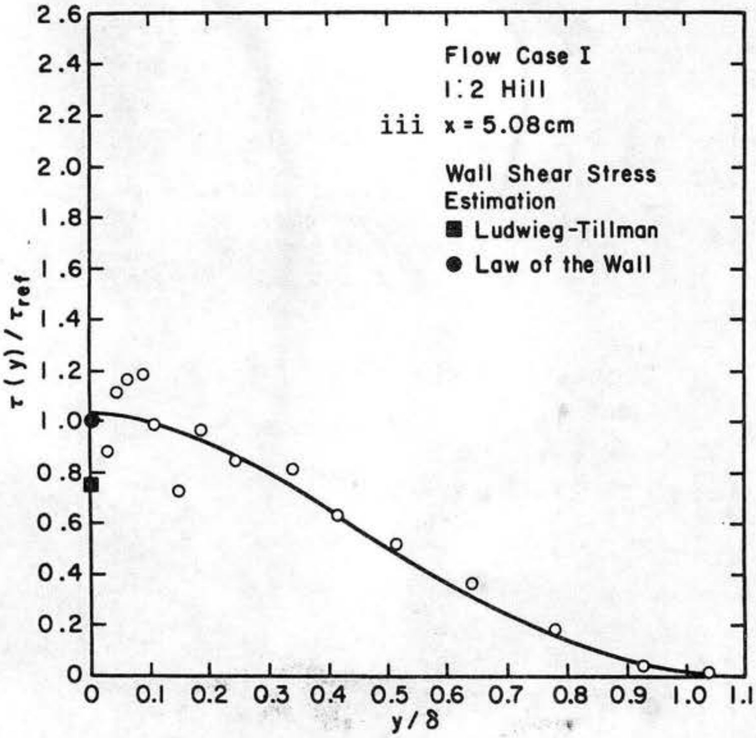

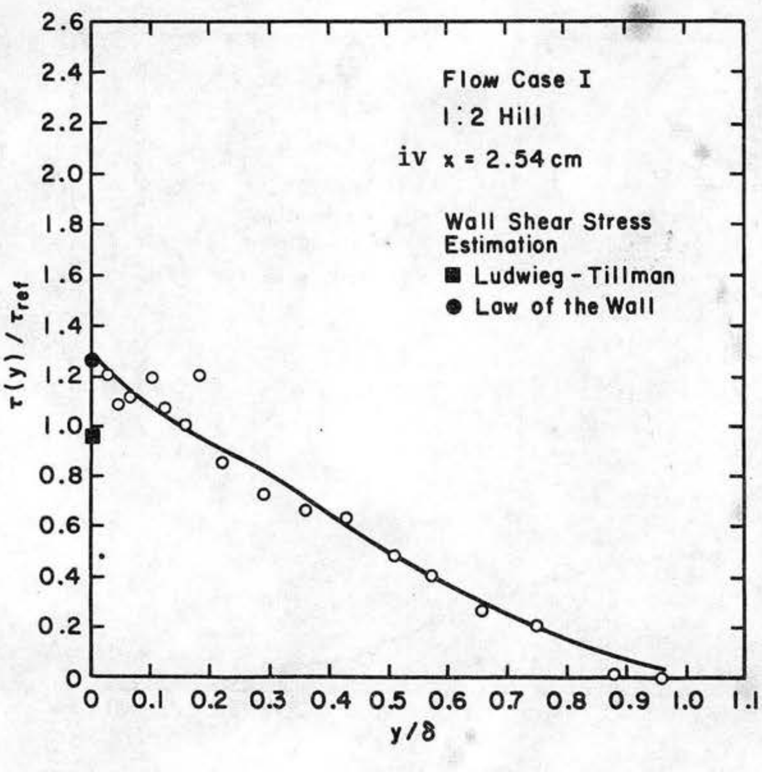

Figure 28. Shear stress distribution flow case I (continued).

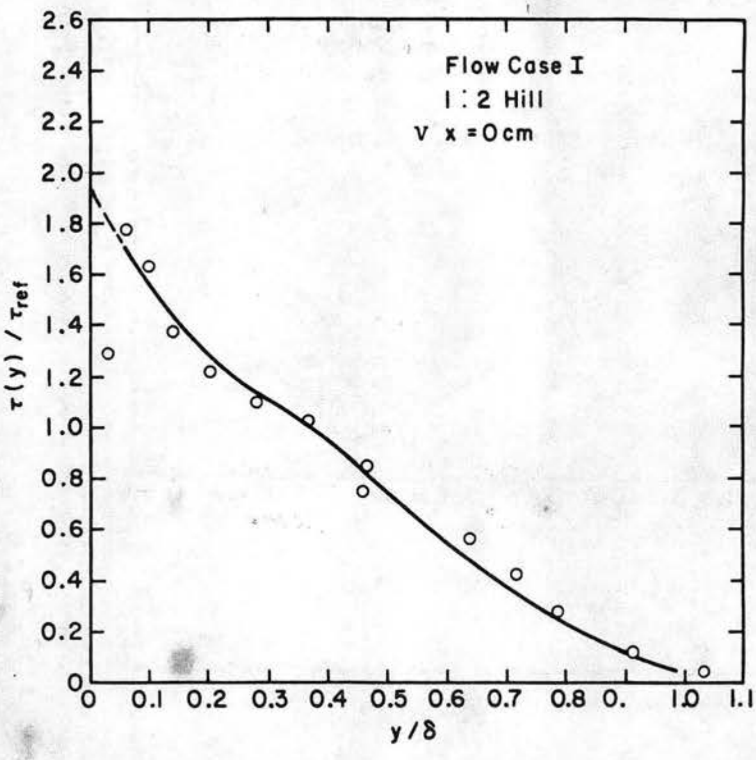

Figure 28. Shear stress distribution flow case I (continued).

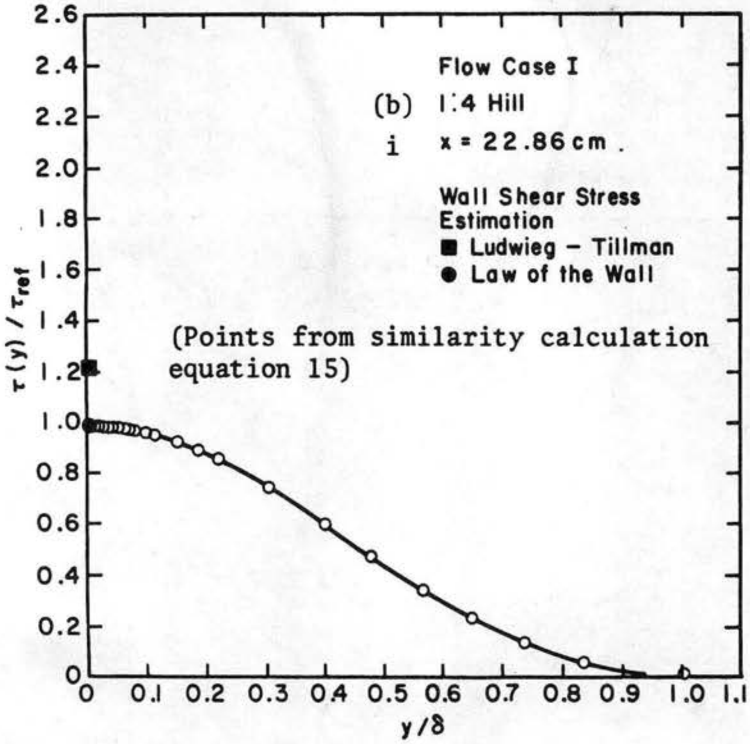

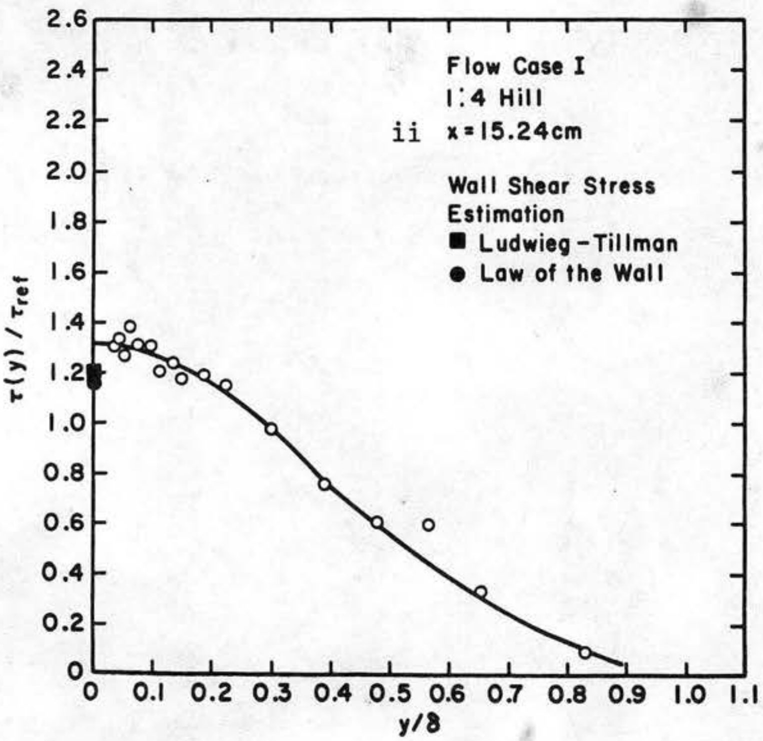

Figure 28. Shear stress distribution flow case I (continued).

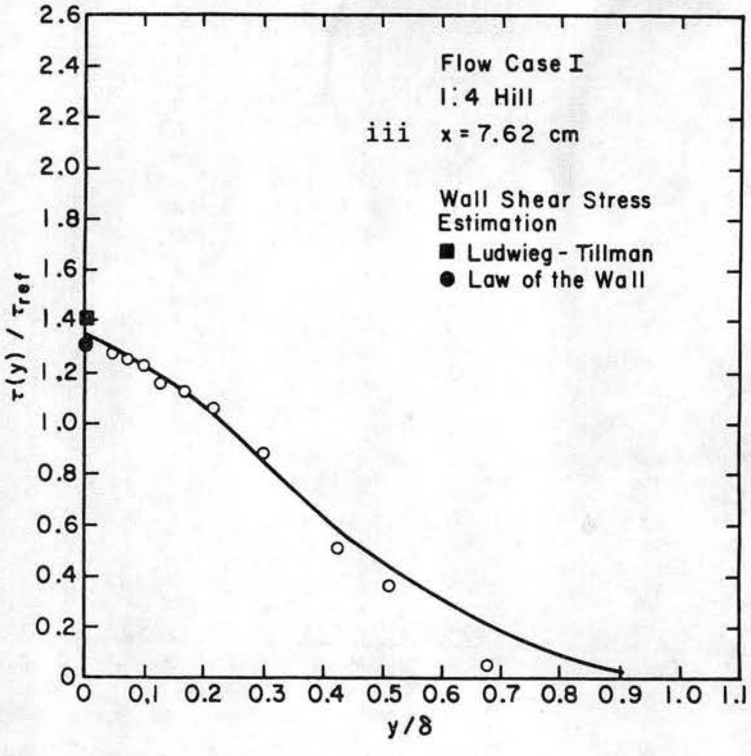

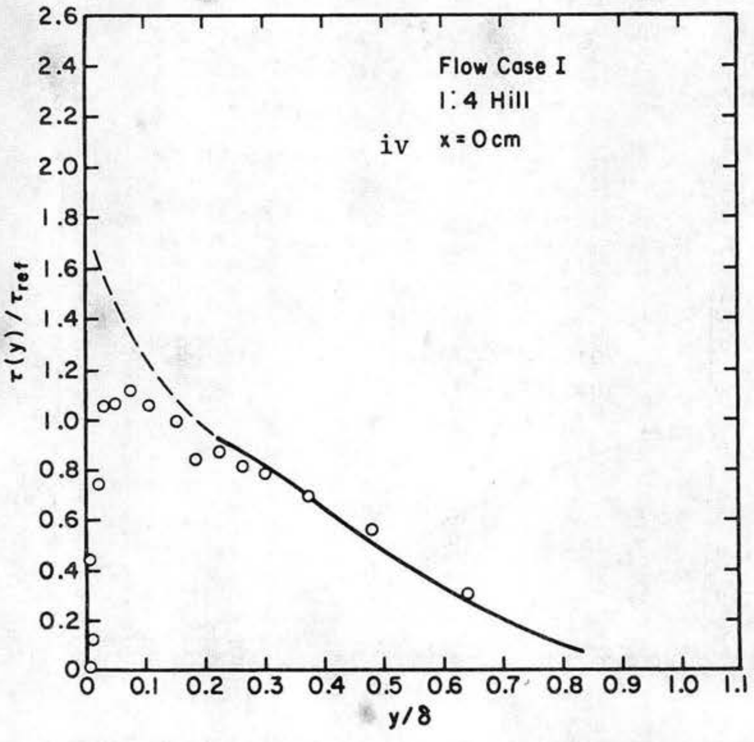

Figure 28. Shear stress distribution flow case I (continued).

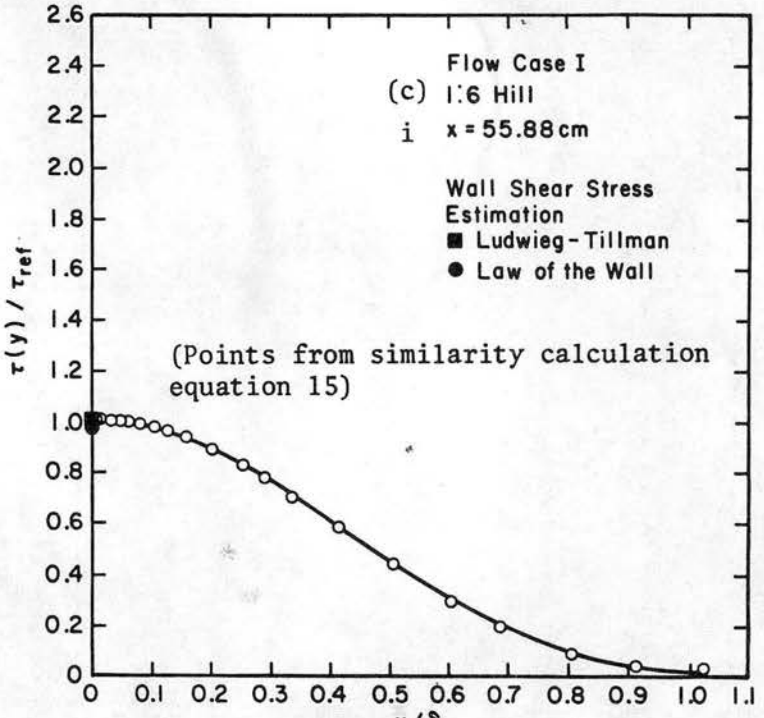

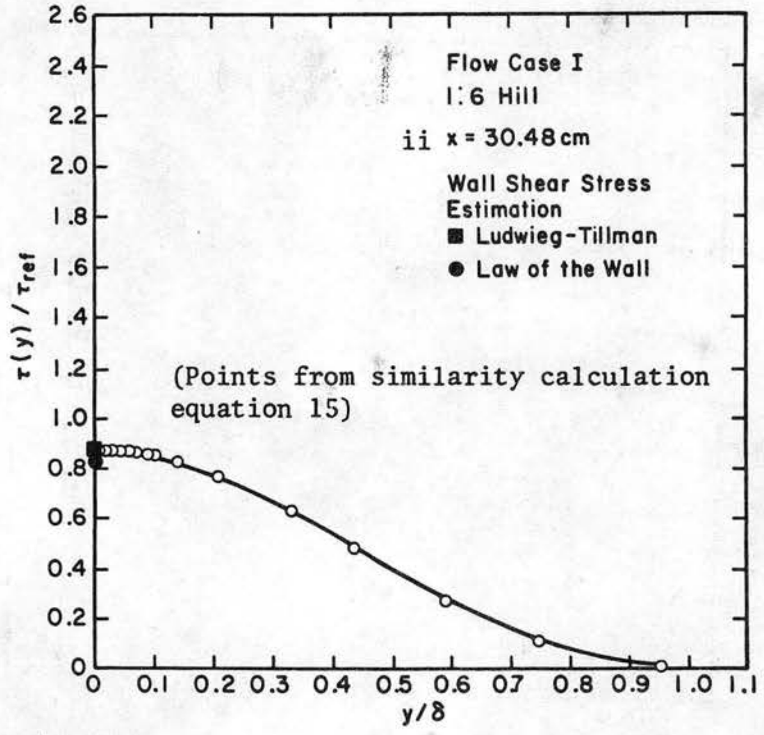

Figure 28. Shear stress distribution flow case I (continued).

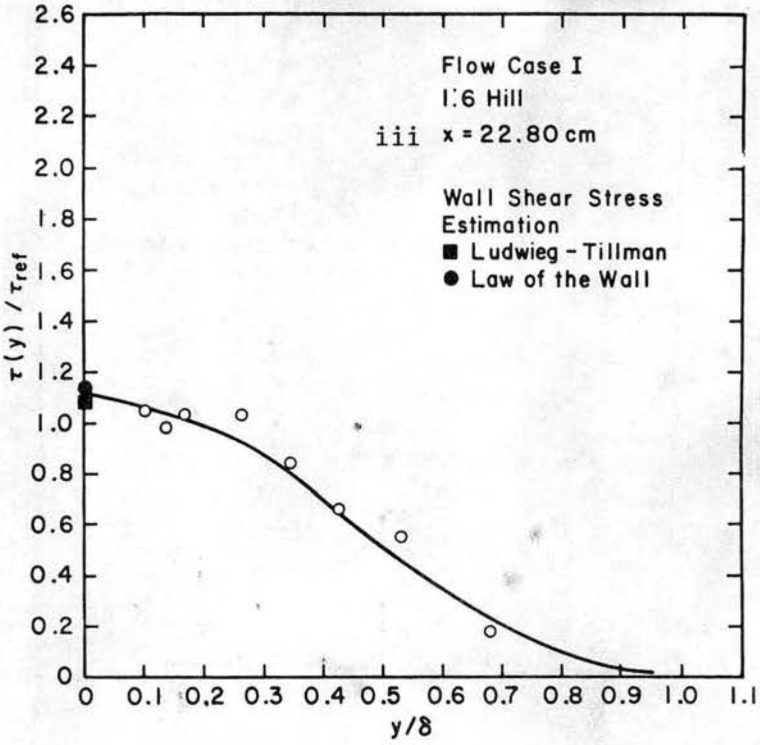

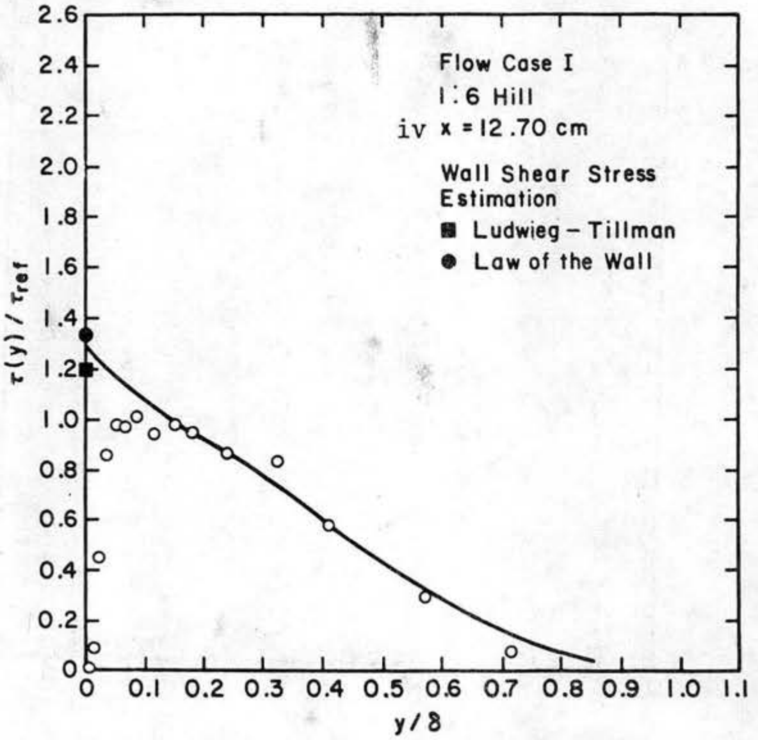

Figure 28. Shear stress distribution flow case I (continued).

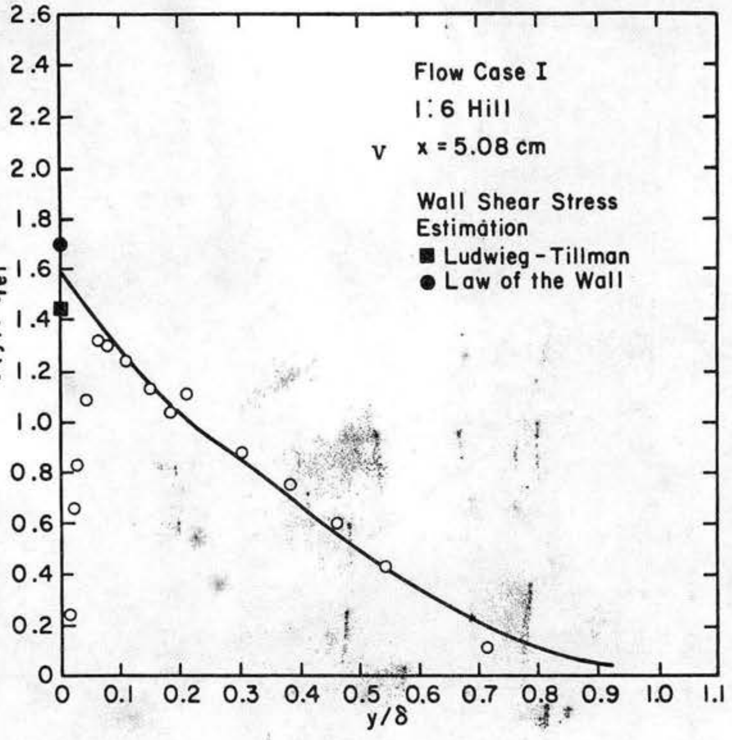

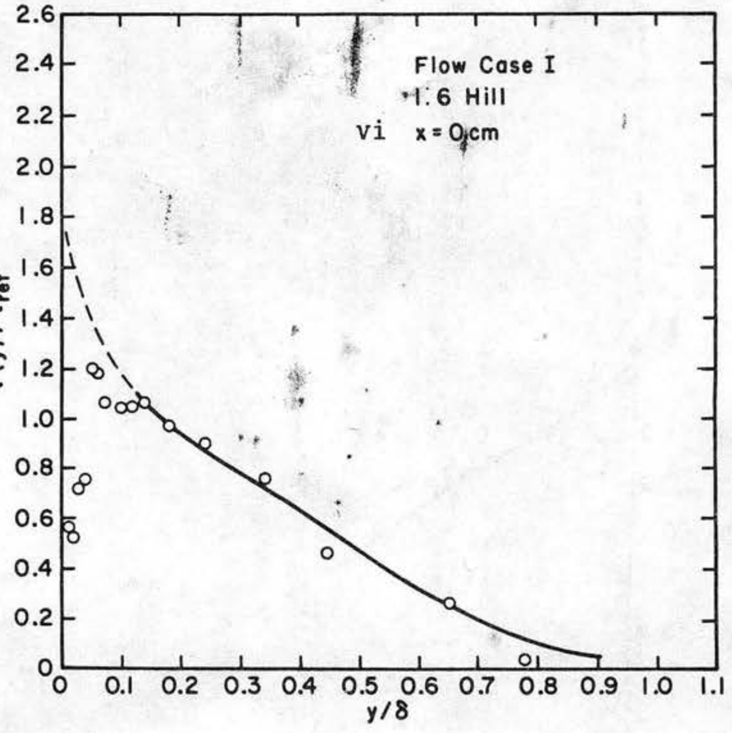

Figure 28. Shear stress distribution flow case I (completed).

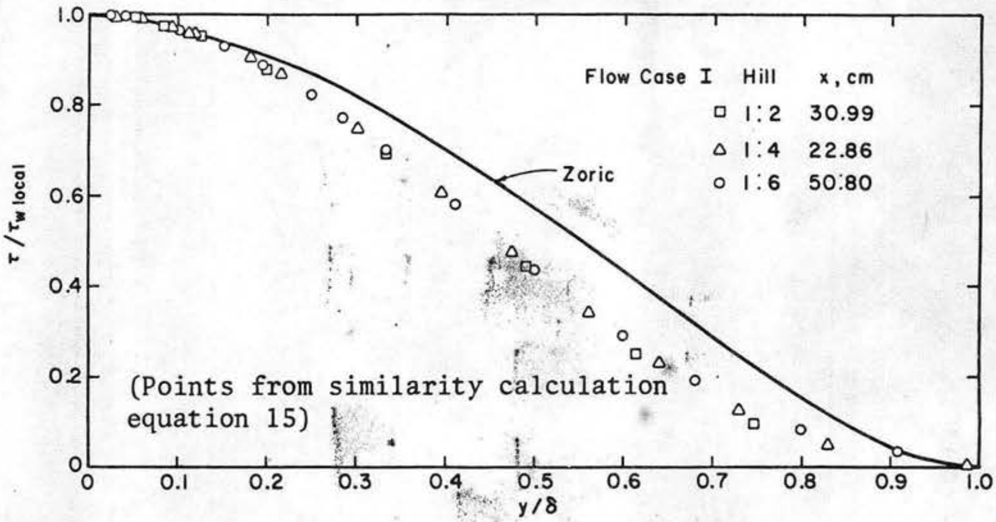

Figure 29. Comparison of upstream shear stress distribution to that of Zoric. Flow case I.

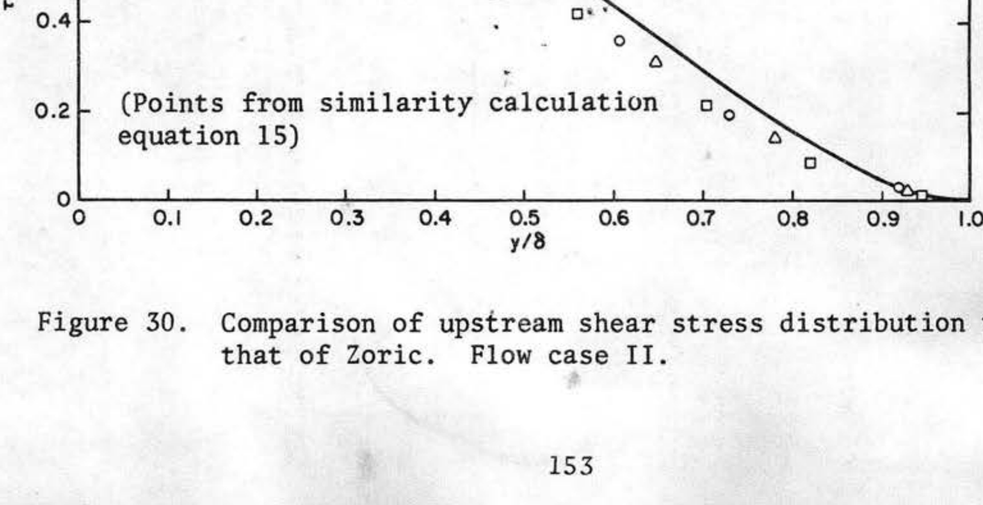

Figure 30. Comparison of upstream shear stress distribution to that of Zoric. Flow case II.

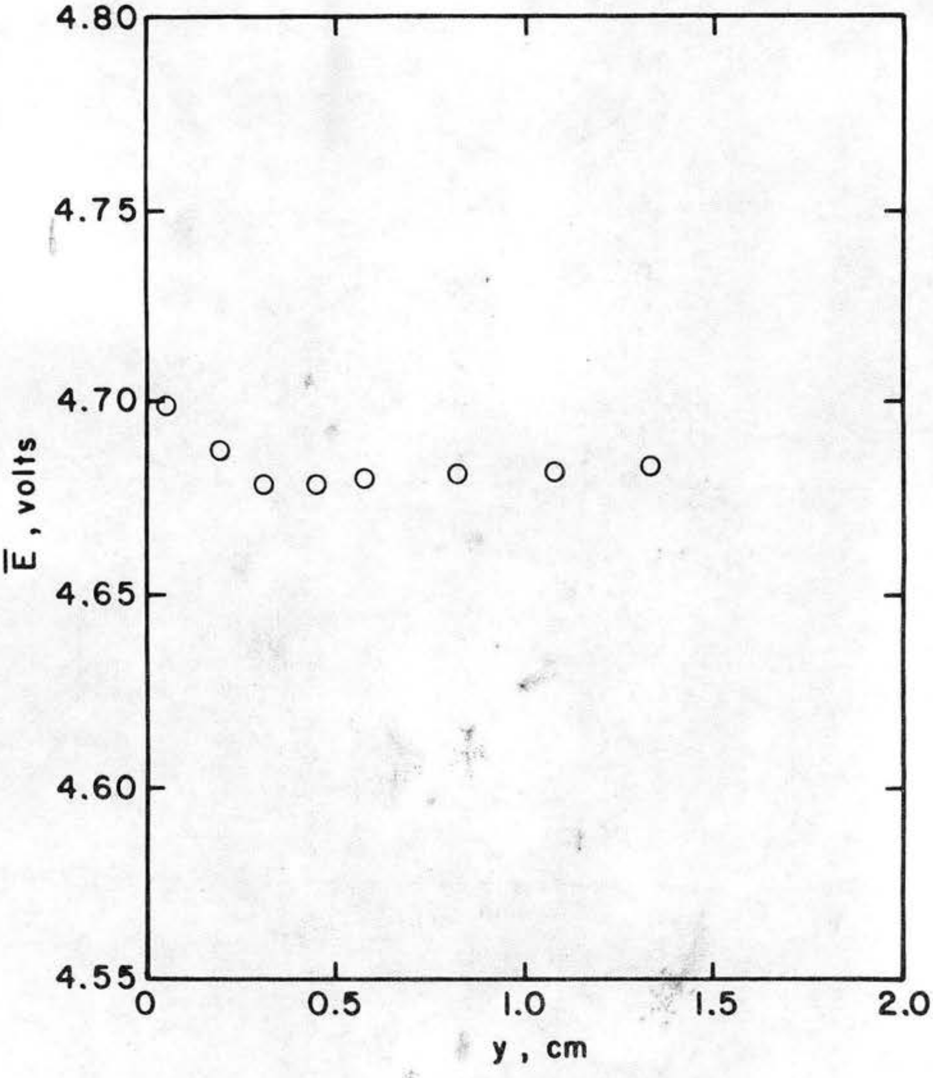

Figure 31. Effect of the wall as a heat sink.

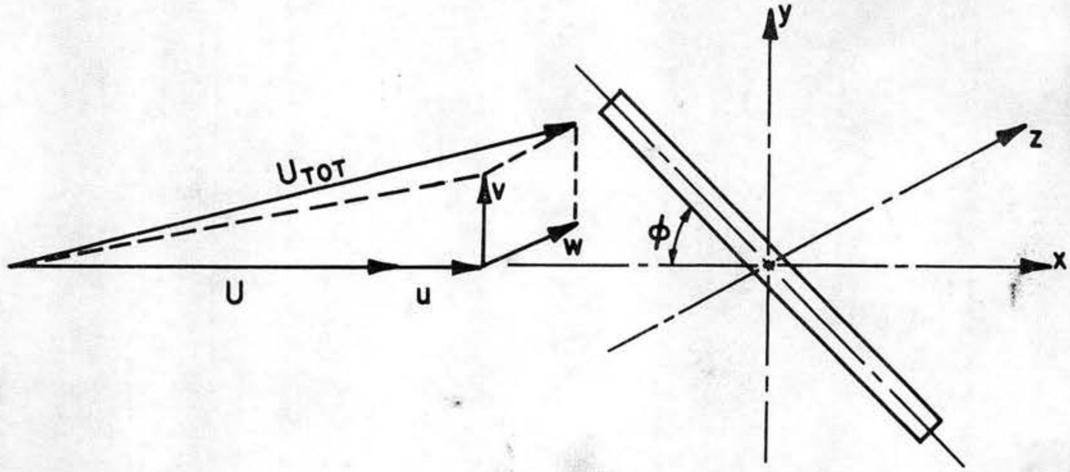

Figure 32. Hot wire with respect to the coordinate system.

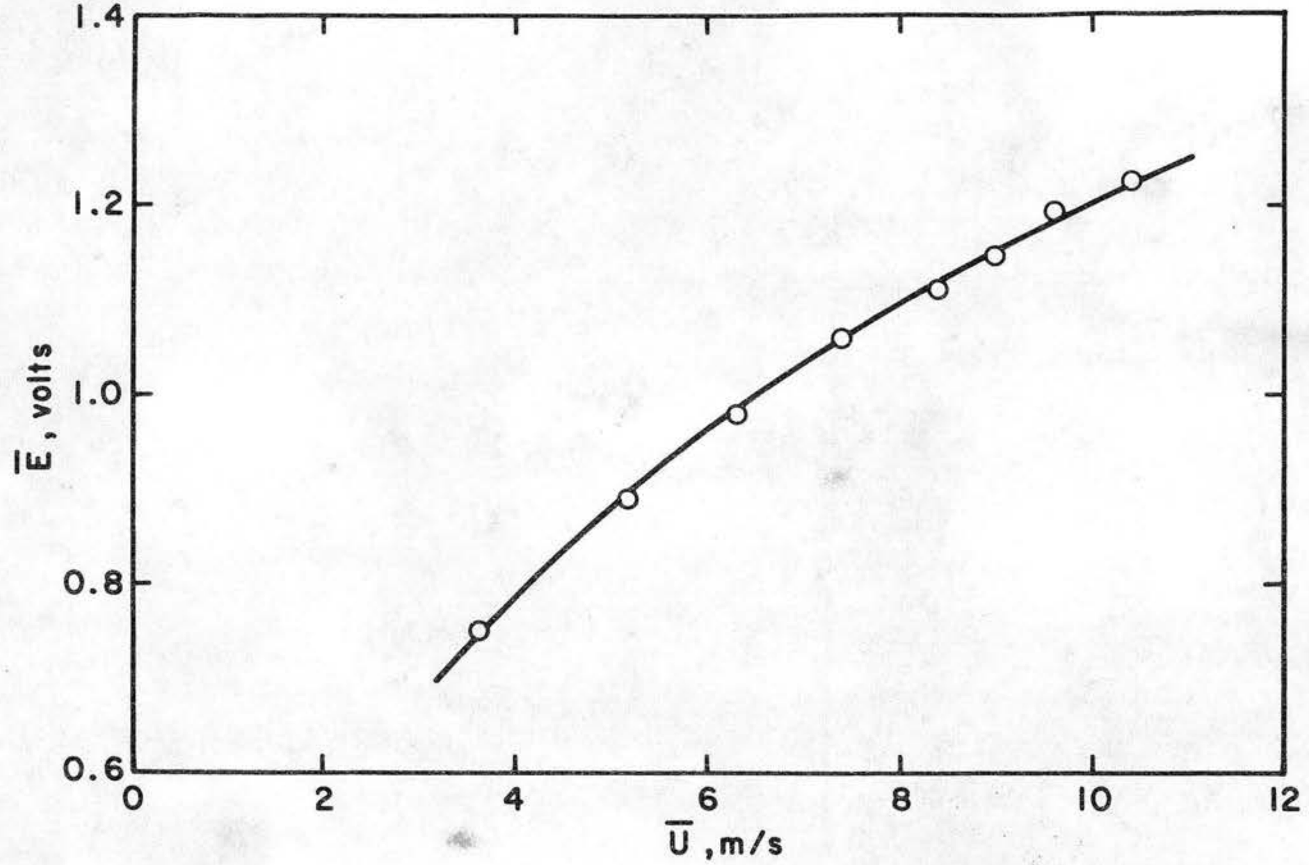

Figure 33. Typical hot wire calibrator curve.

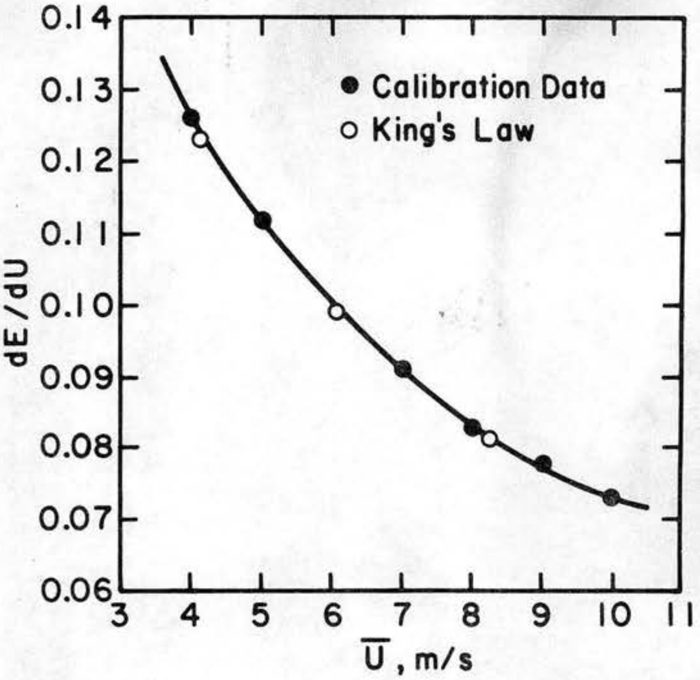

Figure 34. Typical hot wire sensitivity curve to velocity.

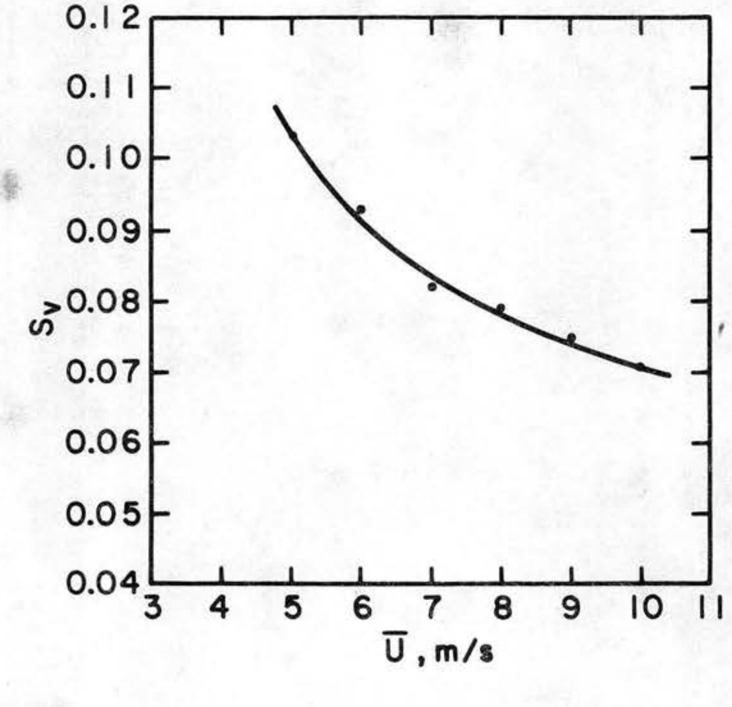

Figure 35. Typical hot wire sensitivity curve to yaw.

TABLES

Table Ia. Tabulated data for flow case I: 1:2 Hill model.

FOR HILL 1/2 POSITION 30.99CM FROM CREST FREE STREAM VELOCIT 9.09M/S

Y/DELTA	U(y)/U F.S.	RMSU(ROE/T)**.5	RMSV(ROE/T)**.5	T(y)/T REF
.005	.380	1.850	1.222	.792
.012	.519	2.223	1.323	.792
.029	.595	2.170	1.170	.790
.053	.641	2.105	1.237	.786
.084	.694	2.010	1.189	.775
.124	.728	1.881	1.245	.755
.196	.771	1.668	1.151	.699
.326	.842	1.606	1.144	.557
.480	.911	1.417	1.115	.359
.602	.949	1.240	.919	.208
.732	.979	.808	.639	.083
.875	.999	.443	.356	.006
1.017	1.000	.246	0.000	-.012

Table Ia. Tabulated data for flow case I: 1:2 Hill model (continued).

FOR HILL 1/2 POSITION 10.16CM FROM CREST FREE STREAM VELOCIT 9.61M/S

Y/DELTA	U(Y)/U F.S.	RMSU(ROE/T)**.5	RMSV(ROE/T)**.5	T(Y)/T REF
.021	.360	1.877	1.217	.550
.037	.469	2.082	1.260	.549
.070	.568	2.032	1.199	.545
.088	.607	2.026	1.170	.541
.123	.675	1.823	1.102	.531
.162	.738	1.838	1.167	.514
.201	.763	1.754	1.154	.493
.250	.795	1.650	1.133	.461
.314	.831	1.569	1.093	.412
.373	.874	1.519	1.113	.361
.458	.907	1.418	1.055	.282
.520	.931	1.378	.982	.226
.612	.947	1.221	.894	.147
.721	.977	.947	.696	.073
.824	.995	.629	.536	.025
.927	.998	.413	.350	.003
1.033	1.000	.284	.227	-.001

Table Ia. Tabulated data for flow case I: 1:2 Hill model (continued).

FOR HILL 1/2 POSITION 2.54CM FROM CREST FREE STREAM VELOCIT 9.53M/S

Y/DELTA	U(Y)/U F.S.	RMSU(ROE/T)**.5	RMSV(ROE/T)**.5	T(Y)/T REF
.022	.707	2.086	1.375	1.198
.041	.728	2.004	1.278	1.076
.060	.758	2.007	1.262	1.104
.099	.805	2.002	1.183	1.181
.120	.823	1.899	1.163	1.061
.153	.841	1.817	1.159	.992
.177	.853	1.907	1.185	1.194
.215	.857	1.694	1.110	.845
.285	.881	1.614	1.096	.720
.356	.899	1.545	1.101	.656
.425	.916	1.471	1.035	.626
.505	.944	1.376	.939	.475
.568	.958	1.307	.846	.394
.653	.978	1.100	.705	.254
.746	.993	.926	.559	.200
.874	1.000	.492	.253	.003
.954	1.000	.369	.099	-.011
1.012	1.000	.275	0.000	-.029

Table Ia. Tabulated data for flow case I: 1:2 Hill model (continued).

FOR HILL 1/2 POSITION 5.08CM FROM CREST FREE STREAM VELOCIT 9.67M/S

Y/DELTA	U(Y)/U F.S.	RMSU(ROE/T)**.5	RMSV(ROE/T)**.5	T(Y)/T REF
.025	.595	1.936	1.256	.878
.038	.628	2.069	1.251	1.104
.057	.688	2.103	1.196	1.159
.082	.721	1.982	1.196	1.177
.102	.752	1.884	1.153	.979
.143	.789	1.655	1.125	.719
.181	.808	1.808	1.162	.960
.237	.851	1.689	1.141	.839
.333	.883	1.631	1.150	.805
.410	.912	1.521	1.031	.621
.507	.942	1.381	.954	.504
.636	.975	1.162	.781	.355
.775	.990	.866	.508	.171
.924	1.000	.453	.243	.033
1.034	1.000	.292	.090	-.002

Table Ia. Tabulated data for flow case I: 1:2 Hill model (continued).

FOR HILL 1/2 POSITION 0.00CM FROM CREST FREE STREAM VELOCIT 9.68M/S

Y/DELTA	U(Y)/U F.S.	RMSU(ROE/T)**.5	RMSV(ROE/T)**.5	T(Y)/T REF
.005	.723	1.819	1.479	.791
.026	.714	1.980	1.419	1.283
.056	.825	1.997	1.359	1.766
.095	.845	1.882	1.333	1.622
.136	.860	1.763	1.241	1.365
.198	.868	1.634	1.208	1.207
.277	.898	1.547	1.194	1.090
.363	.920	1.500	1.145	1.015
.460	.946	1.388	1.044	.837
.455	.959	1.289	.947	.731
.632	.979	1.108	.828	.554
.712	.993	.911	.737	.415
.783	.999	.696	.614	.269
.909	.999	.405	.391	.108
1.028	1.000	.217	.221	.031

Table Ib. Tabulated data for flow case I: 1:4 Hill model.

FOR HILL 1/4 POSITION 22.86CM FROM CREST FREE STREAM VELOCIT/0.00M/S

Y/DELTA	U(Y)/U F.S.	RMSU(ROE/T)**.5	RMSV(ROE/T)**.5	T(Y)/T REF
.005	.428	1.770	1.166	.979
.010	.484	1.899	1.122	.979
.019	.540	2.003	1.331	.979
.028	.570	2.018	1.358	.978
.039	.610	2.046	1.351	.976
.046	.622	2.049	1.343	.974
.054	.644	2.058	1.357	.972
.062	.640	1.984	1.331	.969
.071	.652	1.972	1.323	.966
.080	.660	1.945	1.323	.962
.096	.676	1.925	1.314	.953
.113	.692	1.879	1.292	.943
.147	.745	1.850	1.276	.916
.181	.777	1.829	1.277	.884
.215	.795	1.771	1.267	.848
.300	.836	1.659	1.215	.735
.395	.865	1.452	1.055	.591
.473	.932	1.353	.959	.465
.558	.955	1.099	.901	.334
.641	.995	.922	.782	.220
.729	1.000	.773	.679	.121
.828	.997	.462	.442	.047
.999	1.000	.214	.100	-.000
1.168	.995	.141	.105	-.000
1.280	.990	.140	.056	-.000

Table Ib. Tabulated data for flow case I: 1:4 Hill model (continued).

FOR HILL 1/4 POSITION 15.24CM FROM CREST FREE STREAM VELOCIT 10.05M/S

Y/DELTA	U(Y)/U F.S.	RMSU(ROE/T)**.5	RMSV(ROE/T)**.5	T(Y)/T REF
.007	.537	1.870	1.421	.708
.011	.542	1.901	1.479	.911
.020	.572	2.010	1.503	1.173
.031	.614	2.067	1.477	1.299
.039	.647	2.049	1.458	1.328
.049	.662	2.008	1.438	1.260
.057	.669	2.031	1.440	1.378
.071	.685	1.976	1.402	1.302
.093	.709	1.920	1.378	1.300
.109	.711	1.850	1.335	1.198
.129	.730	1.838	1.333	1.236
.145	.738	1.781	1.302	1.171
.181	.801	1.769	1.260	1.184
.221	.829	1.739	1.268	1.141
.295	.859	1.612	1.206	.973
.385	.927	1.453	1.032	.752
.472	.960	1.352	.941	.596
.561	.965	1.147	.945	.588
.649	1.005	.857	.750	.324
.823	1.000	.521	.480	.086
1.066	1.000	.164	0.000	-.038
1.289	.995	.136	0.000	-.035

Table Ib. Tabulated data for flow case I: 1:4 Hill model (continued).

FOR HILL 1/4 POSITION 0.00CM FROM CREST FREE STREAM VELOCIT 9.70M/S

Y/DELTA	U(Y)/U F.S.	RMSU(ROE/T)**.5	RMSV(ROE/T)**.5	T(Y)/T REF
.005	1.072	1.920	.862	.109
.001	1.070	1.765	1.200	.434
.016	1.052	1.778	1.374	.737
.025	1.014	1.821	1.496	1.044
.045	.977	1.762	1.456	1.055
.072	.957	1.737	1.453	1.105
.104	.941	1.671	1.414	1.046
.148	.934	1.599	1.376	.984
.182	.934	1.531	1.316	.834
.221	.934	1.494	1.310	.861
.260	.932	1.458	1.267	.806
.297	.934	1.426	1.239	.775
.370	.938	1.344	1.182	.685
.477	.954	1.241	1.056	.551
.637	.977	1.035	.815	.291
.822	.994	.643	.311	-.078
1.033	1.000	.220	.148	-.272

Table Ib. Tabulated data for flow case I: 1:4 Hill model (continued).

FOR HILL 1/4 POSITION 7.62CM FROM CREST FREE STREAM VELOCIT 9.95M/S

Y/DELTA	U(Y)/U F.S.	RMSU(ROE/T)**.5	RMSV(ROE/T)**.5	T(Y)/T REF
.005	.529	1.341	1.289	-.061
.014	.538	1.368	1.368	.114
.021	.553	1.455	1.462	.388
.032	.567	1.509	1.481	.565
.042	.709	1.921	1.567	1.266
.067	.738	1.861	1.497	1.244
.095	.772	1.766	1.460	1.216
.122	.799	1.733	1.421	1.146
.163	.878	1.662	1.366	1.112
.212	.899	1.611	1.333	1.048
.294	.930	1.500	1.229	.875
.421	.953	1.268	.990	.495
.505	.965	1.114	.859	.351
.671	.989	.822	.558	.039
.842	1.000	.333	0.000	-.236
1.001	.993	.129	0.000	-.292

Table Ic. Tabulated data for flow case I: 1:6 Hill model.

FOR HILL 1/6 POSITION 55.88CM FROM CREST FREE STREAM VELOCIT 9.48M/S

Y/DELTA	U(y)/U F.S.	RMSU(ROE/T)**.5	RMSV(ROE/T)**.5	T(y)/T REF
.004	.396	2.395	.916	1.000
.010	.530	2.332	1.150	1.000
.027	.608	2.182	1.138	.998
.043	.655	2.110	1.208	.995
.057	.688	2.143	1.209	.991
.075	.730	1.892	1.183	.984
.100	.760	1.907	1.186	.971
.122	.788	1.835	1.228	.956
.153	.814	1.784	1.252	.930
.196	.825	1.624	1.202	.887
.248	.869	1.569	1.206	.823
.285	.869	1.510	1.205	.773
.333	.899	1.444	1.174	.701
.409	.923	1.366	1.144	.580
.500	.950	1.196	1.000	.436
.599	.975	1.033	.875	.289
.682	.988	.802	.643	.187
.799	.997	.585	.441	.083
.908	.999	.394	.150	.035
1.020	1.000	.123	0.000	.025
1.178	1.000	.075	0.000	.025

Table Ic. Tabulated data for flow case I: 1:6 Hill model (continued).

FOR HILL 1/6 POSITION 30.48CM FROM CREST FREE STREAM VELOCIT 9.50M/S

Y/DELTA	U(y)/U F.S.	RMSU(ROE/T)**.5	RMSV(ROE/T)**.5	T(y)/T REF
.004	.321	2.342	.964	.867
.017	.500	2.015	1.121	.866
.026	.556	2.138	1.139	.865
.041	.594	2.097	1.169	.863
.053	.630	2.074	1.135	.861
.065	.653	2.011	1.220	.857
.084	.697	1.957	1.186	.850
.099	.707	1.941	1.218	.843
.134	.748	1.867	1.267	.822
.204	.813	1.751	1.302	.764
.324	.883	1.510	1.225	.622
.432	.931	1.326	1.150	.472
.585	.976	1.052	.894	.264
.740	.999	.671	.537	.102
.948	1.000	.202	0.000	.009
1.149	1.000	.080	0.000	.006

Table 1c. Tabulated data for flow case I: 1:6 Hill model (continued).

FOR HILL 1/6 POSITION 12.70CM FROM CREST FREE STREAM VELOCIT 9.59M/S

Y/DELTA	U(y)/U F.S.	RMSU(ROE/T)**.5	RMSV(ROE/T)**.5	T(y)/T REF
.010	.680	2.052	.915	.080
.018	.711	2.002	1.163	.443
.031	.741	2.040	1.342	.853
.047	.779	2.008	1.343	.972
.063	.788	1.950	1.359	.961
.082	.806	1.885	1.394	1.008
.111	.842	1.765	1.371	.939
.147	.867	1.728	1.378	.976
.176	.875	1.638	1.376	.943
.233	.900	1.530	1.313	.857
.318	.923	1.444	1.279	.828
.405	.962	1.235	1.097	.570
.566	.996	.980	.852	.283
.709	1.000	.650	.583	.068
.872	1.000	.253	0.000	-.134
1.022	1.000	.140	0.000	-.136
1.159	1.000	.081	0.000	-.143

Table 1c. Tabulated data for flow case I: 1:6 Hill model (continued).

FOR HILL 1/6   POSITION 22.86CM FROM CREST   FREE STREAM VELOCIT 9.58M/S

Y/DELTA	U(Y)/U F.S.	RMSU(ROE/T)**.5	RMSV(ROE/T)**.5	T(Y)/T REF
.005	.589	1.975	1.263	-.186
.013	.602	2.075	1.440	.377
.020	.637	2.146	1.454	.664
.031	.670	2.085	1.441	.749
.045	.681	2.018	1.369	.803
.059	.702	1.948	1.348	.857
.097	.752	1.902	1.347	1.042
.133	.789	1.738	1.268	.973
.164	.825	1.726	1.260	1.024
.259	.876	1.619	1.217	1.022
.342	.909	1.442	1.085	.829
.421	.933	1.254	.974	.651
.527	.966	1.146	.887	.541
.675	.991	.756	.541	.169
.845	.999	.358	0.000	-.053
.991	.997	.144	0.000	-.106
1.144	1.000	.080	0.000	-.115

Table Ic. Tabulated data for flow case I: 1:6 Hill model (continued).

FOR HILL 1/6 POSITION 0.00CM FROM CREST FREE STREAM VELOCIT 9.68M/S

Y/DELTA	U(Y)/U F.S.	RMSU(ROE/T)**.5	RMSV(ROE/T)**.5	T(Y)/T REF
.006	1.021	2.590	.916	.558
.014	.943	2.318	1.018	.514
.023	.986	2.076	1.262	.712
.033	.964	1.901	1.349	.747
.046	.949	2.063	1.507	1.190
.058	.949	2.021	1.479	1.168
.067	.927	1.903	1.453	1.054
.095	.934	1.826	1.458	1.033
.114	.942	1.787	1.453	1.035
.134	.919	1.715	1.392	1.051
.173	.912	1.611	1.398	.959
.236	.919	1.524	1.351	.891
.337	.934	1.396	1.253	.747
.440	.964	1.144	1.002	.449
.645	.964	.880	.782	.254
.772	.986	.626	.521	.027
.938	.996	.345	0.000	-.105
1.153	1.000	.198	0.000	-.113
1.405	1.000	.144	0.000	-.110

Table Ic. Tabulated data for flow case I: 1:6 Hill model (continued).

FOR HILL 1/6 POSITION 5.08CM FROM CREST FREE STREAM VELOCIT 9.66M/S

Y/DELTA	U(y)/U F.S.	RMSU(ROE/T)**.5	RMSV(ROE/T)**.5	T(y)/T REF
.009	.801	2.030	.981	.232
.017	.827	2.027	1.218	.651
.023	.844	2.020	1.320	.824
.039	.861	2.024	1.399	1.082
.057	.885	2.029	1.476	1.312
.073	.893	1.969	1.467	1.293
.105	.901	1.876	1.437	1.232
.145	.909	1.717	1.504	1.121
.179	.917	1.637	1.375	1.026
.206	.924	1.633	1.376	1.099
.298	.947	1.501	1.257	.869
.380	.967	1.388	1.173	.742
.458	.977	1.254	1.059	.594
.538	.990	1.106	.929	.422
.708	1.000	.741	.571	.101
.883	1.000	.296	0.000	-.136
1.006	1.000	.136	0.000	-.162
1.154	1.000	.101	0.000	-1.276

Table IIa. Tabulated data for flow case II
1:2 Hill model.

FOR HILL 1/2 POSITION 50.80CM FROM CREST FREE STREAM VELOCIT 9.48M/S

Y/DELTA	U(Y)/U F.S.	RMSU(ROE/T)**.5	T(Y)/T REF
.001	.351	2.435	.956
.003	.438	2.334	.956
.006	.485	2.365	.956
.008	.512	2.390	.956
.012	.540	2.447	.956
.016	.566	2.511	.955
.028	.614	2.607	.954
.062	.671	2.460	.948
.128	.718	2.376	.918
.192	.748	2.203	.871
.257	.776	2.200	.808
.354	.822	2.118	.691
.453	.877	1.968	.552
.582	.934	1.597	.361
.776	.989	.761	.117
.983	1.000	.269	.000

FOR HILL 1/2 POSITION 30.48CM FROM CREST FREE STREAM VELOCIT 9.74M/S

Y/DELTA	U(Y)/U F.S.	RMSU(ROE/T)**.5	T(Y)/T REF
.001	.294	2.297	.850
.003	.390	2.518	.850
.005	.429	2.497	.850
.008	.432	2.409	.850
.019	.490	2.578	.849
.036	.540	2.641	.847
.064	.612	2.664	.842
.093	.645	2.555	.832
.124	.655	2.413	.818
.188	.707	2.327	.777
.250	.737	2.234	.722
.345	.778	2.120	.616
.457	.837	2.004	.469
.563	.885	1.787	.320
.752	.957	.963	.085
.953	1.000	.340	0.000

Table IIa. Tabulated data for flow case II
1:2 Hill model (continued).

FOR HILL 1/2 POSITION 15.24CM FROM CREST FREE STREAM VELOCIT 9.69M/S

Y/DELTA	U(Y)/U F.S.	RMSU(ROE/T)**.5	T(Y)/T REF
.001	.193	2.044	.702
.003	.277	2.561	.702
.005	.296	2.622	.702
.007	.313	2.590	.702
.012	.340	2.646	.702
.028	.418	2.862	.701
.059	.497	2.730	.698
.089	.538	2.602	.692
.119	.597	2.419	.683
.181	.657	2.332	.656
.270	.739	2.250	.597
.364	.799	2.131	.515
.486	.872	1.948	.388
.646	.939	1.485	.214
.777	.934	.671	.091
.927	1.000	.268	.009

FOR HILL 1/2 POSITION 10.16CM FROM CREST FREE STREAM VELOCIT 9.71M/S

Y/DELTA	U(Y)/U F.S.	RMSU(ROE/T)**.5	T(Y)/T REF
.001	.050	.548	.607
.003	.105	1.343	.607
.005	.136	1.673	.607
.007	.168	1.953	.607
.012	.213	2.254	.607
.022	.284	2.500	.606
.055	.466	2.814	.604
.085	.532	2.022	.600
.117	.592	2.293	.593
.187	.677	2.124	.569
.266	.730	1.382	.526
.358	.820	.546	.459
.480	.878	1.720	.352
.625	.947	1.395	.216
.761	.985	.788	.102
.918	1.000	.286	.023

Table IIa. Tabulated data for flow case II
1:2 Hill model (continued).

FOR HILL 1/2 POSITION 7.62CM FROM CREST FREE STREAM VELOCIT 9.70M/S

Y/DELTA	U(Y)/U F.S.	RMSU(ROE/T)**.5
.001	.824	3.607
.003	.277	1.709
.005	.298	1.772
.007	.308	1.918
.014	.360	2.124
.034	.428	2.462
.064	.520	2.552
.094	.589	2.386
.155	.671	2.212
.218	.734	2.118
.307	.790	2.063
.398	.844	2.000
.520	.905	1.759
.703	.976	.976
.897	1.000	.295

FOR HILL 1/2 POSITION 2.54CM FROM CREST FREE STREAM VELOCIT 9.70M/S

Y/DELTA	U(Y)/U F.S.	RMSU(ROE/T)**.5
.001	.440	2.032
.003	.482	1.809
.005	.492	1.724
.012	.507	1.760
.020	.542	1.915
.033	.576	2.117
.060	.650	2.204
.092	.690	2.211
.154	.734	2.158
.217	.780	2.077
.314	.831	2.052
.415	.873	1.994
.504	.913	1.783
.695	.963	1.096
.900	.999	.036

Table IIa. Tabulated data for flow case II
1:2 Hill model (continued).

FOR HILL 1/2 POSITION 0.00CM FROM CREST FREE STREAM VELOCIT 9.71M/S

Y/DELTA	U(Y)/U F.S.	RMSU(ROE/T)**.5
.001	.602	2.011
.003	.635	1.748
.006	.640	1.670
.008	.643	1.750
.021	.681	2.006
.046	.691	2.145
.087	.729	2.161
.130	.753	2.094
.164	.772	2.073
.228	.802	2.047
.294	.836	2.039
.390	.876	1.946
.489	.912	1.792
.653	.966	1.222
.748	.985	.815
.892	1.000	.327

Table IIb. Tabulated data for flow case II 1:6 Hill model.

FOR HILL 1/6 POSITION 50.80CM FROM CREST FREE STREAM VELOCIT 9.57M/S

Y/DELTA	U(y)/U F.S.	RMSU(ROE/T)**.5	T(y)/T REF
.001	.340	2.350	1.000
.003	.452	2.367	1.000
.005	.483	2.410	1.000
.008	.501	2.366	1.000
.014	.545	2.449	1.000
.024	.579	2.518	.999
.036	.620	2.521	.997
.061	.648	2.440	.992
.093	.690	2.332	.980
.123	.787	2.404	.964
.185	.763	2.201	.918
.248	.790	2.168	.855
.341	.845	2.080	.737
.434	.889	1.964	.601
.558	.929	1.713	.405
.705	.975	1.168	.191
.821	.987	.452	.059
.946	1.000	.221	0.000

FOR HILL 1/6 POSITION 35.56CM FROM CREST FREE STREAM VELOCIT 9.40M/S

Y/DELTA	U(y)/U F.S.	RMSU(ROE/T)**.5	T(y)/T REF
.001	.304	2.294	.925
.003	.411	2.443	.925
.005	.450	2.442	.925
.007	.472	2.450	.925
.012	.501	2.472	.925
.028	.591	2.604	.924
.059	.649	2.538	.918
.100	.696	2.403	.905
.140	.728	2.282	.884
.184	.760	2.195	.854
.244	.794	2.143	.803
.304	.832	2.076	.739
.394	.871	2.031	.627
.486	.918	1.841	.501
.608	.960	1.286	.331
.731	.987	.880	.177
.921	1.000	.314	.032

Table IIb. Tabulated data for flow case II
1:6 Hill model (continued).

FOR HILL 1/6 POSITION 20.32CM FROM CREST FREE STREAM VELOCIT10.21M/S

Y/DELTA	U(y)/U F.S.	RMSU(ROE/T)**.5
.001	.356	2.432
.003	.456	2.497
.005	.494	2.341
.008	.503	2.346
.014	.523	2.489
.027	.559	2.626
.052	.608	2.637
.088	.655	2.594
.157	.698	2.464
.220	.761	2.421
.284	.797	2.356
.376	.884	2.308
.473	.927	2.087
.594	.972	1.665
.720	.992	1.110
.919	1.000	.266

FOR HILL 1/6 POSITION 12.70CM FROM CREST FREE STREAM VELOCIT10.78M/S

Y/DELTA	U(y)/U F.S.	RMSU(ROE/T)**.5
.001	.407	2.589
.003	.520	2.542
.005	.549	2.307
.008	.570	2.225
.013	.591	2.214
.026	.633	2.394
.052	.677	2.414
.080	.708	2.368
.116	.748	2.327
.181	.811	2.315
.235	.832	2.269
.332	.881	2.202
.460	.923	1.955
.639	.979	1.344
.758	.995	.912
.919	1.000	.350

Table IIb. Tabulated data for flow case II
1:6 Hill model (continued).

FOR HILL 1/6 POSITION 7.62CM FROM CREST FREE STREAM VELOCIT 9.54M/S

Y/DELTA	U(y)/U F.S.	RMSU(ROE/T)**.5
.001	.500	2.568
.003	.613	2.428
.006	.643	2.196
.008	.650	2.091
.015	.685	2.176
.027	.696	2.270
.063	.741	2.287
.127	.793	2.209
.209	.826	2.138
.289	.859	2.146
.387	.892	2.037
.517	.938	1.791
.645	.994	1.306
.777	1.000	.751
.919	1.000	.320

FOR HILL 1/6 POSITION 0.00CM FROM CREST FREE STREAM VELOCIT 9.26M/S

Y/DELTA	U(y)/U F.S.	RMSU(ROE/T)**.5
.001	.767	2.462
.003	.860	2.264
.006	.883	2.036
.008	.880	2.040
.014	.872	2.003
.021	.877	2.109
.033	.886	2.195
.067	.874	2.168
.107	.860	2.107
.174	.860	2.062
.275	.870	2.032
.375	.889	1.911
.524	.951	1.572
.654	.980	1.246
.781	.995	.822
.917	1.000	.402

APPENDIX

Turbulence Measurements

Following is a short discussion of the general principles involved in hot-wire anemometry. The specifics used in the data evaluation are also discussed.

The basis of hot-wire anemometry is measuring the instantaneous heat loss from a cylinder due to change in surrounding conditions. The sensing elements used in this study were extremely small metal wires. These wires were heated above the ambient temperature by a commercial anemometer. As the flow conditions in the tunnel varied, the anemometer responded to the change in heat loss by balancing a wheatstone bridge. The response is considered instantaneous up to at least frequencies of 5,000 hertz. The rate of heat loss is indicated by the change in voltage required to maintain the wire at a desired temperature.

There is a variety of conditions which will cause a change in the heat transfer rate, 1) flow velocity, U; 2) change in the ambient air temperature; 3) physical properties of the air; 4) the length of the wire; 5) orientation of the wire with respect to the flow; and 6) solid objects which act as heat sinks.

Heat is lost from the wire in three ways: radiation, conduction, and convection. Generally in hot-wire anemometry the first two are considered negligible and not compensated for. The third, convection, is made up of two parts, free convection and forced convection. Free convection is important only with extremely low velocities. In this experiment the velocities were great enough so that free convection was not a problem. As a result, forced convection governed the measurements.

Stated earlier were six factors which will change the heat transfer rate from the wire. It was assumed that the physical properties of the air and the wire did not change. In addition the temperature of the air was held constant. The only solid body encountered during the testing was that of the tunnel floor. With no flow a check was made of the heat loss to the tunnel floor. There was no significant heat loss for the region of interest of this study, Figure 31. It was concluded that the heat loss from the hot wire was a result of the instantaneous velocities, mean velocity, and the geometric positioning of the probe.

Providing that the previous assumptions are valid, then voltage output from the hot wire would be a function of U_{tot} and ϕ, the angle of attack.

$$E_{out} = E(U_{tot}, \phi) . \tag{A-1}$$

The angle ϕ is that angle the wire makes with the instantaneous velocity and the x axis, Figure 32.

Following a discussion presented by Sandborn (9) where he writes that a perturbation in the velocity results in a perturbation in the voltage then the response of a hot wire for a two-dimensional flow

$$e = \frac{dE}{dU} u + \frac{dE}{d\phi} \frac{v}{U} . \tag{A-2}$$

This equation is the basis of the valuation of the hot-wire data. Squaring the equation and taking the mean, gives

$$\overline{e^2} = \left(\frac{dE}{dU}\right)^2 \overline{u^2} + 2 \frac{dE}{dU} \frac{dE}{d\phi} \frac{\overline{uv}}{U} + \left(\frac{dE}{d\phi}\right)^2 \frac{\overline{v^2}}{U^2} \tag{A-3}$$

and letting

$$S_u = \frac{dE}{dU} \quad \text{and} \quad S_v = \frac{1}{U}\frac{dE}{d\phi}$$

then

$$\overline{e^2} = S_u^2\overline{u^2} + a\ S_uS_v\overline{uv} + S_v^2\overline{v^2} \tag{A-4}$$

This equation can be used for either the cross-wire probe or the single horizontal wire. The cross-wire probe application is discussed first followed by the horizontal wire probe.

As described earlier the cross-wire probe is made up of two individual wires. One mounted parallel to the y-axis and the other lying in the x-y plane. (This configuration makes the data reduction less complicated than the usual x cross wire.) A wire placed parallel to the y-axis or normal to the flow is insensitive to the velocity component in the y-direction. As shown by Sandborn (9) the sensitivity to angle, S_u, varies as approximately the cosine of the angle. Thus for even slight misalignment up to 5° the value of S_v is essentially zero. This reduces equation for a normal wire to

$$\overline{e_n^2} = S_u^2\overline{u^2} \quad . \tag{A-5}$$

Henceforth S_u for the normal wire will be called S_1.

The second wire of the cross-wire probe was yawed approximately 40° from horizontal. This wire then calls for a calibration with respect to the mean velocity for each angle of incidence. The $\overline{e^2}$ of the yawed wire is the same as equation (A-4) or

$$\overline{e_y^2} = S_2^2\overline{u^2} + 2\ S_2S_v\overline{uv} + S_v^2\overline{v^2} \tag{A-6}$$

where S_u for the yawed wire is not S_2. At this point the equations governing the A.C. output of the hot wires have three unknowns $\overline{u^2}$, $\overline{v^2}$ and $\overline{uv}$. To evaluate the flow properties a third equation was needed. This equation came from multiplying the A.C. output of the two wires, which yielded

$$\overline{e_n e_y} = S_1 S_2 \overline{u^2} + S_1 S_v \overline{uv} \tag{A-7}$$

where $\overline{e_n e_y}$ will be represented as $\overline{e_1 e_2}$.

The evaluation of the turbulence sensed by the horizontal wire is very similar to that of the normal wire on the cross-wire probe. Because the probe is parallel to the x-axis any rotation about the z-axis causes no change in the voltage due to change in angle or S_v is zero. For the horizontal wire

$$\overline{e^2} = S_u^2 \overline{u^2} \ . \tag{A-8}$$

To summarize, the turbulent terms evaluated from the cross-wire data were found using the following equations:

$$\sqrt{\overline{u^2}} = \sqrt{\overline{e_1^2}}/S_1 \tag{A-9}$$

$$\overline{uv} = (\overline{e_1 e_2} - S_1 S_2 \overline{u^2})/(S_1 S_v) \tag{A-10}$$

$$\sqrt{\overline{v^2}} = [(\overline{e^2} - S_2^2 \overline{u^2} - 2\, S_2 S_v \overline{uv})/S_v^2]^{1/2} \ . \tag{A-11}$$

For the horizontal probe data

$$\sqrt{\overline{u^2}} = \sqrt{\overline{e^2}}/S_u \tag{A-12}$$

HOT-WIRE CALIBRATION

To calibrate the hot-wire probes the carriage was moved forward of the model and the probes raised to the free stream. When situated in the free stream the probes were outside the boundary layer, which reduces turbulence to a minimum for calibration. The standard used was a pitot-static tube mounted directly on the probe support. The wires were then subjected to a number of flow velocities ranging from 3.5 m/s to 16 m/s. The mean voltage required to maintain the overheat was recorded. This same procedure was repeated several times during the testing. Because the cross-wire probe needed additional calibration for angle change the probe was rotated in the x-y plane. The angles varied from -10° to +30° from the measuring position. At each angle setting chosen a complete velocity calibration, as described above, was made.

Once the hot-wire probes were heated they were not disconnected until the testings were complete. This helps to reproduce the same calibration from one time to the next. During the surveys the mean velocity was measured with a total pressure probe. This gave a check for the calibration during the actual sampling period.

Two methods were used to reduce the calibration data. The first used for the cross-wire data was a graphical method. The second and more adaptable to computers was the application of King's Law.

To find the sensitivity of a hot wire a relation must be known between the mean voltage of the hot wire for a known velocity, $\overline{U}$. A plot of $\overline{E}$ versus $\overline{U}$ from the calibration was made for both wires of the cross-wire probe data, Figure 33. From these plots the mean velocity for the surveys were taken. To find the sensitivity of the hot wire for a given velocity a second curve was constructed. The curve was formed by graphically evaluating $\frac{dE}{dU}$ for both wires at known velocities, Figure 34, and then plotting $\overline{U}$ versus S_u.

The method used to evaluate the data digitally employed King's Law. This involves relating the output of the hot wire to the velocity by an equation. The form used was

$$\overline{E^2} = A + B\ U^m \tag{A-13}$$

where A represents the equivalent square of the voltage for U = 0 and B and m are constants. Although m is different for each wire in most instances it is very close to .5. Differentiating gives S_u or

$$\frac{dE}{dU} = \frac{mB}{2EU^{(m-1)}} \ . \tag{A-14}$$

For the data at hand, setting m = .5 to find velocity and sensitivity proved to be very satisfactory, Figure 34.

The sensitivity of the wire to change in angle of incidence was done graphically. As stated earlier a complete voltage-velocity calibration was recorded for each angle setting of the probe. A series of velocity curves worked up. The individual curves represented different probe rotations. From each of the curves a voltage output for a designated velocity was read. A voltage versus angles was plotted. The relation is a linear one so the slope of the line gave $\frac{dE}{d\phi}$ for the designated velocity. The final result is S_v for the given velocity. Again

$$S_v = \frac{dE}{d\phi}\frac{1}{U} \ .$$

This evaluation was continued until the wire had a complete curve of $\overline{U}$ versus S_v. Figure 35 is an example of a sensitivity to angle curve.